Topology Optimization of Conjugated Heat Transfer Devices : Experimental and Numerical investigation

Vignaesh Subramaniam

N° d'ordre :

IMT LILLE DOUAI

IMT Lille Douai
École Mines-Télécom
IMT-Université de Lille

UNIVERSITÉ DE LILLE

Université de Lille

THESE

présentée en vue
d'obtenir le grade de

DOCTEUR

en

Discipline : Mécanique et Énergétique

par

Vignaesh SUBRAMANIAM

DOCTORAT DE L'UNIVERSITÉ DE LILLE
DÉLIVRÉ PAR IMT LILLE DOUAI

Titre de la thèse :

Topology Optimization of Conjugated Heat Transfer Devices: Experimental and Numerical Investigation

Soutenue le 7 Décembre 2018 devant le jury d'examen :

Président de Jury et Rapporteur	Julien REVEILLON, Professeur, Université de Rouen, CORIA UMR 6614
Rapporteur	Jean-Marie BUCHLIN, Professeur, Von Karman Institute for Fluid Dynamics, Department of Environmental and Applied Fluid Dynamics
Examinateur	Chérifa ABID, Maître de conférences, Aix Marseille Université
Examinateur	Lilla KAPA KOLOSZAR, Research Engineer, Von Karman Institute for Fluid Dynamics, Department of Environmental and Applied Fluid Dynamics
Encadrant	Talib DBOUK, Maître-Assistant, IMT Lille Douai, Département Energétique Industrielle
Directeur de Thèse	Jean-Luc HARION, Professeur, IMT Lille Douai
Examinateur	Rainier HREIZ, Maître de Conférence, Université de Lorraine, Laboratoire Réactions et Génie des Procédés - UMR 7274

Laboratoire d'accueil : Département Énergétique Industrielle (DEI), IMT Lille Douai

Ecole Doctorale SPI 072 (Lille I, Lille III, Artois, ULCO, UVHC, Centrale Lille, IMT Lille Douai)

What you imagine, is what will transpire. What you believe is what you will achieve.

A.P.J. Abdul Kalam

Acknowledgments

Undertaking this PhD has been a truly life-changing experience for me and it would not have been possible without the support and guidance of many individuals. I would like to extend my sincere thanks to all of them.

First and foremost, I would like to express my sincere gratitude to my thesis director, Prof. Jean-Luc HARION, who introduced me to this exciting and challenging field of topology optimization applied to thermal systems which is nicely shaping up as a highly promising topic for future industrial applications. I would like to thank him for his valuable guidance, scientific inputs and above all the trust he placed in me. Specifically, I thank him for his key inputs for the design of the experimental test bench and its various components which were very crucial for the success of one of the first kind of such experiments in the field of topology optimization applied to heat conduction problems. I am highly grateful to him for his continuous support and consistent motivational encouragement during these last three years.

I would like to express my special appreciation and thanks to my thesis guide, Dr. Talib DBOUK, for his continuous supervision and involvement during each and every stage of my PhD research. I thank him for his scientific advice, knowledge he shared and many long insightful discussions we had during several important stages of my PhD. He is my primary resource for getting all my scientific and numerical doubts clarified in a quick and efficient manner. Furthermore, his immense knowledge of CFD, OpenFOAM® and Linux operating systems really helped me during the implementation and debugging stages of the topology optimization numerical solver. I could not have imagined having a better advisor and mentor for my PhD research.

I would like to thank both Prof. Jean-Luc HARION and Dr. Talib DBOUK for giving me several opportunities to present my research work in various national and international conferences, in the process allowing me to grow as a more complete and confident scientific researcher. Their advice on both research as well as on my career have been invaluable.

My sincere thanks goes to the jury members of the thesis defence committee: Prof. Jean-Marie BUCHLIN, Prof. Julien REVEILLON, Dr. Chérifa ABID, Dr. Lilla KAPA KOLOSZAR and Dr. Rainier HREIZ for their encouragement, insightful comments, and interesting queries.

I am also hugely appreciative and thankful to Dr. Dmytro VASIUKOV from the Department of Polymers and Composites Technology and Mechanical Engineering at IMT Lille Douai, for his useful scientific discussions and his continuous efforts and guidance for selecting and preparing the appropriate polymer material for the experimental investigations.

Furthermore, I would also like to thank the complete staff of Energy Engineering Department at IMT Lille Douai, in particular, Nadine LEVEQUE and Valérie DRUELLE for guiding me through various administrative procedures and Engr. Chrystèle EVRARD, who provided me with all the required equipment and the necessary materials to successfully conduct my experiments.

My thanks and appreciations also goes to my friends Bineet MEHRA, Sanjeev SHARMA, Remi GAUTIER, Souria HAMIDOUCHE, Hassan KARKABA, Joseph JABBOUR and Hatim BELKHOU for the great working environment and for all the fun we have had in the last three years. Special mention goes to Bineet MEHRA for helping me with MATLAB post-processing scripts apart from the endless fun conversations we had during the last three years.

Last but not the least, I would like to thank my family: my parents Vijaya and Muthukrishnan Saila SUBRAMANIAM, my sister Lakshmi, my nephew Prithvi and my loving wife Sonam for their unconditional support and encouragement during this work. They are the most important people in my world and I dedicate this thesis to them.

Contents

List of Figures

Nomenclature

Roman Symbols

$\boldsymbol{n}$	Normal vector	$-$
$\boldsymbol{u}$	Velocity vector	$m \cdot s^{-1}$
$\boldsymbol{x_j}$	Design variable vector	$-$
$\dot{q}$	Volumetric heat generation rate	$W \cdot m^{-3}$
$\tilde{T}$	Normalized temperature	$-$
$\tilde{u}$	Normalized velocity	$-$
$\tilde{x},\ \tilde{y}$	Normalized system of coordinates	$-$
A	Length of the domain	m
a	Base cell size	m
C	Size of the heat sink	m
C_p	Specific heat capacity	$J \cdot kg^{-1} \cdot K^{-1}$
D	Thermal diffusivity	$m^2 \cdot s^{-1}$
d	Hydraulic diameter	m
E	Surface emissive power	$W \cdot m^{-2}$
e	Thickness	m
F	Aggregated objective function	$-$
f_0	General objective function	$-$
f_d	Friction factor	$-$
h	Heat transfer coefficient	$W \cdot m^2 \cdot K^{-1}$
J_f	Dissipated fluid power	W
J_{th}	Recoverable thermal power	W
K	Thermal conductivity	$W \cdot m^{-1} \cdot K^{-1}$
k	Penalty parameter	$-$
L	Lagrange function	$-$
l	Length of the pipe	m
L_x	Maximum dimension in x-direction	m

L_y	Maximum dimension in y-direction	m
m	Mass flow rate	$kg \cdot s^{-1}$
$nCells$	Number of square elements	$-$
OS	Object signal	$digital\ level\ (DL)$
P	Pressure	Pa
p	penalization factor	$-$
q	Surface heat flux	$W \cdot m^{-2}$
r_{min}	Filter radius	m
T	Temperature	K
V	Volume of the domain	m^3
$x,\ y,\ z$	System of coordinates with dimension	m

Greek Symbols

α	Pseudo inverse permeability	$-$
$\Delta x,\ \Delta y$	Mesh size	mm
ϵ	Emissivity	$-$
η	Design variable	$-$
Γ	Domain boundary	$-$
γ	Ratio of thermal diffusivity	$-$
λ	Lagrange multiplier	$-$
ν	Kinematic viscosity	$m^2 \cdot s^{-1}$
Ω	Design domain	$-$
ω	Scalar-valued weight factor	$-$
ϕ_{max}	Maximum volume fraction	$\%$
ρ	Density	$kg \cdot m^{-3}$
σ	Stefan-Boltzmann constant	$W \cdot m^{-2} \cdot K^{-4}$
θ	Field of view	$^\circ(deg)$
ε	Convergence criterion	$-$

Abbreviations

Da	Darcy number
Re	Reynolds number

BC	Boundary condition
BEM	Boundary element method
BESO	Bi-directional evolutionary structural optimization
CAD	Computer-aided design
CAE	Computer-aided engineering
CFD	Computational fluid dynamics
CHT	Conjugate heat transfer
CPU	Central processing unit
DOF	Degree of freedom
ESO	Evolutionary structural optimization
FDM	Finite difference method
FEM	Finite element method
FVM	Finite volume method
GA	Genetic algorithm
GCMMA	Globally convergent method of moving asymptotes
GPU	Graphics processing unit
IC	Integrated circuit
ICE	Internal combustion engine
KKT	Karush-Kuhn-Tucker
LBM	Lattice Boltzmann methods
LES	Large eddy simulation
LHTES	Latent heat thermal energy storage
LP	Linear programming
LSM	Level-Set method
MBB	Messerschmitt-Bölkow-Blohm
MMA	Method of moving asymptotes
MOO	Multi-objective optimization
N-S	Navier-Stokes
NLP	Non-linear programming
NUC	Non-uniformity correction
OCM	Optimality criteria method
OpenFOAM	Open source Field Operation And Manipulation
PCB	Printed circuit board

PSO	Particle swarm optimization
PSPG	Pressure-stabilizing/Pedrov–Galerkin
RAMP	Rational approximation of material properties
RANS	Reynolds averaged Navier-Stokes
SA	Simulated annealing
SIMP	Solid isotropic material with penalization
SQP	Sequential quadratic programming
SUPG	Streamline-upwind/Pedrov–Galerkin
TO	Topology optimization
VP	Volume-to-Point

Chapter 1

Introduction

Thermal systems are components of a large part of industrial and household applications. They appear in automobile engines, motors, modern electronic equipments, refrigeration and air conditioning units, household appliances and several other devices which are increasingly being designed to be more compact, light-weight and power efficient. Meanwhile, rapid product design cycles are becoming more of an industrial standard than a demand. As a consequence, designing efficient thermal systems is a very crucial step for developing new products. The need to develop optimization methodologies in order to design efficient thermal systems is currently drawing the attention of a large number of industrial and university researchers. Sizing, shape and topology optimization methods have a great potential to advance cooling structure design. The rapid growth of computational power and Computer-Aided-Engineering (CAE) software makes it possible to model complex geometries and accurately take into account physical processes and material behaviour with reasonable computational efforts. Still, the development procedure of thermal components depends predominantly on the traditional trial-and-error method, which is very time consuming and requires enormous experimental data. Moreover, the trial and error method may become problematic because the outcome depends mainly on the expertise of the designer, and there is no guarantee of design improvement during the design process. Hence, there is a need to develop automated and computerized design optimization approaches, such as sizing, shape and topology optimization, which automatically determine a design change and furthermore guarantee the improvement of the structure design. These automated optimization processes speed up the design process and reduce development cost.

Of the computer-aided optimization methods that exists in literature, namely topology, size and shape, topology optimization can be seen as the most promising automated design procedure because of its ability to produce complex non-intuitive optimal designs which could not have been guessed beforehand [18]. It has been successfully applied to many structural design optimization problems and is recently finding its application in several other domains like aerospace, electrical, energy systems, telecommunications, etc. Moreover, with the rise of modern fabrication technologies like rapid prototyping and 3D printing, topology optimization has major scope for future industrial developments for real world applications.

1.1 Thermal system design optimization

Thermal systems are important features in automobile, power, electronics, chemical processing and other industries which involve energy transfer and fluid flows. These thermal systems are comprised of some specific components like pumps, compressors, heat exchangers, ducts and similar related devices. When a thermal system meets all the specifications and performs the required function during the design process, it is reffered as an efficient system that can be fabricated [19]. However, due to ever increasing global completion and need of high-performance thermal systems, it is no longer sufficient to have an efficient system, rather it has become indispensable to optimize the existing systems in order to find the best or the "optimal" design in terms of some predefined criteria out of the several available or previously known designs. As an example, efficient underhood thermal management in an automobile requires the cooling ducts to evacuate enough heat to allow proper

functioning of the internal combustion engine (ICE) and uniformly distribute the heat. Inefficient cooling duct designs may result in considerable overheating of engine compartment which might eventually lead to system failure from engine bay all the way down to the exhaust line. This requires the need of optimization methodologies for cooling ducts with an objective to evacuate maximum heat from the system.

Over the years, scientists and engineers have been trying to optimize thermal components using different computational optimization design techniques that can be broadly classified as follows:

- ***Trial and error optimization***: This approach optimizes an already known design by intuitively changing the design parameters on the basis of a trial and error procedure. This approach requires high-level of technical expertise in addition to significant amount of time to complete the optimization process, on the other hand, the final design obtained has no guarantee to be an optimum.
- ***Sizing and shape optimization***: This approach optimizes an existing design by modifying its shape or size on the basis of some predefined objectives and constraints. For example, several authors used size optimization methods to optimize pin-fin heat sink design to achieve higher thermal performance [1,2,20]. Figure 1.1 presents the optimal heat sink design obtained through size and shape optimization obtained by Yang *et al.* [1,2]. Likewise, shape optimization methods were used, as example to optimize dimple shape in a cooling channel for heat transfer enhancement in laminar and turbulent flows [21, 22].
- ***Topology optimization***: This approach works by modifying the structural topology during the optimization process in order to achieve an optimal design based on predefined objective and constraints. The main difference in this approach as compared to earlier ones is that the final designs do not depend on the initial configuration. Fig. 1.2 compares the topology optimization method with the size and shape optimization methods for cooling of a CPU by using a heat sink.

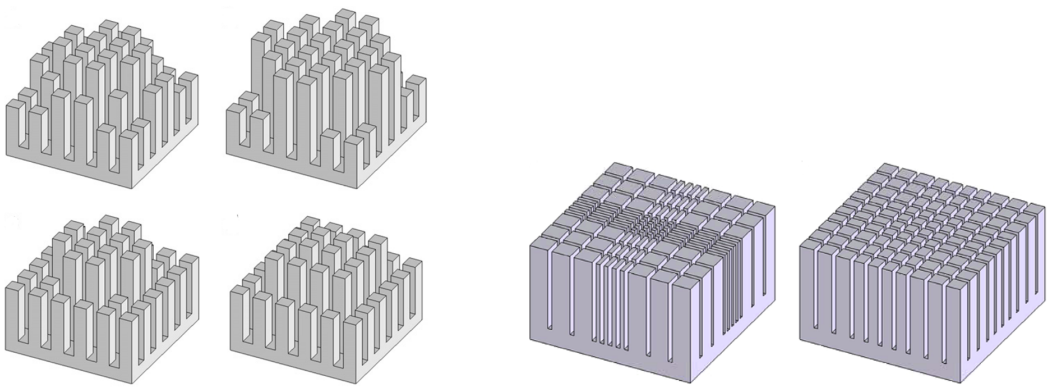

a) Size Optimization **b) Shape Optimization**

Figure 1.1 – Schematic representation of optimal designs for pin fin heat sink obtained by: a) Size optimization [1] and b) Shape optimization [2].

The automated design optimization techniques like size, shape and topology optimization are more efficient compared to the traditional trial and error manual optimization approach in terms of time required to complete the optimization process. Additionally, an improvement over the initial design is mathematically guaranteed. Of the automated optimization techniques, size and shape optimization approach, although comparatively easy to implement, substantially decreases the flexibility of the design as these are characterized by only few parameters. As a result, both these approaches are restricted to a limited number of possible design outcomes as a virtue of a priori assumptions

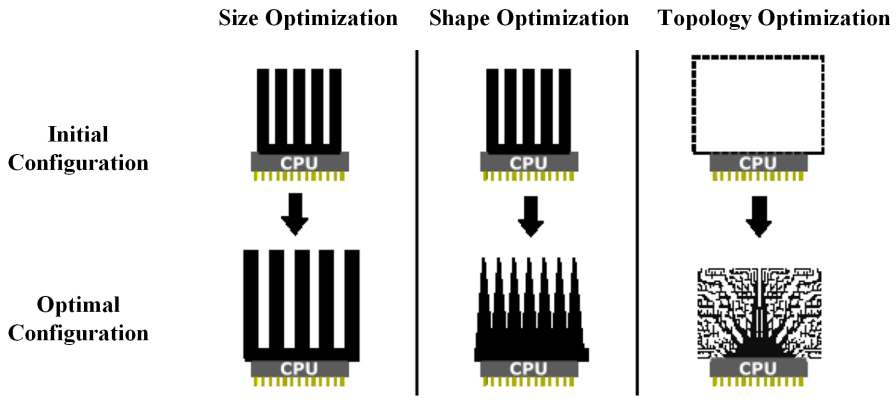

Figure 1.2 – Three different approaches of computational optimization applied to a CPU heat sink.

made about the design. Another major drawback of size and shape optimization approach is their inability to create new holes in the design domain which sometimes might play a crucial role in thermal system design optimization for some specific applications [23, 24]. On the other hand, the number of degree of freedom (DOF) associated with a topology optimization problem is substantially large as compared to its size/shape optimization counterpart. Consequently, topology optimization has the ability to produce complex and non-intuitive optimal designs due to its independence on the initial design. Today, with modern industrial manufacturing processes like additive manufacturing and 3D printing, it has become possible to fabricate even the most complex geometries obtained through topology optimization. This has opened a new era for applications of topology optimization for thermal system design optimization.

1.2 Topology Optimization

Topology optimization (TO) addresses the basic engineering problem of placing the materials within a given design domain that obeys a predefined objective function. Mathematically, the main purpose of topology optimization lies in minimizing or maximizing some objective function while taking into account one or more constraints. Initially introduced for structural mechanics by Bendsøe and Kikuchi in 1988 [25], topology optimization now finds its application to a wider range of physical problems including acoutsics [26], electromagnetics [27, 28], fluid dynamics [9, 29, 30] and heat transfer [5, 7, 15, 31, 32]. For example, in heat transfer problems, TO can be used to find the optimal material distribution to minimize the overall average temperature in a system. Similarly, in fluid dynamics, TO is often used with an objective to minimize the pressure drop across a fluid channel.

A general topology optimization problem can be defined mathematically as follows:

Minimize/Maximize:

$$f_0(\boldsymbol{x}) \tag{1.1a}$$

subject to:

$$f_i(\boldsymbol{x}) \leq 0, i = 1, 2, ..., m \tag{1.1b}$$
$$R_h(\boldsymbol{x}) = 0, h = 1, 2, ..., e \tag{1.1c}$$
$$\boldsymbol{x} \in \mathbf{X}, \tag{1.1d}$$

where $\boldsymbol{x} = (x_1, ...x_n)^T \in R^n$ are the so called design variables with $\mathbf{X} = \{\boldsymbol{x} \in R^n \mid x_j^{min} \leq x_j \leq (x_j)^{max}, j = 1, ..., n\}$ and $f_0, f_1, f_2, .., f_m$ are provided continuously differentiable (at least twice) real valued function on $\mathbf{X}$. x_j^{min} and x_j^{max} belongs to R such that $x_j^{min} \leq x_j^{max}$ $\forall j$. The design variable vector $\boldsymbol{x}$ is bounded numerically such that its final value represents only one value i.e either

x_j^{min} or x_j^{max}. This represents the interpolation of two materials in the design domain which is obtained by a specific penalization technique.

The constraints $R_1, R_2, .., R_e$ represents the state equations for the physical problem being solved. For example, in TO problem applied to fluid flows the constraint will be the mass and momentum conservation equations.
For solving a system of equations represented by equation 1.1, the following basic steps are involved in any TO process :

- *Numerical Modelling*: This step involves specifying a computational domain with a generated mesh, discretization of the governing equations and solving for the field variables (i.e., the velocity field or the temperature distribution).
- *Sensitivity analysis*: This second step involves calculating the objective function f_0 in equation 1.1 and its derivative with respect to the design variable $\boldsymbol{x}$. The process of calculation of these derivatives is known as the sensitivity analysis. The sensitivities determine the direction of descent for the update of the density variables in each element.
- *Optimization algorithm*: Using the sensitivity analysis, TO algorithms are used to update the design variables. In this regard, various updating schemes exist in literature for example, the popular MMA (Method of Moving Asymptotes) algorithm introduced by Svanberg [33].
- *Material Distribution*: Once the optimal direction has been found, a material scheme is used to determine how the material distribution will take place within the design domain. Various material interpolation schemes exist in the literature with their own advantages and drawbacks [34].
- *Filtering*: In conventional topology optimization method, several numerical instabilities may be encountered. One such problem is formation of alternating solid and void elements, sometimes resembling a checkerboard. To overcome such difficulties, some filtering techniques are used in order to obtain a better optimized final structure [35].
- *Post-processing*: Before one begins the fabrication of the final topology optimized structure, the results obtained from TO solver needs to be post-processed in order to display the two dimensional or the three-dimensional solution better on paper.

The above mentioned procedure will be dealt in detail in the forthcoming sections emphasizing mostly on methods and techniques that shall be used in the present thesis.

1.2.1 Topology optimization approaches

Originally based on homogenization theory [25], topology optimization methods have now evolved in different directions such as density approach [36] [37] [38]; level-set method [39] [40]; topological derivatives [41]; phase field [42]; and evolutionary approaches [43]. All these techniques differs on the basis of methodology used to represent the optimal material distribution in a given design domain. The fundamentals of these approaches will be briefly summarized in the following subsections.

1.2.1.1 The density approach

In TO, the aim is to find the optimal distribution of a given material within a design domain in order to achieve some predefined objective. In this purpose, a local design variable field is introduced and used as a characteristic function to represent the optimal material distribution within the design domain in density based TO. The optimization problem in equation 1.1 is essentially solved by discretizing the design domain into a large number of finite volumes or elements and describing the design variable vector $\boldsymbol{x}$ for each cell or element. Thus, for a single material TO problem, Eqn. 1.1d in the design problem 1.1 can be rewritten as follows:

$$x_j = 0 \ or \ 1, \quad j = 1, 2, ..., N \tag{1.2}$$

The optimum solution is then represented in terms of discrete values of x_j (0 or 1) where the value 0 represents void and 1 represents the solid material. This can clearly illustrate the optimal distribution of the material in the domain. However, it is numerically very difficult to reach direct solutions using directly defined discrete variables formulation represented by equation 1.2. This problem can be solved by using a popular material interpolation technique from literature known as the Solid Isotropic Material with Penalization (SIMP) [18]. The SIMP technique replaces the integer variables with continuous ones, and then introduces some sort of penalty that steers the solution towards discrete 0-1 values. In the SIMP approach the relation between design variable and material property is given by a power law as follows:

$$k(x_j) = x_j^p \; k_0 \tag{1.3}$$

where p is the penalization factor such that $p \geq 1$ and k_0 is the material property of the solid material (for example thermal conductivity). The main motivation behind using a SIMP type density approach is to facilitate a continuous interpolation between the solid material and void with a penalization of intermediate values between 0 and 1.

Chosing a right value of p is always important as choosing p value too low causes too much grey-scale (i.e., intermediate x_j values in between 0 or 1). On the other hand, choosing a very high value of p may result in a rapid convergence to local minima/maxima [44]. Note that this penalization effect works only in presence of a volume constraint or some other constraint that directly or indirectly limits the volume fraction of the solid material to be imposed [34]. Moreover, the correct choice of penalization factor p is non-unique as it depends predominantly on the physical problem under consideration. For example, for fluid flow TO problems where the objective is to minimize the pressure loss across a given channel, the interpolation function needs to be adjusted in order to smoothen the affect of the material distribution on the flow [9]. In the literature, it is always advised to follow a continuation approach starting from $p = 1$ and gradually increasing it during the optimization process until the final design is achieved after convergence [6, 7, 34].

It is quite evident from the literature that density approach is one of the most widely used material representation technique for topology optimization problems [45]. However, this technique does not help the ill-posedness of the TO problem i.e., it still remains heavily mesh dependent. One explanation can be that by using these type of non-optimal materials (the material distribution obtained from SIMP like interpolation schemes), the macroscopic approach tries to mimic an optimal material but the fact is that the material in continuum mechanics is always defined on a lower length scale that can never be reached by any-sort of mesh refinement. One solution is to mitigate the mesh-dependency using "density filters" which will be discussed later.

1.2.1.2 The level set approach

Level-Set Methods (LSM) define the interfaces between different materials implicitly by iso-contours of a Level-set Function [39, 40]. This function implicitly provides a crisp description of boundaries. Here, the boundary of the design domain is defined by the zero-level contour of the level set function $\phi(\mathbf{x})$ and the structure is defined by domain where the level-set function takes positive values.

For a material-void structural optimization problem, given a level set function $\phi(\mathbf{x})$, the level-set method defines the material domain Ω, the void domain D$\backslash\Omega$ and the material interface as Γ inside the design domain as follows [46]:

$$\begin{aligned} \phi(\mathbf{x}) &> c \quad \forall \quad \mathbf{x} \in \Omega \; (material) \\ \phi(\mathbf{x}) &= c \quad \forall \quad \mathbf{x} \in \Gamma \; (interface) \\ \phi(\mathbf{x}) &< c \quad \forall \quad \mathbf{x} \in (D \setminus \Omega) \; (void), \end{aligned} \tag{1.4}$$

where c is a constant (usually $c = 0$) and $\mathbf{x}$ is a point in design domain. Fig. 1.3 represents an example of a level set function $\phi(\mathbf{x})$ and corresponding material domain Ω before and after a design update for a 2D design. The main advantage of using a level set method over density approach is

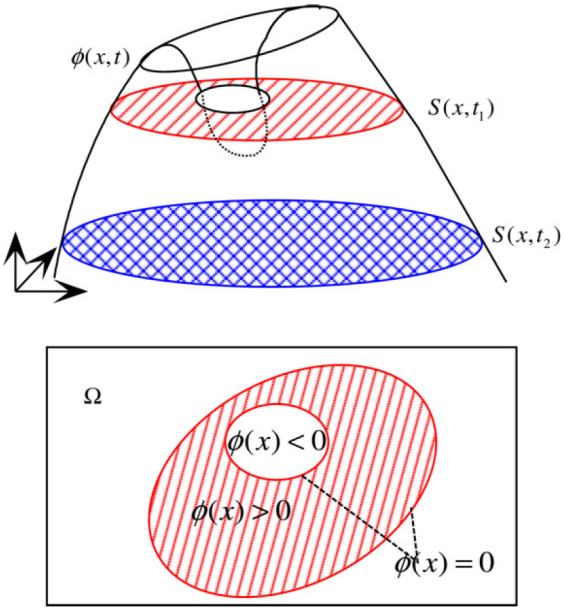

Figure 1.3 – Diagram of a level set function and its implicit boundary at some time [3].

that the results obtained from a level set based TO methods do not involve mesh-dependent spatial oscillations of the interface (i.e, the staircasing phenomenon observed with SIMP). On the contrary, one major drawback of the level set method is the limitation on the geometries that only can evolve from existing boundaries. Present level-set methods in literature are belived to be highly dependent on the initial design and the position of the level-set function [47]. This drawback questions the acceptability of optimal solutions obtained from LSM. Another limitation is the inability of the level set methods to generate new holes at points surrounded by solid materials in 2D problems [34], however some recent developments have been made to mitigate these problem [48].

1.2.1.3 The topological derivatives

Topological derivatives, also named the "bubble method" by Eschenauer *et al.* [49] , consists of introducing holes at a specific locations in the design domain. These holes are taken as a starting point for the generation of new holes. Topological derivatives determine where to place new holes and either modify the shape of the boundaries of existing holes [49], or update the presence of holes element-wise [50].

1.2.1.4 Discrete or 'Hard-kill' approach

Discrete design variable approach forces the design variable to be either 0 or 1 which means it does not allow for intermediate grey zones as observed in continuous design variable approach like SIMP. These methods progressively remove or add material from the design domain explicitily for each iteration step based on some specific optimization criterion evaluated in each element in order to reach the desired optimum. As the original TO problem in Eqn. 1.1 uses discrete design variable i.e. 0 (void) or 1 (solid material) it seems obvious to try solving it utilizing a discrete optimization approach. However, when formulated directly in discrete design variable, the TO problem becomes numerically very difficult to solve and till now a very limited number of problems have been solved in literature for global optimality [51]. Nevertheless, there still exist dedicated discrete approaches in literature like the evolutionary structural optimization (ESO) [43], bi-directional evolutionary structural optimization (BESO) [52] and cellular automaton [53].

The concept of evolutionary structural optimization (ESO) was introduced by Xie and Steven [43] back in 1993 as a simple hard-kill strategy to remove elements with lowest strain energy density. The basic idea behind ESO is to gradually remove inefficient material from the structure and thus

iteratively update the design to more optimal topology.

The idea has now been extended to bi-directional evolutionary structural optimization scheme (BESO) [52] where material can also be reintroduced in the system if considered favourable. Although initially the concept being solely based on intuition, it now uses adjoint gradient analysis and filtering techniques to stabilize algorithms and results, similar to the ones used in the density approach [54].

The process doesn't always guarantee the best optimal solution but still provides useful ways to explore new shapes in the conceptual phase of design. The common drawback of all discrete approaches is that they become very sensitive to parameter variations and eventually might end up in non-convergent and oscillating solutions. According to Sigmund and Maute [34], it is very easy to suggest schemes that could perform discrete updates, but the difficulty lies in finding parameters and update strategies that make them converge to stable and good design. In specific, ESO/BESO approaches are criticized for flaws pertaining to design density updates [55] citing some particular examples like compliant mechanism design problems with thin hinges that makes the discrete approach fail.

1.2.2 Optimization Algorithms

Optimization algorithms are iterative in nature. Starting with an initial guess for the value of the design variable in each cell the algorithm tends to generate a sequence of improved estimates until a final solution is reached based on some convergence criterion. Different optimization algorithms are distinguished on the bases of their approach used to proceed from one iteration to another. Most of them uses the objective function values, constraints values and probably the gradients and/or hessians of the objective function.

For many optimization problems, there is a possibility of finding more than one optimum design, commonly referred as the local optimum. A local optimum for a minimization problem is a point at which the objective function value is less than at all other feasible points in its neighborhood. Local optimization algorithms tends to find a local optimum which may or may not be a global one. These algorithms usually depend on the gradients of the objective function and constraints to search for the optimal vector. As a result, some stringent requirements are imposed on the problem input like the chosen objective function must be real valued and atleast twicely continuous and differentiable. Additionally, local optimization algorithms are also sensitive to the initial guess [56]. Global optimal solutions are much desired in some applications, but they are generally very difficult to identify and locate. Global optimization algorithms compartively posses much less restrictions on the problem input. It is worth mentioning that although these algorithms have a much better chance of finding a global or near-global optimum solution than the local algorithms, no algorithm can guarantee convergence to a global optimum in a general sense [57].

The general constrained TO problem of equation 1.1 requires some specific numerical algorithms to be solved in order to find an optimum. The complexity of any optimization problem depends on numerous factors like the number of design variables, degree of convexity/non-convexity and linearity/non-linearity of the equations, the smoothness of the functions (nondifferentiable or differentiable) and the numerical difficulties associated with them. Thus, choosing an efficient optimization algorithm is a very important step in TO process to ensure a stable convergence to an optimum solution. Researchers over the years have developed various optimization algorithms for the solution of different types of optimization problems ranging from some classical methods of differential calculus to the most advanced linear (LP) and non-linear programming methods (NLP) [58]. Although optimization algorithms in general can be classified in many different ways, but for TO of heat transfer and fluid flow systems, the majority of algorithms can be broadly classified as gradient-based or gradient-free algorithms.

- **Gradient-based algorithms:** These algorithms use the gradient of the objective function to identify the most favorable direction for finding the optimum solution. They are widely used in TO of thermo-fluid systems because of their ability to handle problems with large number of design variables, and they require minimum problem specific parameter tuning. However, there are few drawbacks associated with these algorithms such as their tendency to converge to a

local optimum. These are complex algorithms that are somewhat difficult to implement and they have difficulty in handling discrete optimization problems [59]. The most commonly used algorithms for design optimization are the gradient-based steepest-descent algorithm, conjugate gradient algorithm, the hessian-based Newton's method and Quasi-Newton method [60].

For a general optimization problem, a gradient-based algorithm updates the design variable at each iteration k as:

$$\boldsymbol{x}_{k+1} = \boldsymbol{x}_k + \underbrace{\alpha_k p_k}_{\Delta \boldsymbol{x}_k} \tag{1.5}$$

where p_k is the search direction for the iteration k, and α_k is the optimum step size. Most gradient-based algorithms uses a two-step approach to find the optimum where the first step is to compute a search direction p_k using gradient information. The second step is to proceed in this direction until no further improvement of the objective function can be made. The second step is referred as the line search which provides the optimum step size α_k. The two-step approach of a gradient based optimization algorithm is illustrated in Fig. 1.4. The different gradient-based algorithms that exist in literature are distinguished based on the technique used to determine the search direction (the first step of the two-step approach).

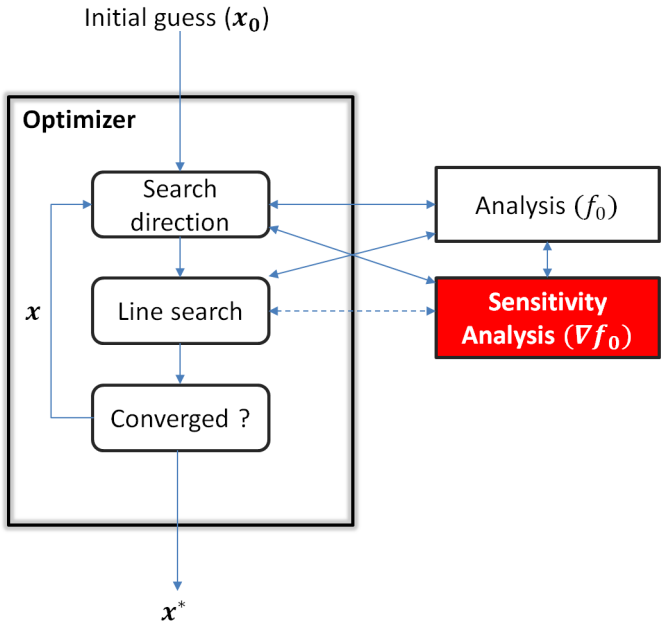

Figure 1.4 – General gradient-based optimization algorithm methodology: "Analysis" is the computation of the objective function, and "Sentivity Analysis" is the process of computation of gradient of the objective function.

Once the gradient information is obtained, the Karush-Kunh-Tucker (KKT) conditions are necessary conditions to identify if a constrained local optima has been reached. They can be explained as the following:

1. The optimum solution point $\boldsymbol{x}^\star$ must be feasible.
2. The gradient of the Lagrangian must vanish at the optimum solution point

$$\nabla f_0(\boldsymbol{x}^\star) + \sum_{i=1}^{m} \lambda_i \nabla f_i(\boldsymbol{x}^\star) + \sum_{h=1}^{e} \lambda_{m+h} \nabla R_h(\boldsymbol{x}^\star) = 0 \tag{1.6}$$

   where the Lagrange multiplier $\lambda_i \geq 0$ and λ_{m+h} are not restricted in sign.
3. For each inequality constraint $\lambda_i f_i(\mathbf{X}) = 0$, where $i = 1, m$.

The KKT conditions are helpful to identify a local optimum, however cannot ensure if the identified local optimum is also a global one [60].

As most topology optimization problems for thermal systems require large number of design variables, a specific gradient based algorithm called the Method of Moving Asymptotes (MMA), initially introduced by Svanberg [33] is frequently used in the literature [5, 13–15, 61] because of its robustness and its ability to handle multiple constraints.

- **Gradient-free algorithms:** These algorithms do not need any gradient information and usually employs a set of design points referred as a population to search for a optimum solution. They either mimic some phenomena observed in nature or use heuristics. As compared to gradient-based algorithms, these are easy to implement and are well suited for discrete optimization problems. Additionally, many of the gradient-free algorithms are formulated to work as global optimizers and hence are able to obtain multiple local optima in search of the global optimum. The main disadvantages of these type of algorithms include high computational cost, restricted problem size, problem specific parameter tuning, and their poor constraint handling ability [57]. The most commonly used gradient-free algorithms in engineering optimization problems are Genetic Algorithm (GA) [62], Simulate Annealing (SA) [63], Particle Swarm Optimization (PSO) [64] and evolutionary programming [65].

  Genetic Algorithms for optimization are based on process of natural evolution of organisms. It starts by creating a random initial population and consists of the following three main features:

  - *Selection:* Survival of the fittest.
  - *Crossover:* Process of reproduction where genetic traits are passed on.
  - *Mutation:* Variation.

  As compared to gradient-based algorithms, where a single solution point is updated from one iteration to another, a whole set of solution points (population) is iterated towards the optimum at the same time. By doing so, it allows for exploration of multiple local optima simultaneously, increasing the chances of finding a global optimum. In the field of TO of heat transfer system, Xianghua *et al.* [66] used a combinatorial optimization algorithm composed of SA and GA for topology optimization of 2D steady volume-to-point heat conduction problems. Yoshimura *et al.* [67] used GA associated with some specific surrogate models for TO of fluid from problems coupled with heat transfer to search for global optimum solutions.

1.2.3 Numerical Instabilities:

Topology optimization methods have evolved to maturity in the past decade, specially in the field of structural optimization. However, there still exist specific important numerical problems that sometimes hinders the use of TO for real world applications. These numerical problems can be broadly classified into three major categories: Checkerboards, mesh dependence and local minima/maxima. These numerical problems, their causes and prevention are discussed in detail by Sigmund and Petersson [35] and briefly summarized below:

1.2.3.1 Checkerboards

Checkerboards refer to the problem of formation of alternating solid and void elements, sometimes resembling a checkerboard. Earlier believed to be certain kind of micro-structures, but later proved to be an outcome of bad numerical modelling by Diaz and Sigmund [68]. Fig. 1.5 shows the checkerboard formations in optimal structure obtained in a classical "Volume-to-Point"(VP) heat conduction TO problem. Several methods have been proposed by different authors to help with the appearance of checkerboard patterns.

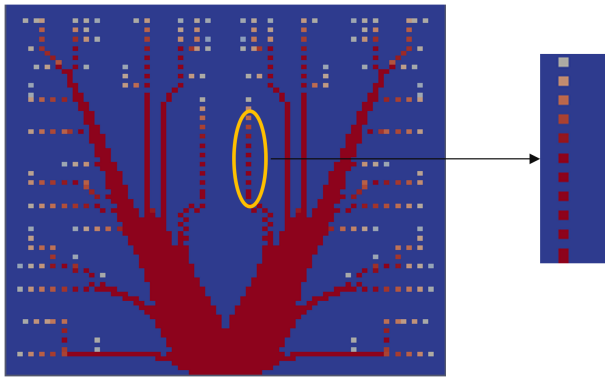

Figure 1.5 – Checkerboards observed in optimal structure obtained for a Volume-to-Point heat conduction topology optimization problem.

- *Smoothing:* It is a process of removing checkerboards through image processing. However, the underlying numerical problem behind the checkerboards is completely ignored in this method, and it focuses solely on image processing algorithm. This method is not advised very often.

- *Higher-order finite elements:* Many authors suggest the use of higher-order elements to avoid the formation of checkerboards. Homogenization approach requires eight or nine noded finite elements to prevent chekerboards whereas the SIMP technique requires the penalizatipn factor p to be small enough in addition to eight or nine noded elements to avoid checkerboards [68]. However, it should be noted that higher order elements results in significant increase in the computational time.

- *Patches:* To prevent checkerboards without losing on cpu-time Bendsøe *et al.* [69] proposed the use of patch technique. This technique introduces a kind of super-element to the finite element formulation and thus dampens the appearance of checkerboards. The problem is: it does not remove them entirely in topology optimization problems.

- *Filter:* This method is based on filtering techniques from image processing, and was introduced by Sigmund in 1994 [70]. Checkerboards are prevented by modifying either the densities or the sensitivities used in each iteration of the optimization algorithm. The filter makes the density or the sensitivity of a given element dependent on the weighted-average over the element and its direct neighbours. This technique has shown to be very efficient in removing checkerboards.

1.2.3.2 Mesh-dependence

Mesh-dependence refers to the problem of obtaining qualitatively different solutions for different grid-size or discretization schemes. Conceptually, mesh-refinement is expected to provide a better numerical modelling of the same optimal configuration with a better description of boundaries, not in a completely different configuration qualitatively. Mathematically, mesh-dependence can be attributed to non-existence or non-uniqueness of the solution. To limit the mesh-dependence the following method of local gradient constraint is used in literature [71].

- *Local constraint on gradient of material density:* This method introduces a constraint on the local density variation. This is written as a point-wise constraint on the gradients of the function x_j (element density). This method was shown to be effective in minimizing many numerical instabilities but proved to be very slow for practical design problem as it adds $2N$ (N is the total number of nodes) extra constraints in the optimization problem.

1.2.3.3 Local Minima

It refers to the problem of obtaining different optimal solutions to the same discritized problem when choosing different algorithmic parameters. For example, choosing different initial conditions, number of elements, geometry of design constraint or a different filtering technique could drastically change the optimal structure. The issue of obtaining local minima can be attributed partially to the flatness of objective function, but more importantly, due to the choice of numerical optimization procedure adopted to solve the problem. For non-convex functions, algorithms in general, tends to converge to a nearby stationary point, which may or may not be the global solution. To obtain a near global solutions, different type of continuation were proposed by different authors [72, 73].

- *Continuation methods:* The concept behind continuation methods is to slowly change the optimization problem from an artificial convex problem to the original non-convex design problem in a certain number of steps. A gradient-based optimization algorithm is then to be used in each step until convergence is achieved. Allaire and Francfort [72] proposed a continuation method where the structure is first optimized allowing grey-zones or perforated regions and after convergence, penalization scheme is cautiously introduces in the system to produce a $0/1$ design. Guedes and Taylor [73] also proposed a continuation method where the costs of intermediate density elements are slowly increased by adjusting a weighing function ω in the volume constraint as follows :

$$\int \omega x_j \leq \ V \tag{1.7}$$

Although such continuation methods were seen in literature, but still the concept of continuation in TO are not very consistent and require more research in this direction to obtain general stable methods in combination with other global optimization methods.

1.3 Heat transfer

Thermal energy is related to the temperature of matter. For a given material and mass, the higher the temperature, the greater its thermal energy. Heat transfer is a study of the exchange of thermal energy through a body or between bodies which occurs when there is a temperature difference. When two bodies are at different temperatures, thermal energy transfers from the one with higher temperature to the one with lower temperature. Heat always transfers from hot to cold [74].

Primarily, there are three modes of heat transfer: conduction, convection, and radiation. Any energy exchange between bodies occurs through one of these modes or a combination of them. Conduction is the transfer of heat through solids or stationery fluids. Convection uses the movement of fluids to transfer heat. Radiation does not require a medium for transferring heat; this mode uses the electromagnetic radiation emitted by an object for exchanging heat.

- **Conduction**: The basic microscopic mechanism of conduction is the motion of molecules and electrons. It can occur in solids, liquids and gases. In non-metallic solids the transfer of heat energy is due mainly to lattice vibrations. In metallic solids we have both lattice vibrations and random motions of free electrons. As a consequence, metals are more conductive than non-metals. In gases, we have mainly random motions of molecules. In liquids we have partly random molecular motions and some sort of vibration of the liquid lattice structure. It is possible to quantify heat transfer process in terms of appropriate rate equations. These equations can be used to compute the amount of energy being transferred per unit time. For heat conduction processes, the rate equation is known as the Fourier's law which states that the heat flux q $[Wm^{-2}]$, resulting from thermal conduction is proportional to the magnitude

of the temperature gradient and opposite to it in sign. Mathematically, it can be expressed for a one-dimensional plane as follows:

$$q = -K\frac{dT}{dx} \tag{1.8}$$

The constant, K $[Wm^{-1}K^{-1}]$, is called the thermal conductivity which is characteristic of the material.

- **Convection**: Convection is associated with the transport of a mass of liquid or gas. It can be forced when assisted by a pump or fan, or free (also called natural convection) when the motion of a fluid occurs due to density differences. If there is an electrical heating element at the corner of a room and air is blown onto the element by a fan, this is forced convection. In the absence of a fan the air surrounding the heating element will get hotter, its density will decrease and the air will move upwards causing natural circulation within the room, as the hot air is replenished by colder air, which gets hot and rises again. Regardless of the particular nature of the convection heat transfer process, the appropriate rate equation for convection processes is give by Newton's law of cooling:

$$q = h(T_{body} - T_{\infty}) \tag{1.9}$$

where q $[Wm^{-2}]$, the convective heat flux, is proportional to the difference between the body and fluid temperature, T_{body} and T_{∞}, respectively. h $[Wm^2K^{-1}]$ is the convective heat transfer coefficient and it depends on conditions in the boundary layer, which are influenced by the surface geometry, the nature of the fluid motion and various fluid thermodynamic and fluid properties [74]. All convection heat transfer analysis ultimately reduces to a study of the means by which this convective heat transfer coefficient can be determined.

- **Radiation**: Radiation involves electromagnetic waves which are emitted by a body as a result of its temperature. The electromagnetic radiation has a broad spectrum from radio waves to x-rays. Between the two extremes a narrow portion of the radiation spectrum is the visible light and a broader one covers the thermal radiation. The earth is heated by sun's radiation. Radiation that is emitted by the surface of an object originated from the thermal energy of matter bounded by the surface, and the rate at which energy is released per unit area $[Wm^{-2}]$ is termed the surface emissive power E. There is an upper limit to this emissive power prescribed by the Stefan-Boltzmann law as follows:

$$E_b = \sigma {T_s}^4 \tag{1.10}$$

where T_s is the absolute temperature $[K]$ of the surface and σ is the Stefan-Boltzmann constant ($\sigma = 5.67 \times 10^{-8}\ Wm^{-2}K^{-4}$. Such a surface is called an ideal radiator or black body [74].

On the other hand, the heat flux emitted by the real surface is less than that of a black body maintained at the same temperature which is given by:

$$E = \epsilon\sigma {T_s}^4 \tag{1.11}$$

where ϵ $(0 \leq \epsilon \leq 1)$ is the radiative property of the surface knows as its emissivity. Emissivity provides a measure of how efficiently a surface emits energy relative to a black body. It is highly dependent on the surface material and the surface finish.

It is possible to carry out relatively accurate calculations of temperature rise, drop or distribution and the energy requirements, by applying the principle of conservation of mass, momentum and energy, and the equations of heat conduction, convection and radiation. For conduction the thermal conductivity of the materials involved must be known. For convection the key step is the determination of the heat transfer coefficients, which are usually available as correlations involving the Reynolds number of the flow. Radiation calculations require the material emissivities and the relative geometrical orientation of the radiating surfaces [75].

1.3.0.1 Conjugate heat transfer

The term conjugate heat transfer is used to describe processes which involve variations of temperature within solids and fluids, due to the thermal interaction between the solids and the fluids. A typical example is the heating or cooling of a solid object by the flow of air in which it is immersed [76].

In the past, the flow field and the solid thermal field were solved separately and no coupling between the two solutions occurred. The solid temperature was usually calculated and then applied as a fixed boundary condition on the fluid domain. This numerical method had a lack of accuracy and it often provided results which were not in agreement with the real physics. Several safety coefficients were applied to cooling system design. In the last decades, the requirements of coupling the solid heat flux and the fluid thermal flow has become almost mandatory.

In a conjugate heat transfer (CHT) approach, the fluid and solid domains are solved with the same or different method (Finite Element, Finite Volume or Finite Difference Method) however, embedded in the same monolithic solver. In particular the CFD code models both fluid and solid domains, neighbouring the fluid. The solid thermal diffusion is described by the scalar unsteady parabolic partial differential equation, while Navier- Stokes equations describe the fluid flow advection. It is the most flexible and accurate approach. One of the main problems related to a conjugate heat transfer approach is the existence of two different characteristic times for thermal/heat and the fluid flow diffusion/convection (advection). Considering the accuracy requirements, a large amount of time is spent in grid generation and a high number of cells is required for solving the total field. Moreover, many problems related to CHT, such as nano-channels or cooling system of turbine blades are heavy to discretize with a body fitted mesh [77].

With the aim to cope with this problem, some authors [78] have proposed boundary element method (BEM) for solving the thermal conduction inside the solid body. The heat transfer equation is then traduced in a boundary integral equation, which can be solved using the boundary surface discretization available from the convective grid. This method does not require any volumetric mesh inside the solid, but only surface grid is needed for solving Laplace equation. It is an iterative approach falling anyway in the coupled method family because two different solvers are used. It is apparent the lack of accuracy in the solid heat transfer that this method provides.

On the other hand, Rigby *et al.* [79] have been among the pioneers in the conjugate methods family, using the energy flow equation to solve the solid temperature field and forcing fluid flow speed equal to zero in the solid regions. The interface fluid-solid is treated, assuming the temperature field to be known inside the solid, and transferring back this information to the fluid. However, a difference of about 50 % is found in the code prediction with respect to experimental data for some tested configurations. No stability analysis and considerations have been performed at this step. Some other authors [80] have proposed large eddy simulation (LES) with an immersed boundary technique, thus reducing drastically the mesh generation time thanks to the immersed boundary, but requiring a very fine grid. Iaccarino*et al.* [81] proposed a Reynolds averaged Navier-Stokes (RANS) incompressible solver on an immersed boundary technique applied to an electric motor, and a comparison with a body fitted mesh was performed.

1.4 OpenFOAM® (Open source Field Operation And Manipulation)

OpenFOAM® (Open source Field Operation And Manipulation) is a registered C++ toolbox maintained by the OpenFOAM® Foundation. It is mainly a computational fluid dynamics software package and includes a fair amount of pre- and post-processing utilities. Its syntax allows for the creation of custom solvers with relative ease thanks to object-oriented programming and encapsulation. It was first released as open source in 2004 and has in recent years become more widely used in both academia and industry. The relatively simple implementation of custom solvers, and its increasing popularity in industry are the main reasons behind choosing it as the prefferred CFD toolbox in the present thesis. The first implementation of the continuous adjoint formulation of the Navier-Stokes equations in OpenFOAM® was presented in 2008 [82]. Since then, research groups at universities and from industry have published results of adjoint based sensitivity analysis and optimization using OpenFOAM®. This includes optimization of exhaust systems [83, 84], optimization of train head

cars [85], buoyancy-driven flows with heat transfer [86], optimization of engine intake port [87] and mapping of surface sensitivities to morphing control points [88].

1.5 Organization of the PhD thesis

In this thesis, the concepts of topology optimization and heat transfer introduced in section 1.2 and 1.3 are combined using OpenFOAM® software package in the framework of thermal systems focusing on TO of conductive and conjugate heat transfer systems. Globally, this thesis is composed of two major parts:

- **Part 1:** Experimental investigations of topology optimized configuration. For this purpose, infrared thermal measurements are performed on a conductive heat transfer tree-like structure obtained numerically by TO of a 2D Volume-to-Point heat conduction problem. The objective here is to examine experimentally the thermal performance of a topology optimized structure under some specific thermal loads and boundary conditions. The optimized conductive structure under investigation is obtained by density based TO approach which was developed in-house code via OpenFOAM® by coupling the gradient-based Method of Moving Asymptotes (MMA) algorithm to the SIMP bi-material distribution technique. This investigation will question the validity of developed topology optimization numerical tools in really producing efficient cooling/heating real applicable devices.

- **Part 2:** Numerical developments, simulations and investigations on topology optimization of conjugate heat transfer (CHT) systems. For this purpose, a density based bi-objective TO technique is developed with to maximize heat recovery from a fluid/solid domain and minimize pressure drop in the system, simultaneously. The MMA algorithm is chosen as the preferred optimizer based on its performance verification for thermal problems observed during experimental investigations conducted in part 1. For gradient computation, continuous adjoint system of equations and the associated boundary conditions are derived for the multi-objective function under consideration. The developed numerical solver uses the finite volume method discretization for solving the primal and adjoint system of equations inside the OpenFOAM® CFD software package. The objective of this part is to search for physically logical optimal designs for CHT systems that can best manage trade-off between **two conflicting criteria** of heat transfer enhancement and pressure drop reduction. In addition to this, an in-depth investigation of the obtained optimal designs is carried out in terms of convergence study, performance evaluation, local analysis of the results at critical regions and comparison with similar studies in literature in terms of objective function values.

The present thesis consisting of the two above mentioned parts is organized as follows: Chapter 2 presents a detailed state of the art for topology optimization applied to heat transfer and fluid flows. Chapter 3 presents experimental investigations of results obtained from a TO method applied to a 2D heat conduction problem. The complete experimental methodology is presented in detail describing each and every component of the experimental test bench. The appendix A gives the complete details regarding the IR camera setup used for the infrared thermography including the field of view calculations, the camera calibration procedure and the non-uniformity correction (NUC) procedure. Chapter 4 presents a topology optimization method for conjugate heat transfer systems. This chapter describes all the ingredients involved in the bi-objective topology optimization technique for CHT systems including the rigorous derivation of the continuous adjoint system of equations. The developed numerical solver is tested on some specific numerical examples from literature and the obtained optimal designs obtained are analyzed in detail. The appendix B described in detail the FVM discretization implemented in the OpenFOAM® solver, appendix C describes the gradient-based method of moving asymptotes optimization algorithm (MMA) and the density filtering technique used in the present study is described in appendix D. Chapter 5 presents a detailed discussion of some critical numerical and physical issues encountered in density based topology optimization of thermal systems in the context of its validity in real world applications. Finally, at the end, the major

conclusions derived from the work realized during this thesis and some perspectives for future studies in topology optimization of heat transfer and fluid flow systems are presented.

Chapter 2

State of the art: TO applied to heat transfer and fluid flows

Topology optimization applied to structural design has undergone a tremendous development since its introduction by Bendsøe and Kikuchi in 1988. However, Topology optimization applied to heat transfer and fluid flows is still not mature as compared to its structural counterpart. In the last two decades, various TO techniques have been developed in the literature for optimization of thermal systems based on conductive, convective and conjugate heat transfer, however, without enough comparisons between them. This chapter provides a comparative and critical review of topology optimization methods applied to design optimal thermal systems. At the end, a brief summary is presented which highlights the major challenges for topology optimization of thermal system design optimization.

2.1 Topology optimization applied to heat conduction systems

Heat conduction systems are widely used in several industrial applications like automotive cooling and electronic thermal management. There is an increasing demand of compact high performance passive cooling and heat dissipating devices in today's rapidly growing electronics industry. Modern computers, smartphones and tablets are designed to be thin and light without compromising on performance. Integrated Circuit (IC) boards are getting denser and silicon chips are clustered in closer proximity. Moreover, the need for compact and power-efficient electronics has led to minimized use of moving parts like fans and blowers. Consequently, the ability to extract heat form an increasingly restricted space is currently a very critical and challenging issue. Such applications can be modelled by the well known "Volme-to-Point" (VP) heat conduction problems proposed by Bejan [89] where the aim is to seek an optimal distribution of a specified quantity of high conductive material in regions of low conductivity heat generating material. Many researches in the past decade applied TO techniques to optimize this particular type of thermal conduction systems. Various numerical solvers applied to TO of heat conduction systems are present in literature. An indepth review of these solvers applied to heat transfer and fluid flows can be found in [45]. Majority of the studies were limited to 2D steady state applications with the few exceptions of Burger *et al.* [7], Donoso [90] and Dede *et al.* [13, 91].

A general topology optimization problem for steady state heat conduction within a volume V can be stated mathematically as following:

Minimize/Maximize:

$$f_0(\boldsymbol{x}) \tag{2.1a}$$

subject to:

$$\nabla \cdot (K_{eff} \nabla T) + \dot{q}_{eff} = 0 \tag{2.1b}$$

$$\frac{1}{V} \sum_{j=1}^{nCells} x_j \leq \phi_{max} \tag{2.1c}$$

where $f_0(\boldsymbol{x})$ is the objective function to be optimized (minimized or maximized), K_{eff} is the effective thermal conductivity in $[Wm^{-1}K^{-1}]$, T in Kelvin (K) is the temperature distribution in the system, $\dot{q}_{eff}$ $[Wm^{-3}]$ is the effective volumetric heat generation and ϕ_{max} is the maximum allowed porosity (ratio of the volume of higher conductivity material to the total volume of the design domain) which is introduced in the system as the volume constraint. The choice of objective function depends on the problem under consideration. As an example, if the mean temperature in the system is used as the objective function then the above system of equations can be visualized as TO problem to minimize the overall average temperature in the volume V using specified amount of conducting material to be used.

Qing *et al.* [92] were among the firsts to apply topology optimization to 2D steady state heat conduction problems. They used the Evolutionary Structural Optimization (ESO) technique which incorporates an evolutionary iterative process into the Finite Element Method (FEM) solver over 2D structures uniform mesh. They concluded that the ESO technique is capable of handling various optimal objectives by choosing an appropriate evolutionary criteria e.g., temperature or heat flux. They applied different numerical examples to printed circuit board design (PCB) and concluded that the algorithm works well for both single and multiple loads (heat sources). However, the solver was limited to 2D problems and there was no information regarding the computational time behind the solver.

Zhang and Liu [4] applied density based TO to investigate the 2D design of conducting paths to solve the VP heat conduction problem using the SIMP material interpolation method in a FEM solver. The authors used a gradient-based sequential quadratic programming (SQP) algorithm coupled with filtering techniques suggested by Sigmund and Petersson [35] to avoid the onset of checkerboards. The VP problem had an adiabatic boundary everywhere except for a small isothermal cold spot. They calculated the best distribution of the high-conductive material in the domain with an objective to minimize the highest temperature (hotspot) while obeying a specific volume constraint. However, they noticed that the position of hotspot changes as the material distribution changes, concluding that the highest temperature, as a function of material distribution is non-continuous in some cases. This non-continuity makes the optimization process difficult. They finally compared their optimal structures with structures obtained by bionic optimization and constructal theory and found better performing structures. They observed that the configuration of the optimal paths with different conductivity ratio corresponded to the configuration of a tree in different stages of growing. With the increase of the ratio of high conductivity material to low-conductivity material $(\tilde{K} = K_H/K_L)$, number of branches of tree increased (refer Fig. 2.1). Later in the same year, the authors introduced a novel thermal performance index by the name of geometric average temperature as a better alternative objective function compared to maximum temperature for heat conduction systems [93]

Gersborg-Hansen *et al.* [94] were among the firsts to use the Finite Volume Method (FVM) in TO to discretize the energy equation. However, both FEM and FVM were used to calculate the cost-function. Additionally, the authors used arithmetic and harmonic averages to compute element interface heat fluxes using material conductivities at element boundaries. They used the method of moving asymptotes (MMA) as the optimizer, discrete adjoint method for gradient computation and SIMP interpolation technique for material distribution. They compared their results with those based on FEM approach and studied the effect of both arithmetic and harmonic average on the final topologies and the numerical instabilities (for e.g., the checkerboard problem). They observed that checkerboards were not encountered while using a harmonic average to calculate the conductivity at the interface of elements, but did, however, encounter checkerboards when using an arithmetic average. The authors finally concluded that thermal topology optimization is indeed possible using FVM for heat conduction and that it only requires minor deviations in the gradient computation when compared with FEM.

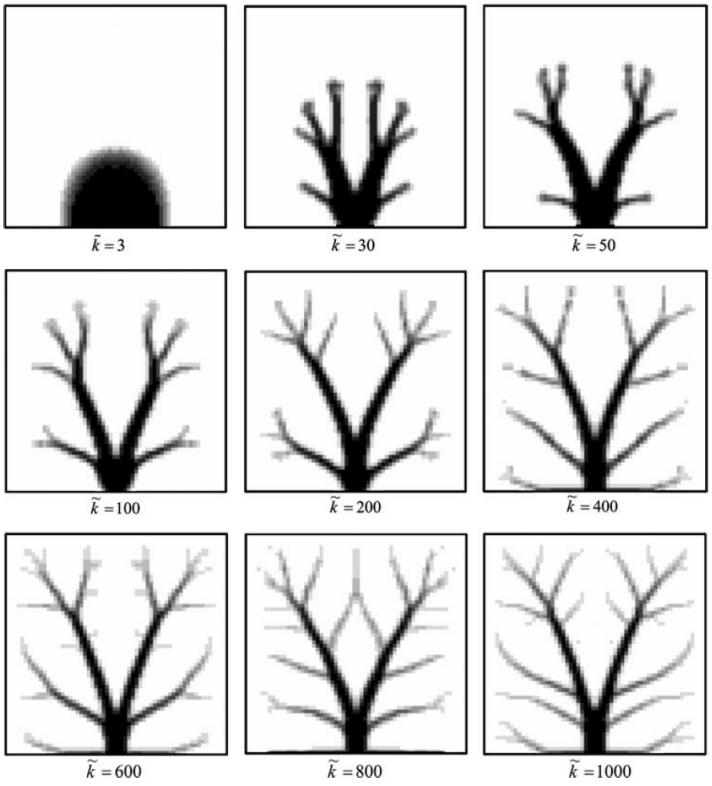

Figure 2.1 – Material distribution at different thermal conductivity ratios obtained by Zhang and Liu [4] by using density-based TO.

Zhuang *et al.* [31] investigated 2D heat conduction using a level set method for multiple load cases. The authors used the level set method to implicitly represent the boundary of the conductive material. They used a topological derivative through the finite element solver to generate holes in the material at a fixed cutting ratio. By using numerical examples, they concluded that the level set approach is effective in the topology optimization of a heat conduction problem.

Gao *et al.* [95] studied 2D TO of heat conduction problems under two different load conditions: design-dependent and design-independent loads using a Bi-directional Evolutionary Structural Optimization (BESO) scheme. They studied uniformly heated square domains as well as point loads. The authors used a modified BESO procedure to handle the non-monotonicity of the objective function defined by a heat potential capacity. Their FEM based methodology with a discrete adjoint system for sensitivity analysis, proved its efficiency in the layout design of electronic components and it was effective in the dissipation of heat generated using conductive path.

Donoso [90] was among the first researchers to analyze an optimal design problem in three-dimensional (3D) heat conduction. The author used Finite Difference Method (FDM) numerical scheme on a structured uniform mesh with an objective to minimize the quadratic mean temperature gradient in the domain. The author used the Optimality Criteria Method (OCM) as the optimization algorithm and solved several examples taking a cubical design domain $\Omega = [0, 1]^3$. Donoso also incorporated a volume constraint for the high conductivity material. The author concluded that very similar results were obtained when different mesh sizes and different starting points are used.

The problem of heat evacuation from finite-sized heat generating volumes by optimal allocation of the high conductivity materials in a 2D design domain was also analysed by Marck *et al.* [5]. The authors used a density based TO method coupled with a a bi-objective function strategy to tackle the TO problem in a FVM solver. They used the following bi-objective function (f_{bo}) based on a linear combination of average temperature (f_{av}) and variance temperature (f_{vr}) objective functions:

$$f_{bo} = w f_{av} \; + \; (1 - w) f_{vr} \tag{2.2}$$

where w is the scalar-valued weight ranging from 0 to 1. To take advantage of both the objective

functions they used a Pareto-front to present the optimal structures. The authors used discrete adjoint method for sensitivity analysis, the gradient-based MMA as the optimizer along with a volume constraint on the high-conductivity material. They observed that higher the porosity constraint, the more the whole set of solutions is closed to the Pareto frontiers i.e., structures with large porosity constraints are less sensitive to local optima due to the low variations of the objective function according to small structural changes, making them easier to avoid. Conversely, the lower the maximal porosity, the more is the chances of the optimization process to not succeed in avoiding local minima.

The authors also studied the effect of different numerical instabilities like mesh independence study and role of filtering in modifying the final topologies. They concluded that elementary structures does not vary with mesh size, however, additional second scale structures appear along the elementary layout on increasing the mesh size which is shown below in Fig. 2.2.

Figure 2.2 – Mesh indendance analysis performed by Marck *et al.* [5]: a) 200×200 elements $f_{av} =$ 2.98 °C, b) 100×1000 elements $f_{av} =$ 6.97 °C and c) 50×50 elements $f_{av} =$ 8.73 °C.

In recent times, Dirker and Meyer [6] studied the TO of heat conduction in a 2D square domain by introducing some novel concepts. The MMA algorithm in a Finite Difference Methodology (FDM) framework and a discrete adjoint system was used in their studies. They introduced two new concepts of "thermal conduction performance" and "definiteness measure". The thermal conduction performance represents a non-dimensional temperature (τ) that includes both the thermal properties of the base material and the main characteristics of the system.

$$\tau = \frac{K_0}{\dot{q}_0 A^2}(T - T_0) \tag{2.3}$$

where K_0 $[Wm^{-1}K^{-1}]$ is the thermal conductivity of the low conductivity base material, $\dot{q}_0$ $[Wm^{-3}]$ is the volumetric heat generation inside the base material, A $[m]$ is the length of the square domain, and T_0 $[K]$ is the heat sink temperature. This performance criteria can be used as a measure to compare the conduction effectiveness of different optimal structures.

The definiteness measure represents the measure of the narrowness (definiteness) of the boundaries between two materials in the domain. Dirker and Meyer [6] expressed the definiteness measure in terms of the local elemental design variables ($\boldsymbol{x}_j$), the volume fraction occupied by the higher conductive material (ϕ), and the number of elements used (N).

$$\varepsilon_{final} = \frac{\sum_{j=1}^{N} \left(x_j^2 - x_j\right)}{(\phi^2 - \phi)N} \tag{2.4}$$

They applied it to the problem in Fig. 2.3 (for $\phi_{max} = 0.1$), using different objective functions, at different schemes and at different control methods to improve the definiteness of the boundaries between the heat-generating and high-conduction regions in the 2D design domain. They showed that the type of objective function used and the choice of the numerical scheme (especially the algorithm parameters and the penalization factor p) have a significant effect on the optimized material distribution in the final converged topologies. However, no deep information was provided about the computational speeds and convergence criterion.

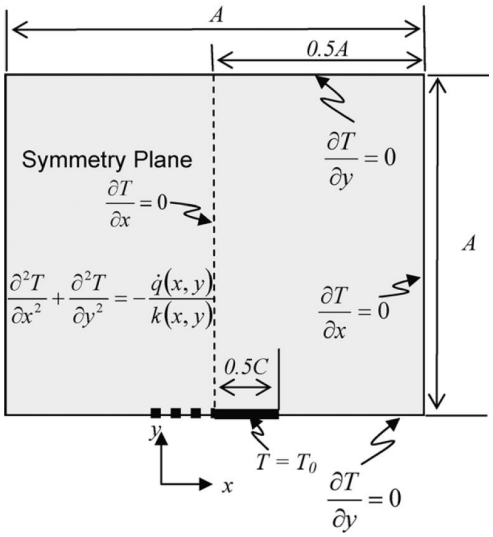

(a) Initial and boundary conditions. Taken from [6]

$p = 3$	Scheme 2A			Scheme 2B		
	$\gamma = 100$	$\gamma = 200$	$\gamma = 500$	$\gamma = 100$	$\gamma = 200$	$\gamma = 500$
τ_{max}	0.1858	0.1315	0.0723	0.0900	0.0554	0.0247
ε_{final}	0.9732	0.9750	0.9561	0.9444	0.9364	0.8826
$\mathbf{x}_{final}$				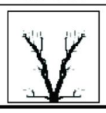		
$p = 3$	Scheme 4A			Scheme 4B		
	$\gamma = 100$	$\gamma = 200$	$\gamma = 500$	$\gamma = 100$	$\gamma = 200$	$\gamma = 500$
τ_{max}	0.1860	0.1319	0.0742	0.0903	0.0567	0.0302
ε_{final}	0.8874	0.9452	0.9332	0.9550	0.9408	0.9001
$\mathbf{x}_{final}$				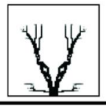		

(b) 2D optimal structures: Influence of thermal conductivity ratio (γ) on material distribution. Taken from [6]

Figure 2.3 – "Volume-to-Point" 2D heat conduction TO problem studied by Dirker and Meyer [6].

Burger *et al.* [7] further extended the 2D works of Dirker and Meyer [6] for 3D steady heat conduction applications. However, this time in a FVM framework keeping the gradient based MMA algorithm as optimizer for the TO problem, and retaining the discrete approach for the adjoint system of sensitivities. Fig. 2.4 below shows an example of a 3D topology design for minimizing the average temperature in a cubic domain for the porosity (ϕ_{max}) of 0.05 and the conductivity ratio (γ) of 500.

Pizzolato *et al.* [96] presented TO for heat transfer enhancement in Latent Heat Thermal Energy Storage (LHTES) tanks involving phase change. The authors developed a TO method to find optimal layout of high conductivity material inside the regions of low conductivity phase changing material. The Stefan problem for solidification was solved with a fixed grid FEM based on the apparent heat capacity technique. The density based TO method used SIMP technique for material distribution and discrete adjoint method for sensitivity analysis. 2D and 3D transient numerical examples were solved for two alternate problem formulations of the Energy Minimization approach which minimizes the residual energy in the tank at a fixed time and the Time Minimization approach which minimizes the time required to discharge the tank down to a specified energy fraction, respectively. Very different optimal designs were obtained for the two different objective functions. The authors concluded that

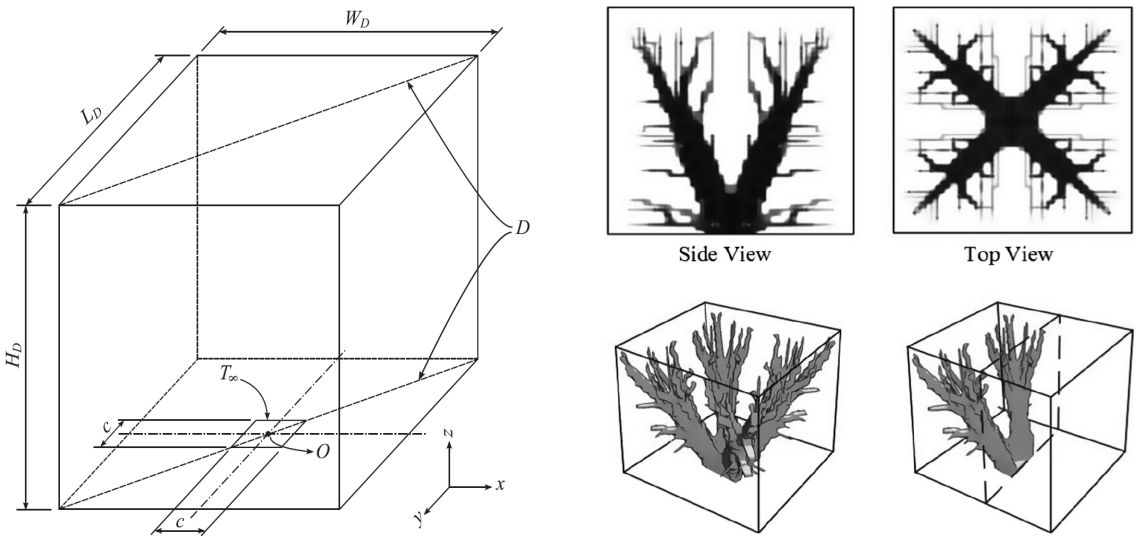

(a) 3D design domain (b) 3D optimal structures

Figure 2.4 – 3D steady state heat conduction problem analysed by Burger*et al.* [7]

the 3D optimal designs contains features not visible in 2D which gives a discharge time reduction of around 20 % w.r.t 2D optimal designs.

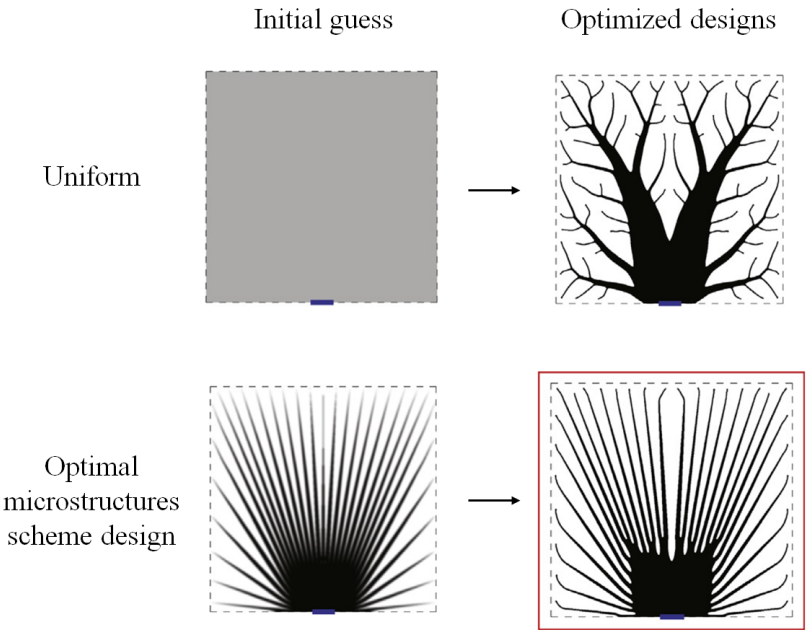

Figure 2.5 – Optimized design for 2D "Volume-to-Point" heat conduction problem for minimum thermal compliance obtained by Yan *et al.* [8] using the RAMP scheme. Left column shows the starting initial guesses used and the red box indicate design with the best objective function value.

Lastly, in a very recent study Yan *et al.* [8] revisited the 2D volume-to-point heat conduction problem for minimizing thermal compliance and minimizing maximum temperature in the domain, respectively. The authors used three different material interpolation models from literature for material density and effective thermal conductivity: the optimal rank-1 microstructure scheme [97], the penalized density approach via RAMP interpolation [98] and the simple variable thickness sheet model [99]. The gradient-based MMA algorithm was used to solve the optimization algorithm over a highly refined mesh of 800×800 elements for the density approach. The authors stated that lamellar needle structures as shown in Fig. 2.5 and not the trees-like structures are the optimal topologies for the volume-to-point heat conduction problems. They further advocated the use of

good initial-guesses and very slow continuation strategies for the penalization process to avoid the TO solver to get stuck in local-optimum solution. Finally, the authors concluded that a uniform material distribution is not a good initial guess for the volume-to-point heat conduction problems.

2.2 Topology optimization applied to fluid flow systems

Fluid flows are encountered in many industrial and day-to-day applications such as flow around a moving car, water flowing in pipes, blood flows in arteries and many others. Shape and size optimization of fluid flow systems existed long before, however, topology optimization found its applicability only in the last decade. The main advantage with TO is that in addition to modification of the boundary shape, it allowed creation of new boundaries as well. The general TO problem for steady incompressible fluid flow in a volume V can be expressed mathematically as follows:

Minimize/Maximize:

$$f_0(\alpha(\boldsymbol{r}), \boldsymbol{u}, P) \tag{2.5a}$$

subject to:

$$\nabla \cdot \boldsymbol{u} = 0 \tag{2.5b}$$

$$\rho_f(\boldsymbol{u} \cdot \nabla)\boldsymbol{u} + \alpha \boldsymbol{u} = -\nabla P + \nabla \cdot (2\mu_f D(\boldsymbol{u})) + \boldsymbol{f} \tag{2.5c}$$

$$\frac{1}{V} \sum_{j=1}^{nCells} x_j \leq \phi_{max} \tag{2.5d}$$

where f_0 is the objective function to be minimized, ρ_f is the fluid density, $\boldsymbol{u}$ is the fluid flow velocity vector, P is the pressure and μ_f is the dynamic viscosity of the fluid. ϕ_{max} is the maximum allowed volume fraction of the high viscosity material. $D(\boldsymbol{u})$ is rate of strain 2^{nd} rank tensor and $\boldsymbol{f}$ represent the gravity and external body forces. $\alpha(\boldsymbol{r})$ represents the inverse of the local permeability of the medium at position $\boldsymbol{r}$. Most of the topology optimization methods in literature are based on immersed boundary method which uses the Brinkman penalization approach [100, 101] to penalize the momentum equation by a source term in order to account for the presence of immersed solid regions in the fluid flow domain. The main idea behind this approach is to force a zero velocity inside the stationary solid material regions by means of the Brinkman penalization source term $(\alpha \boldsymbol{u})$ in equation 2.5c when α tends to a very large value of the order $O(10^5)$.

Borvall and Petersson [9] were the first researchers to consider topology optimization of fluids in Stokes flow. In Stokes flow ($Re = \frac{\text{Inertial forces}}{\text{Viscous forces}} << 1$), the inertial terms on the left hand side of equation (2.5c) are very small as compared to the viscous terms on the right and hence are neglected. The authors formulated the optimization problem to minimize the total potential power, which in the absence of body forces is reduced to minimization of the dissipated power in the fluid. They discretized the partial differential equations using the Finite Element Method (FEM) and solved it by a preconditioned conjugate gradient method. Various numerical examples were considered. Fig. 2.6 shows results obtained for optimal double pipe for two different lengths of 1 and 1.5, respectively. The authors illustrated through their examples that the obtained TO solutions are not prone to numerical instabilities, such as mesh-dependence or checkerboards and explained that the choice of the objective function (total potential power) is the reason for obtaining nice mathematical results. They further suggested that for an application which requires use of another objective, additional or alternative measures may be needed to obtain satisfactory results.

Olesen *et al.* [30] extended the works of Borvall and Petersson in topology optimization and were among the firsts to consider full incompressible Navier-Stokes (N-S) equations in steady-state. Their implementation was based on the commercial FEM software package FEMLAB which allowed a selection of a wide range of optimization objectives. The authors used the same objective function of minimizing the power dissipation in the fluid and the MMA as the preferred optimization algorithm. They implemented their solver on two fluid flow examples in 2D. In the first example,

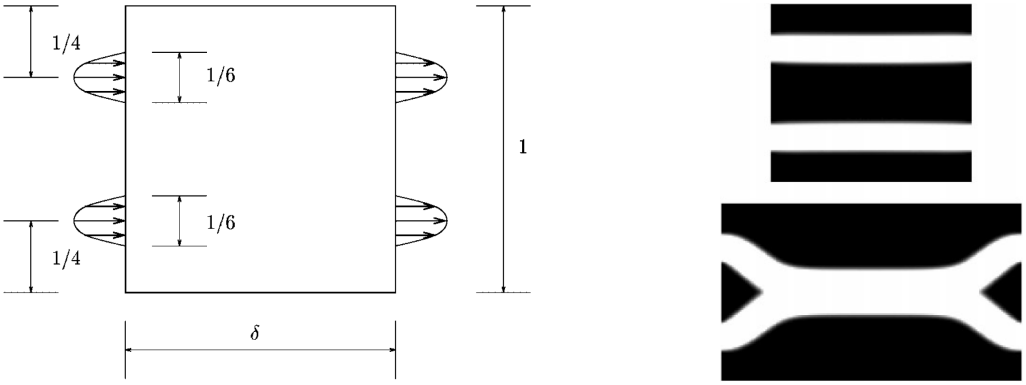

(a) 2D design domain (b) Optimal double pipes for length of 1 and 1.5

Figure 2.6 – Optimal double pipe designs for Stokes flow obtained by Borvall and Petersson [9].

they considered a channel with reversed flow and demonstrated the influence of the Reynolds number ($Re = \frac{\text{Inertial forces}}{\text{Viscous forces}}$) and the Darcy number ($Da = \frac{\text{Viscous forces}}{\text{Porous friction forces}}$) on the solutions. They showed that the choice of Darcy number has a major influence on the solution when the structure contains barriers to deflect the fluid stream. In the second example, they considered minimization of the power dissipation in a four-terminal device and expressed the problems of determining the global minimum in the presence of two strong minima and finally concluded that in highly convex problem the solution depends on initial conditions.

Following the works of Borvall and Petersson [9], numerous studies have been performed. Wiker *et al.* [102] added effective viscosity variation as an additional property control of two-phase material. Gersborg-Hansen *et al.* [103] suggested a topology optimization method for Navier-Stokes flow, which is similar to the Borrvall and Petersson's work. Various example problems followed such as Stokes flow [94], 3D Stokes flow [104], mixing [105], reactor design [106] and fluid-structure interaction problem [107]. Chen [108] presented a detailed review of topology optimization of microfluidics in different flow state, including Stokes flow, Darcy-Stokes flow, Navier-Stokes flows, unsteady Navier-Stokes flows and non-Newtonian flows. Duan *et al.* [109] demonstrated topology optimization for Stokes' flow and Navier-Stokes' flow via variational level set method. Pingen *et al.* [110, 111] presented topology optimization for nano-fluid problem by using Lattice Boltzmann equation. Later, Pingen and Maute [10] extended their Lattice Boltzmann Method (LBM) based TO to solve non-Newtonian flows for the first time in the literature. The authors used a Carreau-Yasuda model to approximate the non-Newtonian fluid viscosity. The developed TO method was used to solve the classical double pipe flow optimization problem to highlight the difference between optimal topologies for Newtonian and non-Newtonian fluids at different Reynolds number (refer Fig. 2.7).

Kreissl *et al.* [11] were the first to consider topology optimization of unsteady flow problems governed by the incompressible N-S equations for low to moderate Reynolds number (with $Re_{max} = 1000$). The authors used a streamline-upwind/Pedrov–Galerkin (SUPG), pressure-stabilizing/Pedrov–Galerkin (PSPG) finite element formulation and the corresponding discrete adjoint equations over unstructured non-uniform meshes. Using a Brinkman penalization technique to track the fluid-solid interface, they investigated the feasibility of the material interpolation approach in optimizing unsteady flow designs. The authors reported non-physical artifacts at higher Reynolds number due to insufficient resolution of the flow field and incorrect pressure field predictions in the solid region. Physically logical designs were later obtained by using sufficiently refined grid. Several numerical examples were solved to show that the optimum unsteady flow designs are significantly different from their steady-state counterparts (see Fig. 2.8). Later Deng *et al.* [112] also studied the transient TO for 2D and 3D incompressible N-S flows with FEM formulation however, with continuous adjoint system of equations. The authors also emphasized on the high sensitivity of the transient flow optimum designs to the Reynolds number. Recently, Nørgaard *et al.* [113] analyzed TO for 2D transient incompressible N-S flows using the lattice Boltzmann method and the corresponding discrete adjoint equations. A partial bounceback model was used to model solid/fluid phase transition

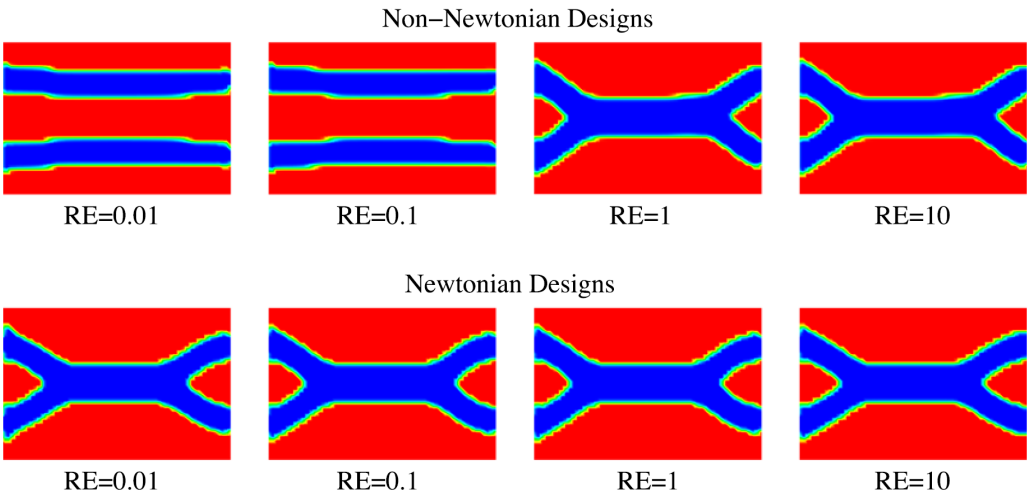

Figure 2.7 – Optimal double pipe designs for Newtonian and non-Newtonian fluids at different Reynolds numbers obtained by Pingen and Maute [10].

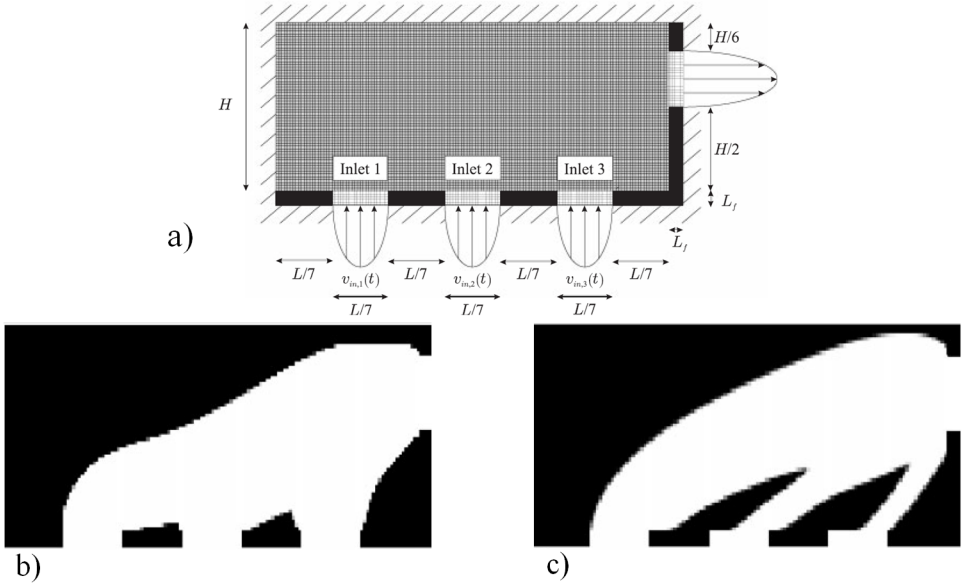

Figure 2.8 – Topology optimization of a 3-inlet, 1-outlet manifold studied by Kreissl *et al.* [11]: a) Design domain, b) Steady-state optimized manifold design and c) Unsteady optimized manifold design.

in the TO problem and the gradient-based MMA algorithm was used as the optimizer. The authors showed that for moderate Reynolds number flows, TO can account for unsteady effects like vortex shedding and time-varying boundary conditions which are critical in many engineering applications, i.e., fluid pumps and control valves.

For the the fluid dynamics TO problem of Eqn. 2.5, Othmer *et al.* [12,82] derived the continuous adjoint formulations taking into account the appropriate boundary conditions for the computations of surface and topological sensitivities of ducted flows and demonstrated its implementation into the OpenFOAM® CFD environment. For the automotive industry, they implemented several objective functions like dissipated power, equal mass flow through different outlets and flow uniformity. They demonstrated the capability of the continuous adjoint formulation by solving for various 2D and 3D geometries. In particular, they emphasised on the versatility of this approach w.r.t changes in the objective function. However, the turbulence field is assumed to be "frozen" where the variation of turbulence field w.r.t design variables are neglected and the authors did not take into account any

wall functions in the adjoint formulation. Fig. 2.9 below shows the optimization for a automotive air-conditioning duct as demonstrated by Othmer *et al.*

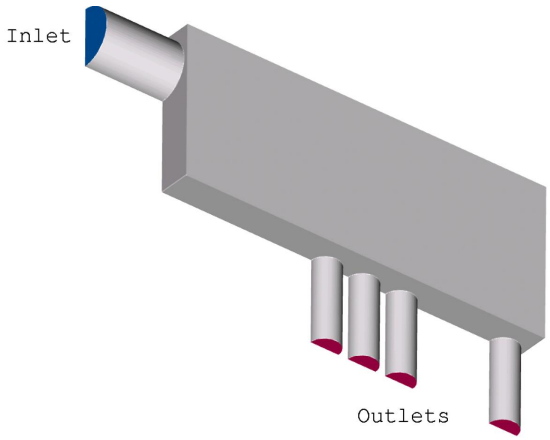

(a) Flow splitter manifold geometry

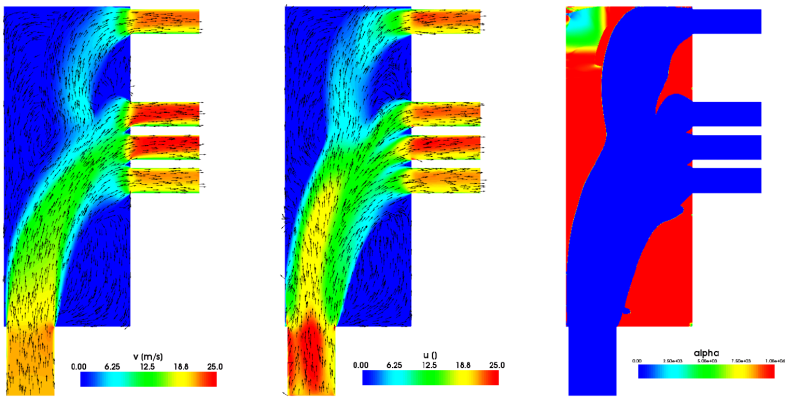

(i) (ii) (ii)

(b) Optimized result: i) Primal velocity, ii) Adjoint velocity and iii) Porosity (blue: favourable, red: non favourable)

Figure 2.9 – Optimized result for the design of flow splitter manifold used in automotive air-conditioning. Taken from [12].

In recent studies, Duan *et al.* [114] introduced an adaptive local mesh refinement method based on material distribution information to obtain high-resolution fluid/solid interface in the context of TO of 2D steady-state fluid flow problems. The authors used the FEM formulation coupled with the OCM from literature [18] to tackle the optimization problem. They considered several numerical examples to successfully demonstrate the proposed adaptive mesh refinement technique. Jensen [115] also demonstrated the feasibility of performing TO of Stokes flow on dynamic unstructured meshes. The author presented an anistropic mesh adaption technique through a custom MATLAB script to efficiently resolve the physical length scale associated with the Brinkman penalization term near the solid boundaries. The OCM is used as the optimization algorithm for minimizing the viscous dissipation subject to a volume constraints. Several 2D and 3D numerical examples for different Darcy numbers were considered to demonstrate the use of the developed mesh adaption technique for accurate resolution of small localized length scales. Koch *et al.* [116] proposed a new technique to combine topology optimization to shape optimization for 2D fluid flow problems with an aim to use shape optimization to further refine a solution found by TO. A transitional procedure was developed that post-processes 2D adjoint TO results, fitting the interface between the solid and fluid domains

to generate a parameterized solution which can be further used as a CAD-compatible representation or a source for grid generation from which a shape optimization loop can be initialized. The author used the level set method to clearly define the solid/fluid interface throughout the TO process in addition to a geometric, fluid volume constraint. The authors solved three specific 2D internal flow problems with an objective to minimize the pressure drop between inlet and outlet. They showed that the developed transitional procedure was able to capture both converged and pre-converged TO solution, allowing the user to switch to shape optimization befor TO has found an optimal solution. The shape optimization allowed for a significant decrease in the objective function as compared to the solutions found by TO alone, with the improvements being more significant the further from convergence the TO solution was.

Yoon *et al.* [117] developed a topology optimization method for turbulent flows with the one-equation Spalart-Allmaras turbulent model. The author modified the wall equation and transport equation for eddy viscosity to allow for free material distribution using SIMP technique during the TO process. For sensitivity analysis, a custom FEM script was developed in COMSOL to solve the discrete adjoint equations. To demonstarte the validity of the developed TO formulation several steady-state 2D numerical examples were solved for Reynolds number between 3000 to 5000 with an objective to minimize the dissipated fluid energy and the resulting optimal fluid channel layouts were compared to it laminar counterparts. The author pointed out that by considering the turbulent effects, the eddy viscosity is added to the N-S equations and thus it increases the influence of the viscosity forces. Hence, laminar flow designs are not effective in turbulent flow regimes. Dilgen *et al.* [118] presented a topology optimization approach based on discrete-adjoint systems for turbulent flow problems. The authors used a FVM discretization for solving Reynolds Averaged Navier-Stokes (RANS) equations coupling it with either one equation (Spalart-Allmaras model) or two equation ($k-\omega$ model) turbulence closure models. The authors then solved some classical 2D and 3D optimization flow problem to demonstrate the importance of exact sensitivity analysis over the previously used frozen turbulence assumption.

2.3 Topology optimization applied to conjugate heat transfer systems

After successful application of TO for heat conduction and fluid flows separately, the next obvious step was to combine these two phenomena to optimize coupled thermal-fluid systems. Early implementations of TO modeled the thermal-fluid systems by combining 2D heat conduction problem with convective heat transfer to the surrounding fluid through Newtons' law of cooling by either using a constant heat transfer coefficient [119–121] or employing some specific surrogate based models [122] to the convective boundaries. In conventional TO methods, it is not easy to clearly define boundary locations in the middle of the process, since they are blurry and constantly changing. Hence, practical implementation of optimal designs obtained from such assumptions (or approximations) is not feasible.

Such limitations can be avoided by adopting a comprehensive conjugate heat transfer approach to optimize thermal-fluid systems. As discussed earlier, the term conjugate heat transfer is used to describe processes which involve variations of temperature within solids and fluids, with thermal interaction between them. A typical example is the heating or cooling of a solid object by the flow of air in which it is immersed. From mathematical point of view, all the physical problems that solve the general constrained TO formulation of the three coupled equations i.e., mass, momentum and energy conservation are categorized under conjugate heat transfer. This phenomenon is observed in several industrial thermal systems like heat exchangers, heat regenerators, finned surfaces and heat sinks. The design of such heating or cooling equipments involves a consideration of both the heat transfer between different media and the mechanical pumping power spend to overcome the fluid friction in order to move the fluid through the device. In other words, the objective is to increase the heat transfer while keeping the pressure drop as low as possible. Optimizing designs that best manage trade-offs between these two conflicting criteria is currently a very critical issue and has attracted many academic and industrial researchers.

A general steady-state TO problem for conjugate heat transfer systems can be expressed mathematically as follows:

Minimize/Maximize:

$$f_0(\alpha(\boldsymbol{r}), \boldsymbol{u}, P, T) \tag{2.6a}$$

subject to:

$$\nabla \cdot \boldsymbol{u} = 0 \tag{2.6b}$$

$$(\boldsymbol{u} \cdot \nabla)\boldsymbol{u} + \alpha \boldsymbol{u} = -\nabla p + \nabla \cdot (\nu \nabla \boldsymbol{u}) + \boldsymbol{f} \tag{2.6c}$$

$$\boldsymbol{u} \cdot \nabla T - \nabla \cdot (D(\alpha) \nabla T) = 0 \tag{2.6d}$$

$$\frac{1}{V} \sum_{j=1}^{nCells} x_j \leq \phi_{max} \tag{2.6e}$$

where ν is the fluid kinematic viscoity and D is the thermal diffusivity of either a fluid or a solid depending on the Brinkmann penalization term α.

Gil Ho Yoon [32] was among the first researchers to consider topology optimization for a coupled thermo/hydraulic system in 2D. He analysed the use of TO for designing a heat dissipating structure that use forced convective heat transfer, however, buoyancy and viscous dissipation inside the fluid were not considered. Also for simplicity, the material non-linearities of the viscosity, the conductivity and the specific heat capacity were neglected. He used the FEM formulation for discretizing the governing equations over a structured uniform mesh. Using MMA as the optimization algorithm and SIMP technique for material distribution, Yoon [32] found the optimal topologies of heat dissipating structures. In particular, three examples were analysed for the problem of thermal compliance minimization. As a nonlinear multiphysics system was under consideration, Yoon encountered many numerical difficulties such as multiple local optima, instabilities on the mesh-scale and the final topologies were highly sensitive to initial guesses.

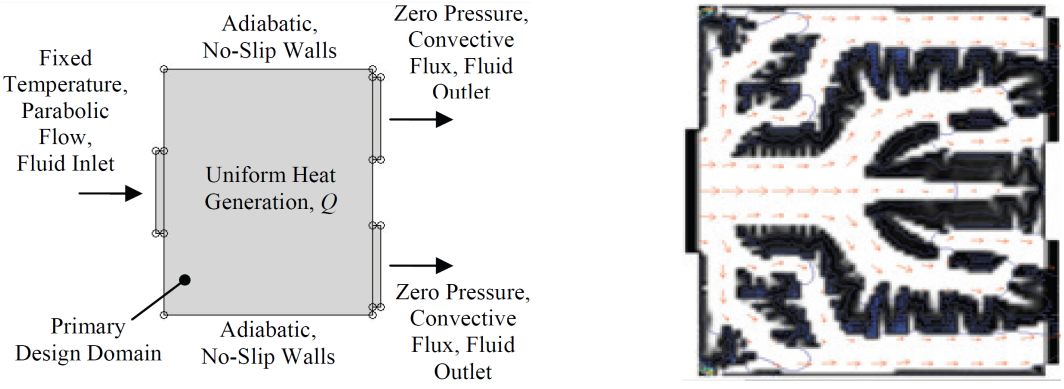

(a) 2D design domain and boundary conditions

(b) Optimal topology

Figure 2.10 – Topology optimization of a conjugate heat transfer three-terminal device analysed by Dede [13]: Undesirable dead-ends observed in the structure.

Dede [13] introduced a bi-objective function strategy to minimize simultaneously both the mean temperature and the pressure drop in the system using a custom COMSOL/MATLAB solver. A continuous adjoint method for gradient computation and MMA as the optimizer algorithm was used. However, fluid density, heat capacity and viscosity were assumed to be unity in all the examples. Additionally, high values of pressure drop were observed in the system due to undesirable dead-ends in the structure. As a conclusion, the author emphasized on the need of better weighting strategies for multi-objective topology optimization.

Lee [61] applied density based TO approach to design convective cooling channels in both 2D and 3D using FEM formulation coupled with discrete adjoint method for sensitivity analysis and

Rational Approximation of Material Properties (RAMP) [98] functions for interpolating material properties. Many interesting optimal structures were produced using, first a single objective function (mean temperature minimization), and then introducing a bi-objective function (minimizing mean temperature and kinetic energy dissipation) in order to tackle high pressure drop observed in the former case.

Matsumori *et al.* [123] studied topology optimization for coupled fluid-thermal problem to design heat exchangers under a constant input power using sequential quadratic programming (SQP) algorithm [124] and RAMP-type interpolation functions in the FEM based COMSOL software package. Surprisingly, the authors did not consider the thermal conductivity differences between the solid and fluid regions (i.e., assuming $K_s = K_f$). Kontoleontos *et al.* [125] extended the TO of coupled fluid-thermal problems to turbulent flows using a finite volume method (FVM) formulation and continuous adjoints for gradient computation coupled with the steepest-descent optimization algorithm. However, the authors did not solve the temperature field in the solid region by numerically imposing a constant value of temperature.

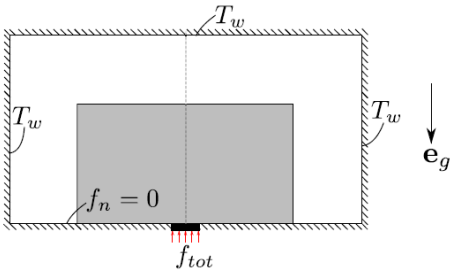

(a) Boundary condition for TO of heat sink: Grey zone is the design domain

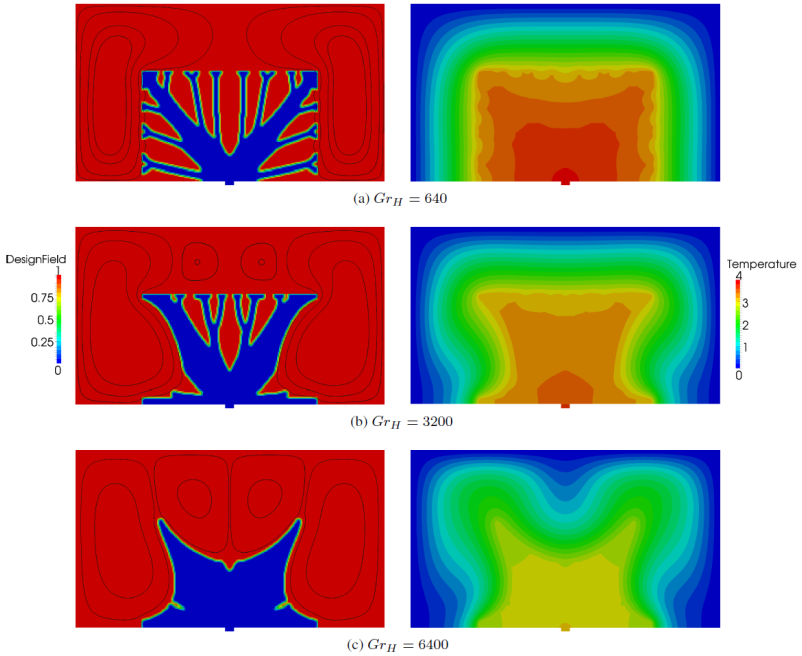

(b) Optimal designs at different Grashof numbers

Figure 2.11 – Topology optimization of a heat sink cooled by natural convection. Taken from [14].

Alexandersen *et al.* [14] introduced density based topology optimization for natural convection problems using Boussinesq approximation to design heat sinks and micropumps in a FEM formulation. The strongly coupled physical phenomena associated with natural convection heat transfer problems makes optimization for such kind of sytems even more difficult. The authors pointed out that the

buoyancy effects in the system greatly influence the final optimized topologies. It is worth to mention that the authors for the first time used a parallelized version of method of moving asymptotes (MMA) algorithm to solve the 3D conjugate heat transfer optimization problem. Fig. 2.11 shows the optimal natural convection heat sink designs obtained at various Grashof numbers.

$a)\ \omega = 0.00$
$f_d = 4.98 \times 10^{-9}\ W$
$f_r = 1.94 \times 10^{-5} W$

$b)\ \omega = 0.75$
$f_d = 1.34 \times 10^{-7}\ W$
$f_r = 2.77 \times 10^{-5} W$

$c)\ \omega = 1.0$
$f_d = 6.32 \times 10^{-7}\ W$
$f_r = 2.94 \times 10^{-5} W$

Figure 2.12 – Single pipe with constant wall temperatures: structures going from $f_d(w = 0)$ minimization to $f_r(w = 1)$ maximization. Taken from [15].

Koga *et al.* [126] presented a complete product development cycle for a topology optimized heat exchanger. The authors developed a heat sink device for electronic cooling using topology optimization for Stokes flows (inertial effects in fluid were not considered) using a FEM formulation and the Sequential Linear Programming (SLP) optimization algorithm. The authors used the RAMP function for interpolating Brinkman penalization term and the SIMP interpolation function for thermal properties. 3D prototypes of numerically obtained 2D optimal structures were fabricated through electrical discharge machining and precision computer numerical control (CNC) milling. The authors reported a good match between experimental and numerical results. Marck *et al.* [15] also considered the topology optimization for conjugate heat transfer systems. They efficiently coupled the finite-volume method (FVM), for the direct solver, with the discrete adjoint formulation, for the sensitivity analysis taking MMA as the optimizer, in order to handle both fluid dynamic and heat transfer optimization in 2D laminar flows. They used a bi-objective function stratergy as they did previously for heat conduction problems [5], however, this time with an objective to minimize the pressure drop ($f_d(\boldsymbol{u}, P)$) while maximizing the recoverable thermal power ($f_r(\boldsymbol{u}, T)$), simultaneously. The authors presented a Pareto set of optimal solutions for the multi-objective optimization (MOO) of a single pipe with constant wall temperature. However, they reported non physical optimal structures (i.e., fluid flow blockage) for some designs specifically when the thermal objective function is more prioritized ($\omega > 0.75$).

Haertel and Nellis [127] used TO to design 3D-printed air-cooled heat exchangers. Density-based TO was used to design the air-side surface of dry-cooled power plant condenser with a steady-state, incompressible, fully developed laminar flow assumption. A cross-flow heat exchanger optimization model was developed with explicit modelling of both fluids (air and water) flowing perpendicular to each other. However, the water-side geometry was fixed and only the air-side geometry was considered for optimization. Polymer with infilled thermal conducting filaments was used as the heat exchanger material to allow for cost effective 3D printing. The objective was to maximize conductance of the heat exchanger for a prescribed pressure-drop and prescribed air-side temperature change across the heat exchanger. The optimization was conducted with the FEM based COMSOL Multiphysics software package using the globally convergent version of Method of Moving Asymptotes algorithm (GCMMA) with the air bulk temperature as the global constraint. The authors found that optimized designs tend to require finer feature sizes with increasing polymer conductivities. In reality, the smallest feature obtained is limited by the minimum feature size that can be conveniently 3D printed. However, actual experiments and 3D printed fabrication of the numerically obtained polymer structures were kept as perspectives for future studies.

In recent studies, Qian and Dede [128] presented density based 2D TO of conjugate heat transfer

systems with a tangential thermal gradient constraint by using a bi-objective function approach. The authors used the continuous adjoint method to derive gradients of both the objective function and tangential thermal constraint in a FEM formulation. Additionally, they used a RAMP function for interpolating fluid properties and SIMP for thermal properties. The authors emphasized the role of appropriate material interpolation schemes in producing clear fluid/solid designs. Zeng *et al.* [129] used a multi-stage optimization approach to obtain a non-conventional 2D design of a heat sink under forced convection in COMSOL. 3D representations of the optimal structure was then numerically and experimentally investigated. However, in their formulation, while evaluating heat transfer coefficient in the solid domain, heat conduction was considered only in the height direction (spanwise heat conduction was neglected even though the width of the base is very large as compared to its height). A similar study was performed by Haertal *et al.* [130] in COMSOL using the GCMMA algorithm to optimize the design of a thermo-fluid heat sink where in 2D results obtained from the topology optimization process were numerically validated in 3D. Lastly, in contrast to density based TO approach, Dugast *et al.* [131] developed a Level-Set Method (LSM) coupled to adjoint Lattice Boltzman Method (LBM) for topology optimization of thermal fluid flows. The authors presented optimal thermo-fluid designs for fixed pressure drop values with three different cost functions: minimization of mean temperature in the domain, maximization of recoverable thermal power by the fluid, and maximization of the heat exchange with heated solid parts.

2.4 Discussions

During the last two decades, TO applied to heat transfer and fluid flows has attracted a large number of researchers. However, no research can be deemed good until it finds its application in solving existing industrial problems. Despite the huge amount of fruitful research conducted in this field, topology optimization is still not the preferred numerical tool for designing optimal thermal systems due to several reasons. In authors' point of view, the following are the main issues or the existing "research gaps" in the field of topology optimization applied to thermo-fluid systems:

1. **Lack of benchmark studies:** Topology optimization techniques are evolving in many different directions, including density, level set, topological derivative, phase field, evolutionary and several others. However, these numerical techniques are too dispersed in literature without enough comparisons. Moreover, there have been no benchmark studies conducted in this field which hinders the application of such studies in real world application. In industrial field, only Daimler-Chrysler [132] and Volkswagen engineers [133] demonstrated the possibility of topology optimization for air channel flow design. Recently, Dirker and Meyer [6] introduced the concepts of "thermal conduction performance" and "definiteness measure" as performance criteria for comparing different heat conduction optimal structures. In future, more such performance criteria should be established in order to perform benchmark studies in topology optimization. In structural design optimization, compliance minimization of the Messerschmitt-Bölkow-Blohm (MBB) beam is considered to be a standard benchmark problem [34]. In heat conduction systems, average temperature minimization in "Volume-to-Point" problems acts as a benchmark case [5, 7]. In fluid flow systems, the total pressure drop minimization in a double pipe can be seen as a benchmark problem [9, 10, 15]. However, no such benchmark problem exists for conjugate heat transfer systems mainly due to the uncertainty associated with the correct choice of objective function for such problems. Creating standard benchmark problems and performing methodological benchmark studies in future can lead to establishment of best practice guidelines for researchers and engineers developing TO methods applied to heat transfer and fluid flows.

2. **Handling complex boundary conditions:** For the classical VP heat conduction problem, it is observed that almost all of the studies used an internal volumetric heat source $[Wm^{-3}]$ in the low conductivity material. However, no instance was found which tackled a surface heat source as the boundary condition in the literature. In the future, it will be an interesting topic of investigation to characterize properly a surface heat flux $[Wm^{-2}]$ in the TO formulation

where the structure is continuously changing in the domain with iterations untill convergence. Similarly, for heat transfer coupled with fluid flows problems, many researchers consider heat convection by just using the heat transfer coefficient (h) in addition to solving for heat conduction [120, 134]. In conventional topology optimization methods, it is not easy to clearly define boundary locations in the middle of the process, since they are blurry and constantly changing. Therefore, previous research assumed constant heat convection coefficient without considering fluid motion, which varies significantly according to the geometry. Subsequently, these approaches may be infeasible for designing cooling channels that prevent re-circulation areas and hotspots. To overcome this issue, Iga *et al.* [122] recently applied the design-dependent topology optimization method developed by Chen and Kikuchi [135]. They approximated design dependent heat convection coefficient by using the flow simulation of a simplified periodic fin model. Yet, the possibility of practical implementation of their assumption is an open question.

3. **Performance of optimization algorithms:** Another trend that is clearly evident from the literature is the increasing use of the method of moving asymptotes (MMA) contrained optimization algorithm by most authors. However, no enough information is available about its performance in TO applied to heat transfer and fluid flows. Moreover, there has been no enough comparison in the literature between various optimizers. For instance, in future it will be very interesting to see how the MMA algorithm performs as compared to other methods like the Optimality Criteria Method (OCM). Only Dbouk and Harion [136] showed a detailed analysis about the general performance of MMA and its variant the globally convergent method of moving asymptotes (GCMMA).

4. **Complex thermo-fluid systems:** Majority of industrial thermal equipment involve turbulent flow regimes. Hence, it becomes important to develop techniques to take into account turbulence in TO of compex thermo-fluid system. Although, there exists topology optimization approaches [82] with a simplified frozen-turbulence assumptions (variation of turbulence field w.r.t design variables are neglected), to authors' knowledge, no studies in literature tackled TO of complete turbulent conjugate heat transfer problems without any unrealistic simplifications. Another important consideration in future could be to develop TO methodologies to incorporate radiation heat transfer which could be critical for some applications.

5. **Unrealistic or Non-physical optimal designs:** Designing optimal conjugate heat transfer systems requires consideration of both heat transfer maximization and pressure drop reduction in the domain. As a result, optimization of CHT systems falls under the scope of multi-objective optimization (MOO) where the goal is to search for a solution that best manages trade-offs between conflicting criteria and that cannot be transformed into a common measure [137]. However, combining these two conflicting objectives causes **complex numerical instabilities** in the overall TO method (due to their different nature and magnitudes) specifically when heat transfer maximization is more prioritized. Due to this, several authors reported non-physical artifacts in the final optimal design such as broken flow paths, dead ends and blocked fluid flow [13, 15, 128]. This can be attributed to the way the optimization problem is formulated, the choice of objective function or the adopted material interpolation scheme. For this particular reason, no study in literature clearly demonstrated the evolution of optimal designs at high influences of the thermal objective function. Nevertheless, such non-physical designs are highly undesirable from fabrication point of view.

6. **Lack of experimental studies:** While there exist several numerical studies related to TO of thermal systems, only very few experimental investigations [126, 129] of topology optimized configurations exists in the literature which really questions the ability of existing TO algorithms for producing optimal thermal designs for real world applications (especially when most of optimization algorithms currently used by the TO community are local optimization algorithms i.e., they tends to produce different optimal solution for the same discretized problem). Experimental studies can address several critical issues associated with the complex unconventional designs obtained through topology optimization. For example, the the minimum length scale

that can be fabricated using available manufacturing techniques will influence the minimum mesh size to be used for TO process. For bi-material structures, the actual inter-facial contact between the two material after fabrication may affect the intended ideal performance of the final optimal structure in terms of objective function values. All these critical factors can only be quantified through experimental studies which is one of the objective in the present thesis.

7. **Need for non-FEM based analysis:** Most of the studies in literature used a FEM formulation to solve TO problems. Very few studies investigated the FVM [15, 125] and LBM [131, 138] discretization techniques for CHT systems. For some specific physical problem such as compressible flows, FVM, being a conservative method, is conventionally believed to perform better that FEM for its ability to better handle the advective term in the Navier-Stokes equations. Hence, to tackle wide variety of physical problem, non-FEM based TO approaches needs to be explored.

8. **Numerical issues:** Finally there still exists specific numerical challenges associated with present TO methods such as: minimizing the influence of initialization parameters, understanding effect of different mesh types and size to ensure mesh-independent convergence, spatial filtering techniques, incorporating multiple constraints, minimizing problem specific tuning parameters and implementing efficient adaptive mesh refinement techniques. These critical issues require immediate attention for making TO a robust numerical technique for thermal system design optimization.

Although TO applied to heat transfer and fluid flow systems has come a long way since its inception, a lot of work still needs to be done in this field. In this context, the present PhD thesis attempts to address some answers for the above mentioned issues concerning topology optimization of thermal systems.

Chapter 3

Topology optimization of conductive heat transfer devices: An experimental investigation

Abstract: This chapter presents a first approach dedicated to experimental investigation of a conductive heat transfer tree-like structure obtained numerically by topology optimization (TO) applied to a bi-material "volume-to-point" heat conduction problem. In the configurations presented in this work, density based TO is implemented to define thermally optimal solutions for cooling heat generating volumes by organizing a high conductive metallic material as complex tree-like structure inside regions of lower thermal conductivity heat generating volumes. Since it is not easy to impose a 3D volumetric heat source experimentally in bi-material domain, a 2D TO numerical problem was considered. The resulting 2D optimal structure is realized experimentally by keeping the thickness of the structure very small as compared to its sides and in addition to this, a thin film silicone heater is used as a surface heat source $[Wm^{-2}]$ on one side of the test-section to facilitate the use of an infrared (IR) camera for steady-state temperature measurement on the other side.

To construct this bi-material structure experimentally, two materials, Aluminum and a two-part epoxy polymer, with a very high diffusivity ratio are carefully selected after testing several combinations of the two materials for their suitability to this experiments. The fabrication of the complex bi-material optimal structure is presented through a step-by-step procedure starting from the post-processing of the TO numerical results to the final surface treatments on the structure required for the IR acquisitions. Two different optimal structures are fabricated using water-jet cutting for two values of the amount of high diffusivity material in the structure, 17.92 % Al and 28.6 % Al, respectively. Experimental thermal measurements are carried out on the optimal structures using a non-intrusive infrared thermography technique in order to qualify the heat transfer performance of the geometries obtained by the developed TO numerical method.

Simultaneously, 3D CFD simulations are performed for the two optimal structure (in order to simulate the exact environmental boundary conditions that exist during the experiments) whose results are then eventually compared to the IR thermal measurement data. All the experimental results are presented with an in-depth comparison of the similarities and dissimilarities with the numerical findings. It is found that the experimental results are in good agreement with the numerical ones in terms of objective function values (overall average temperature), and the maximum temperature in the structure. As a conclusion, this study demonstrates a methodological experimental approach to fabricate and investigate the thermal performance of the complex tree-like optimal structures under some specific loads and boundary conditions. In authors' opinion, this study could constitute a relevant approach for future experimental studies of structures resulting from topology optimization, aimed at testing the validity and comparing the structures obtained from different optimization algorithms for producing efficient cooling/heating industrial devices. This part of the thesis was published in Applied Thermal Engineering, vol. 131, pp. 390–411, 2018, https://doi.org/10.1016/j.applthermaleng.2017.12.026

Résumé: Ce chapitre présente une première approche dédiée à la caractérisation expérimentale d'une structure arborescente conductrice de chaleur obtenue numériquement par optimisation topologique (TO) appliquée à un problème bi-matière de conduction thermique de type textquote volume-vers-point. Dans les configurations présentées dans ce chapitre, une méthode d'optimisation topologique basée sur la densité est mise en œuvre pour définir les solutions thermiquement optimales pour refroidir un volume générant de la chaleur. L'optimisation conduit à des structures arborescentes du matériau métallique à haute conductivité incluses au matériau plus faiblement conducteur. La génération volumique de chaleur dans un volume pleinement tridimensionnel étant d'une mise en œuvre très complexe, il a été choisi de se placer dans une configuration bidimensionnelle pour réaliser l'analyse expérimentale. La structure optimale 2D résultant de l'optimisation topologique est réalisée expérimentalement pour une épaisseur très petite par rapport à ses côtés. Un chauffage en couche mince est utilisé comme source de chaleur surfacique $[Wm^{-2}]$ sur une face de la structure arborescente, permettant ainsi sur l'autre face, l'utilisation d'une caméra infrarouge (IR) pour mesurer le champ de température en régime permanent.

Pour construire expérimentalement cette structure bi-matières, deux matériaux, l'aluminium et un polymère époxy bi-composant, avec un rapport de diffusivités très élevé, ont été soigneusement sélectionnés après avoir testé de nombreuses combinaisons de deux matériaux pouvant satisfaire aux contraintes expérimentales. La fabrication de la structure optimale bi-matière complexe est détaillée pas-à-pas à partir du post-traitement des résultats d'optimisation topologique jusqu'aux traitements de surface finaux permettant les acquisitions de mesures de température par IR de bonne qualité. Deux structures optimales différentes ont été fabriquées en utilisant la découpe au jet d'eau pour usiner l'élément de structure en aluminium. Ces deux structures correspondent respectivement à deux valeurs de la quantité de matériau à diffusivité élevée, respectivement 17,92 $\%$ Al et 28,6 $\%$ Al. Des mesures thermiques expérimentales sont effectuées sur les structures optimales en utilisant une technique de thermographie infrarouge non intrusive afin de qualifier les performances de transfert de chaleur des géométries obtenues par la méthode numérique d'optimisation topologique.

Parallèlement, des simulations CFD tridimensionnelles ont été effectuées pour les deux structures optimales en intégrant de façon la plus exhaustive possible l'ensemble des conditions limites correspondant aux conditions expérimentales. Les résultats sont ensuite comparés aux données de mesure thermique IR. Tous les résultats expérimentaux sont présentés avec une comparaison détaillée des similitudes et des différences avec les résultats numériques. On constate que les résultats numériques sont en bon accord avec les résultats expérimentaux en termes de valeurs de la fonction objective (température moyenne globale) et de température maximale dans la structure. En conclusion, cette étude présente une approche méthodologique expérimentale pour fabriquer et étudier les performances thermiques de structures optimales bidimensionnelles complexes dans les conditions expérimentales s'approchant au plus près des conditions numériques. Selon les auteurs, cette étude pourrait constituer une approche pertinente pour les futures études expérimentales de structures issues de l'optimisation topologique, visant à tester la validité et à comparer les structures issues d'algorithmes d'optimisation pour la production de dispositifs industriels efficaces de refroidissement / chauffage. Cette partie de la thèse a fait l'objet d'une publication parue dans la revue Applied Thermal Engineering, vol. 131, pp. 390–411, 2018, https://doi.org/10.1016/j.applthermaleng.2017.12.026

Topology optimization of conductive heat transfer devices: An experimental investigation

V. SUBRAMANIAM[a,b], T. DBOUK[a,b,*], J.-L. HARION[a,b]

[a] *IMT Lille Douai, Industrial Energy Engineering Department, F-59500 Douai, France*
[b] *University of Lille, F-59000 Lille, France*

Abstract

For optimal tree-like heat conductive structures obtained numerically by topology optimization (TO), few experimental investigations exist in the literature to author's knowledge. In this context, the present study deals with an experimental investigation of tree-like structures obtained by topology optimization (known also by bi-material volume-to-point problems). For a volume (of lower conductivity material) that is continuously generating heat, TO predicts tree-like structures (of higher conductivity material) to evacuate efficiently the amount of heat being generated. Experimental measurements were carried out on two tree-like structures using infrared thermography in order to test the validity of the developed numerical topology optimization approach. It is found that the experimental thermal measurements are in good agreement with numerical data obtained by TO, which was developed in this work by coupling the method of moving asymptotes (MMA) as optimization algorithm to the solid isotropic material with penalization (SIMP) as a bi-material distribution technique.

Keywords: Topology optimization, heat conduction, volume-to-point problem, infrared thermography, method of moving asymptotes, solid isotropic material with penalization (SIMP)

Nomenclature

Greek Symbols

Symbol	Description	Unit
α	Thermal diffusivity	$\mathrm{m}^{-2} \cdot \mathrm{s}^{-1}$
γ	Ratio of thermal diffusivity	$-$
$\Delta x,\ \Delta y$	Mesh size	mm
ε	Convergence criterion	$-$
θ	Field of view	$^{\circ}$(deg)
ρ	Density	$\mathrm{kg} \cdot \mathrm{m}^{-3}$
σ	Standard deviation	$-$
ϕ_{max}	Maximum volume fraction	%

*Corresponding author
Email address: talib.dbouk@imt-lille-douai.fr (T. DBOUK)

Ω	Dimensions of the optimal structure	mm

Roman Symbols

Symbol	Description	Unit
A	Length of the domain	m
C	Size of the heat sink	m
C_p	Specific heat capacity	$\mathrm{J \cdot kg^{-1} \cdot K^{-1}}$
D	Height of thermal insulation	mm
e	Thickness	mm
f_0	Objective function	–
k	Thermal conductivity	$\mathrm{W \cdot m^{-1} \cdot K^{-1}}$
h_{ext}	Convective heat transfer coefficient	$\mathrm{W \cdot m^{2} \cdot K^{-1}}$
L_x	Maximum dimension in x-direction	m
L_y	Maximum dimension in y-direction	m
$\boldsymbol{n}$	normal vector	
M^2	Number of square elements	–
OS	Object signal	digital level (DL)
p	penalization factor	–
$\dot{q}$	Volumetric heat generation rate	$\mathrm{W \cdot m^{-3}}$
T	Temperature	K
$\tilde{T}$	Normalized temperature	–
$\boldsymbol{x_j}$	Design variable vector	–
$x,\ y,\ z$	System of coordinates with dimension	m
$\tilde{x},\ \tilde{y}$	Normalized system of coordinates	–

1. Introduction

Designing efficient thermal systems is a very crucial step for developing many new products. Electronic components are getting denser and faster and multiprocessor computer system chips are clustered in closer proximity. This compactness makes power density of components higher and causes a constant increase of thermal load. As a consequence, the ability to efficiently remove heat from an increasingly restricted space is currently a very critical issue. The need to develop optimization methodologies in order to design efficient cooling systems is for years drawing the attention of a large number of industrial and university researchers. Of the automated optimization methods that exist in literature, namely topology, size and shape, topology optimization (TO) is the most recent one which was initially introduced by Bendsøe and Kikuchi [1]. Recently, it has been successfully applied to wide range of applications including thermal systems when an optimal material distribution is required. This kind of applications can be modelled by the well-known "volume-to-point" heat conduction problem which has been extensively studied by the scientific community [2][3][4][5]. The aim is to minimize the thermal resistance in a given domain by distributing a fixed percentage of high conductive material in an optimal way within the domain to improve heat transfer to the evacuation points.

This problem of distribution of high conductive material in areas of low conductivity heat generating material has been approached by several methods in the literature such as

constructal theory [2], bionic optimization [6], simulated annealing and genetic algorithms (SAGA) [7], solid isotropic material with penalization (SIMP) [8] and many others. Most of the studies for the heat conduction TO problem were limited to two dimensions (2D) [9], however, contrary to its name, numerous authors still referred it to the "volume-to-point" problem for the sake of consistency and convenience [5][10][11][7]. Henceforth, the same terminology will be used in this article.

Qing *et al.* [12] were among the first to apply topology optimization to 2D steady state heat conduction problems by using the Evolutionary Structural Optimization (ESO) technique within a Finite Element Method (FEM) solver over 2D structured uniform mesh. They concluded that the ESO technique is able to handle various optimal objectives by choosing an appropriate rejection criteria e.g. temperature or heat flux. However, the solver was limited to 2D problems and there was no information regarding the solver's computational time.

Gersborg-Hansen *et al.* [13] were the firsts to use the Finite Volume Method (FVM) in TO to tackle the 2D heat conduction problem. However, they used both Finite Element Method (FEM) and Finite Volume Method (FVM) to calculate the cost-function. Discrete adjoint method [14] was used to calculate the sensitivities of the objective function, the method of moving asymptotes (MMA) [15] as optimizer, and Solid Isotropic Material with Penalization (SIMP) technique was used to force the solution towards a 0-1 solution [8]. They compared their results with those based on FEM approach and studied the effect of both arithmetic and harmonic average on the final topologies and on the numerical instabilities (for e.g. the checkerboard problem). The authors used the filter method proposed by Sigmund and Bendsøe to avoid the checkerboards [16].

Thereafter, many authors used the FVM discretization method for solving heat conduction TO problems [7][11][10]. Xianghua *et al.* [7] developed a FVM numerical solver to solve non-linear two dimensional Volume-to-Point (VP) steady heat conduction problems. They used the simulated annealing and genetic algorithm (SAGA) as optimization algorithm and showed that it produces better results than the Bionic Optimization (BO) algorithm and constructal theory for VP problems.

Donoso [17] was among the first researchers to analyze an optimal design problem in three-dimensional (3D) heat conduction. The author used Finite Difference Method (FDM) numerical scheme on a structured uniform mesh with an objective to minimize the quadratic mean temperature gradient in the domain. The author used the Optimality Criteria Method (OCM) defined in [8] as the optimization algorithm and solved several examples taking a cubical design domain. Donoso also incorporated a volume constraint for the high conductivity material. The author concluded that very similar results were obtained when different mesh sizes and different starting points are used. However, the main disadvantage of using OCM as the optimization algorithm is that it is applicable to only single-constraint optimization problems i.e. it can handle only the volume constraint and it is very difficult to use in problems with multiple constraints [18].

Marck *et al.* [11] used a multi objective function strategy as a linear combination of average and variance temperature objective functions to solve the volume-to-point heat conduction problem for a 2D domain. The authors coupled the SIMP material interpolation scheme with an Aggregated Objective Function approach (AOF) for the topology optimization problem. FVM numerical scheme with discrete adjoint system for sensitivity analysis

and the gradient based MMA as the optimization algorithm were used. The authors observed that the structures with large volume constraints are less sensitive to local optima due to the low variations of the objective function according to small structural changes, making them easier to avoid. The authors also studied the effect of different numerical instabilities like mesh independence study and the effect of filtering in modifying the final topologies. The authors concluded that elementary structures does not vary with mesh size, however, additional second scale structures appear along the elementary layout on increasing the mesh size.

During the last two decades, TO applied to conductive heat transfer has attracted a large number of researchers. By now, the concept is developing in many directions, including density, level set, topological derivative, phase field, evolutionary, etc. However, these numerical methods and tools are too dispersed without enough comparison between them. Moreover, to authors's knowledge, there have been no benchmark studies conducted in this field which hinders the application of such studies in industrial real applications. Recently, Dirker and Meyer [10] introduced the concepts of "thermal conduction performance" and "definiteness measure" as performance criteria for comparison between different optimal structures obtained by topology optimization. In the future, more performance criteria are needed in order to construct benchmark like studies for topology optimization. Another trend that clearly appears from the literature is the use, by most authors, of the method of moving asymptotes (MMA) which is a constrained optimization algorithm introduced by Svanberg [15]. However, no enough information is available about its performance in TO applied to heat transfer and fluid flows. Only Dbouk and Harion [19] showed a detailed analysis about the general performance of MMA and its variant, the globally convergent method of moving asymptotes (GCMMA). While, many numerical studies have been conducted for topology optimization applied to VP heat conduction problem, to the author's knowledge, only few experimental studies [20] of topology optimized configuration exist in literature which questions the ability of TO algorithms for producing optimized solutions for real world applications. Therefore, the objective of this study is to investigate experimentally the results obtained from a topology optimization method applied to a volume-to-point heat conduction problem.

In this manuscript, first the mathematical definition of the topology optimization problem is introduced outlining all the components involved in solving a classical volume-to-point heat conduction TO problem. Thereafter, the complete experimental setup is presented in detail elaborating every aspect of the experimental test bench. The next section demonstrates the CFD simulations for the optimal structures whose results are then eventually compared to the experimental measurements results. Finally, all the experimental data are presented with an in-depth analysis of similarities and dissimilarities with the numerical ones. Finally conclusions are drawn and some perspectives are proposed for the near future.

2. Topology Optimization

Topology optimization (TO) addresses the basic engineering problem of placing different materials within a given design domain that obeys a predefined objective function. Mathematically, the main purpose of topology optimization lies in minimizing or maximizing some objective function while taking into account one or more constraints.

A general TO problem can be defined mathematically as the following:

Minimize/Maximize:

$$f_0(\boldsymbol{x}) \tag{1a}$$

subject to:

$$f_i(\boldsymbol{x}) \leq 0, i = 1, 2, ..., m \tag{1b}$$

$$R_h(\boldsymbol{x}) = 0, h = 1, 2, ..., e \tag{1c}$$

$$\boldsymbol{x} \in \mathbf{X}, \tag{1d}$$

where $\boldsymbol{x} = (x_1, ...x_n)^T \in R^n$ are the so called design variables with $\mathbf{X} = \left\{\boldsymbol{x} \in R^n \mid x_j^{min} \leq x_j \leq (x_j)^{max}, j = 1, ..., n\right\}$ and $f_0, f_1, f_2, .., f_m$ are provided continuously differentiable (at least twice) real valued function on $\mathbf{X}$. x_j^{min} and x_j^{max} belongs to R such that $x_j^{min} \leq x_j^{max}\ \forall j$. The design variable vector $\boldsymbol{x}$ is bounded numerically such that its final value represents only one value i.e either x_j^{min} or x_j^{max}. This represents the interpolation of two materials in the design domain which is obtained by a penalization technique.

The constraints $R_1, R_2, .., R_e$ represents the state equations for the physical problem being solved. For example, for a pure steady state heat conduction application, $R_1 = 0$ will be the steady state heat equation. In TO problem applied to fluid flows with no heat transfer $R_1 = 0$ and $R_2 = 0$ will be the mass and momentum conservation equations, respectively.

The general TO problem of equation 1 requires some specific TO methods and numerical algorithms to be used in order to find an optimum. The complexity of any optimization problem depends on numerous factors like number of design variables, degree of convexity/ non-convexity and linearity/non-linearity of the equations and the numerical difficulties associated with them. Thus, choosing an efficient TO method and an equally reliable optimization algorithm is very important to ensure a stable convergence to an optimum solution. Figure 1 demonstrates the basic steps involves in any TO process.

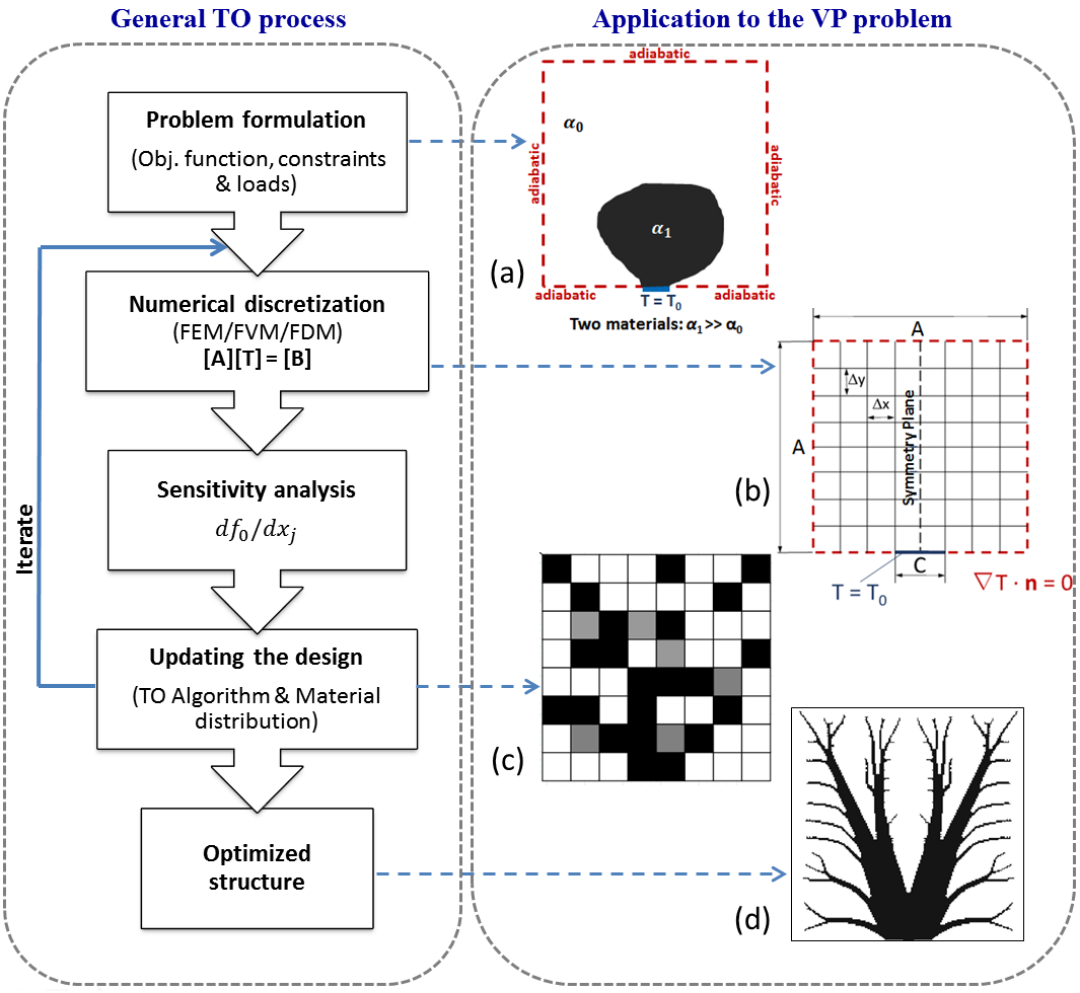

Figure 1: The topology optimization process.

2.1. The heat conduction topology optimization problem

Figure 1(a) and 1(b) represents the 2D computational domain and boundary conditions of a heat conduction topology optimization problem. The domain has lengths of $A(m)$ in the both the x and y directions and the thickness (e) is considered negligible as compared to the side A $(e << A)$. All the boundaries are adiabatic except for the small center part of the lower boundary (length C) which is at a constant temperature of T_0 and thus acts as a heat sink. Heat can only escape from the heat sink at the lower boundary. An effective constant volumetric heat generation rate $\dot{q}_{eff}$ $[Wm^{-3}]$ is applied as heat source. Under these conditions, the aim is to find the best topology of a material of high thermal diffusivity α_1 with an objective to minimize the overall average temperature in the domain.

Mathematically, the above TO problem can be expressed as follows:

Minimize:

$$f_0 = \frac{1}{M^2} \sum_{j=1}^{M^2} T_j \tag{2a}$$

subject to:

$$\nabla \cdot (\alpha_{eff} \nabla T) + S_{eff}(x, y) = 0 \tag{2b}$$

$$\frac{1}{M^2} \sum_{j=1}^{M^2} x_j \leq \phi_{max} \tag{2c}$$

where f_0 is the objective function to be minimized, subjected to a steady state heat equation 2b and an inequality constraint 2c. The amount of high thermal conductivity material is limited by restricting the ratio of its effective volume to the total domain volume, given by ϕ_{max} i.e. the maximum allowed relative quantity of material of high thermal diffusivity. M^2 is the number of square elements used to discretize uniformly the 2D domain in a Cartesian frame of reference. α_{eff} is the effective thermal diffusivity in $[m^2\ s^{-1}]$. S_{eff} is a thermal source term such that:

$$S_{eff} = \frac{\dot{q}_{eff}}{\rho_{eff} C_{p_{eff}}} \tag{3}$$

T is the temperature in Kelvin $[K]$, and $k_{eff}[Wm^{-1}K^{-1}]$ is the effective thermal conductivity. $x_j = (x_1, x_1, ..., x_{M^2})$ represents the design variable vector describing two materials such that $x = 1$ for material with diffusivity α_1 and $x = 0$ for material with diffusivity α_0.

The system of equations 2 can be seen as to minimize the average temperature in a domain, given a specified amount of two (conducting and insulating) materials in this domain. On closer observation, one can see that equations 2a and 2c concern the topology optimization part of the problem 2 whereas equation 2b represents physics involved. In a sense, system 2 can be interpreted as a coupling between the topology optimization process and the physics being solved.

In such topology optimization problems, the optimal solution is represented by integer discrete variables x_j (0-1 values) which shows clearly the optimal distribution of two materials in the domain. However, it is numerically very difficult to reach direct solutions using directly defined discrete variables formulation. To avoid this difficulty, the Solid Isotropic Material with Penalization (SIMP) technique [8] is used in the literature. The SIMP technique replaces the discrete integer variables with continuous ones, and then introduces some kind of penalty that forces an evolution of the solution towards discrete 0-1 values as the following:

$$S_{eff} = S_0 + x_j^p (S_1 - S_0) \tag{4a}$$

$$\alpha_{eff} = \alpha_0 + x_j^p (\alpha_1 - \alpha_0) \tag{4b}$$

with $p \geq 1$ and the subscript indices 0 and 1 represents two materials of different thermal diffusivities (or conductivities).

For the current problem, $x_j(t = 0) = \eta_{initial}\ \forall j$ (initially homogeneous material); $\gamma = \frac{\alpha_1}{\alpha_0} = 760$; and two cases are considered for $\phi_{max} = 20$ % and $\phi_{max} = 30$ % respectively.

2.2. Numerical Methods

The system of equations 2 is solved by using the method of moving asymptotes (MMA) algorithm introduced by Svanberg [15]. The method of moving asymptotes algorithm is

a gradient-based iterative optimization algorithm which is used to solve a non-linear constrained optimization problem by introducing a strictly convex sub-problem. This algorithm has proved to be well suited for various structural and multi-disciplinary optimization problems, especially where reciprocal and reciprocal-like approximations are used and therefore MMA has gained remarkable interest from the optimization community [21].

The gradient information of the objective function which is required by the gradient-based MMA algorithm is computed using the adjoint method. The adjoint method provides an efficient option for calculating the sensitivity field of the objective function, df_0/dx_j and has successfully been implemented in volume-to-point (VP) heat conduction problems in the past [13]. The adjoint equations are generally derived by using either the continuous or the discrete approach [14]. The continuous approach starts by deriving the adjoint equations in their analytical form and then discretizing the equations. The discrete adjoint approach on the other hand starts with the discretization of the equations and then transposing the equations in order to end at the adjoint code. A continuous adjoint formulation is used in the current study.

The SIMP material interpolation technique is used in order to achieve design variables of discrete nature for a two-material representation (values 0 or 1). Recent studies by Dirker and Meyer [10] showed that different schemes for updating the penalization factor p in SIMP (eq. 4), heavily affects the final topologies obtained by the MMA algorithm. The evolution strategy of the penalization factor p has been chosen according to a dedicated study based on this work in [10] i.e. linearly ramped up values over a preselected 40 MMA iterations, followed by constant p values over 30 MMA iterations limited by $p_{max} = 4$. The partial differential equation 2b is discretized spatially over the computational domain of figure 1 using the Finite Volume Method (FVM) in order to find the temperature field.

Density and sensitivity filtering techniques are very popular in topology optimization. They play an important role in producing mesh-independent and checkerboard-free solutions [16]. In this work, density filtering technique is used with a filter radius of 1.428 mm. Initially introduced by Bruns and Tortorelli [22], a density filter works by changing the element density to a function of the densities in a specified neighborhood of an element [23].

The steady state results in this work are produced using a structured uniform square-cells mesh of $\Delta x = \Delta y$ with $M = 140$ as shown in figure 1(b). All the above mentioned elements of this topology optimization solver are coupled in a OpenFOAM software package. The stopping criterion is usually related to the design variable changes in the last iteration (when the squared-norm of the Karush-Kuhn-Tucker (KKT) conditions becomes less than a positive real number ε such that $\varepsilon << 1$).

3. Objective of the experiment

The topology optimization method provides a "tree-like" material distribution of the high diffusivity material for heat evacuation from the areas of low diffusivity material as depicted below in figure 2. Two cases are solved in this study for $\phi_{max} = 20$ % and 30 %, respectively. On the left the repartition values of high and low diffusivities materials are shown and the right hand side presents the final optimized configurations obtained.

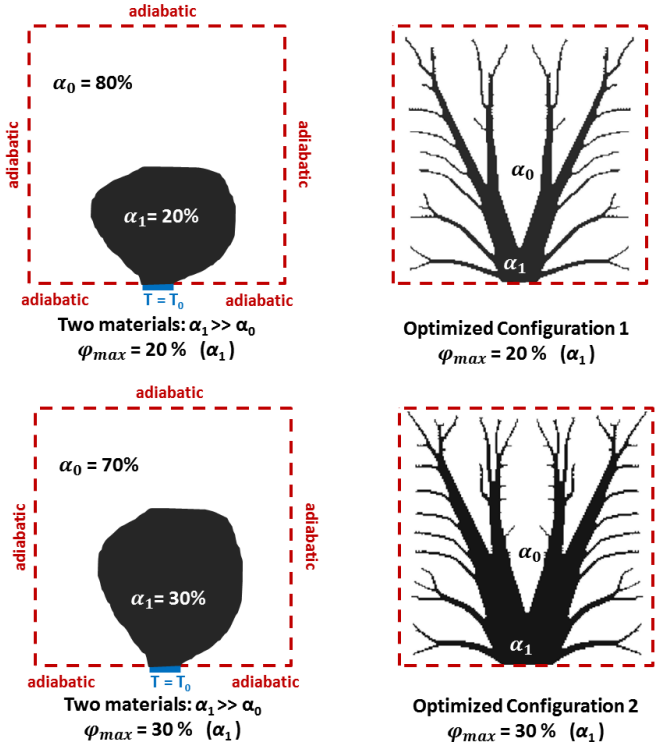

Figure 2: 2D heat conduction topology optimization: two configurations of the VP problem - $\phi_{max} = 20$ % and 30 %.

The objective of the current experiment is to investigate the thermal performance of the above optimal structure under some specific thermal loads and boundary conditions. For the current scenario, the thermal performance criteria is the overall average temperature in the domain which was also the objective function for the TO numerical process.

4. Experimental Setup

The heat transfer problem in this experiment is analyzed under steady-state conditions. Steady-state conditions in heat conduction problems are sensitive to several factors such as the surrounding environment, the thermal diffusivity of the materials involved, the type and quality of insulation and many others, however, such conditions are more desirable because the results can be directly interpreted and compared to the steady-state TO results. For this reason a steady state approach is preferred in this experiment. This requires the use of constant heating and cooling sources.

Some important requirements of the experiment which characterizes the test section are as follows. These requirements are derived from the design domain used during the numerical process in the previous section (figure 1).

- The optimal structure is fabricated with the dimensions of $\Omega = 100\ mm \times 100\ mm$.
- The heat sink size (C) corresponds to the relation C/A = 0.05.

– The high diffusivity material for the two optimal structures under consideration should respect the volume constraint of $\phi_{max} = 20$ % and $\phi_{max} = 30$ %, respectively for the two cases.

– The thermal diffusivity of the materials should be in the ratio $\gamma = \dfrac{\alpha_1}{\alpha_0} = 760$.

4.1. Material selection

One of the main critical aspect for this experiment is the proper selection of the two materials. The first step is to identify two materials which can form a good bi-material structure with a significant high ratio of thermal diffusivities. Once the two materials for the experiment are identified , TO is performed (as discussed in section 2.1) with the same values of diffusivities and more importantly with the same ratio. As a prerequisite, the materials are required to have excellent inter-facial contact in order to minimize the thermal contact resistance along the interface. Fundamentally being a heat transfer problem, the selected materials should allow for expansion or contraction during heating and cooling, without separating from each other at least under operating temperature range (0-80°C). While it is relatively easy to find a cost effective high conductivity (or diffusivity) material, matching an economical low conductive material that is both heat resistant and easy to fabricate is quite difficult. Moreover, the highly intricate shape of the "tree-like" optimal structure makes it even complicated for the surrounding material to be moulded around. After testing many combinations of the two materials, aluminum and a specific epoxy resin polymer were selected as high and low thermal diffusivities materials, respectively.

Figure 3 shows one of the sample test conducted for the selection of the low diffusivity material. In this case, the Polymer B clearly is a better choice as compared to Polymer A for a better inter-facial contact with aluminum.

To further ensure the proper choice of materials, the selected aluminum and the epoxy resin polymer were analyzed for their exact thermal properties both at an external laboratory and at the in-house thermal conductivity measurement system. The thermal properties of the two materials are listed in Table 1. It can be seen that the thermal diffusivity of aluminum and epoxy resin are $8.89 \times 10^{-5}\ m^2 s^{-1}$ and $1.17 \times 10^{-7}\ m^2 s^{-1}$, respectively and the thermal diffusivity ratio matches the one used in topology optimization solver. TO numerical process have then been computed with the right ratio of thermal diffusivities to define the final optimal geometries.

$$\gamma = \frac{\alpha_1}{\alpha_0} = \frac{8.89 \times 10^{-5}}{1.17 \times 10^{-7}} = 759.82 \simeq 760 \tag{5}$$

Material properties	Aluminium	Epoxy resin polymer
Thermal conductivity, $k(W\ m^{-1}\ K^{-1})$	214.04	0.19663
Density, $\rho(kg\ m^{-3})$	2700	1100
Specific heat, $C_p(J\ kg^{-1}\ K^{-1})$	891	1522.72
Thermal diffusivity, $\alpha(m^2\ s^{-1})$	8.89×10^{-5}	1.17×10^{-7}

Table 1: Material properties for aluminum and epoxy resin polymer.

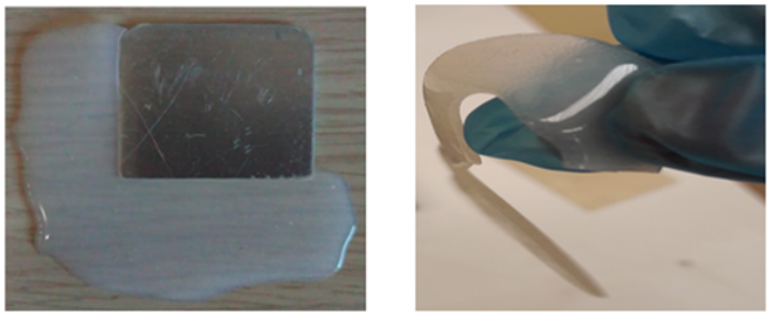

a) Polymer A + Aluminium: bad interface contact; elastic in nature (lacks rigidity)

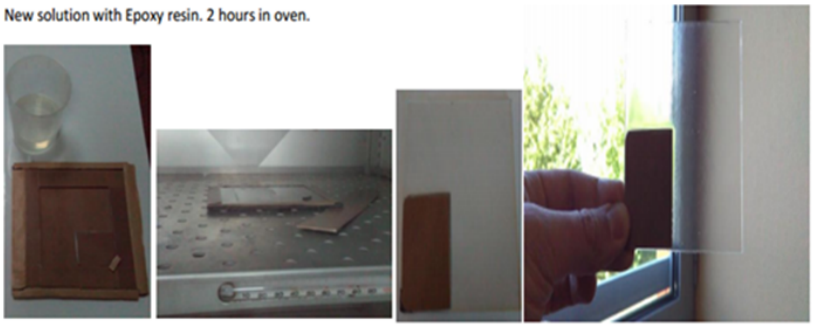

b) Polymer B + Aluminium (post curing): excellent interface contact (analysed under microscope); rigid in nature

Figure 3: Testing material combinations : a) aluminum with polymer A and b) aluminum with polymer B.

4.2. Fabrication of the test section

The aim is to build the test section with the two selected materials in such a way that it represents exactly the material distribution obtained from the TO solver (see figure 2). However, before fabricating the optimal tree structure the results obtained from TO solver needs to be post-processed in order to display the two dimensional solution. Even though a density filter is used in the current TO numerical process still intermediate densities (or gray zones) always exist in the solution in SIMP like density-based topology optimization due to the relaxation of the original 0/1 problem [16]. Hence, post-processing of the final design is needed in order to obtain a pure black and white solution. Post-processing and industrial fabrication of structures obtained from TO is a critical issue and therefore is a subject of many ongoing research [24]. Nevertheless, in this study, the optimal structure is extracted from the image file and exported into a suitable CAD format(for example - .dxf or .dwg) after treating the intermediate densities. As a result, the ϕ_{max} of 20 % and 30 % for the two different optimal structures is reduced to 17.92 % and 28.6 % respectively, without affecting the optimality of the solution and respecting the design constraint.

The fabrication is actually a two step process where the first step is to cut the aluminum sheet of some prescribed thickness in the shape of the tree structure and then in the second step the polymer is molded around the tree structure to fill the design domain of $\Omega = 100\ mm \times 100\ mm$. The intricate tree-structure is carved out from an aluminum plate using

water-jet cutting which was found to give better surface finish on the edges as compared to laser cutting. Figure 4 compares the two sample tree structures carved out from laser cutting and water-jet cutting, respectively.

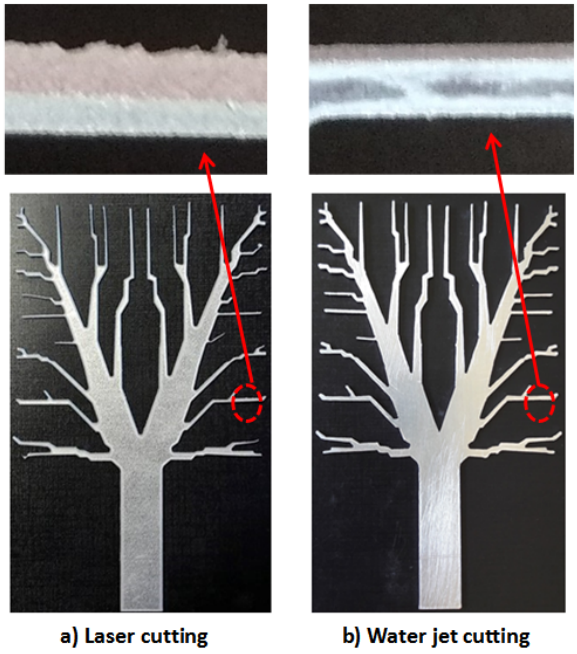

Figure 4: Tree structures obtained from: a) Laser cutting and b) Water-jet cutting.

To mold the polymer around the aluminum structure, the epoxy resin polymer is mixed with the hardener in a specified ratio and the mixture is poured in a special mold cavity fabricated in the dimensions of 100 mm x 100 mm x 1.5 mm and then polymerizes and cures in the oven at 80 $^{\circ}C$ for at least two hours (see figure 5). For easy de-molding of the test section, a thin layer of Teflon^{TM} (Polytetrafluoroethylene -PTFE) sheets are applied all over the mold cavity before pouring the resin. The epoxy resin is then carefully de-molded from the mold cavity to obtain the test section in its final form.

Figure 6 shows the final fabricated test section for the two optimized configurations based on different ϕ_{max} values. Furthermore, two samples of each optimized configuration is fabricated which shall be used for testing the reproducibility of thermal measurements during experiments (see figure 6(a)). Finally, one side of the optimal structure is painted with a high emissivity coating in order to enhance infrared acquisitions (see figure 6(b)).

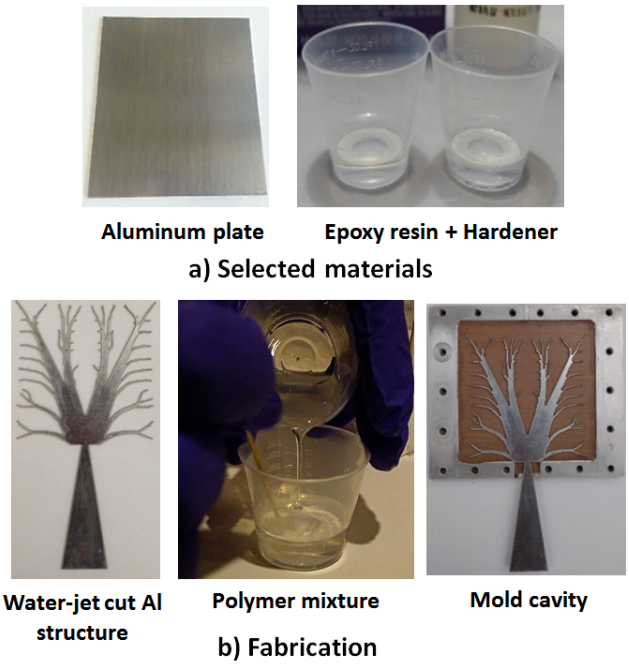

Figure 5: Fabrication process.

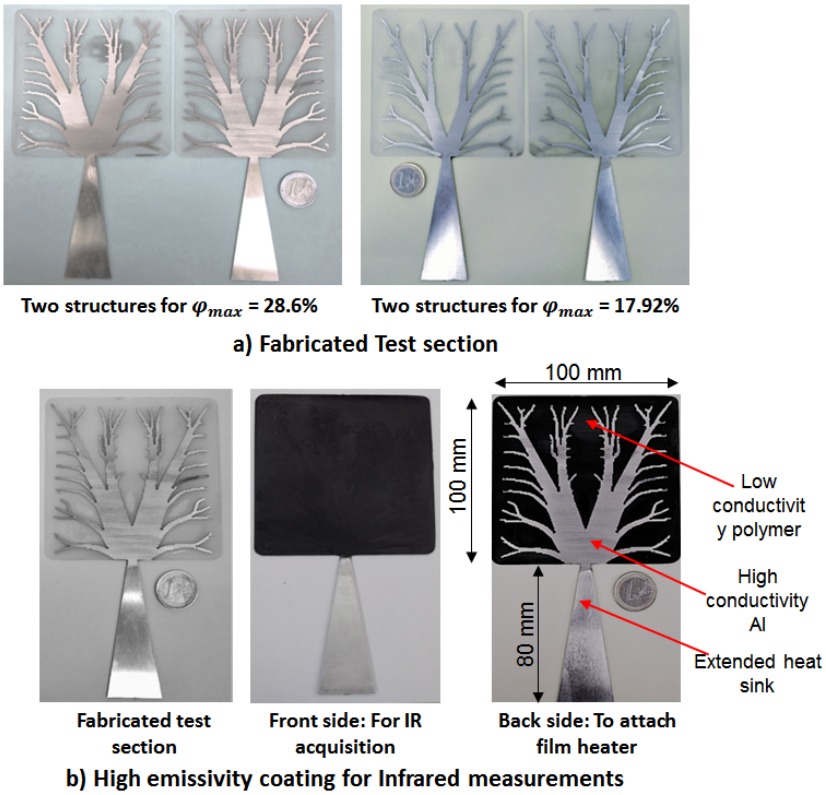

Figure 6: Fabricated test section.

4.3. Experimental test bench

The original TO problem was solved numerically for a two-dimensional domain where the heat transfer would occur only in the x and y directions (see figure 1(b)). To construct this scenario experimentally, the thickness of the test section (e) should be taken very small as compared to the sides to minimize the temperature variation along the thickness (z-direction). On the other hand, the thickness should be sufficient enough to facilitate the fabrication of the highly intricate branches of the tree structure. Additionally, the film heater is applied only from one side of the test section to allow the use of an IR camera to capture the surface temperature on the other side. This requires an enclosure of the insulating material of a certain height (D) to be used beyond the face of the test section in order to minimize the atmospheric effect on the steady-state temperature distribution in the optimal structure. 3D CFD simulations were performed to determine these two design parameters and as a result a material thickness of 1.5 mm and the height of the thermal insulation of 350 mm is used in the current experiments.

The TO problem in section 2.1 dealt with heat evacuation from the low conductivity heat generating volumes. A heat generating volume generates heat from within the volume, and can be approximated by applying a constant uniform heat flux on the surface of the test section if provided the test section is very thin ($A >> e$). A classical silicone rubber thin film heater is used as a surface heat source ($W\ m^{-2}$) in this experiment. In addition to this, a carefully monitored thickness of thermal paste is applied between the test section and the film heater to enhance the heat transfer capability.

To extract heat from the system, a constant lower wall temperature is required at the base of tree structure (here $0°C$). To achieve this, the base of the aluminum tree is further extended by 80 mm and clamped on to a cooling plate. A special high conductivity (copper) cooling plate with an inner water circulation that is accurately thermo-regulated ($\pm 0.01°C$ of stability) is used for this purpose.

The experimental facility is sketched in figure 7. The test bench is the integration of the test section and various elements required to perform the experiment. This experimental facility based on a non-intrusive approach allows infrared measurement of steady state temperature distribution on the optimal structure under prescribed boundary conditions.

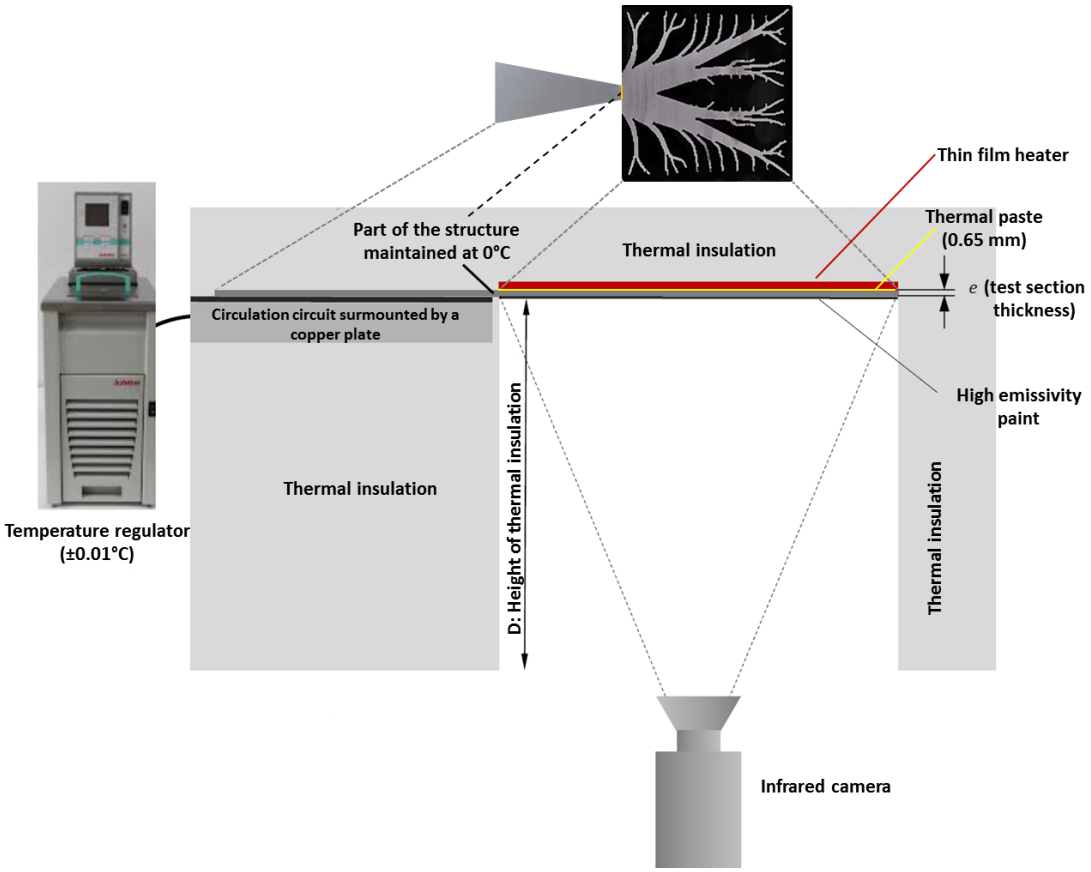

Figure 7: Schematic representation of the experimental test bench.

4.4. Calibration of the IR camera

The temperature measurements on the optimal structure are carried out by IR thermography. It is a very convenient and powerful way to capture the steady state temperature distribution as it allows non-intrusive measurements with a very high spatial resolution. The Cedip Titanium 550M IR camera with a InSb quantum detector is used in this experiment. The technical specifications of this IR camera are listed in table 2. In addition to this, the test section is equipped with a curtain system to shield the thermal scene from surrounding environmental radiations.

Focal length	Field of view ($\theta_H \times \theta_V$)	Aperture	Pixels (resolution)	Sensor size (pitch)	Spectral band
50 mm	$11° \times 8.8°$	$f/2.0$	320×256	30 μm	3.6 -5.1 μm

Table 2: Infrared camera specifications.

The IR camera is calibrated before each measurement. An infrared camera is a "photon counting device". Depending on the number of photons received, it returns an electrical voltage (in volts) expressed as a digital level (DL). A non-linear transfer function can convert

the digital levels returned by the camera into temperatures. The purpose of calibration is to define this experimental transfer function. The calibration is made over the camera measurement range in order to extract a polynomial function that links the "Object Signal" OS (in digital level DL) captured by the IR camera to the "Uniform Temperature" (in $°C$) of the calibration plate as measured by the k-type thermocouple. Figure 8 below shows the calibration curve obtained from this procedure [25].

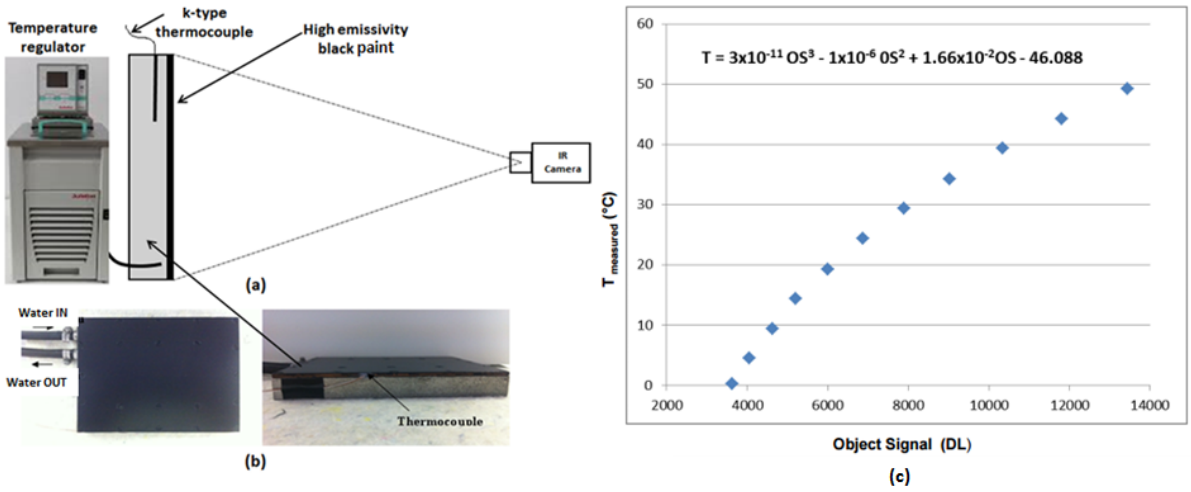

Figure 8: a) Calibration set up; b) Calibration plate (black body), and c) Calibration curve for the infrared camera.

4.5. Experimental procedure

For performing IR measurement, the thin film heater provides a surface heat flux of 588 W/m^2 over the surface of the test section. The heat sink temperature is maintained at $0°C$ at the isothermal boundary (see figure 1(b), $T = T_0$). All other boundaries are well insulated except for the bottom face. The steady-state is achieved when the temperature values in the domain stops changing and then the IR measurements are taken on the bottom face. The raw images from the IR camera are then post-processed in Matlab® to better interpret the results.

The heat transfer problem in this experiment is analysed under steady-state conditions. Steady-state conditions are sometimes difficult to attain due to the sensitivity of the experimental set up to the surrounding environment. However, due to the relatively small scale of the test section (100 mm x 100 mm x 1.5 mm) and efficient use of insulation materials, steady state conditions were reached with less effort. Nevertheless, all the IR acquisitions were made when the temperature values in the domain stopped changing after keeping the test section operating under thermal loads and boundary conditions for a significant amount of time ($\geq$ 15 hours). Figure 20 shows the objective function approaching steady for the two structures with $\phi_{max} = 28.6$ % and $\phi_{max} = 17.92$ % Al, respectively.

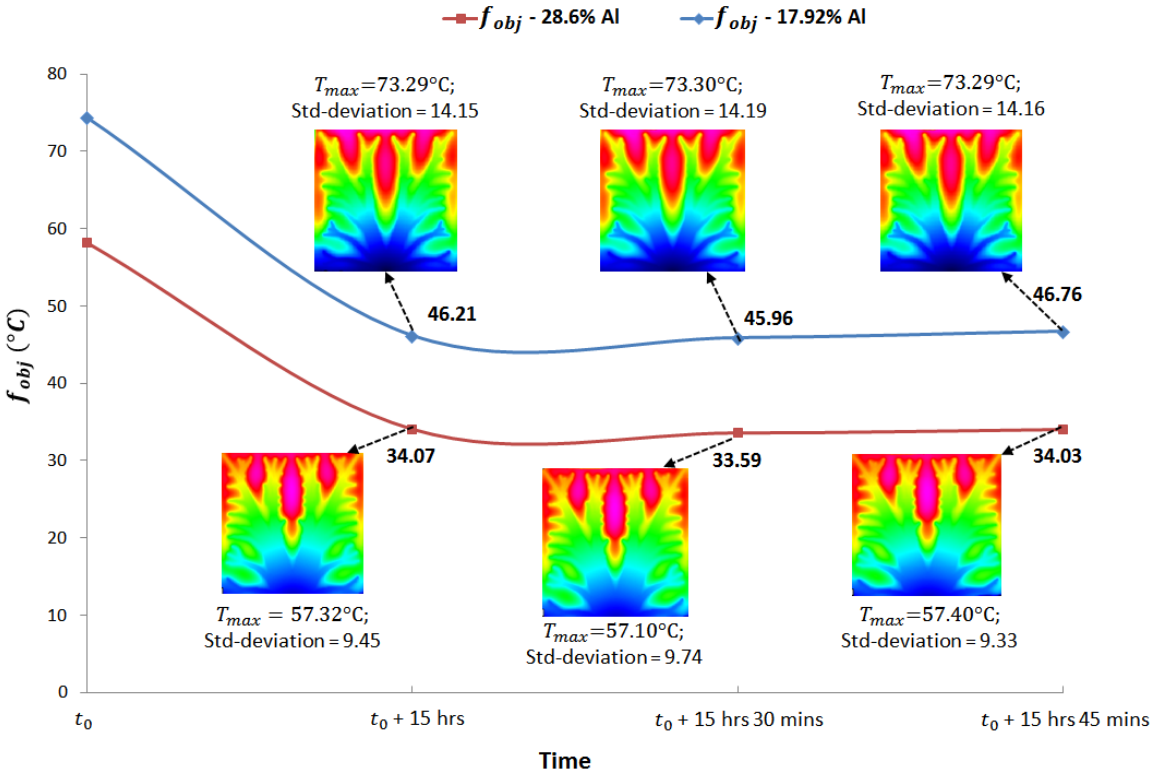

Figure 9: IR images acquired at steady state for $\phi_{max} = 28.6$ % and $\phi_{max} = 17.92$ % with $T_0 = 0°C$.

It is important to note that small fluctuations always exist in IR acquisitions as each film presented here is acquired over an average of 100 images in order to eliminate all the time noise [25].

5. CFD simulations

The results obtained from IR thermal acquisitions cannot be compared directly to those obtained from the TO solver (because the TO obtained structures contain slightly intermediate density values and also a no sharp black-to-white or 1-to-0 interface). Instead, the slightly modified optimal structures obtained from TO (refer figure 2) are simulated into a 3D CFD conjugate heat transfer numerical solver to mimic exactly the same initial and boundary conditions that exist during the experiments. In this way, one can efficiently investigate the thermal performance of the topology optimized structure by drawing a direct comparison between the CFD numerical results and IR thermal measurements.

The computational domain for the CFD simulation used in STAR-CCM+® commercial software is represented in figure 10.

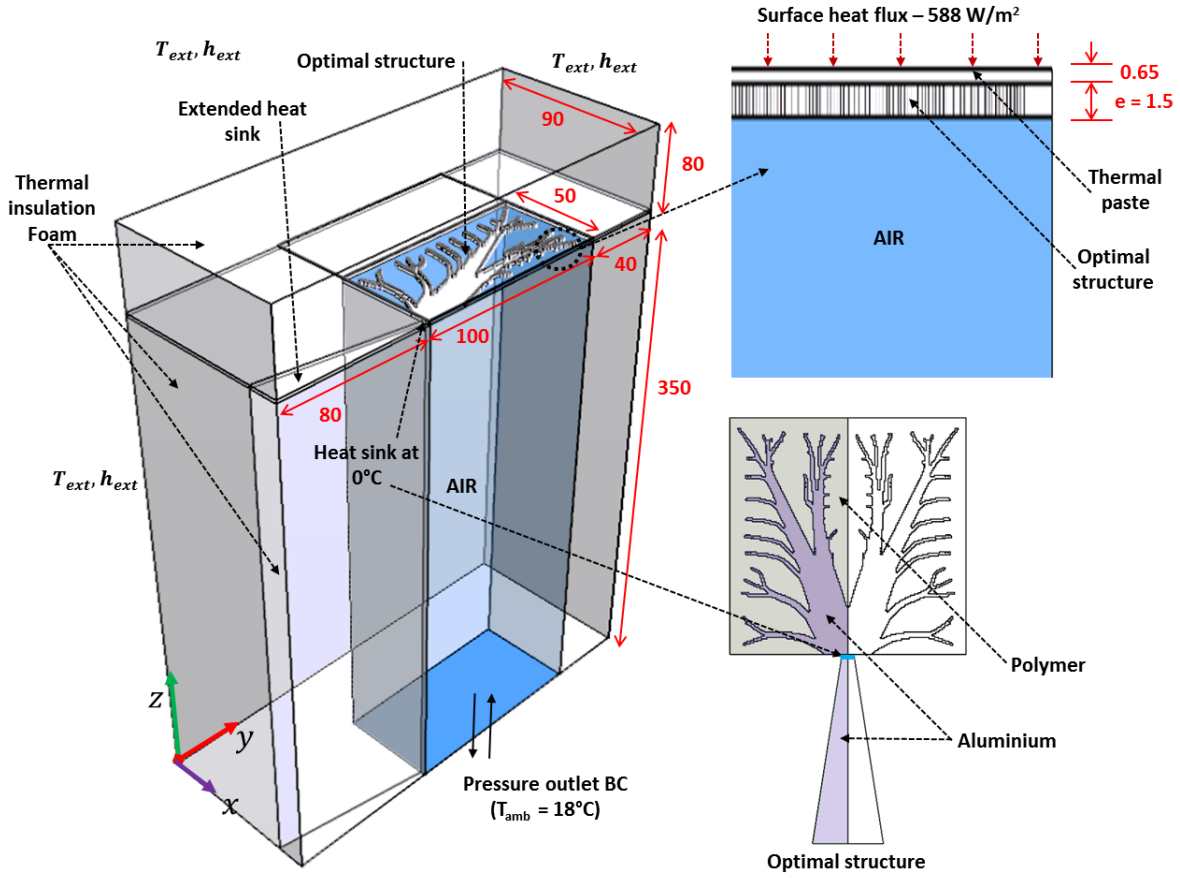

Figure 10: Axisymmetric computational domain in *mm*.

Two important phenomena of heat conduction in the test section and natural convection in the air beneath the heated plate needs to be modeled. Natural convection is modeled with incompressible ideal gas density model with the gravity in z direction and energy equation turned on. As the computational domain is axisymmetric only one half of the domain is modeled to enhance computational speed. Rayleigh number based on film temperature of the air beneath the heated test section of length L ($L = 100\ mm$) is found to be less than 10^9 for the current domain as a result the flow is considered to be laminar [26]. The important parameters and flow conditions for the CFD simulation are as follows:

- *Material*: Air (incompressible ideal gas); Aluminum; polymer; thermal paste and insulation material. Rigid polyurethane foam is used as the insulation material. The properties of air required for simulation is calculated at film temperature which varies for each case. The important thermal properties of all other materials are listed below in table 3.
- *Geometry (in mm)*: Test section = $100 \times 50 \times 1.5$; height of the insulation (D) = 350; length of extended heat sink = 80; axisymmetric model.
- *Mesh*: 1.52 million hexahedral cells, structured mesh; first cell height of 0.1 mm in the fluid domain.

– *Boundary conditions*: Surface heat flux of 588 $W\ m^{-2}$; bottom open surface: pressure outlet boundary condition; heat sink wall temperature = 0°C; ambient surrounding conditions elsewhere (T_{ext}, h_{ext}) .

– *Solver:* 3D steady-state coupled implicit solver; laminar flow; gravity in z-dimension: -9.81 $m\ s^{-2}$.

Material properties	Thermal paste	Aluminium	Epoxy resin	Insulation
k (Thermal conductivity, $W\ m^{-1}\ K^{-1}$)	0.247	214.04	0.1967	0.022
ρ (Density, $kg\ m^{-3}$)	1100	2700	1100	33
C_p (Specific heat, $J\ kg^{-1}\ K^{-1}$)	1396.3	891	1522.72	1450

Table 3: Material properties for CFD simulations.

6. Results

Separate IR thermal measurements are performed on two distinct optimal structures obtained from TO for different volume fractions of 17.92 % and 28.6 %, respectively. The acquired data are then transformed into Matlab® format and gathered into a matrix. Figure 11 is an example of an acquired raw IR thermal image. It represents the object signal in digital levels (DL) at different position of space (in pixels). All acquired images are then cut out in order to save only data corresponding to the square domain of 100 $mm \times 100\ mm$ under consideration. The calibration curve is used to convert these DL into temperatures.

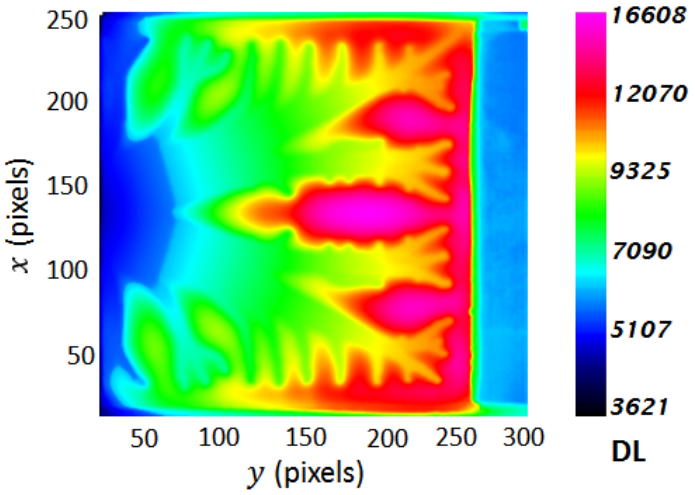

Figure 11: Recorded IR data in DL.

Similarly, 3D CFD simulations are performed in STAR-CCM+ for the two optimal structures to obtain steady state temperature profiles. To better compare the results obtained

from the two sources, the temperature and the lengths are normalized as follows:

$$\tilde{T} = \frac{T - T_{min}}{T_{max} - T_{min}} \tag{6}$$

$$\tilde{x} = \frac{x}{L_x} \tag{7}$$

$$\tilde{y} = \frac{y}{L_y} \tag{8}$$

where $\tilde{T}$ is the normalized temperature, T_{min} is the minimum temperature in the structure (isothermal boundary at the heat sink, T_0), T_{max} is the highest temperature observed in the structure for each measurement and T is the actual temperature in $^{\circ}C$ at each pixel (IR measurement) or cell (CFD simulation). Similarly, $\tilde{x}$ and $\tilde{y}$ are the normalized x and y-coordinates, respectively, and, L_x and L_y are the maximum dimension in x and y-directions, respectively.

Apart from this, experimental investigations are also performed by changing the heat sink boundary condition (figure 1(b), $T = T_0$). The objective is to examine the thermal behavior of the existing structure at different heat sink temperatures and comparing the results with CFD simulations. In addition to the classical heat sink temperature of $0^{\circ}C$, measurements were also performed for heat sink temperatures of $2.5^{\circ}C$and $5^{\circ}C$ with all other boundary conditions unchanged.

Finally, same experiments are repeated on the additional fabricated sample of the two specified volume fractions (see figure 6(a)) in order to ensure reproducibility of results.

6.1. Steady state temperature measurements on the optimal structure

For the optimal structure with $\phi_{max} = 28.6$ % (see figure 12(b)), figure 12(a) shows the normalized steady state temperature field and isotherms as obtained by CFD simulations, whereas figure 12(c) demonstrates the results obtained by IR thermal measurements. In the IR measurements, an average temperature (f_{obj}) of $34.03^{\circ}C$ and a maximum temperature (T_{max}) of $57.40^{\circ}C$ are observed in the domain. On the other hand, CFD simulations provide an average temperature and maximum temperature of $35.41^{\circ}C$ and $60.02^{\circ}C$, respectively.

The accuracy and high spatial resolution of the IR thermography method facilitates clear visualization of heat transfer from individual branches of the tree structure (see figure 12(c)). As a consequence, the value of objective function and maximum temperature measured by IR thermography and to those obtained by CFD simulations are very close.

To further investigate the comparison between the results obtained by IR measurements and CFD, the temperature profiles are extracted and compared at five different locations in the domain (see figure 12(b)), the process being termed here as "line probe measurements". These line probe measurements are performed at three horizontal and two vertical lines in the domain and compared with the CFD data. Figure 12(d) and 12(e) show the temperature profiles at vertical lines $\tilde{x} = 0$ and $\tilde{x} = 0.45$, respectively. Figure 12(f), 12(g) and 12(h) show the temperature profiles at horizontal lines $\tilde{y} = 0.2$, $\tilde{y} = 0.5$ and $\tilde{y} = 0.8$, respectively. The temperature profiles measured at these locations clearly demonstrate the closeness of the

results obtained from CFD and IR measurements. Moreover, when examined closely, one can clearly observe the accuracy with which the IR thermography in the current experimental set-up captures even the smallest of the temperature changes in the system.

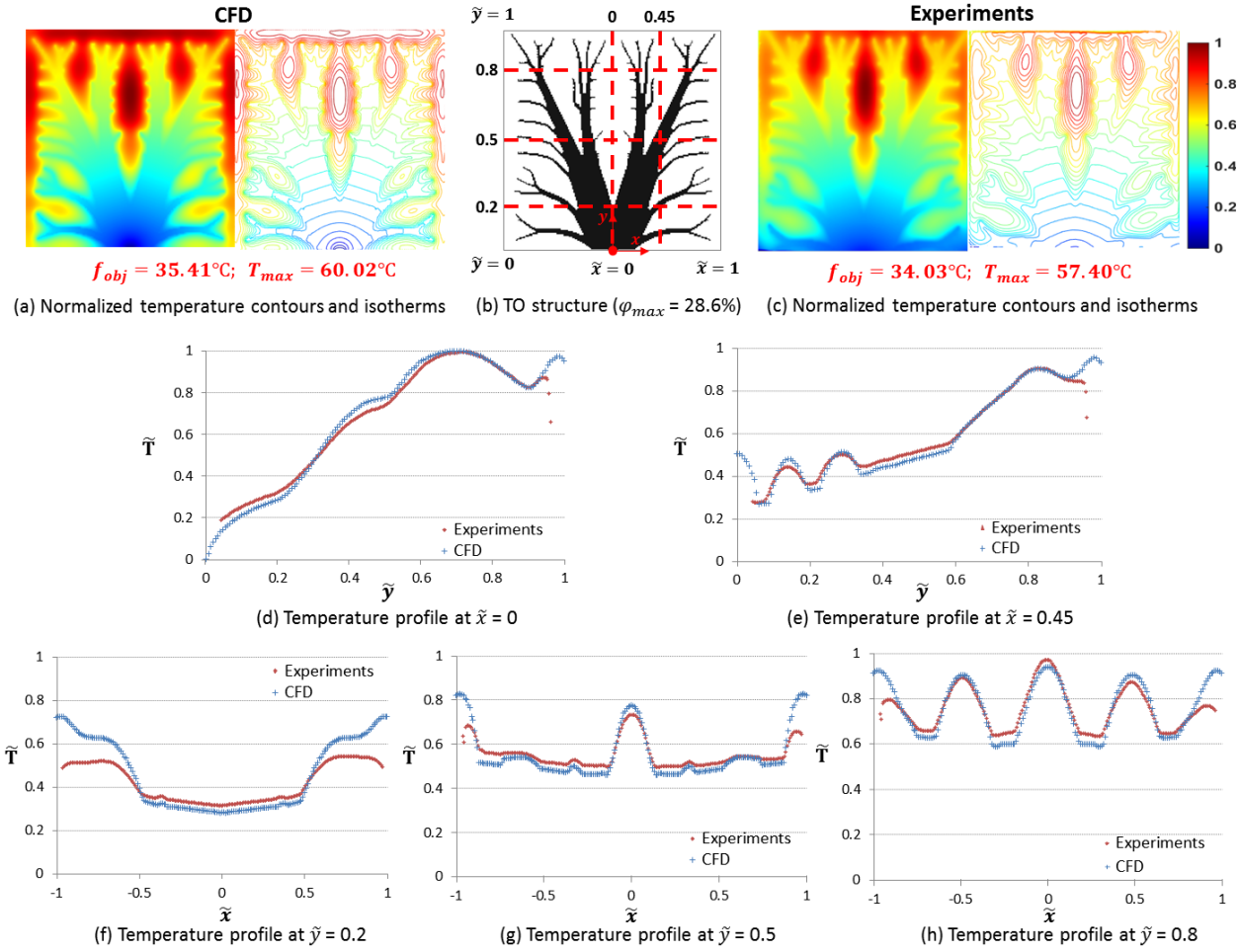

Figure 12: Normalized steady state temperature measurement for the topology optimized structure with $\phi_{max} = 28.6$ % and $T_0 = 0°C$.

Another important observation that can be made in figure 12 from the temperature contours and the line probe measurements is the significant temperature drop that occurs near the edges of the domain for the experimental results. Although important precautions are made to ensure good insulation at edges in the experimental set-up, it is very difficult to reproduce a near-perfect insulating boundaries like those modelled in the CFD simulations. A marginal part of test-section (up to 2 mm) is even inserted inside the insulation foam to establish a good insulation during the experiments (figure 13(a)). Hence, the small differences that exists between the two results can be attributed to the conditions prevailing at the boundary, in other words the heat loss from the boundary.

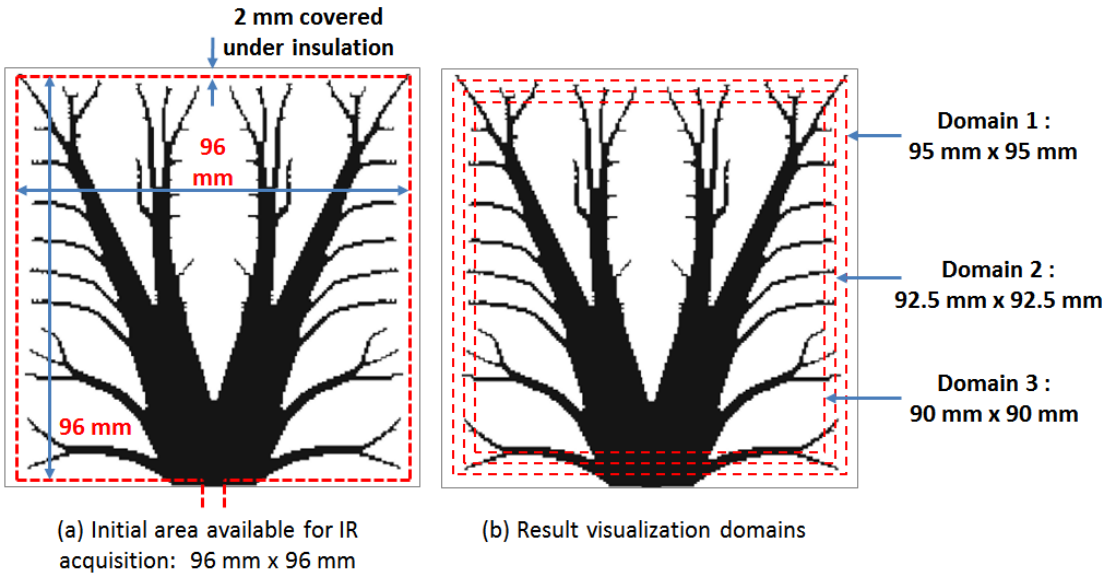

Figure 13: Quantifying the influence of heat loss from the edges - (a) Original area available for IR acquisition after placing the insulation foam in the experiments; (b) Creating three new domains for result visualization.

To quantify the differences in the results due to the heat loss from the edges, the results from CFD and IR experiments are again compared at three different domains obtained by cutting marginal area from the edges of the complete domain (figure 13(b)). Thus, three new domains are created for the dimensions of 95 mm x 95 mm, 92.5 mm x 92.5 mm and 90 mm x 90 mm, respectively and the objective function and maximum temperature is re-evaluated for the new domains.

Figure 14 shows the comparison of normalized temperature contours and isotherms between CFD results and IR measurements in the newly created three domains for visualization. It can be clearly seen that the temperature contours obtained from both the sources become almost exactly similar as the domain under consideration shifts away from the actual boundary (100 mm x 100 mm), especially in domain 3 where the objective functions for the two results become very close.

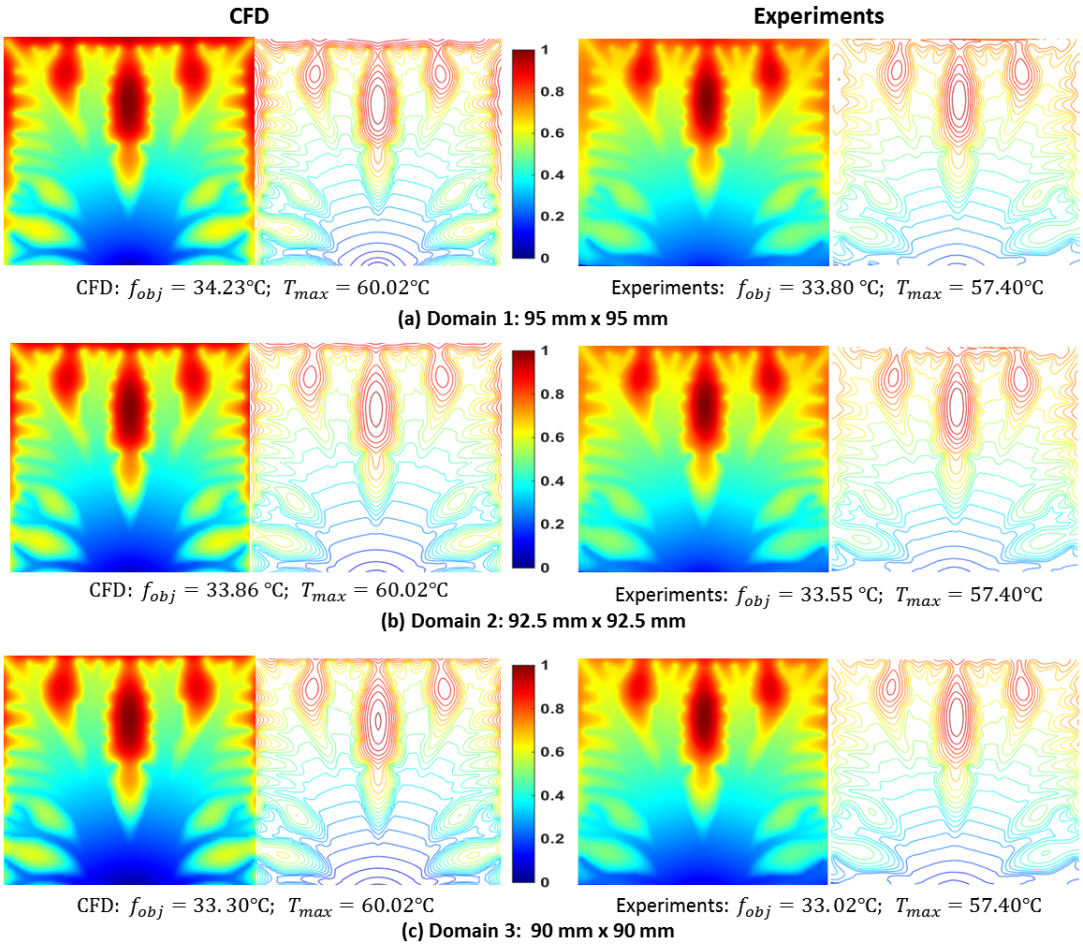

Figure 14: Quantifying the influence of heat loss from the edges (for ϕ_{max} = 28.6 % and $T_0 = 0°C$) - Normalized temperature contours and isotherms at the three new domains: (a)95 mm x 95 mm, (b) 92.5 mm x 92.5 mm and (c) 90 mm x 90 mm.

Figure 15 demonstrates the change in $|\Delta T|$ values on changing the result visualization domain, where $|\Delta T|$ for each domain is evaluated as follows :

$$|\Delta T_{avg}| = |(T_{avg})_{CFD} - (T_{avg})_{IR}| \tag{9}$$

$$|\Delta T_{max}| = |(T_{max})_{CFD} - (T_{max})_{IR}| \tag{10}$$

From figure 15, it is clearly evident that the farther one moves away from the actual boundary, the lesser is the influence of heat loss from the edges and, as a result, there is a significant decrease in $|\Delta T_{avg}|$. However, there is no change in the values of $|\Delta T_{max}|$, which entirely is dependent on the location of maximum temperature in the domain. This shall be discussed later in the article.

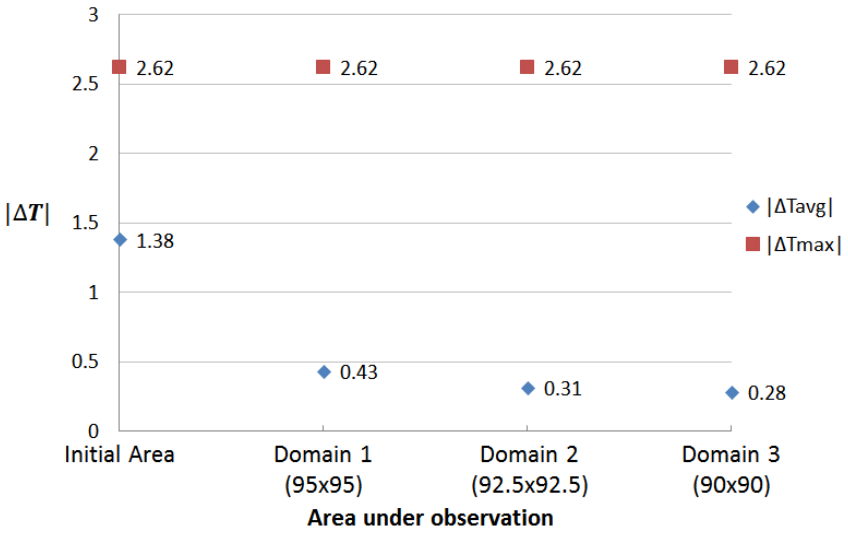

Figure 15: Quantifying the influence of heat loss from the edges (for $\phi_{max} = 28.6$ % and $T_0 = 0°C$) - Variation in $|\Delta T|$ on changing the result visualization domain.

Likewise, for the optimal structure with 17.92 % volume fraction of aluminum, figures 16(b), 16(a) and 16(c) illustrate the normalized steady state temperature field and isotherms obtained by CFD simulations and IR measurements, respectively. For the IR measurements, an average temperature (f_{obj}) of 46.76° and a maximum temperature (T_{max}) of 73.29°C is observed in the domain, whereas CFD simulations provide an average temperature and maximum temperature of 47.92°C and 80.25°C, respectively.

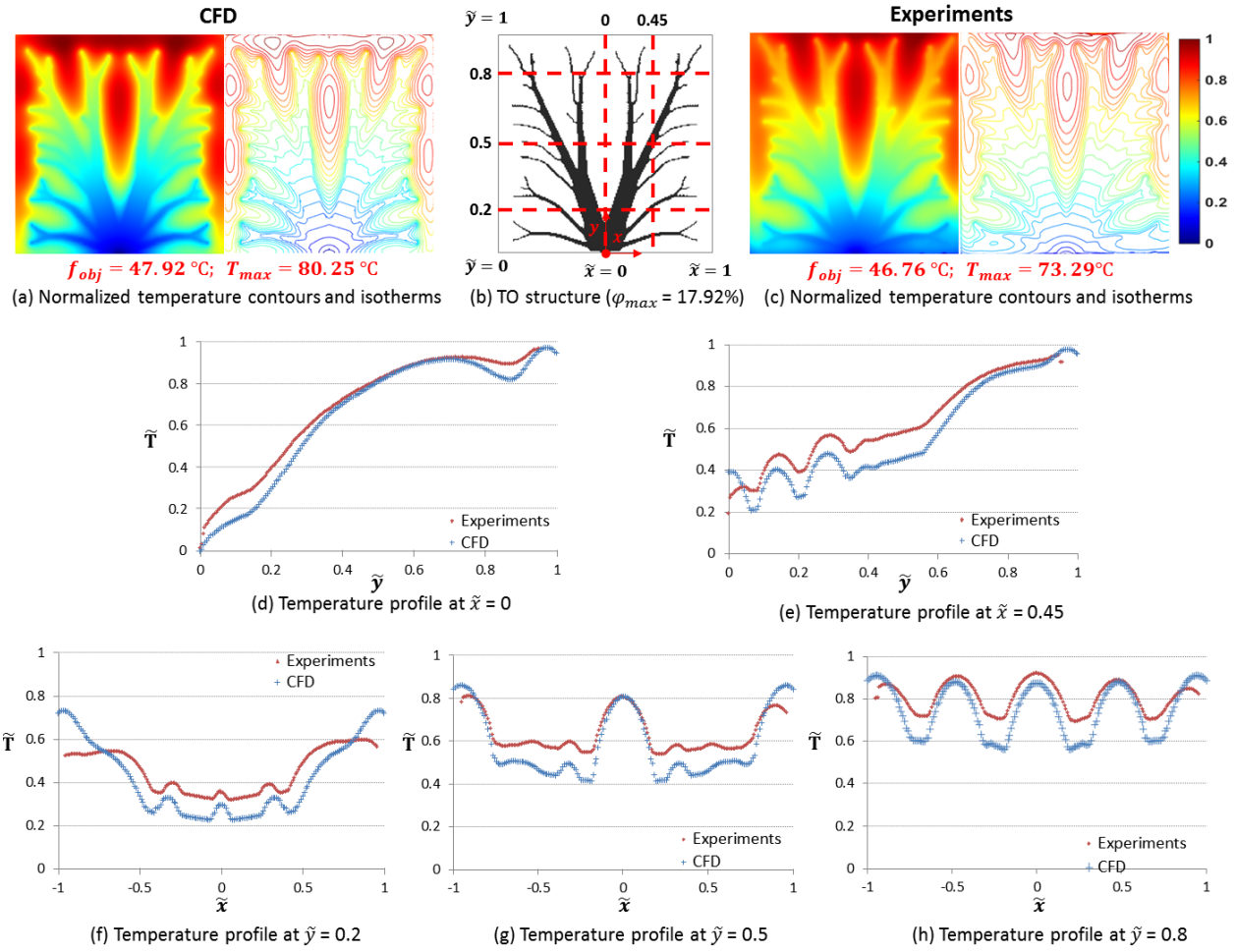

Figure 16: Normalized steady state temperature measurement for the topology optimized structure with $\phi_{max} = 17.92$ % and $T_0 = 0°C$.

The values of objective function (i.e. the average temperature) are in good agreement for the two results, however unlike the previous structure with 28.6 % aluminum, there is a significant difference between the values of maximum temperature observed in the domain. The average temperature is obtained by taking an average of temperature values occurring at each cell/pixel in the domain. However, the maximum temperature occurs at one particular cell/pixel in the whole domain also referred as "hot spot" [2] . The reason for the dissimilarity in the IR results for the two structures lies in the location where the maximum temperature occurs in the domain (see figure 17). In the optimal structure with 28.6 % Al, T_{max} occurs at a considerable distance from the edges, whereas it occurs very close to the boundary in the optimal structure with 17.92 % Al and hence for the latter case, the value of T_{max} is significantly affected by the conditions prevailing at the boundary.

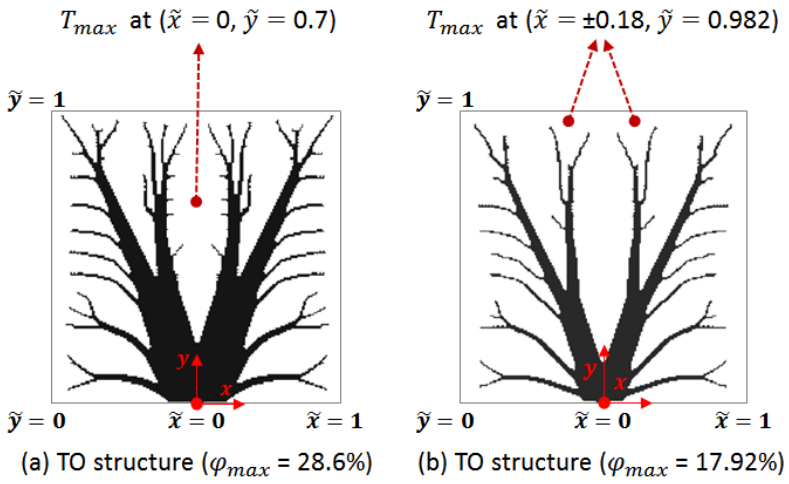

Figure 17: Location of T_{max} ("hot spots").

Figure 16(d) and 16(e) show the temperature profiles at vertical lines $\tilde{x} = 0$ and $\tilde{x} = 0.45$, respectively, and figures 16(f), 16(g) and 16(h) show the temperature profiles at horizontal lines $\tilde{y} = 0.2$, $\tilde{y} = 0.5$ and $\tilde{y} = 0.8$, respectively. The temperature profiles at these five locations demonstrate fairly good agreement between results obtained from CFD simulations and IR measurements. However for the line probe measurements, the differences in the temperature profiles between CFD and IR experiments are slightly higher as compared to the optimal structure with 28.6 % Al (refer figure 12 and 16).

The IR thermal measurements for the two structures were performed at an ambient room temperature of around $18°C$. The average temperature in the domain for the structure with 28.6 % Al and 17.92 % Al are $34.03°C$ and $46.76°C$, respectively. Similarly, the maximum temperature in the domain for the two structures are $57.40°C$ and $73.29°C$, respectively. Evaluating the temperature gradient that exist between the test section and the surrounding environment as follows:

$$(\Delta T_{amb})_{avg} = |T_{avg} - T_{amb}| \tag{11}$$

$$(\Delta T_{amb})_{max} = |T_{max} - T_{amb}| \tag{12}$$

From the above equation, the temperature gradient with the surrounding for the two structures are as follows:

For tree structure with 28.6 % Al :

$$(\Delta T_{amb})_{avg} = |34.03 - 18| = 16.03°C \tag{13}$$

$$(\Delta T_{amb})_{max} = |57.40 - 18| = 39.4°C \tag{14}$$

For the tree structure with 17.92 % Al :

$$(\Delta T_{amb})_{avg} = |46.76 - 18| = 28.46°C \tag{15}$$

$$(\Delta T_{amb})_{max} = |73.29 - 18| = 55.29°C \tag{16}$$

The above results show that the temperature gradient between the surrounding environment and the test section is higher for the tree structure with 17.92 % Al and as a consequence there is relatively more heat loss from the insulating boundaries and the bottom face exposed to the environment. This is the primary reason for comparatively higher differences between CFD results and IR measurements for the optimal structure with less conductive material.

Finally, to quantify the differences in the results due to the heat loss from the boundaries, the results from CFD and IR experiments are compared again at three different domains as described earlier (see figure 13). For the optimal structure with 17.92 % Al, figure 18 shows the comparison of normalized temperature contours and isotherms between CFD results and IR measurements in the newly created three domains of visualization and figure 19 demonstrates the change in $|\Delta T|$ values on changing the result visualization domain.

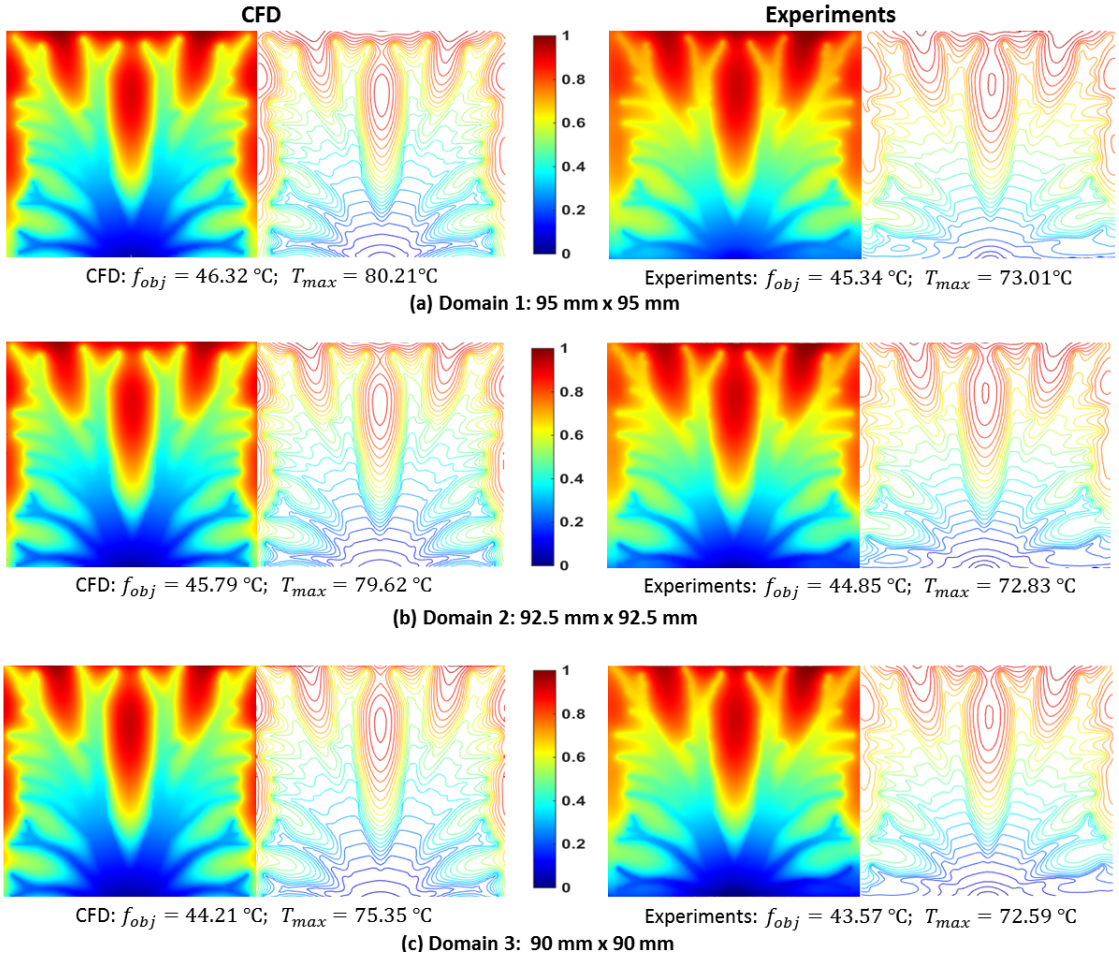

Figure 18: Quantifying the influence of heat loss from the edges (for ϕ_{max} = 17.92 % and T_0 = 0°C) - Normalized temperature contours and isotherms at the three new domains: (a)95 mm x 95 mm, (b) 92.5 mm x 92.5 mm and (c) 90 mm x 90 mm.

As quantified earlier, there is a significant reduction in $|\Delta T_{avg}|$ values for the structure with 17.92 % Al. However, unlike the previous structure (28.6 % Al), there is even greater reduction in the values of $|\Delta T_{max}|$ for this structure as the domain under observation shifts away from the actual boundary. This is primarily due to the location of hot spot in the domain as explained earlier.

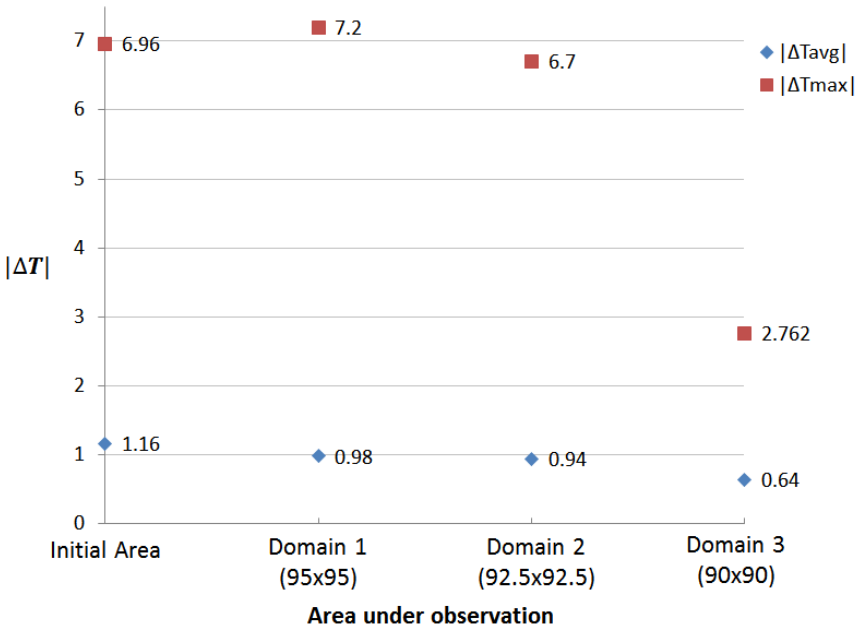

Figure 19: Quantifying the influence of heat loss from the edges (for $\phi_{max} = 17.92$ % and $T_0 = 0°C$) - Variation in $|\Delta T|$ on changing the result visualization domain.

6.2. Mesh independence study

To establish accuracy of the CFD solution, it is important to ensure that the obtained numerical results are independent of the mesh resolution. The grid convergence study is accomplished by performing the same CFD simulation on seven different meshes and monitoring the values of the objective function and maximum temperature on the converged solution. Subsequently, the relative percentage error is evaluated for each case and a suitable mesh is selected when the solution stops changing on further increasing the mesh size. This process is performed on the two different optimal structures.

Figures 20 and 21 represent the results for the mesh independence study performed on the optimal structure with $\phi_{max} = 28.6$ % and $\phi_{max} = 17.92$ %, respectively. For both the optimal structures, the value of f_{obj} and T_{max} becomes stable (within an acceptable range of around ≈ 0.1 % relative error) for a mesh size of 1.52 million cells. Consequently, a mesh size of 1.52 million cells is used for all the CFD simulations performed in the present study.

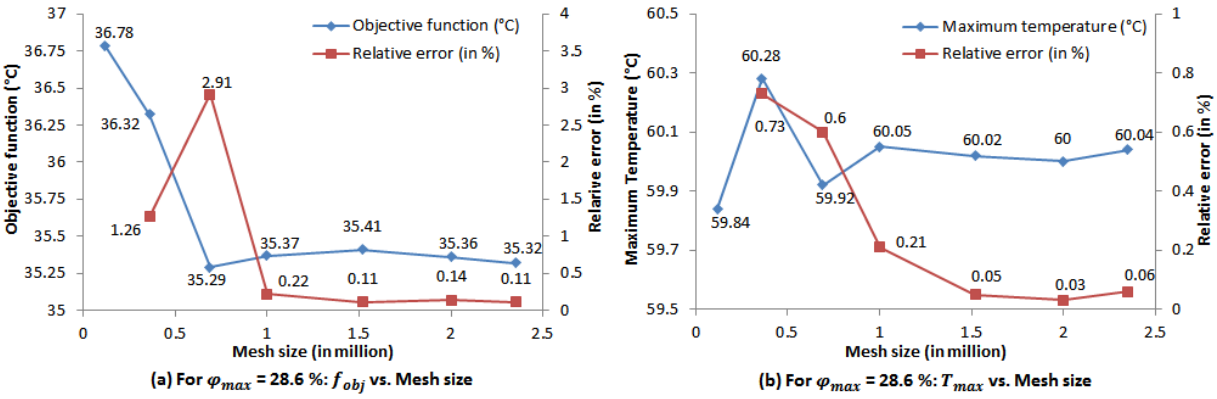

Figure 20: Mesh independence study for the optimized structure with $\phi_{max} = 28.6$ %.

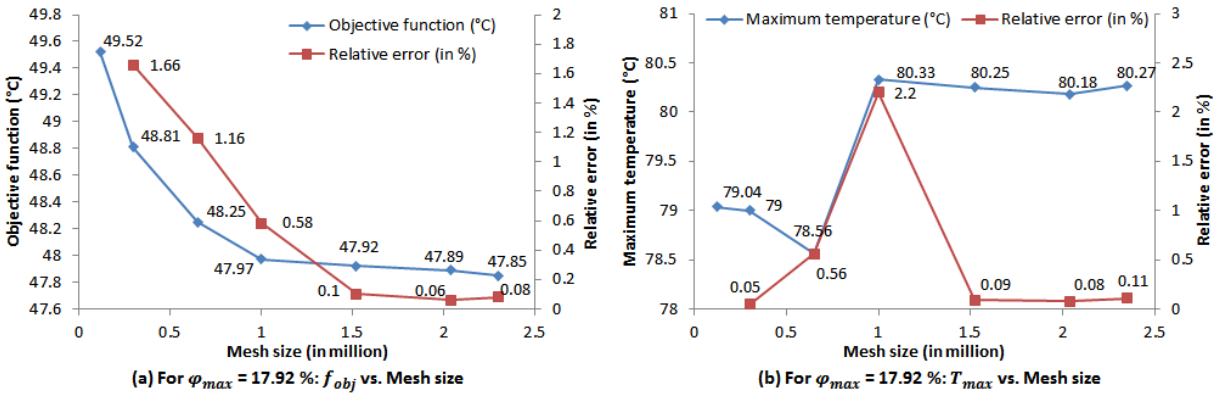

Figure 21: Mesh independence study for the optimized structure with $\phi_{max} = 17.92$ %.

6.3. Modified heat sink boundary condition

To investigate the thermal response of the existing optimal structure to boundary condition modifications, IR measurements and CFD simulations are again produced on the existing structures at two different values of heat sink temperature (T_0) of 2.5 $°C$ and 5 $°C$, respectively (see figure 1(b)). The objective is to test whether the thermal behaviour of the optimal structure changes or remains consistent on modifying the boundary conditions.

6.3.1. $T_0 = 2.5°C$

Figures 22 and 23 show the normalized steady state temperature fields, isotherms and line probe measurements obtained by CFD simulations and IR measurements for the optimal structure with 28.6 % Al and 17.92 % Al, respectively, when the heat sink boundary is maintained at 2.5 °C.

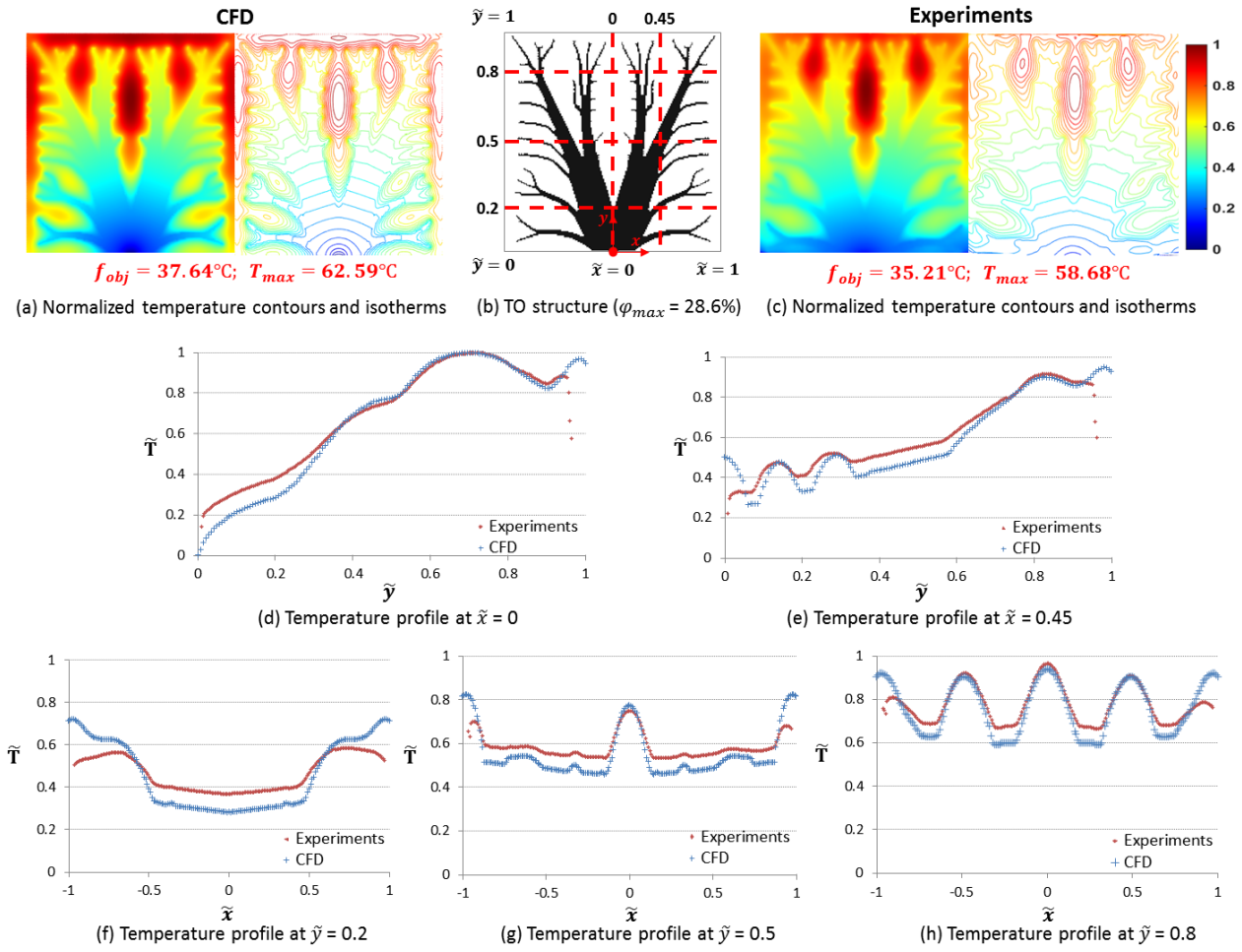

Figure 22: Normalized steady state temperature measurement for the topology optimized structure with $\phi_{max} = 28.6$ % and $T_0 = 2.5°C$.

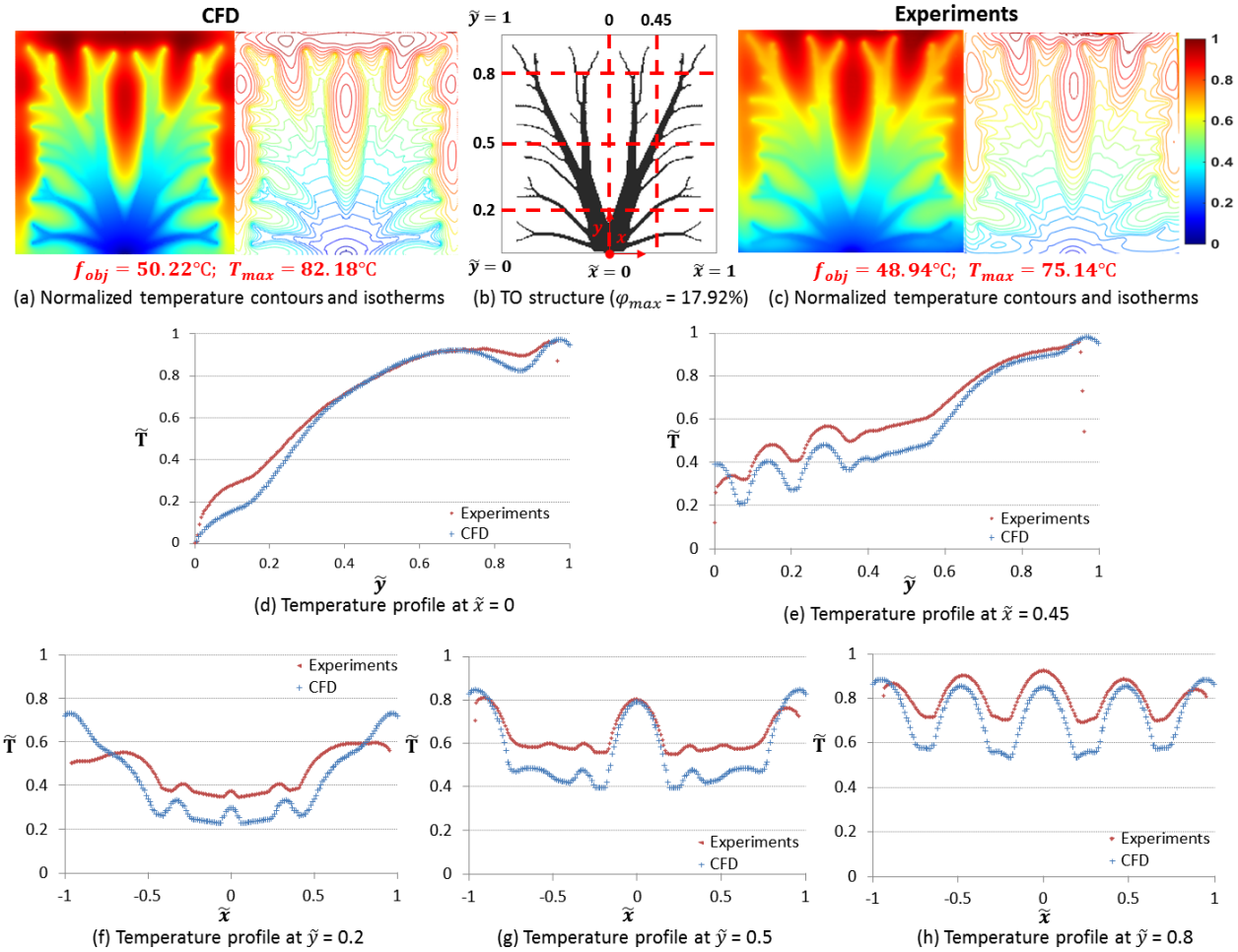

Figure 23: Normalized steady state temperature measurement for the topology optimized structure with $\phi_{max} = 17.92$ % and $T_0 = 2.5°C$.

Figures 24 summarises the change in $|\Delta T|$ values on changing the visualization domain for the optimal structure with 28.6 % Al and 17.92 % Al.

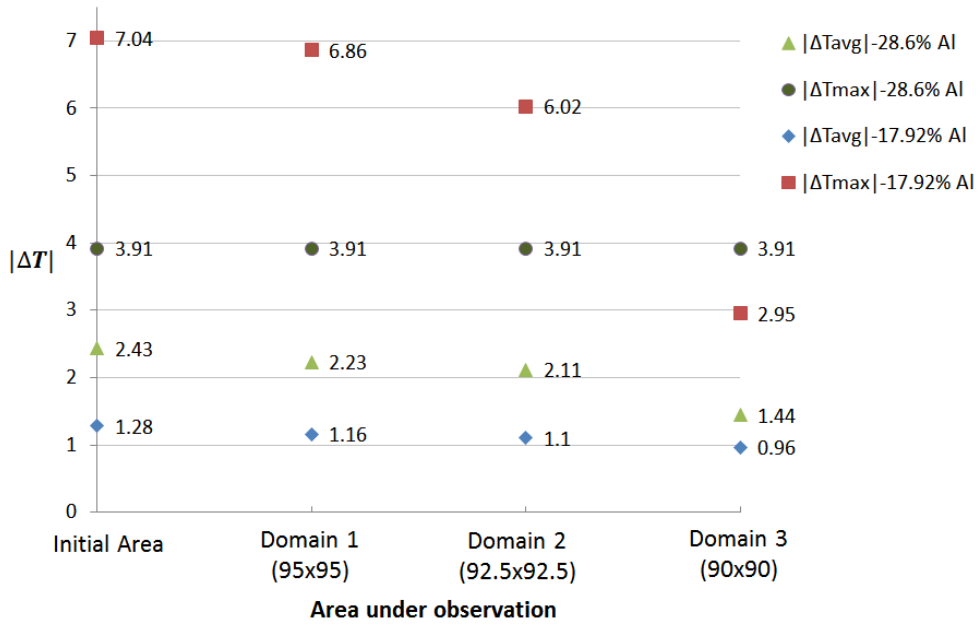

Figure 24: Quantifying the influence of heat loss from the edges (for $\phi_{max} = 28.6$ % and $\phi_{max} = 17.92$ % with $T_0 = 2.5°C$) - Variation in $|\Delta T|$ on changing the result visualization domain.

6.3.2. $T_0 = 5°C$

Similarly, for the heat sink boundary maintained at 5 °C, figure 25 and 26 shows the results obtained for the optimal structure with 28.6 % Al and 17.92 % Al, respectively.

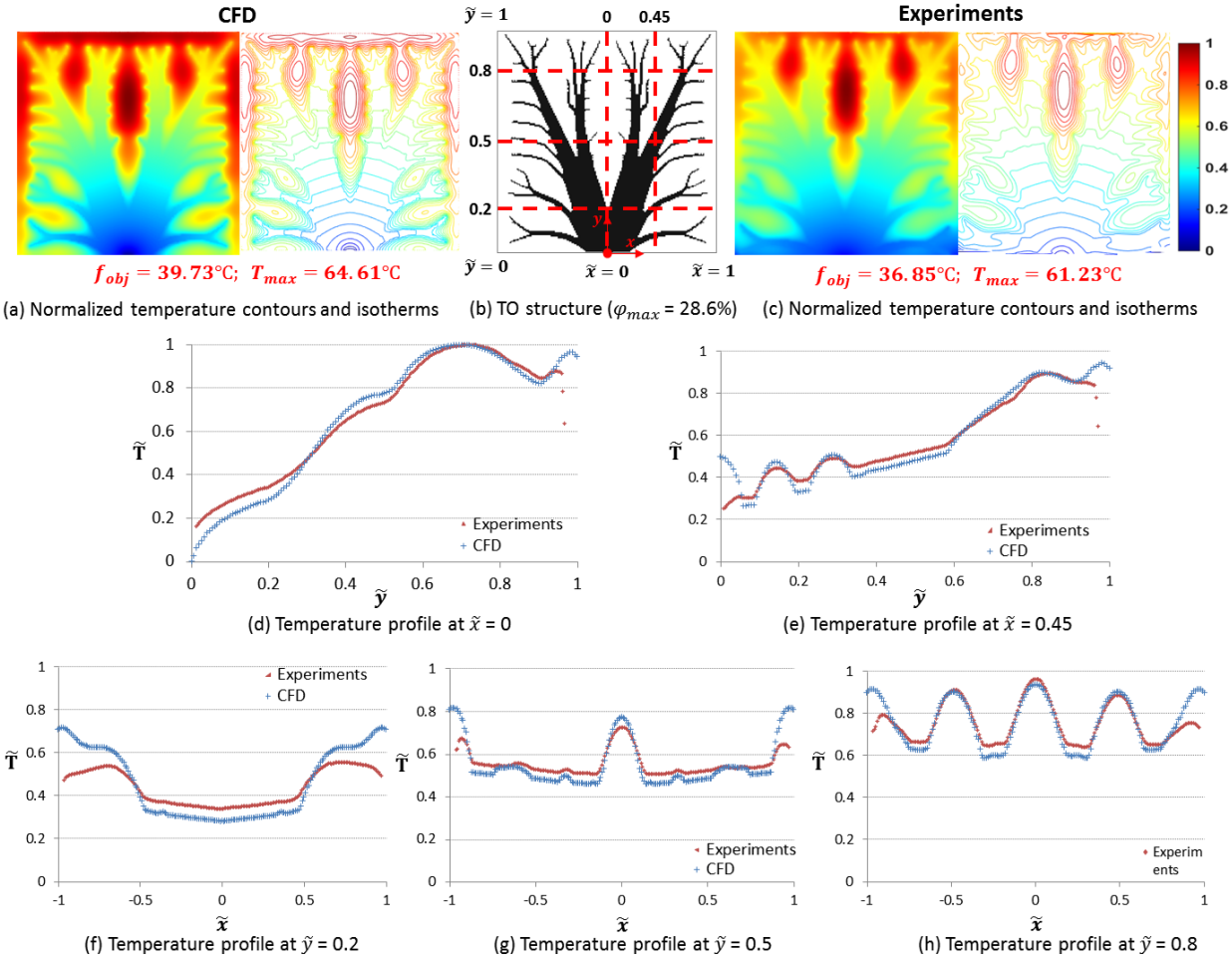

Figure 25: Normalized steady state temperature measurement for the topology optimized structure with $\phi_{max} = 28.6$ % and $T_0 = 5°C$.

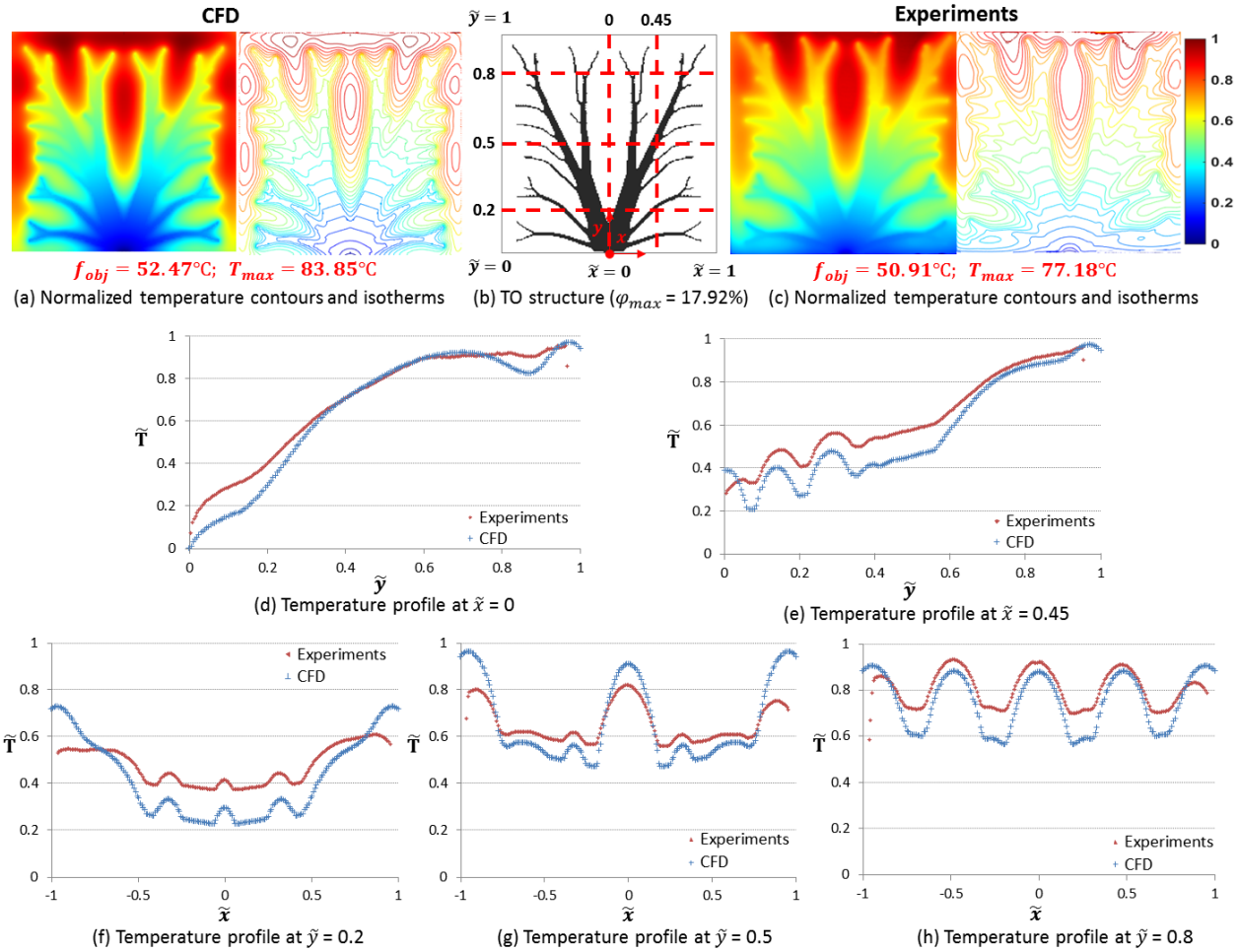

Figure 26: Normalized steady state temperature measurement for the topology optimized structure with $\phi_{max} = 17.92$ % and $T_0 = 5°C$.

Likewise, figure 27 summarises the influence of heat loss on the edges on $|\Delta T|$ values for the optimal structure with 28.6 % Al and 17.92 % Al. As seen previously, the value of $|T_{avg}|$ and $|T_{max}|$ decreases as the domain is moved away from the boundary.

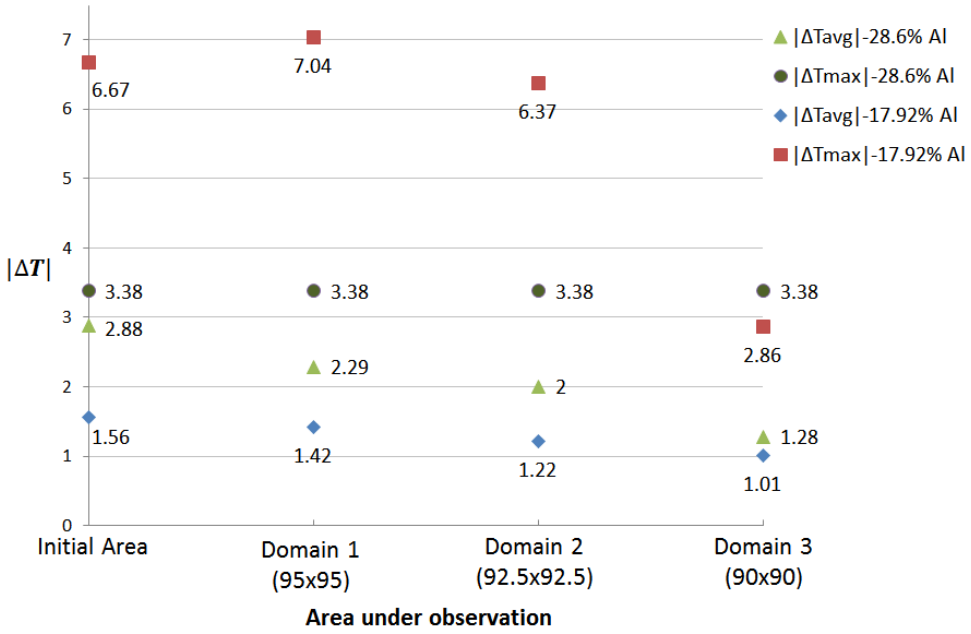

Figure 27: Quantifying the influence of heat loss from the edges (for $\phi_{max} = 28.6$ % and $\phi_{max} = 17.92$ % with $T_0 = 5°C$) - Variation in $|\Delta T|$ on changing the result visualization domain.

In all the above cases, there is a significant increase in the values of the objective function and the maximum temperature observed in the domain due to a decrease in the amount of heat getting removed from the heat sink boundary. But more importantly, the thermal behavior of both the optimal structures remains consistent with the classical case of heat sink boundary maintained at 0 $°C$. This can be well observed from the line probe measurements performed at the five locations. Also, as observed previously, the differences in the temperature profile between CFD and IR measurements are relatively higher for the tree structure with 17.92 % Al.

6.4. Reproducibility of results

To test the reproducibility of results, same experiments are performed again on additional samples fabricated for the two optimal structures with different ϕ_{max} values (refer figure 6(a)).

Figure 28(a) represents the temperature contours obtained from IR thermal measurement of the two fabricated sample with 28.6 % Al and figure 28(b) shows the reproducibility of results for the other two samples with 17.92 % Al.

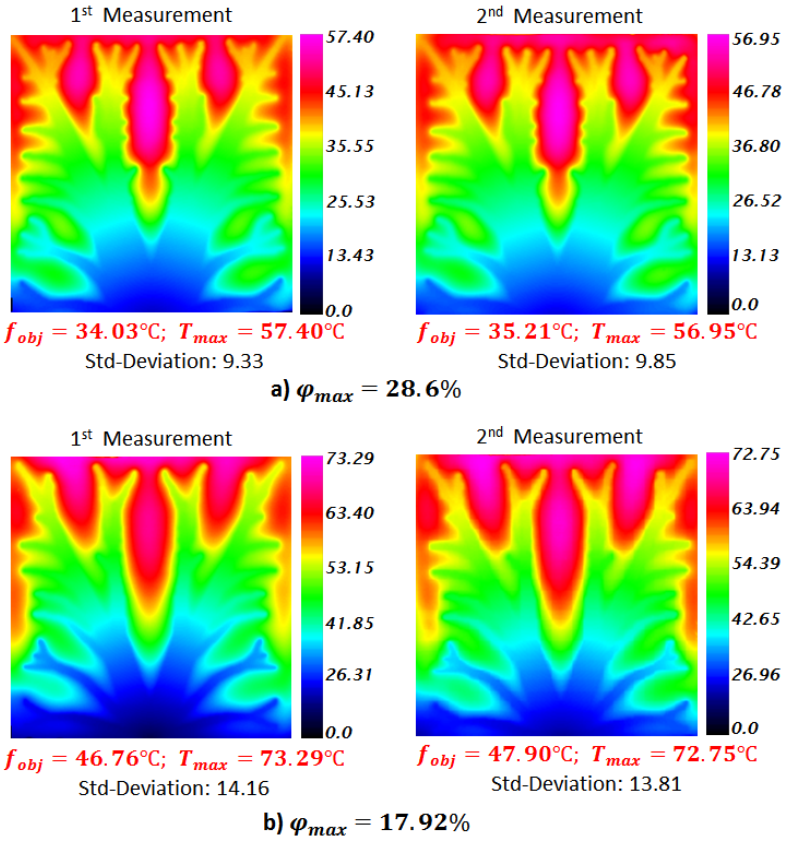

Figure 28: Reproducibility of IR measurements for a) $\phi_{max} = 28.6$ % and b)$\phi_{max} = 17.92$ % with $T_0 = 0$°C: Contours of temperature in $°C$.

Table 4 summarises the maximum temperature, average temperature and standard deviation for the two measurements.

S. No.	T_{max} $(°C)$	T_{avg} $(°C)$	σ
$\phi_{max} = 28.6$ %			
1^{st} Measurement	57.40	34.03	9.33
2^{nd} Measurement	56.95	35.21	9.85
$\phi_{max} = 17.92$ %			
1^{st} Measurement	73.29	46.76	14.16
2^{nd} Measurement	72.75	47.90	13.81

Table 4: Reproducibility of infrared measurements for $\phi_{max} = 28.6$ % and $\phi_{max} = 17.92$ % with $T_0 = 0$°C.

For both the optimal structures, the second set of measurements performed on the additional fabricated samples is in line with the first set of measurements with low differences.

7. Conclusion

This study is a first approach dedicated to experimental investigation of optimized conductive structures obtained by TO applied to volume-to-point heat conduction problem. There exists many numerical studies dedicated to the optimization of the VP configuration, however, to date and to author's knowledge, few experimental studies were conducted. The objective was to investigate experimentally the thermal performance of the topology optimized structure under some specific thermal loads and boundary conditions. The bi-material configuration obtained from TO was fabricated in aluminum-polymer combination and a non-intrusive method of infrared thermography was used to measure the steady state temperature distribution on the tree structure. CFD simulations were performed on the optimized structure with the same thermal loads and boundary conditions that existed during the experiments and the results were then finally compared to the experimental measurements.

As a first conclusion, the optimized structures obtained by TO were experimentally found to be effective in reducing the overall average temperature in the domain. The trees structures with higher ϕ_{max} values resulted in lower average temperature in the domain as a virtue of higher amount of conductive material and vice-versa.

Secondly, the values of objective function measured by IR thermography and those obtained by CFD simulations were found to be very close for the two optimal structures under observation with $\phi_{max} = 28.6$ % and $\phi_{max} = 17.92$ %, respectively.

However, for the maximum temperature in the domain (hot spot), there was a significant difference observed between the CFD and experimental results for the tree structure with $\phi_{max} = 17.92$ % which is due to the proximity of the location of hot spot to the boundary edges and as a result T_{max} is significantly affected by the conditions prevailing at the boundary.

Further experimental measurements were performed on existing optimal structures by modifying heat sink boundary conditions. The thermal behavior of the optimal structures remained consistent on modified boundary conditions.

Finally, results of IR measurements reproduced on additional fabricated samples for optimal structures were found to be in agreement with the original IR thermal measurements thus ensuring consistency of experimental results. As perspectives it will be very interesting to conduct in the future thermal experimental measurements on three-dimensional structures or optimal designs obtained numerically by topology optimization and to be fabricated by the additive manufacturing technology.

8. Acknowledgements

The authors appreciate and thanks Dr. Dmytro VASIUKOV from the Department of Polymers and Composites Technology and Mechanical Engineering at IMT Lille Douai, for his useful scientific discussions and his continuous efforts and guidance for selecting and preparing the appropriate polymer material applied in the present study.

References

[1] M. P. Bendsøe, N. Kikuchi, Generating optimal topologies in structural design using a homogenization method, Computer methods in applied mechanics and engineering 71 (2) (1988) 197–224.

[2] A. Bejan, Constructal-theory network of conducting paths for cooling a heat generating volume, International Journal of Heat and Mass Transfer 40 (4) (1997) 799813–811816.

[3] S. Wei, L. Chen, F. Sun, volume-point heat conduction constructal optimization with entransy dissipation minimization objective based on rectangular element, Science in China Series E: Technological Sciences 51 (8) (2008) 1283–1295.

[4] S. Wei, L. Chen, F. Sun, The area-point constructal optimization for discrete variable cross-section conducting path, Applied Energy 86 (7) (2009) 1111–1118.

[5] S.-b. ZHOU, L.-g. CHEN, F.-r. SUN, Entropy generation minimization for volume-point conduction based on constructional theory, Journal of Thermal Science and Technology 4 (2007) 004.

[6] Z. Xia, Z. Li, Z. Guo, Heat conduction optimization: high conductivity constructs based on the principle of biological evolution, in: Twelfth Int. Heat Transfer Conf., Grenoble, France, 2002, pp. 18–23.

[7] X. Xu, X. Liang, J. Ren, Optimization of heat conduction using combinatorial optimization algorithms, International journal of heat and mass transfer 50 (9) (2007) 1675–1682.

[8] M. P. Bendsoe, O. Sigmund, Topology optimization: theory, methods, and applications, Springer Science & Business Media, 2013.

[9] T. Dbouk, A review about the engineering design of optimal heat transfer systems using topology optimization, Applied Thermal Engineering 112 (2017) 841–854.

[10] J. Dirker, J. P. Meyer, Topology optimization for an internal heat-conduction cooling scheme in a square domain for high heat flux applications, Journal of Heat Transfer 135 (11) (2013) 111010.

[11] G. Marck, M. Nemer, J.-L. Harion, S. Russeil, D. Bougeard, Topology optimization using the simp method for multiobjective conductive problems, Numerical Heat Transfer, Part B: Fundamentals 61 (6) (2012) 439–470.

[12] Q. Li, G. P. Steven, O. M. Querin, Y. Xie, Shape and topology design for heat conduction by evolutionary structural optimization, International Journal of Heat and Mass Transfer 42 (17) (1999) 3361–3371.

[13] A. Gersborg-Hansen, M. P. Bendsøe, O. Sigmund, Topology optimization of heat conduction problems using the finite volume method, Structural and multidisciplinary optimization 31 (4) (2006) 251–259.

[14] A. Evgrafov, M. M. Gregersen, M. P. Sørensen, Convergence of cell based finite volume discretizations for problems of control in the conduction coefficients, ESAIM: Mathematical Modelling and Numerical Analysis 45 (6) (2011) 1059–1080.

[15] K. Svanberg, The method of moving asymptotesa new method for structural optimization, International journal for numerical methods in engineering 24 (2) (1987) 359–373.

[16] O. Sigmund, J. Petersson, Numerical instabilities in topology optimization: a survey on procedures dealing with checkerboards, mesh-dependencies and local minima, Structural optimization 16 (1) (1998) 68–75.

[17] A. Donoso, Numerical simulations in 3d heat conduction: minimizing the quadratic mean temperature gradient by an optimality criteria method, SIAM Journal on Scientific Computing 28 (3) (2006) 929–941.

[18] A. Shukla, A. Misra, Review of optimality criterion approach scope, limitation and development in topology optimization, International Journal of Advances in Engineering & Technology 6 (4) (2013) 1886.

[19] T. Dbouk, J.-L. Harion, Performance of optimization algorithms applied to large nonlinear constrained problems, American Journal of Algorithms and Computing 2 (1) (2015) 32–56.

[20] E. M. Dede, S. N. Joshi, F. Zhou, Topology optimization, additive layer manufacturing, and experimental testing of an air-cooled heat sink, Journal of Mechanical Design 137 (11) (2015) 111403.

[21] M. Bruyneel, P. Duysinx, C. Fleury, A family of mma approximations for structural optimization, Structural and Multidisciplinary Optimization 24 (4) (2002) 263–276.

[22] T. E. Bruns, D. A. Tortorelli, Topology optimization of non-linear elastic structures and compliant mechanisms, Computer Methods in Applied Mechanics and Engineering 190 (26) (2001) 3443–3459.

[23] O. Sigmund, Morphology-based black and white filters for topology optimization, Structural and Multidisciplinary Optimization 33 (4) (2007) 401–424.

[24] B. S. Lazarov, F. Wang, O. Sigmund, Length scale and manufacturability in density-based topology optimization, Archive of Applied Mechanics 86 (1-2) (2016) 189–218.

[25] FLIR Systems, Inc., 9 Townsend West Nashua, NH 03063 USA, The Ultimate Infrared Handbook for R&D Professionals (2012).

[26] T. L. Bergman, F. P. Incropera, D. P. DeWitt, A. S. Lavine, Fundamentals of heat and mass transfer, John Wiley & Sons, 2011.

Chapter 4

Topology optimization of conjugate heat transfer systems: A numerical investigation

Abstract: Finding optimal designs for conjugate heat transfer (CHT) systems is a very critical task as it requires consideration of both the heat transfer enhancement and pressure drop reduction in the system. These two design objectives are conflicting in nature. In this context, chapter 4 presents an innovative bi-objective optimization technique for topology optimization of CHT systems. The design goals are to maximize thermal power recovery and minimize pressure drop in the system, simultaneously. The two objective functions are combined linearly using a linear weighted sum method. The inequality constrained bi-objective TO method is developed inside the OpenFOAM® open source CFD software package using the Finite Volume Method (FVM) for flow field discretization and the continuous adjoint method for gradient computation. The adjoint equations and their associated boundary conditions are derived for the bi-objective function under consideration. The developed numerical solver couples the Method of Moving Asymptotes (MMA) optimizer to update the design variables with the Rational Approximation of Material Properties (RAMP) interpolation technique for material distribution in the domain.

The present developed numerical solver is applied to a 2D numerical example from literature to generate unconventional Pareto optimal solutions for steady-state incompressible flows at low to moderate Reynolds number. The obtained optimal structures are justified on the basis of an in-depth analysis performed in terms of convergence study, performance evaluation, local analysis of the results at the domain boundaries and order of magnitude analysis of the objective function values. It is observed that the present TO solver produces realistic optimal designs for CHT systems staring from pressure drop reduction to thermal power maximization based on the value of user-dependent weighing function. Apart from this, in order to analyze the influence of the discretization technique on the final optimal topologies, the results from the present FVM-based TO solver are compared to other studies from literature based on FVM and Lattice Boltzmann Method (LBM) by solving identical thermo-fluid optimization problems for the same objective functions. Comparison of the results for the objective function values of the obtained designs emphasized that the present FVM-based TO solver outperformed the existing FVM-based and LBM-based TO solvers from literature. To be specific, marginally higher thermal power is obtained but with 50% less pressure drop as compared to results from the LBM-based TO solver. In conclusion, the results of this work highlight that the performances associated with the "optimal" structures presented in literature could, in fact, be improved. These results further emphasize the importance of various detailed numerical analysis presented in this study to effectively justify optimal designs for coupled thermo-fluid systems obtained by topology optimization. This part of the thesis was published in International Journal of Heat and Fluid Flow, vol. 75, pp. 165-184,2019, https://doi.org/10.1016/j.ijheatfluidflow.2019.01.002

Résumé: La recherche de conceptions optimales pour les systèmes de transferts thermiques conjugués est une tâche complexe car elle nécessite de prendre en compte à la fois l'amélioration des transferts de chaleur et la réduction des pertes de charge dans le système. Ces deux objectifs de conception sont de nature antinomique. Ce chapitre présente une technique d'optimisation bi-objective innovante pour l'optimisation de la topologie des systèmes ou composants de transferts thermiques conjugués. Les objectifs de conception sont de conjointement maximiser le transfert d'énergie thermique et de minimiser la perte de charge dans le système. Les deux fonctions objectives correspondant à ces deux objectifs sont combinées linéairement en utilisant une méthode linéaire de somme pondérée. La méthode d'optimisation topologique bi-objective à contrainte d'inégalité est développée dans le progiciel Open Source OpenFOAM® en utilisant la méthode des volumes finis pour la discrétisation des champs de flux et la méthode adjointe continue pour le calcul des gradients. Les équations adjointes et leurs conditions aux limites associées sont dérivées pour la fonction bi-objective considérée. Le solveur numérique développé couple l'optimisation MMA (Method of Moving Asymptotes) pour mettre à jour les variables de conception (variables de design) à l'aide de la technique d'interpolation RAMP (approximation rationnelle des propriétés du matériau) pour la distribution du matériau solide dans le domaine.

Le solveur numérique développé est appliqué à une configuration bidimensionnelle classique issue de la littérature, afin de générer des solutions optimales non conventionnelles pour des écoulements incompressibles en régime permanent à un nombre de Reynolds faible à modéré. Les structures optimales obtenues sont analysées de façon approfondie en termes d'étude de convergence, d'évaluation des performances, d'analyse locale des résultats aux limites des domaines et d'analyse de l'ordre de grandeur des valeurs de la fonction objective. On observe que le solveur d'optimisation topologique développé produit des conceptions optimales réalistes pour les systèmes thermiques conducto-convectifs, allant de la réduction des pertes de charge à la maximisation de la puissance thermique en fonction de la valeur de pondération définie dans la fonction bi-objective, et fixée par l'utilisateur.

De plus, afin d'analyser l'influence de la technique de discrétisation sur les topologies optimales finales obtenues, les résultats du solveur développé et basé sur une méthode par volumes finis sont comparés, pour des configurations et fonctions objectives objective identiques à des résultats issus de la littérature, basés sur une méthode volumes finis et une méthode Lattice Boltzmann. Les résultats des valeurs de fonction objective des designs optimaux ont montré que le solveur développé dans cette thèse et basé sur la méthode des volumes finis produit des solutions plus performantes que les solveurs volumes finis ou Lattice Boltzmann existant dans la littérature. Plus précisément, une puissance thermique légèrement plus élevée est obtenue, mais avec une perte de charge de $50\ \%$ plus faible que celle obtenue par le solveur basé sur la méthode Lattice Boltzmann.

En conclusion, les résultats de ce travail mettent en lumière que les performances associées aux structures « optimales » présentées dans la littérature pouvaient en fait être améliorées Ils soulignent en outre l'importance de diverses analyses numériques détaillées présentées dans cette étude pour effectivement justifier de conceptions optimales pour les systèmes thermiques conducto-convectifs obtenus par optimisation topologique. Cette partie de la thèse a fait l'objet d'une publication parue dans la revue International Journal of Heat and Fluid Flow, vol. 75, pp. 165-184,2019, https://doi.org/10.1016/j.ijheatfluidflow.2019.01.002

Topology optimization of conjugate heat transfer systems: A competition between heat transfer enhancement and pressure drop reduction

V. SUBRAMANIAM[a,b], T. DBOUK[a,b,], J.-L. HARION[a,b]

[a] *IMT Lille Douai, Energy Engineering Department, 59500 Douai, France*
[b] *University of Lille, 59000 Lille, France*

Abstract

Topology optimization method is developed for a multi-objective function combining pressure drop reduction and thermal power maximization (incompressible flows at low to moderate Reynolds numbers). Innovative optimal designs are obtained, discussed and presented on a Pareto-frontier. The numerical developments (continuous adjoint technique) have been conducted inside an open source CFD platform via the finite volume method. Comparisons have been presented with an optimal design obtained by a Lattice Boltzmann Method from the literature. Finally, this contribution presents and discuss several detailed numerical vitrification steps which are essential to be conducted in topology optimization method when applied with multi-objective functions.

Keywords: Topology optimization; conjugate heat transfer; optimal design; computational fluid dynamics;

Nomenclature

Greek Symbols

Symbol	Description	Unit
α	Pseudo inverse permeability	–
γ	Ratio of thermal diffusivity	–
Γ	Domain boundary	–
η	Design variable	–
ν	Kinematic viscosity	$\mathrm{m}^2 \cdot \mathrm{s}^{-1}$
ρ	Density	$\mathrm{kg} \cdot \mathrm{m}^{-3}$
ϕ_{max}	Maximum volume fraction	%
ω	scalar-valued weight factor	–
Ω	Design domain	–

*Corresponding author
ORCID ID: 0000-0002-9710-4978
Email address: talib.dbouk@imt-lille-douai.fr (T. DBOUK)

Roman Symbols

Symbol	Description	Unit
A	Length of the domain	m
C_p	Specific heat capacity	$\mathrm{J \cdot kg^{-1} \cdot K^{-1}}$
d	Hydraulic diameter	m
D	Thermal diffusivity	$\mathrm{m^{-2} \cdot s^{-1}}$
f_d	Friction factor	$-$
F	Aggregated objective function	$-$
J_f	Dissipated fluid power	W
J_{th}	Recoverable thermal power	W
k	Penalty parameter	$-$
K	Thermal conductivity	$\mathrm{W \cdot m^{-1} \cdot K^{-1}}$
l	Length of the pipe	m
m	Mass flow rate	$\mathrm{kg \cdot s^{-1}}$
$\boldsymbol{n}$	Normal vector	$-$
$nCells$	Number of square elements	$-$
P	Pressure	Pa
T	Temperature	K
$\tilde{T}$	Normalized temperature	$-$
$\boldsymbol{u}$	Velocity vector	$\mathrm{m \cdot s^{-1}}$
$\tilde{u}$	Normalized velocity	$-$
V	Volume of the domain	$\mathrm{m^3}$
$x,\ y$	System of coordinates with dimension	m
$\tilde{x},\ \tilde{y}$	Normalized system of coordinates	$-$

1. Introduction

The term conjugate heat transfer refers to the processes which involve variation of temperature within fluids and solids due to thermal interactions between them. This phenomenon is observed in many industrial thermal equipments like heat exchangers, finned surfaces, microelectronic equipment and heat sinks. The design of such heating or cooling devices involves a consideration of both the heat transfer between different media and the mechanical pumping power spend to overcome the fluid friction in order to move the fluid through the device [1]. In other words, the objective is to increase the heat transfer while keeping the pressure drop as low as possible. Optimizing designs that best manage trade-offs between these two conflicting criteria is currently a very critical issue and has attracted many academic and industrial researchers. On the other hand, rapid product design cycles in development of modern thermal equipment has led to extensive use of automated design and optimization processes. Of the automated optimization techniques that exist in the literature, topology optimization introduced by Bendsøe and Kikuchi [2], can be seen as one of the most promising optimization tool and is presently an active topic of research, development and innovation in the field of heat transfer and fluid flows [3][4].

Topology optimization has its roots in structural design optimization but recently has gained a lot of attention in thermal engineering applications. Originally based on homogenization theory [2], topology optimization has now evolved in different directions which can

be broadly categorized as: density approach [5][6][7], level-set method [8][9][10], topological derivative [11], phase field [12] and evolutionary approaches [13]. These methods in literature have been successfully applied to various problems related to fluid and thermal optimizations. The fundamentals of these techniques are discussed in detail by Sigmund and Maute [14].

TO of heat transfer systems in literature can be broadly classified into three categories: pure heat conduction problems, fluid flow problems and coupled thermal-fluid problems. For heat conduction systems, TO has been found to provide unconventional tree-like optimal structures of high conductivity material for efficient heat evacuation from low conductivity heat generating volumes [15]. Such problems commonly referred as the "volume-to-point" heat conduction problem has been extensively studied in the literature for both 2D [16][17] and 3D [18] cases and recently has also been experimentally investigated [19]. For fluid flow problems, Borrvall and Petersson [20] introduced the concept of TO for Stokes flow by adding a Brinkman penalization sink term into the momentum equation with an objective to minimize the dissipated power in the fluid. This pioneering work was then extended by Gersborg-Hansen et al. [21] to TO for incompressible laminar flows by solving the complete Navier-Stokes equations. After this, several studies were conducted for topology optimization of laminar flows with the objective to either minimize the pressure drop in the channel or to maximize the flow uniformity at the outlet [22][23][24][25]. A detailed review of topology optimization applied to heat transfer and fluid flow problems can be found in [3].

After successful application of TO for heat conduction and fluid flows separately, the next obvious step was to combine these two phenomena to optimize coupled thermal-fluid systems. Early implementations of TO modeled the thermal-fluid systems by combining 2D heat conduction problem with convective heat transfer to the surrounding fluid through Newtons law of cooling by either using a constant heat transfer coefficient [26][27][28] or employing some specific surrogate models [29] to the convective boundaries. In conventional TO methods, it is not easy to clearly define boundary locations in the middle of the process, since they are blurry and constantly changing. Hence, practical implementation of optimal designs obtained from such assumptions (or approximations) is not feasible.

Such limitations can be overcome by adopting a comprehensive conjugate heat transfer approach to optimize thermal-fluid systems. Yoon [30] was among the first researchers to consider TO for a coupled thermo/hydraulic system to optimize for heat dissipating structures under forced convection. A 2D Finite Element Method (FEM) formulation was considered with the objective to minimize the thermal compliance in the domain using the density based Solid Isotropic Material with Penalization (SIMP) [5] approach coupled with method of moving asymptotes (MMA) optimization algorithm, introduced by Svanberg [31]. The author reported several numerical difficulties such as local optima due to high sensitivity of the final design to initialization values. Dede [32] introduced a dual objective function strategy to minimize simultaneously both the mean temperature and the fluid power dissipated in the system with a custom COMSOL/MATLAB solver. A continuous adjoint method for gradient computation and MMA as the optimizer algorithm was used. However, fluid density, heat capacity and viscosity were assumed to be unity in all the examples. Additionally, high values of pressure drop were observed in the system due to undesirable dead-ends in the structure. As a conclusion, the author emphasized on the need of better weighting strategies for multi-objective topology optimization. Lee [33] applied TO to design convective cooling

channels in both 2D and 3D using FEM formulation coupled with discrete adjoint method for sensitivity analysis and Rational Approximation of Material Properties (RAMP) [34] functions for interpolating material properties. Many interesting optimal structures were produced using first a single objective function (mean temperature minimization) and then introducing a bi-objective function (minimizing mean temperature and kinetic energy dissipation) in order to tackle high pressure drop observed in the former case.

Matsumori et al. [35] studied topology optimization for coupled fluid-thermal problem to design heat exchangers under a constant input power using sequential quadratic programming (SQP) algorithm [36] and RAMP-type interpolation functions in the FEM based COMSOL software package. Surprisingly, the authors did not consider the thermal conductivity differences between the solid and fluid regions (i.e. assuming $K_s = K_f$). Kontoleontos et al. [37] extended the TO of coupled fluid-thermal problems to turbulent flows using a finite volume method (FVM) formulation and continuous adjoints for gradient computation coupled with the Steepest-descent optimization algorithm. However, the authors did not solve the temperature field in the solid region by numerically imposing a constant value of temperature. Alexandersen et al. [38] introduced density-based topology optimization for natural convection problems using Boussinesq approximation to design heat sinks and micropumps in a FEM formulation. It is worth to mention that the authors for the first time used a parallelized version of method of moving asymptotes (MMA) algorithm to solve the 3D conjugate heat transfer optimization problem. Koga et al. [39] developed a microchannel heat sink device for electronic cooling using topology optimization for Stokes flows (inertial effects in fluid were not considered) using a FEM formulation and the Sequential Linear Programming (SLP) optimization algorithm. The authors used a RAMP function for interpolating Brinkman penalization term and SIMP for thermal properties. 3D prototypes of numerically obtained 2D optimal structures were fabricated for experimental examination. Marck et al. [40] studied TO of multi-objective heat and mass transfer problems by constructing an overall objective function from linearly weighted two objective functions of pressure drop minimization and thermal power recovery maximization. A FVM based TO formulation with discrete-adjoint method for sensitivity analysis and MMA algorithm was used in their study. The authors presented a Pareto set of optimal solutions for the multi-objective optimization (MOO) of a single pipe with constant wall temperature.

In recent studies, Qian and Dede [41] presented density-based 2D TO of conjugate heat transfer systems with a tangential thermal gradient constraint by using a bi-objective function approach. The authors used the continuous adjoint method to derive gradients of both the objective function and tangential thermal constraint in a FEM formulation. Additionally, they used a RAMP function for interpolating fluid properties and SIMP for thermal properties. The authors emphasized the role of appropriate material interpolation schemes in producing clear fluid/solid designs. Zeng et al. [42] used a multi-stage optimization approach to obtain a non-conventional 2D design of a heat sink under forced convection in COMSOL. 3D representations of the optimal structure was then numerically and experimentally investigated. However, in their formulation, while evaluating heat transfer coefficient in the solid domain, heat conduction was considered only in the height direction (spanwise heat conduction was neglected even though the width of the base is very large as compared to its height). A similar study was performed by Haertal et al. [43] in COMSOL using globally convergent version of MMA (GCMMA) algorithm to optimize the design of a thermo-fluid

heat sink where in 2D results obtained from the topology optimization process were numerically validated in 3D. Lastly, in contrast to density based TO approach, Dugast et al. [44] developed a Level-Set Method (LSM) coupled to adjoint Lattice Boltzman Method (LBM) for topology optimization of thermal fluid flows. The authors presented optimal thermo-fluid designs for fixed pressure drop values with three different cost functions: minimization of mean temperature in the domain, maximization of recoverable thermal power by the fluid, and maximization of the heat exchange with heated solid parts.

Topology optimization applied to CHT systems is an active field of research. During the past decade many numerical techniques have been developed to optimize such systems. Majority of the studies in literature used a FEM formulation and a density approach based on SIMP or RAMP like interpolation scheme for material distribution in the domain. Very few studies investigated the FVM [40][37] and LBM [44][45] discretization techniques for CHT systems. As for the choice of objective function, most of the studies in literature consider either mean temperature minimization in the domain [32][33][35][39][41] or thermal compliance minimization [30][38]. Almost all the studies in literature use a gradient-based optimization algorithm coupled with either discrete or continuous adjoint method for gradient computation. But most importantly, all these numerical techniques in literature, they are too dispersed without enough comparisons in between. Furthermore, to author's knowledge, no benchmark studies exist in this field which hinders the implementation of such studies in real world applications. For example, as most of the studies in literature for CHT systems strive to optimize for heat transfer maximization and pressure drop minimization, it could be interesting to compare different numerical techniques to optimize for some standard academic or industrial configurations on the basis of their respective objective function values. Such studies in future can lead to establishment of best practice guidelines for TO applied to heat transfer and fluid flows.

Another challenge in optimization of CHT systems is to search for optimal designs that can maximize heat transfer in the domain without increasing the pressure drop in the fluid channels (neither blocking the fluid flow). To tackle this issue, some studies optimize only heat transfer enhancement for a prescribed pressure drop values [35][43][44], or optimize only pressure drop with heat transfer performance as a constraint [42]. In reality, optimization of CHT systems falls under the scope of multi-objective optimization (MOO) where the goal is to search for a solution that best manages trade-offs between conflicting criteria and that cannot be transformed into a common measure [46]. Therefore, many researchers adopted the bi-objective function strategy for this task [39][37][32][41][40]. Nonetheless, some studies restricted themselves to Stokes flows [39], whereas others made some unrealistic simplifications in their studies [37][32]. Usually, a bi-objective optimization strategy for CHT systems uses the weighted-sum method to form the overall objective function from the two linearly weighted criteria, a fluid objective (J_f) and a thermal objective (J_{th}), as follows:

$$F = \omega_1 J_f + \omega_2 J_{th} \tag{1}$$

where ω_1 and ω_2 are user-defined scalar-valued weights. The solution of 1 can be unclear, because a single point that optimizes (minimize or maximize) both the objectives simultaneaoulsy usually does not exist. Hence, the solution of such a problem aims at identifying a Pareto set of optimal points also referred as the Pareto frontier [46][47]. Except [40], all

implementations of this bi-objective problem showed the results at a maximum of only two or three optimal points without identifying the Pareto frontier. In other words, most studies in the literature did not exploit the full potential of bi-objective function strategy and consequently did not explore the complete optimal solutions space. On the other hand, as a result of ill-suited boundary conditions opted for the optimization problem Marck et al. [40], reported non physical optimal structures for some designs (i.e. blocking the fluid flow). Precisely speaking, the authors assumed a fixed velocity boundary condition with exactly same value for inlet and outlet, which is an impractical assumption. Finally, one common outcome that can be clearly observed in the literature for such formulations is that whenever the weight of the thermal objective exceeds that of the fluid objective ($\omega_2 > \omega_1$), broken flow paths, dead ends or non-physical artifacts are obtained in the optimal designs [41][40][32]. For this particular reason, no study in literature clearly demonstrated the evolution of optimal design at very high influences of the thermal objective function. This can be due to the formulation itself of the optimization problem, the choice of the objective function or the choice of material interpolation scheme. Nevertheless, such non-physical artifacts are highly undesirable from manufacturing point of view.

In this paper, a multi-objective optimization technique is developed for topology optimization of conjugate heat transfer systems. The design goals are to maximize recoverable thermal power in the domain and minimize the power dissipated by the fluid flow, simultaneously. The two objectives are combined linearly using a linear weighted sum method. In contrast to the commonly used thermal objective functions in literature (thermal compliance or average temeparture in the domain), the recoverable thermal power objective function [40][44] is used in this study as it combines both a tempearture term multiplied by a velocity term. The finite volume method (FVM) is used to solve the coupled thermal-fluid equations over a uniform structured mesh with the open source OpenFOAM CFD software package. A density-based topology optimization approach is adopted and a continuous-adjoint method is used for conducting the sensitivity analysis. The developed topology optimization numerical platform is used to optimize for a fluid channel with single inlet and outlet with constant wall temperature. Several optimal designs are generated for different combination of weighting factors and the Pareto frontier is constructed as the solution of the overall multi-objective optimization problem. The results obtained are compared with those obtained by Marck et al. [40] in terms of objective function values who tackled the similar problem but using a discrete-adjoint method for sensitivity analysis. In addition to this, an another numerical example from literature [44] is solved in order to compare the optimal designs obtained from the present TO numerical platform to the adjoint LBM coupled to LSM based TO in terms of objective function values.

To summarize, the main novelty of this work can be summed up as follows:

– Multi-objective topology optimization technique of CHT systems is developed methodologically by linear combination of two objective functions for pressure drop reduction and heat transfer enhancement which is a very critical task in terms of producing physically realistic optimal designs as it induces severe numerical difficulties in the overall optimization problem due to the physical contradiction behind enhancing heat transfer by material insertion combined to reduction in pressure drop.

– The developed TO technique produces Pareto optimal solutions with more realistic and physically logical structures even at higher influence of thermal objective function without any dead ends or blocked fluid flow which were never reported before in the literature, to authors' knowledge.

– An in-depth analysis of the obtained optimal fluid channel designs in terms of convergence study, performance evaluation, local analysis of the results at the domain boundaries and order of magnitude analysis of the objective functions is presented for the first time, to authors' knowledge.

– Finally, a detailed comparison of the performance of different topology optimization approaches for optimizing conjugate heat transfer systems is presented. In that purpose, the results produced from the **present FVM coupled to density approach based** TO solver are compared to other studies in literature [40] (**FVM coupled to density approach based**) and [44] (**LBM coupled to level-sets based**) by solving identical CHT TO problems for the same objective function. Better optimal designs are obtained in the current study and justified in terms of the objective function values.

The rest of the article is organized as follows: Section 2 presents the mathematical formulation of the inequality constrained topology optimization problem for conjugate heat transfer systems describing the multi-objective function approach, material interpolation techniques, continuous adjoint formulation and numerical implementation of the problem. Section 3 presents the results obtained for the TO problem with an in-depth numerical analysis of the optimal designs obtained and influence of several physical and numerical parameters and finally in section 4, conclusions are drawn and some perspectives are proposed for the near future.

2. Topology optimization for conjugate heat transfer systems

Topology optimization (TO) addresses the fundamental engineering problem of placing different materials within a given design domain that obeys a predefined design objective. Mathematically, the goal of TO is to maximize or minimize some objective function while taking into account one or more constraints. Figure 1 represents the design domain Ω and boundary conditions for the conjugate heat transfer topology optimization problem. The domain under consideration is a square of length $A(m)$ and has one inlet (Γ_{in}) and one outlet (Γ_{out}) of length $A/5$. The inlet flow has a prescribed parabolic velocity profile $\boldsymbol{u}_{in}$ and a constant temperature of $T_{in} = 273$ K. The outlet flow has a zero gradient boundary condition for both velocity and temperature. The top and bottom walls (Γ_{w}) are maintained at a constant temperature of $T_w = 283$ K. All other boundaries (Γ_{ad}) are adiabatic. The boundaries Γ_{w} and Γ_{ad} are subjected to no-slip velocity boundary condition. The fluid under consideration is assumed to be incompressible, Newtonian and under steady-state laminar flow regime with kinematic viscosity of $6.6 \cdot 10^{-6}\ m^2\ s^{-1}$. The Reynolds number varies between Re=3 and Re=100, evaluated on the basis of characteristic length of $A/5$ and a varying inlet fluid velocity. The thermal diffusivity ratio ($\gamma = D_s/D_f$) between solid and fluid material is 10. The amount of the fluid material is limited by restricting the ratio of its effective volume to the total domain volume, given by ϕ_{max} (the maximum allowed

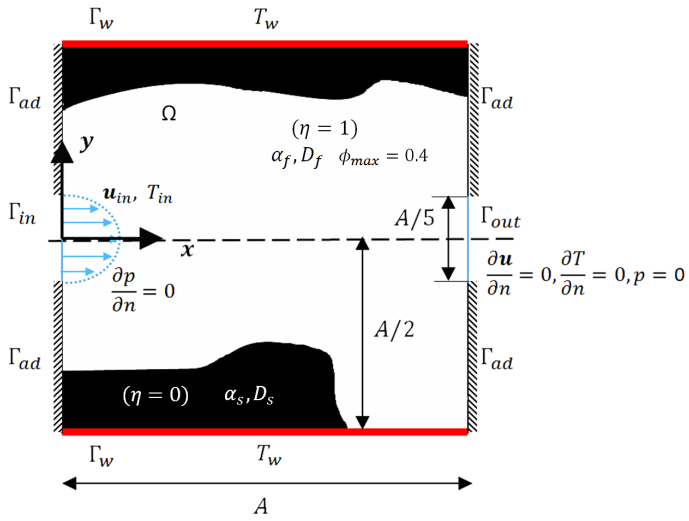

Figure 1: 2D design domain and boundary conditions for conjugate heat transfer topology optimization problem.

relative quantity of fluid material) and for the current problem, $\phi_{max} = 0.4$. As is the case with OpenFOAM CFD software package, 2D simulations here are performed on a 3D mesh with one cell width of 0.005 m in the third direction. Thus, the described design domain represents a typical channel flow with constant wall temperature.

A local design variable field η is introduced which will be used as a characteristic function to represent the optimal material distribution in the design domain. The design variable varies continuously from 0 to 1 in each cell in the domain where $\eta = 0$ represents a solid material and $\eta = 1$ represents a fluid material. The aim of the current topology optimization process is to find an optimal distribution of design variables η in the design domain in order to minimize an objective function F. Mathematically, the above TO problem can be expressed as follows:

Minimize:

$$F(\boldsymbol{u}, p, T, \eta) \tag{2a}$$

subject to:

$$\nabla \cdot \boldsymbol{u} = 0 \tag{2b}$$

$$(\boldsymbol{u} \cdot \nabla)\boldsymbol{u} = -\nabla p + \nabla \cdot (\nu \nabla \boldsymbol{u}) - \alpha(\eta)\boldsymbol{u} \tag{2c}$$

$$(\boldsymbol{u} \cdot \nabla)T = \nabla \cdot (D(\eta)\nabla T) \tag{2d}$$

$$\frac{1}{V} \sum_{j=1}^{nCells} \eta_j \leq \phi_{max} \tag{2e}$$

where F is the objective function to be minimized, subjected to the state equations for incompressible steady-state Navier-Stokes (N-S) equations coupled with heat transfer (2b-2d) and an inequality volume constraint on the fluid material (2e). V is the total volume of

the square domain and $nCells$ is the number of square elements used to discretize uniformly the 2D domain in a Cartesian frame of reference. $\boldsymbol{u}$, p, T and ν represents the fluid velocity vector, pressure, temperature and the fluid kinematic viscosity, respectively. The objective function F is explicitly dependent on velocity, pressure and temperature field and also implicitly dependent on the local design variable η. Here, α is the inverse permeability or the friction coefficient which is linked to the local design variable (η) through an interpolation function. Similarly, in the energy equation the effective thermal diffusivity (D) is dependent on the local design variable (η) via an interpolation function such that:

$$(\alpha(\eta), D(\eta)) = \begin{cases} (\alpha_s, D_s), & \text{if } \eta = 0 \text{ (solid material)} \\ (\alpha_f, D_f), & \text{if } \eta = 1 \text{ (fluid material)} \end{cases} \tag{3}$$

The Brinkman penalization approach [48, 49] is applied here to penalize the momentum equation by a source term in order to account for the presence of immersed solid regions in the fluid flow domain. The main idea behind this approach is to force a zero velocity inside the stationary solid material regions by means of the Brinkman penalization source term $(-\alpha\boldsymbol{u})$ in equation (2c) when α tends to a very large value of the order $O(10^5)$. The

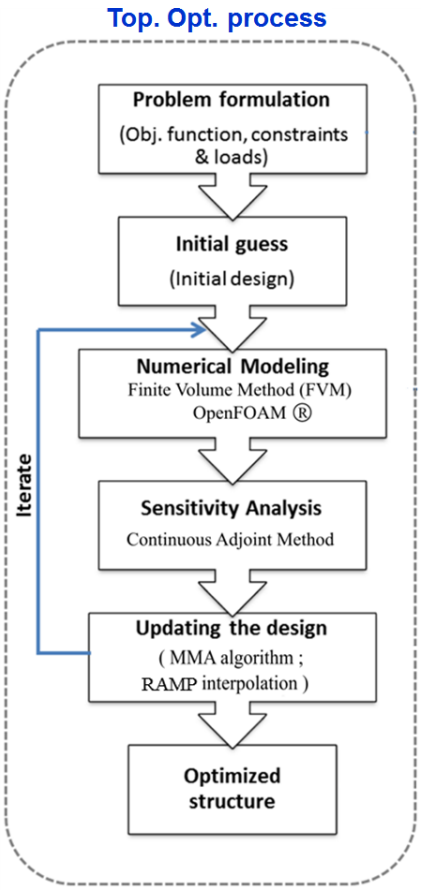

Figure 2: The topology optimization process.

above optimization problem of equation 2 requires some specific numerical algorithms and

TO methods to be used in order to find an optimum. The complexity of any optimization problem depends on various factors like number of design variables involved, degree of convexity/non-convexity and linearity/non-linearity of the equations and the associated numerical difficulties. Therefore, choosing an efficient TO technique and an equally reliable optimization algorithm is very important to ensure a stable convergence to an optimum solution. Figure 2 presents the basic steps involves in the present TO process.

2.1. Interpolation functions

The optimal solution of a topology optimization problem requires discrete variable values only (well defined design) of the design variables η (for example 0 for solid regions and 1 for fluid regions). However, with the continuous medium formulation makes it difficult to reach directly discrete design variables. The density based TO approach [50], overcome this problem by introducing a continuous design field, $\eta(\boldsymbol{x})$ which replaces the discrete variables with continuous ones that is then modified iteratively by a material interpolation technique to reach only discrete design variables. As a result, the friction coefficient (α) and effective thermal diffusivity (D) change with η through the following Rational Approximation of Material Properties (RAMP)-type [34] interpolation functions as following:

$$\alpha(\eta) = \alpha_s + (\alpha_f - \alpha_s)\eta\frac{1+k}{\eta+k} \tag{4a}$$

$$D(\eta) = D_s + (D_f - D_s)\eta\frac{1+k}{\eta+k} \tag{4b}$$

with $0 \leq \eta \leq 1$ and $k > 0$. This penalty parameter k governs the shape of the functions $\alpha(\eta)$ and $D(\eta)$. The above material interpolation scheme interpolates the value of α between the two extrema of $\alpha_f \approx 0$ and $\alpha_s \approx \infty$. Thus, in the fluid domain, the Brinkman penalization term $\alpha\boldsymbol{u}$ approaches zero to recover the classical Navier-Stokes equation in 2c. Conversely, in the solid domain , the friction coefficient α has a very large value, which makes the local velocity approach zero. In the present work, $\alpha_f \approx 0$ and $\alpha_s \approx 10^5$.

2.2. Multi-objective optimization

Efficient optimization of CHT systems requires to optimize for a thermal objective and a fluid objective, simultaneously in order to reach a design that best manages trade-off between the two criteria. A trade-off here means one objective can be improved only by worsening the other one. The solution of such a multi-objective optimization (MOO) problem is not a single point but a set of optimal points (multiple solutions) referred as the Pareto frontier. Thus MOO based on Pareto optimality is divided into two steps: In the first step, the set of pareto optimal solutions is identified and in the second step the final design is selected by a human decision maker based on subjective preferences. The weighted sum method based on linear combination of the objective functions is a suitable method for identifying the Pareto front [51].

For the current problem the multi-objective function is constituted of two objectives inspired from [40][24]. The fluid objective function J_f is to minimize the power dissipated by

the fluid flow in the domain Ω and can be calculated from the total pressure losses through the overall domain boundaries Γ as the following:

$$J_f(\boldsymbol{u}, p) = -\int_\Gamma \Big(p + \frac{1}{2}|\boldsymbol{u}|^2\Big)\boldsymbol{u}\cdot\boldsymbol{n}\ d\Gamma \tag{5}$$

The thermal objective function J_{th} is to maximize the recoverable thermal power from the domain through the inlet and outlet flow boundary conditions. The net thermal power is evaluated as follows:

$$J_{th}(\boldsymbol{u}, T) = \int_\Gamma (\rho C_p T)\boldsymbol{u}\cdot\boldsymbol{n}\ d\Gamma \tag{6}$$

where $\boldsymbol{n}$ is the unit vector normal to the boundary Γ. The weighted sum method or the aggregated objective function is used to linearly combine the two objective functions. As a prerequisite to this approach, the two objective functions are normalized to avoid the huge differences in their numerical values corresponding to two different scales. One simple yet efficient way of normalizing is to divide the objective functions by their respective extrema [47]. The extreme value for each objective function is found independently upon solving the optimization problem (Eqn. 2) for two cases separately: minimizing J_f and maximizing J_{th}, respectively. Finally, the aggregated objective function (F) for the current MOO problem formed from the linear combination of the two normalized objective functions, $\tilde{J_f}$ and $\tilde{J_{th}}$, can be described as follows:

$$F(\boldsymbol{u}, p, T) = (1-\omega)\tilde{J_f} - \omega\tilde{J_{th}} \tag{7}$$

where ω is a scalar-valued weight factor emphasizing the degree of influence or priority of each objective function ($\omega \in (0, 1)$). The thermal objective $\tilde{J_{th}}$ is negatively weighted as it has to be maximized (since the overall F is to be minimized). The weighted-sum approach can obtain the convex part of the Pareto front by progressively varying the weight factor values in the aggregated objective function formulation [46].

2.3. Sensitivity analysis - The continuous adjoint method

In gradient-based TO, the derivative of the objective function with respect to the design variables is required by the optimization algorithm to solve for the design variables in each cell satisfying the optimization problem in equations (2). The adjoint method, either discrete or continuous, provides an efficient option for calculating the sensitivity field of the objective function, $dF/d\eta_j$ and has been applied in many different TO problems (i.e. see [3][37][52][45]). In contrast to Marck et al. [40] who applied a discrete adjoint method, a continuous adjoint method is used here for sensitivity field computation. For this, the adjoint equations and the corresponding boundary conditions are first derived in their analytical form and then discretized to obtain the adjoint equations.

The original constrained optimization problem of Eqn. 2 can be transformed into an unconstrained optimization problem by introduction of a Lagrange function L (also reffered as the augmented objective function) [53]. Reformulating the objective function as follows:

$$L = F + \int_\Omega (\boldsymbol{u}_a,\ p_a,\ T_a)R\ d\Omega \tag{8}$$

where the Lagrange multipliers $\boldsymbol{u}_a,\ p_a$ and T_a are the adjoint velocity, adjoint pressure and the adjoint temperature, respectively, and $R = (R_1, R_2, R_3, R_4, R_5)^T$ represent the state equations for the incompressible steady-state Navier-Stokes equations coupled with heat transfer.

As the objective function is dependent on both the topology (via the design variable η) and the flow field ($\boldsymbol{u},\ p,\ T$), the total variation of the objective function with respect to a design change can be expressed as:

$$\delta L = \delta_\eta L + \delta_{\boldsymbol{u}} L + \delta_p L + \delta_T L \tag{9}$$

Now, if the adjoint variables ($\boldsymbol{u}_a,\ p_a,\ T_a$) are chosen in such a way that the variation of the objective function w.r.t flow field variables vanishes,

$$\delta_{\boldsymbol{u}} L + \delta_p L + \delta_T L = 0 \tag{10}$$

then the sensitivities can be evaluated directly as follows:

$$\delta L = \delta_\eta L = \delta_\eta F + \int_\Omega (\boldsymbol{u}_a,\ p_a,\ T_a)\delta_\eta R \, d\Omega \tag{11}$$

The total variation can also be expressed as $\delta L = \dfrac{\partial L}{\partial \eta}\delta\eta$. Thus, from Eqn. 11, the gradient of the objective function with respect to the design variable η for each cell i can be further simplified as:

$$\frac{\partial L}{\partial \eta_i} = \frac{\partial F}{\partial \eta_i} + \int_\Omega (\boldsymbol{u}_a,\ p_a,\ T_a)\frac{\partial R}{\partial \eta_i} \, d\Omega \tag{12}$$

In density based TO approach, the design variable η is used as a variable to represent a continuous transition between the two materials and as a result there is no explicit dependence of the objective function on the design variable ($\partial F/\partial \eta_i = 0$), hence the above equation can finally be written as:

$$\frac{\partial L}{\partial \eta_i} = \int_\Omega (\boldsymbol{u}_a,\ p_a,\ T_a)\frac{\partial R}{\partial \eta_i} \, d\Omega \tag{13}$$

If the adjoint variables ($\boldsymbol{u}_a,\ p_a,\ T_a$) are known, the topological sensitivities i.e. the gradient of the objective field w.r.t the design variable in each cell can be easily evaluated from the above equation. For this, the governing equations for adjoint variables needs to be derived along with their appropriate boundary conditions which then are solved along with the primal flow field equations to get the adjoint variables.

2.3.1. Continuous adjoint equations and boundary conditions

The requirement of vanishing of variation of Lagrange function L w.r.t the flow field variables (Eqn. 10) serves as the starting point for derivation of adjoint system of equation:

$$\delta_{\boldsymbol{u}} F + \delta_p F + \delta_T F + \int_\Omega (\boldsymbol{u}_a,\ p_a,\ T_a)\delta_{\boldsymbol{u}} R \, d\Omega + \int_\Omega (\boldsymbol{u}_a,\ p_a,\ T_a)\delta_p R \, d\Omega + \int_\Omega (\boldsymbol{u}_a,\ p_a,\ T_a)\delta_T R \, d\Omega = 0 \tag{14}$$

Starting from Eqn. 14, calculating the derivatives of the state equations R w.r.t $\boldsymbol{u}$, p and T; integration by parts; decomposition of the cost function F into contributions from the domain boundary $\Gamma = \partial\Omega$ and the interior Ω and using the Gauss divergence theorem to transform volume integrals to surface integrals, the final adjoint equations are derived. The detailed development of the adjoint equations and the associated boundary conditions can be found in the works of Othmer [24] and Hinterberger et al. [54]. The only addition here is the energy equation due to the coupling of heat transfer with fluid flow. The complete continuous adjoint equation system for the optimization problem described in Fig. 1 is as follows:

Continuous adjoint equations:

$$\nabla \cdot \boldsymbol{u} = \frac{\partial F_\Omega}{\partial p} \tag{15a}$$

$$-2\mathbf{E}(\boldsymbol{u}_a) \cdot \boldsymbol{u} = -\nabla p_a + \nabla \cdot (2\nu \mathbf{E}(\boldsymbol{u}_a)) - \alpha(\eta)\boldsymbol{u}_a + T\nabla T_a - \frac{\partial F_\Omega}{\partial \boldsymbol{u}} \tag{15b}$$

$$-\boldsymbol{u} \cdot \nabla T_a = \nabla \cdot (D(\eta)\nabla T_a) - \frac{\partial F_\Omega}{\partial T} \tag{15c}$$

with rate of strain tensor $\mathbf{E}(\boldsymbol{u}_a) = \frac{1}{2}(\nabla \boldsymbol{u}_a + (\nabla \boldsymbol{u}_a)^{\mathrm{T}})$. The system of adjoint equations are mathematically very similar in structure to the primal N-S equations except that the adjoint convection is upstream to the primal flow due to the minus sign and there are additional volumetric source terms when there is any contribution from interior of the domain Ω to the objective function F. It should be noted that the adjoint variables ($\boldsymbol{u}_a$, p_a, T_a) do not have any physical meaning to them unlike their primal counterparts ($\boldsymbol{u}$, p, T). Depending upon the primal boundary conditions for the N-S equations coupled with heat transfer (described in Fig. 1), the adjoint boundary conditions are derived. The adjoint boundary conditions for the current problem of single channel flow with heat transfer are as follows:

Adjoint boundary conditions for inlet and wall:

$$\boldsymbol{u}_{at} = 0 \tag{16a}$$

$$u_{an} = -\frac{\partial F_\Gamma}{\partial p} \tag{16b}$$

$$\boldsymbol{n} \cdot \nabla p_a = 0 \tag{16c}$$

$$T_a = 0 \tag{16d}$$

Adjoint boundary conditions for outlet:

$$\boldsymbol{u}_a \cdot \boldsymbol{u} + u_{an}u_n + \nu(\boldsymbol{n} \cdot \nabla)u_{an} + TT_a + \frac{\partial F_\Gamma}{\partial u_n} = p_a \tag{17a}$$

$$u_n \boldsymbol{u}_{at} + \nu(\boldsymbol{n} \cdot \nabla)\boldsymbol{u}_{at} + \frac{\partial F_\Gamma}{\partial \boldsymbol{u}_t} = 0 \tag{17b}$$

$$u_n T_a + D(\eta)(\boldsymbol{n} \cdot \nabla T_a) + \frac{\partial F_\Gamma}{\partial T} = 0 \tag{17c}$$

The continuous adjoint equations and the associated boundary conditions described above are generic in nature and can be customized for any objective functions. On closer observation, it can be seen that there are seven derivative of the objective function, highlighted in red in the above equations, required to complete the adjoint system of equations.

A key element of the adjoint method is the choice of correct boundary conditions and their customization for the current objective function. In other words, the complete adjoint system needs to be reformulated on changing the objective function form due to the seven terms described above. This characteristic of adjoint-based TO makes it almost impossible to automate the TO numerical platform to tackle wide range of objective functions. Nevertheless, the two objective functions in the present study in Eqn. 5 and Eqn. 6 are evaluated only on the domain boundary Γ and there is no contribution from the domain interior ($F_\Omega = 0$). As as result the three derivatives in the Eqn. 15 can be neglected and the remaining derivatives are calculated by partial differentiation of the multi-objective function Eqn. 7 with respect to p, u_n, $\boldsymbol{u}_t$ and T. These derivatives are then fed into the adjoint boundary conditions Eqn. 16 and Eqn. 17 to get the specific continuous adjoint equation system for the current multi-objective function.

2.4. Numerical methods and algorithm implementation

The Finite Volume Method (FVM) is used to discretize spatially the system of PDE's in (2) over the computational domain in order to compute the fluid flow and temperature fields. The finite volume formulation for coupled thermo-fluid problems was rarely applied in the literature [40][37]. The SIMPLE algorithm [55] is applied to solve the pressure-velocity coupling for the steady-state incompressible fluid flow under consideration coupled to the heat equation. The SIMPLE algorithm reformulates the initial N-S equations into a momentum prediction and a pressure correction that are solved iteratively such that the resulting velocity field satisfies well the continuity equation (2b). The SIMPLE algorithm can be easily extended to solve the adjoint equations as the primal and adjoint system of equations share similar structure. This facilitates complete gradient computation with just two solver calls for primal and adjoint equations, respectively.

The method of moving asymptotes (MMA) [31, 56] is used as the optimization algorithm in the current TO problem. This gradient-based algorithm is based on logarithmic-based convex separable approximations applied to the objective function and its constraints. It is widely used in literature for various structural and multidisciplinary topology optimization problems [20][32][38][40][30]. A detailed analysis about the general performance of this algorithm can be found in [57].

Density and sensitivity filtering methods are often used in topology optimization to obtain mesh-independent and checkerboard-free solutions [58] with length-scale control. In this work, a density filter is used with a filter radius of 1.51 mm. Initially introduced by Bruns and Tortorelli [59], a density filter modifies the element (or mesh cell) density as a function of the densities in a specified neighborhood of an element [60]. The steady state results in this study are obtained over a 100×100 structured uniform square cells mesh. All the above mentioned components of this TO formulation are implemented in the OpenFOAM C++ open source CFD package.

The above topology optimization solver implementation can be summarized as the following:

1. Provide an initial guess for the design variables η.

2. Solve the governing equations to obtain the flow ($\boldsymbol{u},\ p$) and temperature field (T).

3. Compute the multi-objective cost function $F(\boldsymbol{u}, p, T)$.

4. Calculate the sensitivities using the continuous adjoint formulation.

5. Use the computed sensitivities, fluid flow and temperature distribution to update the design variables using the Method of Moving Asymptotes.

6. If the overall convergence/stopping criterion is not reached, go back to step 1 using the new design variables.

The applied overall convergence/stopping criterion is based on both: the design variable changes in the last iteration to be negligible, and the squared-norm of the Karush-Kuhn-Tucker (KKT) conditions to be less than a very small positive value $\ll 1$.

3. Results

This section presents the optimal numerical designs obtained for multi-objective topology optimization of the conjugate heat transfer (CHT) problem described in fig. 1. In non-dimensional analysis, the temperature and velocity field magnitude values will be normalized as the following:

$$\tilde{T} = \frac{T - T_{in}}{T_w - T_{in}} \tag{18}$$

$$\tilde{u} = \frac{|\boldsymbol{u}|}{|\boldsymbol{u}_{in}|_{max}} \tag{19}$$

where T_{in} is the fluid temperature at the inlet boundary, T_w is the temperature at the top and bottom walls boundaries Γ_w and T is the local steady state temperature in the domain. Similarly, $|\boldsymbol{u}_{in}|_{max}$ is the maximum fluid velocity at inlet and $|\boldsymbol{u}|$ is the local steady state velocity magnitude (in $m\ s^{-1}$) in the domain.

3.1. Optimal designs for CHT systems

The domain under investigation is a square channel with single inlet and single outlet subjected to constant wall temperature on top and bottom walls. The eastern- and western-side walls are considered adiabatic (see figure 1). The multi-objective TO problem is solved for different values of ω in the range of 0 to 1 to take into account the influence of the two participating objective function depending on the value of the scalar weight factor, ω. For the problem description in fig. 1, figure 3 shows various distinct optimal designs obtained by progressively increasing the value of ω along with the corresponding normalized velocity magnitude and normalized temperature fields for the obtained optimal designs.

Here dark regions represents solid material and light regions correspond to fluid material, as demonstrated in fig. 1.

For $\omega = 0$ (Fig 3(a)), when there is no contribution from the thermal objective function J_{th} to F and thus the only objective is to minimize the fluid power dissipation, the optimal design obtained is a direct fluid curved channel symmetric in both x and y directions connecting the inlet to the outlet with an increase of cross section (compared to inlet and outlet) thus corresponding to a decrease of pressure drop. As a result, the value of fluid objective J_f is minimum for this design. In other words, it is the best possible design for least pressure drop under the current flow conditions. Additionally, the recoverable thermal power from the domain in this case is about 0.3 Watts.

Subsequently, the optimal two designs obtained at $\omega = 0.3$ and $\omega = 0.5$ add more priority to increases the thermal objective J_{th} permitting some increase in the J_f value, but the continuity, momentum and energy conservation equations must be always satisfied so that the obtained design/structure to be acceptable and feasible. Note that the velocity fields for the first two structures are almost similar, however for $\omega = 0.5$, the optimal structure tries to slightly increase the velocity at the outlet-center by forming a converging shape at the exit (with the continuity constraint being well preserved as will be shown in Section 3.3). Indeed, this effect is more pronounced for the next structure with $\omega = 0.7$ where the structure becomes narrower to increase more the velocity value at outlet-center. In fact, the thermal objective function J_{th} (refer equation 6) has contribution from both the temperature and the normal component of velocity at outlet. Hence the designs until now can be seen as modifying the straight fluid connection in a way to increase the velocity at the outlet in the flow direction.

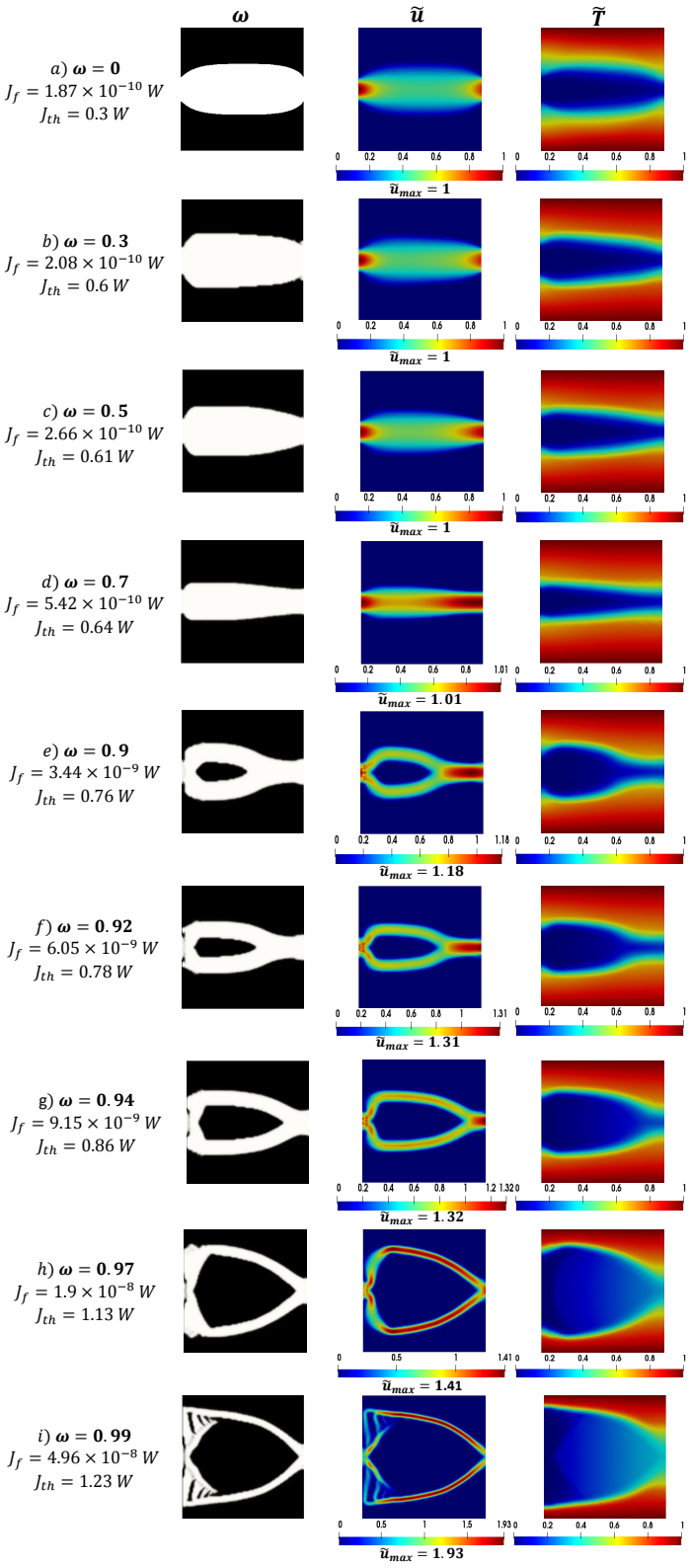

Figure 3: Optimal designs of conjugate heat transfer systems: Starting from fluid objective J_f minimization ($\omega = 0$) to thermal objective J_{th} maximization ($\omega = 0.99$).

Adding more priority in the overall objective function F to maximize J_{th} at $\omega = 0.9$, the fluid flow channel is split into two upper and lower fluid paths with solid material core created in between. The TO solver is trying to place the fluid regions in a way to gain heat from upper and lower solid material regions (knowing that the thermal conductivity of solid is 10 times higher than that of the fluid). Moreover, upon increasing ω, the two divided fluid channels are gradually becoming narrower to rush the exiting fluid where solid material is added at the outlet boundary without totally blocking the fluid flow passage (thus respecting the continuity and momentum conservation equations). At $\omega = 0.94$, 0.97, 0.99, there is a simultaneous increase of both temperature and velocity values at the outlet. These influences will be analyzed in more details in a local analysis of results at the outlet boundary in Section 3.4.2.

At $\omega = 0.99$, the optimal design obtained owns an increased recoverable thermal power of 1.23 W, constituting a significant increase of 310 % as compared to the design obtained at $\omega = 0$. However, this 3-times increased thermal power recovery comes at a cost of 6-times increased fluid power dissipation. Moreover, at very high values of ω, no broken flow paths, fluid flow blockage, dead ends or non-physical artifacts are observed in this work which is a major new finding compared to previous designs obtained previously in the literature which for multi-objective TO of coupled fluid flow and heat transfer problems [17][41][32].

The Pareto frontier in multi-objective optimization problems is an indispensable tool which illustrates the complete solution space and provides the designer with freedom to choose from suitable designs depending on her/his own needs. Unfortunately, most studies in the literature, which dealt with multi-objective TO of CHT systems, did not present this important aspect of the Pareto frontier.

At $\omega = 1$, when there is absolutely no contribution from the objective function J_f, the optimal structure becomes very complex (see Fig. 4) due to an extremely increased non-linearity in the overall optimization problem inducing high numerical instabilities that require large computing efforts to solve at a good precision. This is due to the form of the J_{th} objective function itself that combines both a temperature (T) term multiplied by a velocity term ($\boldsymbol{u} \cdot \boldsymbol{n}$). In fact most studies in the literature, to avoid these numerical complexities, consider either a simple thermal objective that is a function of the temperature field T only or by introducing a convection source term in the energy equation. However, such objective function simplification leads to very limited design space exploration (if not unrealistic designs are obtained), because the fluid flow contribution can not be neither neglected ($\boldsymbol{u} \cdot \boldsymbol{n} = 0$) nor assumed at a velocity value of unity ($\boldsymbol{u} \cdot \boldsymbol{n} = 1$) due to the CHT nature of the system.

Upon comparing the designs obtained in the present study to those obtained by Marck et al. [40], who applied the same objective function F and studied the same problem for single pipe with constant wall temperature with identical flow and thermal conditions (but with discrete adjoint system applied, and $u_{inlet} = u_{outlet}$ imposed boundary condition), the following important critical points can be observed (see Figure 5):

- Upon increasing the weighting factor ω, Marck et al.[40] observed the splitting of the fluid channel at a very lower value $\omega = 0.06$.
- Nonphysical designs like broken flow paths at $\omega = 0.75$ and total fluid flow blockage at $\omega > 0.75$ were reported.

– Finally, the magnitude for the recoverable thermal power objective function J_{th} of the order of magnitude of 10^{-5} W was surprisingly reported.

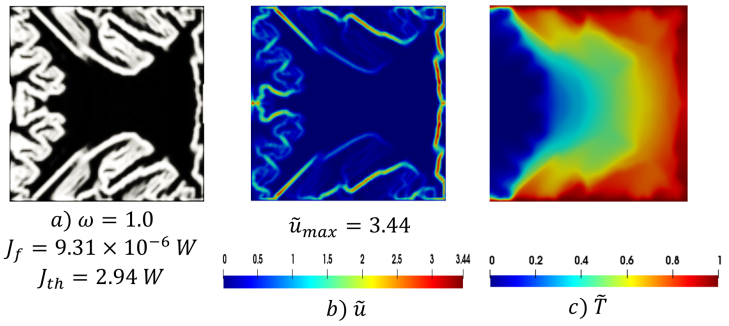

Figure 4: Optimal design obtained by $\omega = 1$.

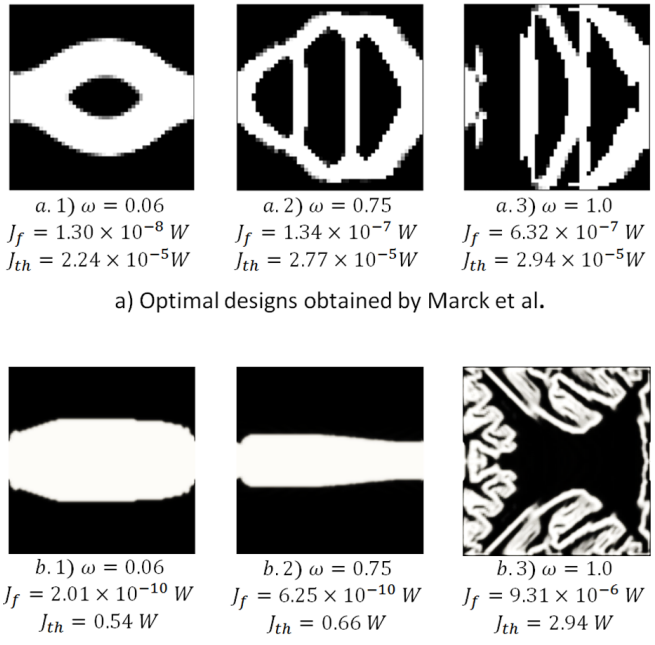

Figure 5: Optimal designs for single pipe with constant wall temperature: a) Obtained by Marck et al.[40] and b) Corresponding designs obtained in the present study.

The above three differences in the two studies will be analyzed in detail in the later sections (refer Section 3.3, Sec. 3.4.2 and Sec. 3.5). Apart from these three major differences, another peculiar observation for the result at $\omega = 1.0$ obtained by Marck et al. [40] is that the order of magnitude of the fluid objective function J_f is same for the two designs at $\omega = 0.75$ and $\omega = 0.1$ even when the flow is totally blocked in the latter. If there is no fluid connection between inlet and outlet at $\omega = 1.0$, as observed by the authors, the pressure drop should

have been very high and consequently the value of J_f should have been significantly higher as compared to other designs. Conversely, in the present study, the order of magnitude for the optimal design at $\omega = 1.0$ (where there is still a fluid connection between inlet and outlet) is much higher to that of $\omega = 0.99$ ($10^{-6} \gg 10^{-8}$) as a result of complex fluid channels in the design (refer Figure 3 and 5).

3.2. Pareto optimal points for multi-objective topology optimization

Figure 6 represents the Pareto frontier obtained for the present multi-objective TO problem for a conjugate heat transfer system. It is obtained by solving the MOO problem for several different weighting factor values between 0 and 1. All the optimal points presented here were verified for convergence satisfying the equality (governing equations) and the inequality (max allowed volume of fluid material) constraints of the TO problem (refer Eqn. 2).

A critical feature of the weighted sum method for MOO is that it can generate the convex part of the Pareto frontier [46]. Hence, the convex shape of the obtained Pareto front (Fig. 6) for the present TO problem is another confirmation of the optimality of the solution points presented here. This Pareto frontier curve constitutes a decision maker tool to select an optimal design based on the needs of the user (i.e. available pumping power, material properties, maximum allowed temperature, etc).

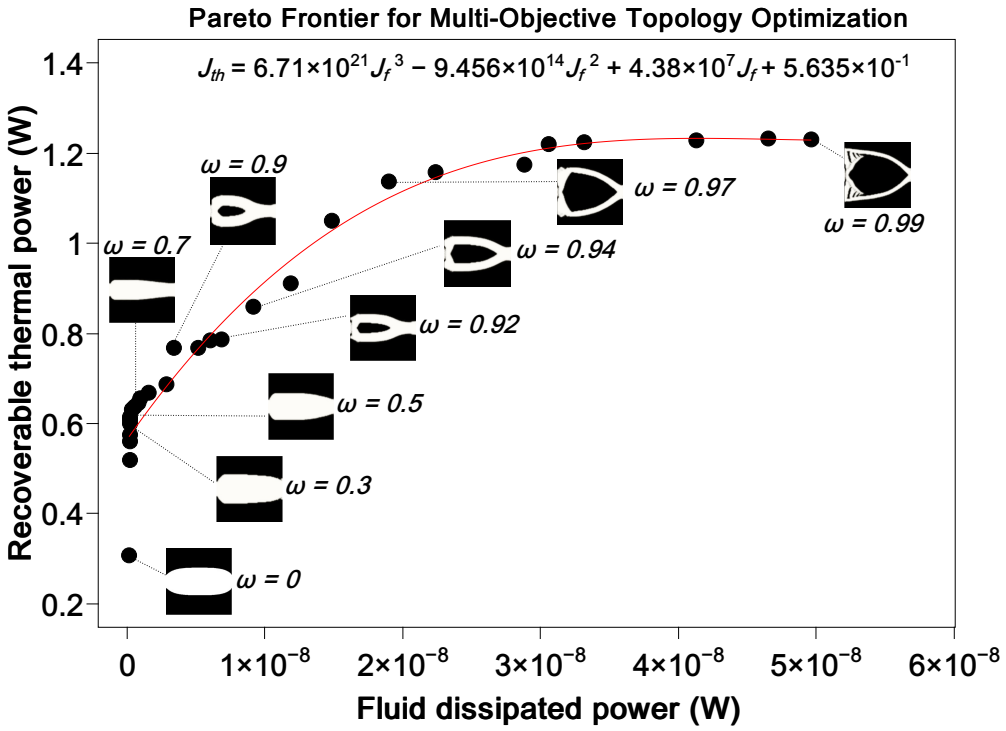

Figure 6: Pareto frontier for multi-objective topology optimization of conjugate heat transfer system.

3.3. Convergence study for the steady-state numerical solutions

For a steady-state numerical simulation, a solution can be deemed converged by observing the evolution of the following quantities:

– The residual values

– The domain imbalances

– Some global quantities of interest

For an iterative numerical simulation, the residual values quantifies the local variance of a conserved variable in the control volume. Therefore, the residual values of a simulation represents the numerical error in the solution of system of equations and as a consequence, it is important to ensure that their values for each equation is very small (typically less than 10^{-5}). As an example, Figure 7 shows the evolution of residual values with iteration for the steady state solution of the TO problem (Eqn. 2) for the three cases at $\omega = 0.0$, $\omega = 0.5$ and $\omega = 0.99$. Although there are some oscillations in the residual values at higher values of ω due to the increased numerical complexities but more importantly, the values are all below 10^{-5} and hence convergence can be stated.

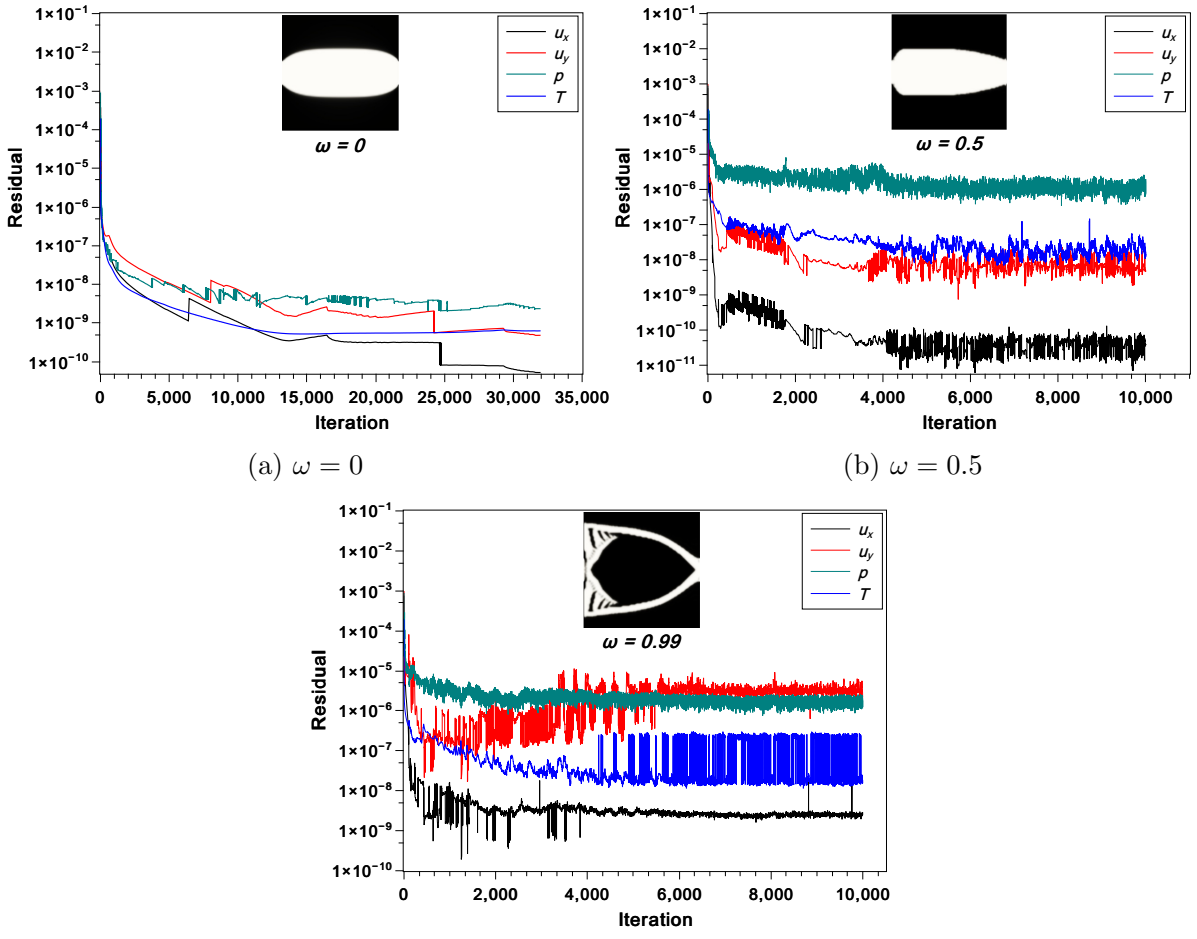

(a) $\omega = 0$

(b) $\omega = 0.5$

(c) $\omega = 0.99$

Figure 7: Residual values for optimal designs obtained from: a) $\omega = 0$, b) $\omega = 0.5$ and c) $\omega = 0.99$.

Secondly, to quantify domain imbalances and to ensure mass conservation in the system, net mass flow rate imbalance is evaluated in the system. Figure 8 presents the difference of

mass flow rate between inlet and outlet (in $kg\ s^{-1}$) as a function of ω (evaluated here for the nine optimal designs in fig. 3 and for $\omega = 1$). It can be seen that the net mass flow rate imbalances are very small of the order of 10^{-15}. Moreover, as the influence of fluid objective function J_f decreases the mass flux imbalance increases marginally to reach its maximum for the optimal design with $\omega = 1$, however, still under the acceptable limits to be deemed mass conserved.

On the contrary, the studies in literature that reported broken flow paths on higher influence of thermal objective function [40][41], may be did not thoroughly respect the mass conservation in the domain. In other words, may be those topology optimization formulation failed to respect the continuity equation equality constraint (Eqn. 2b) during the optimization process.

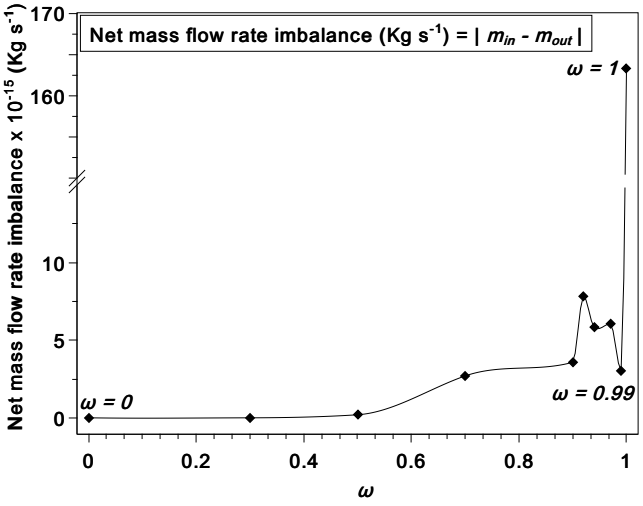

Figure 8: Net mass flow rate imbalances between inlet and outlet of the steady state solution for different optimal designs.

Another criterion to analyze convergence in density based TO is to ensure exact zero velocity values in the solid material for the final design. In the momentum equation (2c), the inverse permeability α is controlled by the design variable η to distinguish the flow in solid and fluid materials which is updated iteratively via the interpolation function (4a). Nevertheless, at a steady state converged solution, the flow motion in solid regions is expected to reach zero velocities. As an example, consider the optimal design obtained at $\omega = 0.99$, where velocity profile is plotted with η values at a randomly selected cross-section ($\tilde{x} = 0.5$) in the domain (Fig. 9). It can be clearly observed that exact zero values are attained in the solid (dark color) regions which testifies convergence at the steady state.

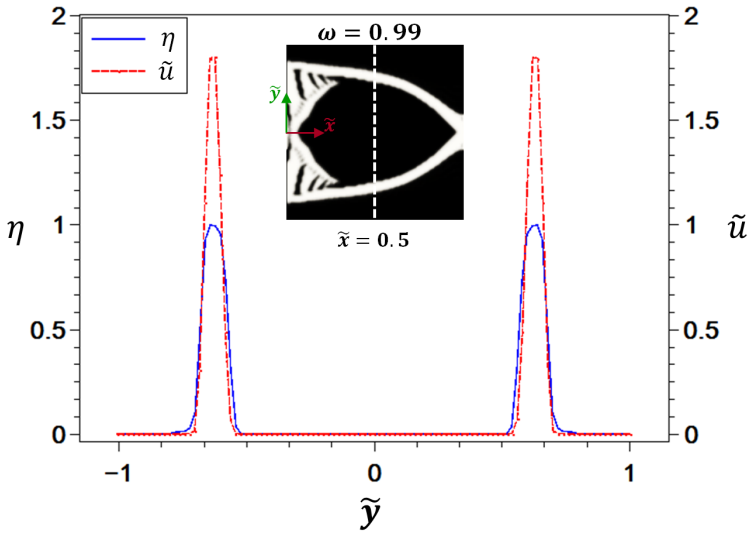

Figure 9: Variation of $\tilde{u}$ with η for the optimal design obtained with $\omega = 0.99$.

Finally, the values of the two objective functions (J_f and J_{th}: evaluated at the domain boundary Γ) itself can be considered as the quantities of interest for the current numerical problem. Additionally, the maximum allowed volume fraction of fluid material ϕ_{max} is also used as a criterion to assure convergence of the numerical TO problem. As an example, Figure 10 shows the convergence history for the TO problem solved iteratively at $\omega = 0.5$ and $\omega = 0.99$.

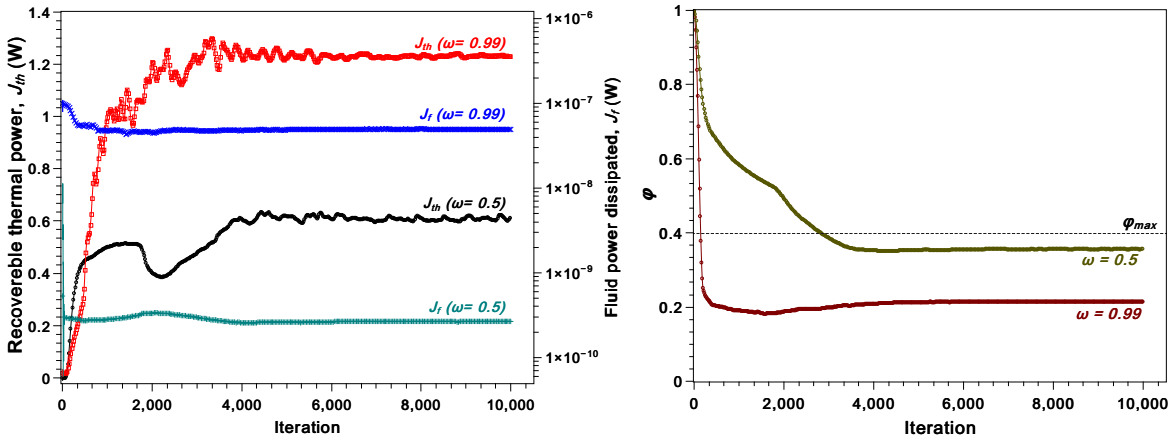

(a) Quantities of interest: J_{th} and J_f

(b) Evolution of ϕ with iteration

Figure 10: Convergence history of the TO problem for the optimal design obtained by $\omega = 0.5$ and $\omega = 0.99$.

3.4. Quantifying the performance of the objective functions

In section 3.1, several designs were presented as an outcome of the multi-objective optimization process. This section attempts to further deepen the understanding of obtained optimal structure by first introducing another performance criteria based on pressure drop

in the fluid channel and then later carrying out an in-depth local analysis at the outlet boundary.

3.4.1. Friction factor (f_d) as the fluid performance criterion

The fluid objective function aims at minimizing the power dissipated by the fluid through the domain and is evaluated from the total pressure losses through the domain boundaries Γ as presented in Eqn. 5. An important criterion from the literature that can be directly associated to pressure drop is the friction factor f_d [61] defined as the following:

$$f_d = \frac{\Delta P}{\frac{1}{2}(l/d)\rho {U_m}^2} \tag{20}$$

where ΔP (in Pa) is the pressure difference between the inlet and outlet boundaries, l (in m) the length of the pipe, d (in m) the hydraulic diameter of the pipe, ρ (in $kg\ m^{-3}$) the density of the fluid and U_m (in $m\ s^{-1}$) is the flow velocity averaged over the cross-sectional area of the pipe outlet. Using equation 20, the friction factor is calculated and shown in Fig. 11 for the different optimal designs presented in Fig. 3. The behavior of the friction factor in the optimal fluid channels is in agreement with that of the fluid objective function J_f. Predictably, the friction factor is of minimum value at $\omega = 0$ and increases rapidly versus increased ω values mainly due to the high pressure drop values between the inlet and outlet. This is due to more priority given in F to maximize J_{th} rather than minimizing J_f. Only at $\omega = 1$, where the fluid path is very complex, the friction factor reaches extremely high values (but still of finite value). The above friction factor (f_d) relation, being more comprehensible as compared to J_f (Eqn. 5) in terms of pressure drop values, gives the user a better insight into the performance of the optimal designs obtained.

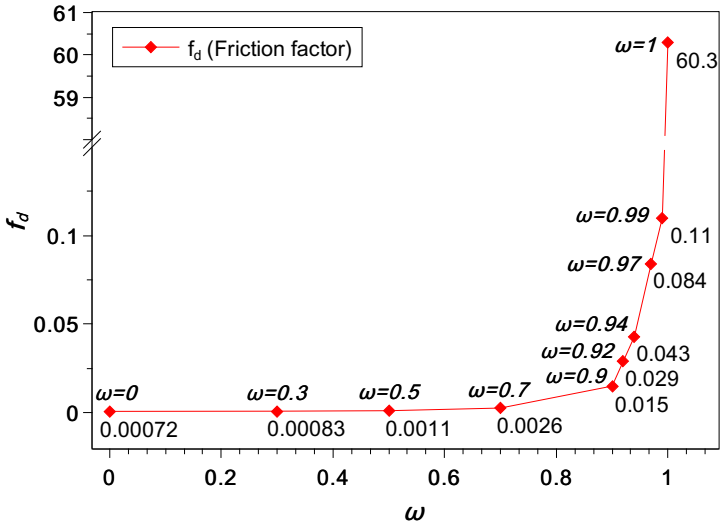

Figure 11: Friction factor (f_d) values for different optimal designs.

3.4.2. Local analysis of the thermal objective J_{th} at the outlet boundary Γ_{out}

The thermal objective function presented in Eqn. (6) computed at the domain total boundary Γ can be detailed as the following:

$$J_{th}(\boldsymbol{u}, T) = \rho C_p \Big[\underbrace{\int_{\Gamma_{\text{in}}} T\boldsymbol{u}\cdot\boldsymbol{n}\, d\Gamma_{\text{in}}}_{\text{constant}} + \underbrace{\int_{\Gamma_{\text{ad}}} T\boldsymbol{u}\cdot\boldsymbol{n}\, d\Gamma_{\text{ad}}}_{=0} + \underbrace{\int_{\Gamma_{\text{w}}} T\boldsymbol{u}\cdot\boldsymbol{n}\, d\Gamma_{\text{w}}}_{=0} + \int_{\Gamma_{\text{out}}} T\boldsymbol{u}\cdot\boldsymbol{n}\, d\Gamma_{\text{out}} \Big] \tag{21}$$

The first term in the above equation remains constant versus iterations because the temperature and velocity profiles are imposed initially at the inlet boundary Γ_{in} (see Fig. 1). The next two terms becomes equal to zero by the virtue of the fact that no-slip velocity boundary condition ($\boldsymbol{u}\cdot\boldsymbol{n} = 0$) was imposed initially at the walls Γ_{ad} and Γ_{w}. Hence, the only term left to optimize (maximize) for the present problem is the fourth term at the outlet Γ_{out} to the right hand side of Eqn. (21). This term is made of two unknown field variables: the temperature and the dot product of the velocity vector and the unit vector normal to the boundary surface at the outlet. Hence, for a more deep analysis of the optimal designs presented in Fig. 3, the normalized temperature and normalized velocity magnitude profiles are plotted at the outlet boundary as shown in Fig. 12 (a) and (b), respectively.

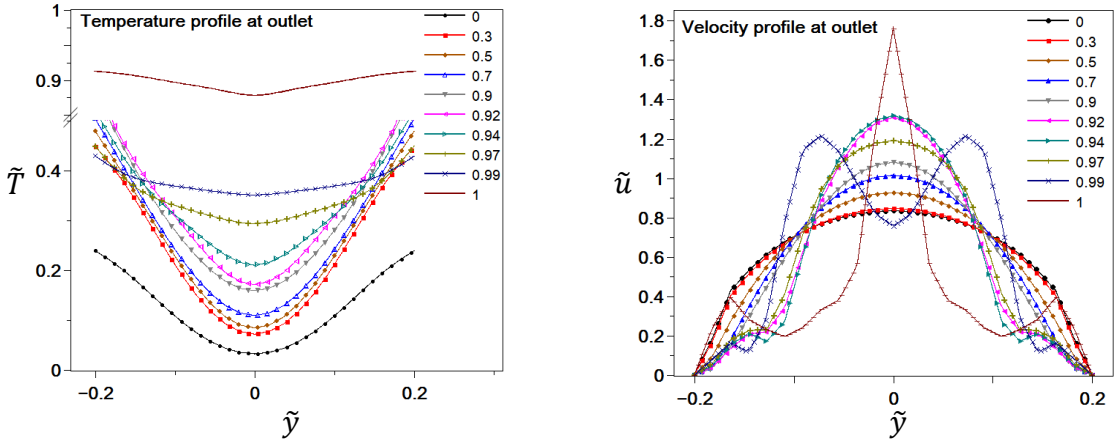

(a) Normalized temperature profiles

(b) Normalized velocity profiles

Figure 12: a) Normalized temperature and b) Normalized velocity magnitude profiles at the outlet boundary Γ_{out}.

It can be seen from figure 12 that the temperature values at the outlet for the optimal designs at $\omega = 0.3,\ 0.5$ and 0.7 are very close because the TO process here is predominantly trying to maximize the velocity at the outlet by changing the shape of the straight fluid channel (converging it or making it narrower). For the optimal designs from $\omega = 0.9$ onwards, there is a significant increase of both temperature and velocity values at the outlet. Now the TO process can be seen as working at its full potential in order to exploit both the contributing factors in the objective function.

On the contrary, Marck et al.[40] used a constant parabolic velocity outlet condition (same value as at the inlet) for the boundary Γ_{out}. Consequently, the only variable left in the

objective function J_{th} which the TO process could exploit (maximize) was the temperature at the outlet. Knowingly or unknowingly, the choice of inappropriate velocity BC at the outlet restricted the performance of their TO numerical tool to a single variable. As a result, the authors observed splitting of the fluid channel from a very early stage as the only alternative for the TO process was to heat up the fluid by moving it closer to the walls. Additionally, in contrast to the present study, the authors did not observe any fluid channel designs that aimed at increasing the velocity of the fluid (for example, converging or narrowing fluid channels).

3.5. Order of magnitude analysis of the thermal objective function

To justify the order of magnitude of recoverable thermal power values obtained in the present study, the following section aims to approximate analytically the values of J_{th} at the domain boundary on one of the optimal designs presented in Fig. 3. For the current problem, the thermal objective function is evaluated on the domain boundaries Γ as described by Eqn. 21. Following the analysis in the previous section, the equation can be re-written here as follows:

$$J_{th}(\boldsymbol{u}, T) = \rho C_p \left[\Big(\int_{\Gamma_{\text{in}}} T\boldsymbol{u} \cdot \boldsymbol{n} \; d\Gamma_{\text{in}} \Big) + \Big(\int_{\Gamma_{\text{out}}} T\boldsymbol{u} \cdot \boldsymbol{n} \; d\Gamma_{\text{out}} \Big) \right] \tag{22}$$

Thus, the computed value of J_{th} has contribution only from the inlet and the outlet boundary. As an example, the optimal design for $\omega = 0.9$ (see Fig. 3(e)) is considered for the current analysis. Now, if it is assumed that the velocity vector ($\boldsymbol{u}$) and the normal vector to the surface at inlet and outlet ($\boldsymbol{u}$) are exactly parallel to each other, then the above equation can be simplified as follows:

$$J_{th}\Big|_{approx} = \rho C_p \Big[\underbrace{- \int_{\Gamma_{\text{in}}} T u_x \; d\Gamma_{\text{in}}}_{\text{I}} + \underbrace{\int_{\Gamma_{\text{out}}} T u_x \; d\Gamma_{\text{out}}}_{\text{II}} \Big] \tag{23}$$

Note that the negative sign in the above equation appears due to the opposite signs of normal vector to the surface at inlet and outlet boundary in OpenFOAM software package. The two integral terms in equation 23 can be easily evaluated from Fig. 13 as the area under the curve for the the function Tu_x at inlet and outlet, respectively. Additionally, for the current study $\rho = 1000 \; kg \; m^{-3}$ and $C_p = 5000 \; Jkg^{-1}K^{-1}$. Hence, the value of thermal objective function for the optimal design with $\omega = 0.9$ can be approximated as:

$$J_{th}\Big|_{approx} = 1000 \times 5000 \Big[- (1.822 \times 10^{-5}) + (1.837 \times 10^{-5}) \Big] = 0.75 \; W \tag{24}$$

The approximate value of thermal objective function obtained by above analysis is very close to the numerical value of 0.76 W reported by the TO method but more importantly this analysis justifies the order of magnitude of the thermal objective function obtained in the present study.

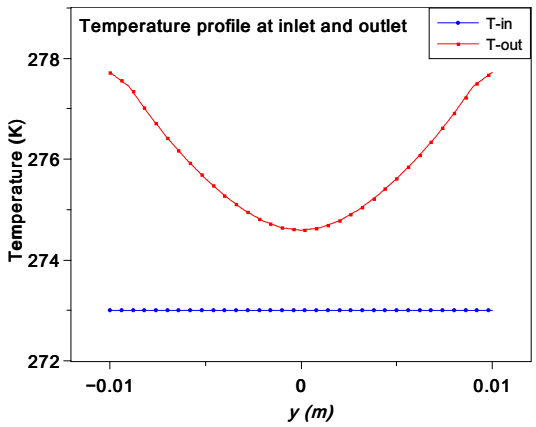

(a) T profile at inlet (blue) and outlet (red).

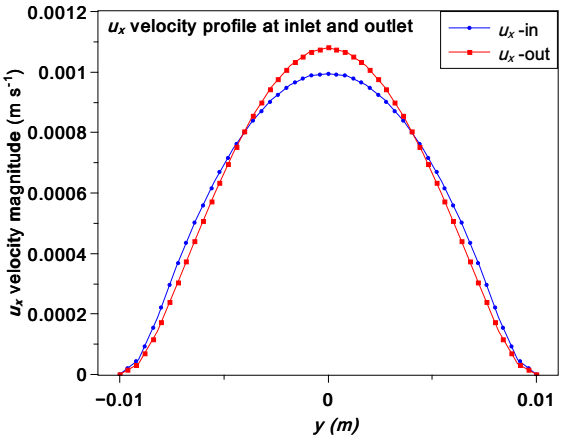

(b) u_x profile at inlet (blue) and outlet (red).

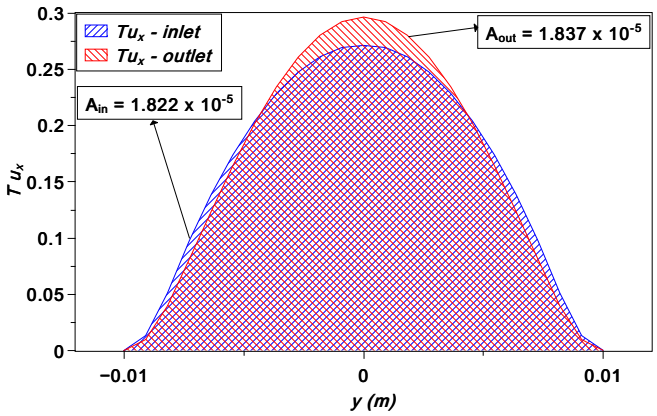

(c) Area under the curve for product (Tu_x) at inlet (blue) and outlet (red).

Figure 13: Analytical evaluation of the thermal objective function J_{th} at inlet and outlet boundaries for the optimal design obtained with $\omega = 0.9$: a) Temperature profile at inlet and outlet, b) u_x velocity profile at inlet and outlet, and c) Area under the curve for the product Tu_x.

3.6. Influence of variation of physical and numerical parameters on the optimal designs for CHT systems

This section demonstrates the effect of variation of some physical and numerical parameters on the final optimal topology of CHT systems. The objective here is to test the ability of developed multi-objective TO numerical solver in producing physically logical structures on varying some important parameters in the optimization problem. For the sake of simplicity, the results in this section are presented only for two values of ω.

3.6.1. Fluid as the higher thermal diffusivity material

All the results obtained in section 3.1 considered solid as the higher thermal diffusivity material in the domain such that $\gamma = D_s/D_f = 10$. Therefore, as the first parameter, the optimization problem described in section 2 is re-evaluated with the reversed thermal diffusivity ratio such that the fluid material now has the higher thermal diffusivity in the domain i.e. $\gamma = D_s/D_f = 0.1$ and all other parameters unchanged.

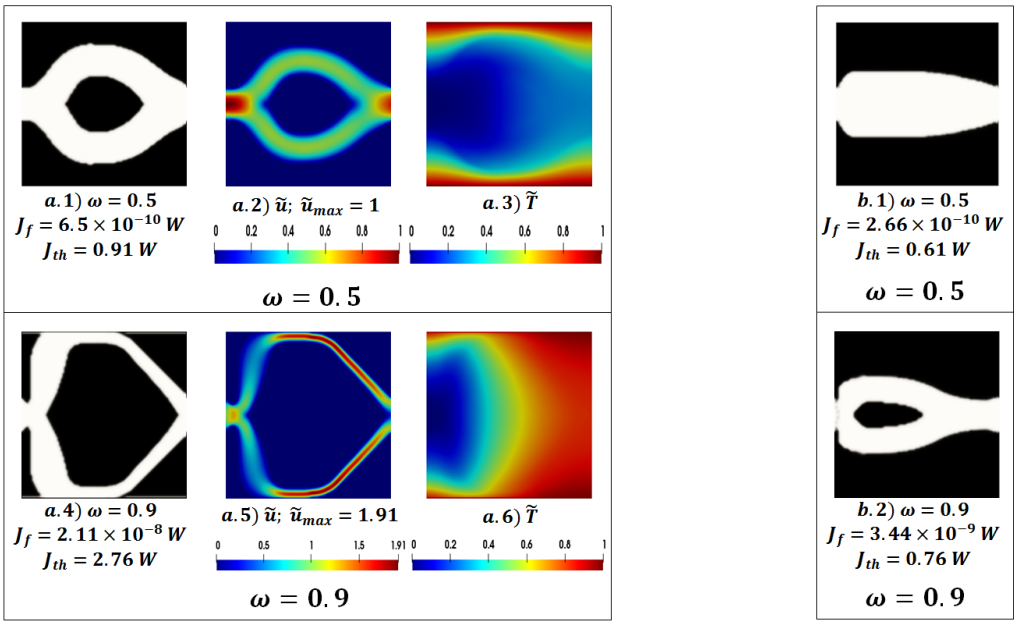

Optimal designs obtained when fluid has higher thermal diffusivity:
$\gamma = D_s/D_f = 0.1$;
$\Delta T = 10K$ & $Re = 3$.

(a) Fluid with the higher thermal diffusivity

Original optimal designs from Fig. 2:
$\gamma = D_s/D_f = 10$;
$\Delta T = 10K$ & $Re = 3$.

(b) Solid with the higher thermal diffusivity

Figure 14: Optimal designs obtained for $\omega = 0.5$ and $\omega = 0.9$ with: a) Fluid as the higher thermal diffusivity material and b) Solid as the higher thermal diffusivity material in the domain.

Figure 14 (a) shows the optimal design obtained for $\omega = 0.5$ and $\omega = 0.9$ with fluid as the higher thermal diffusivity material . In contrast to the previous results (Figure 14 (b)), the fluid channel is already split into two upper and lower fluid paths at $\omega = 0.5$ and moreover these fluid paths move very close to the heated walls at $\omega = 0.9$. This behavior of the optimal fluid channels design can be attributed to the inability of the solid material to conduct more heat to the passing fluid in the current problem. Consequently, on increasing ω, the higher thermal diffusive (or conductive) fluid material attempts to position itself closer to the heat source (the heated walls) in order to extract maximum thermal power from the system. As for the similarities, the fluid channels continue to become narrower on increasing ω in order to increase velocity of the fluid at the outlet which eventually increases the thermal objective function.

3.6.2. Variation of maximum temperature gradient in the system

The problem description in section 2 considered a temperature difference of 10 Kelvin between the cold incoming fluid (T_{in}) and the top and bottom heated walls (T_w). Therefore, the next parameter involves varying the thermal boundary conditions in the domain by changing the maximum temperature gradient in the system. Consequently, the original problem in section 2 is re-evaluated with the modified thermal boundary conditions for the three different cases as follow:

– Cold fluid and hot walls: $\Delta T = (T_w - T_{in}) = 313\ K - 273\ K = 40\ K$

– Cold fluid and hot walls: $\Delta T = (T_w - T_{in}) = 353\ K - 273\ K = 80\ K$

– Hot fluid and cold walls: $\Delta T = (T_w - T_{in}) = 273\ K - 283\ K = -10\ K$

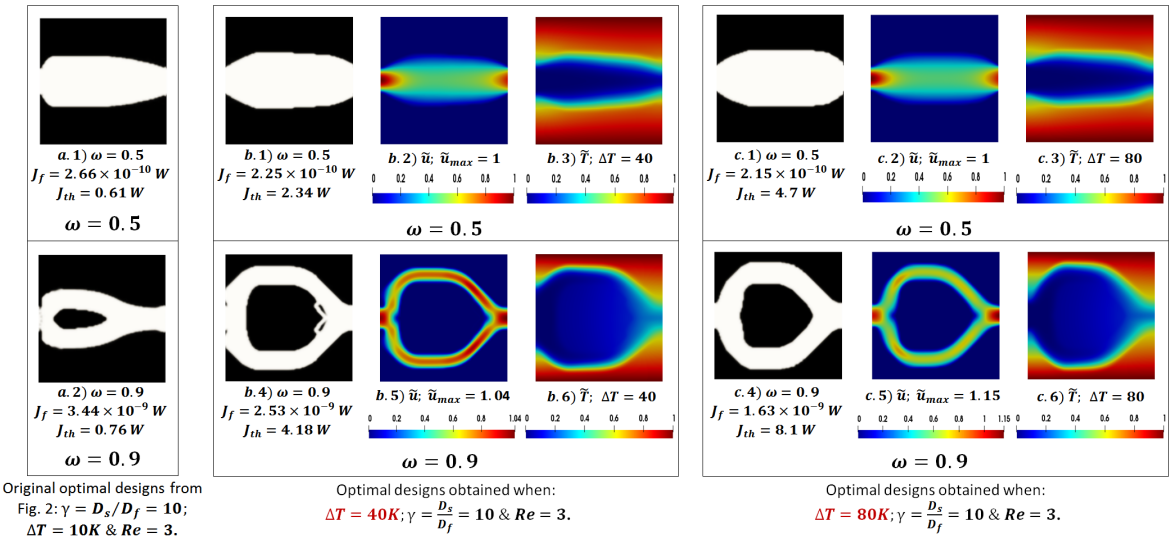

(a) $\Delta T = 10\ K$ (b) $\Delta T = 40\ K$ (c) $\Delta T = 80\ K$

Figure 15: Optimal designs for modified thermal boundary conditions: The thermal diffusivity ratio between solid and fluid maintained as $\gamma = D_s/D_f = 10$ with Cold incoming fluid and hot walls for a) $\Delta T = 10\ K$, b) $\Delta T = 40\ K$ and c) $\Delta T = 80\ K$.

ΔT in (Kelvin)	J_f in (Watts)	J_{th} in (Watts)
$\omega = 0.5$		
10	2.66×10^{-10}	0.61
40	2.25×10^{-10}	2.34
80	2.15×10^{-10}	4.7
$\omega = 0.9$		
10	3.44×10^{-9}	0.76
40	2.53×10^{-9}	4.18
80	1.63×10^{-9}	8.1

Table 1: Objective function values for the optimal designs with $\omega = 0.5$ and $\omega = 0.9$ for the three values of maximum temperature gradient in the domain (ΔT = 10 K, 40 K and 80 K with cold incoming fluid and heated walls).

On comparison with the previous results obtained in with ΔT =10 K (Fig. 15 (a)), Figure 15(b) and (c) show the optimal designs obtained for cold incoming fluid and heated

walls boundary conditions with ΔT =40 K and ΔT =80 K, respectively. Table 1 summarizes the objective function values for the optimal designs with $\omega = 0.5$ and $\omega = 0.9$ for the three values of maximum temperature gradient in the domain (ΔT = 10 K, 40 K and 80 K with cold incoming fluid and heated walls).

The pattern of optimal design evolution with ω remains similar for the three cases whenever the incoming fluid is cold and the top and bottom walls are hot i.e. ($T_w > T_{in}$). Additionally, as expected, the value of thermal objective function significantly increases with increasing value of ΔT because of the possibility of recovering more heat from the domain.

Figure 16 shows the optimal design obtained when the incoming fluid is hot and the top and bottom walls are cold ($T_{in} > T_w$) with $\Delta T = T_w - T_{in} = -10\ K$. Interestingly, in contrast to the previous results, the fluid channel between inlet and outlet attempts to move away as far as possible from the cold walls in order to prevent the heat loss from the passing fluid, on increasing the value of ω. Such optimal designs clearly demonstrate the ability of the developed multi-objective TO numerical solver in producing physically logical designs by appropriately responding to any critical changes in the problem description.

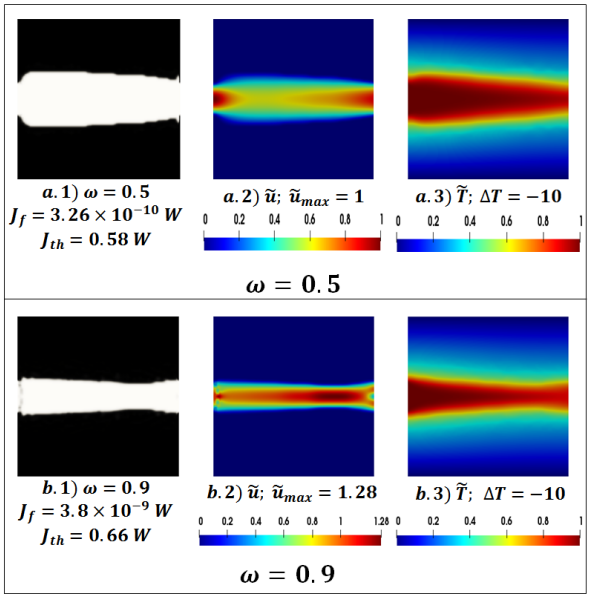

Figure 16: Optimal designs for modified thermal boundary conditions: The thermal diffusivity ratio between solid and fluid maintained as $\gamma = D_s/D_f = 10$ with Hot incoming fluid and cold walls for $\Delta T = -10\ K$

3.6.3. Variation of the Reynolds number

The original problem in section 2 (which considered a Reynolds number of $Re = 3$) is solved again for $Re = 10$ and $Re = 100$ by augmenting the inlet fluid velocity. Figure 17 present the optimal designs for $Re = 10$ and $Re = 100$, respectively compared with the previous results obtained for $Re = 3$ for the two values of ω. Additionally, Table 2 summarizes the objective function values for the optimal designs with $\omega = 0.5$ and $\omega = 0.9$ for the three

different values of Reynolds number of the incoming fluid. Evidently, there is a significant increase in fluid objective function J_f as the Re increases due to the higher fluid velocities in system. Another important observation is the moderate increase in thermal objective function J_{th} on increasing Re even when the thermal boundary condition are same for the three cases. This comes as a direct consequence of the contribution of velocity term in the thermal objective function. Finally, it can be clearly observed from Table 1 and 2 that the objective function J_f is more sensitive to inertial influence of increasing Re whereas the objective function J_{th} is more sensitive to increase of ΔT in the domain.

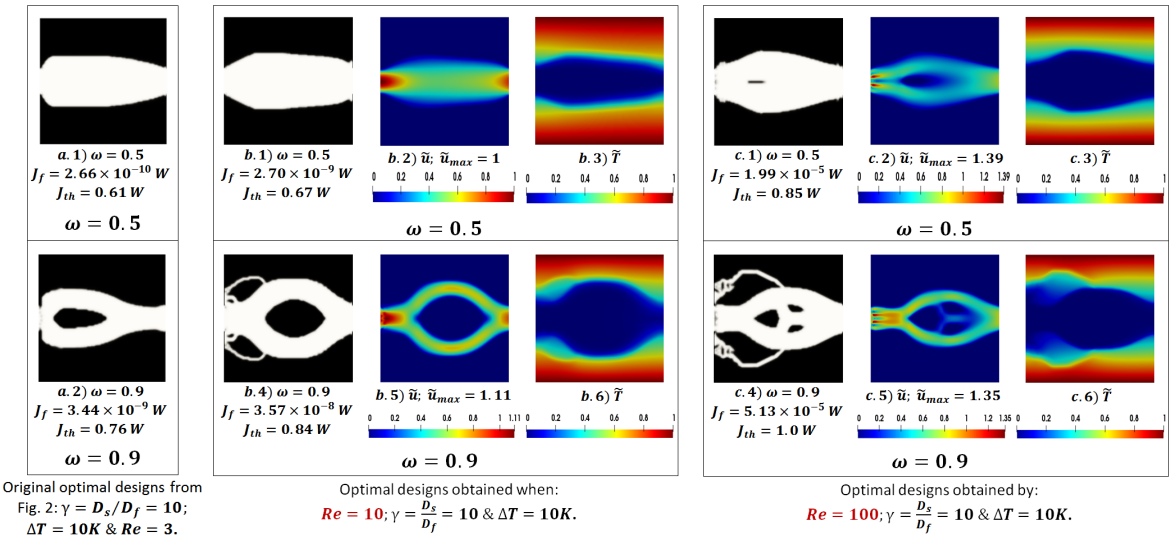

(a) $Re = 3$ (b) $Re = 10$ (c) $Re = 100$

Figure 17: Optimal designs obtained with the thermal diffusivity ratio between solid and fluid maintained as $\gamma = D_s/D_f = 10$ and varying the Reynolds number as: a) $Re = 3$, b) $Re = 10$ and c) $Re = 100$.

Re	J_f in (Watts)	J_{th} in (Watts)
$\omega = 0.5$		
3	2.66×10^{-10}	0.61
10	2.70×10^{-9}	0.67
100	1.99×10^{-5}	0.85
$\omega = 0.9$		
3	3.44×10^{-9}	0.76
10	3.57×10^{-8}	0.84
100	5.13×10^{-5}	1.0

Table 2: Objective function values for the optimal designs with $\omega = 0.5$ and $\omega = 0.9$ for the three different values of Reynolds number of the incoming fluid: Re =3, Re = 10 and Re = 100.

3.6.4. Influence of spatial discretization

Next, the influence of spatial discretization of the computational domain on the topology optimized designs is analysed. The original conjugate heat transfer optimization problem described in section 2 is solved on five different meshes (consisting of 60×60, 80×80, 100×100, 120×120 and 140×140 square-cell design elements, respectively) and the two objective function values are monitored on the converged solution. Subsequently, the relative percentage error is also evaluated for each case. Figure 18 presents the corresponding optimal designs and the associated objective function values (J_f and J_{th}) for two different values of ω: $\omega = 0.5$ and $\omega = 0.94$. For each value of ω, the design with the best (lowest) fluid objective function values is highlighted with a blue box and the one with best (highest) thermal objective function value is highlighted with red box. Additionally, Fig. 19 and 20 plots the variation of the fluid objective function (J_f) and the thermal objective function (J_{th}) along with the associated relative percentage error with increasing mesh size for the two values of ω, respectively.

As a first observation, it can can be seen that the final optimal designs share similar design forms, however, with better and clearer description of fluid channel boundaries with increasing mesh size. Moreover, the plots in Fig. 19 and 20 depicts the general trend of obtaining better objective function values with higher mesh size. On further observation, it can be seen that very close objective function values are obtained with the last two meshes which use 120×120 and 140×140 design elements, respectively. Hence, it can be said that mesh independent designs for the current problem can be obtained by using a mesh resolution of 120×120 cells.

ω	60×60 Cells	80×80 Cells	100×100 Cells	120×120 Cells	140×140 Cells
0.5					
$J_f(\mathbf{W})$	5.21×10^{-10}	2.345×10^{-10}	2.66×10^{-10}	2.34×10^{-10}	2.20×10^{-10}
$J_{th}(W)$	0.52	0.59	0.61	0.63	0.62
0.94					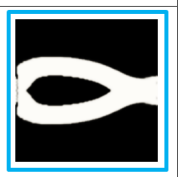
J_f	1.20×10^{-8}	1.04×10^{-8}	9.15×10^{-9}	7.81×10^{-9}	7.2×10^{-9}
J_{th}	0.73	0.85	0.86	0.90	0.87

Figure 18: Optimal designs for $\omega = 0.5$ and $\omega = 0.94$ obtained with five different mesh sizes: 60×60, 80×80, 100×100, 120×120 and 140×140 square-cell designs elements, respectively.

Generally, density-based TO approach is believed to suffer from mesh-dependence problem i.e., the problem of not obtaining qualitatively the same solution for different spatial

discretization also reffered as obtaining *non-unique solutions* or several optima. This problem is acknowledged by several authors who dealt with heat conduction or structural TO problems [17, 58]. However, the results in Fig. 18 clearly show that the current topology optimization model does not suffer from mesh-dependency numerical instability when using a Cartesian grid with orthogonal square elements.

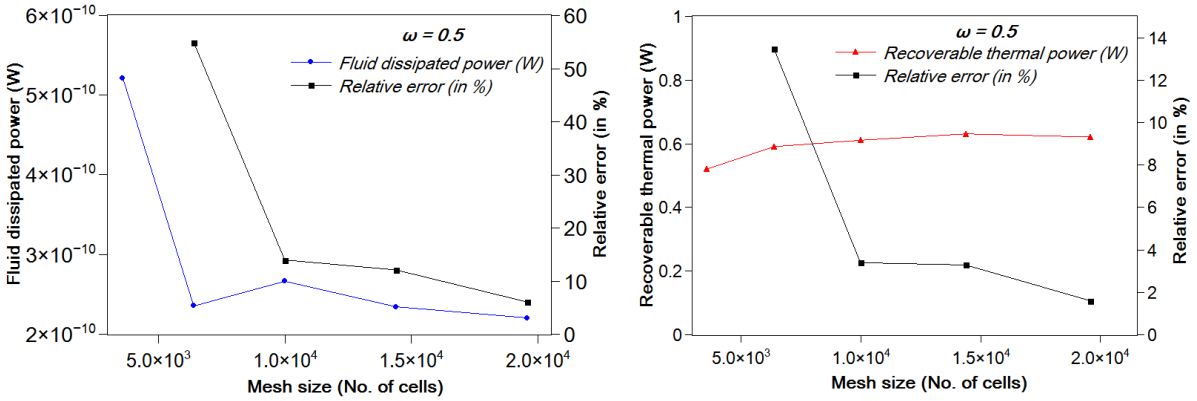

(a) Fluid dissipated power. (b) Recoverable thermal power.

Figure 19: Variation of objective function values and the associated relative percentage error with increasing mesh size for the optimal design obtained with $\omega = 0.5$.

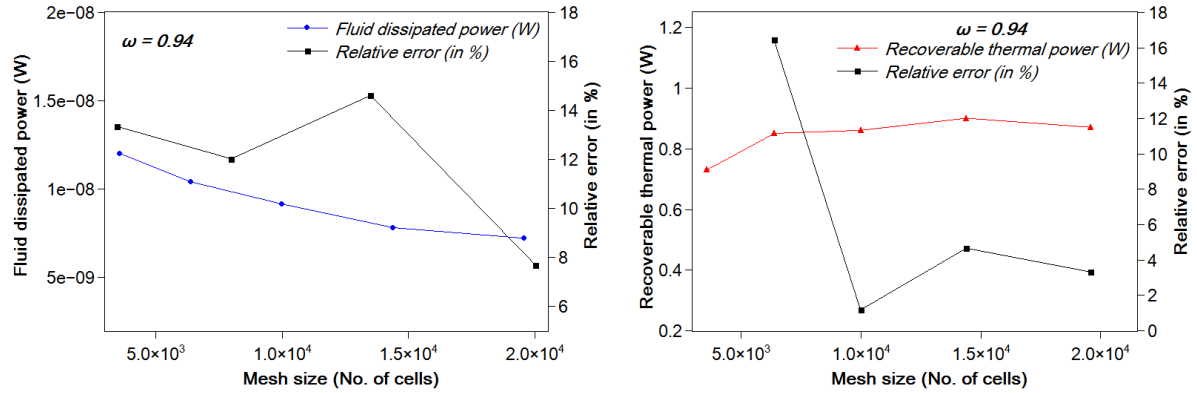

(a) Fluid dissipated power. (b) Recoverable thermal power.

Figure 20: Variation of objective function values and corresponding relative percentage error with increasing mesh size for the optimal design obtained with $\omega = 0.94$.

3.6.5. Comparison of topology optimization approaches

In this section, we analyze the results obtained by two different topology optimization approaches for the same design problem by comparing their optimal designs in terms of objective function values. The present TO numerical platform is based on the Finite Volume Method (FVM) as the discretization technique coupled to a density approach for material distribution in the domain, RAMP-type interpolation functions in this case. It is applied to a recent conjugate heat transfer topology optimization problem taken from the literature by [44] where the authors solved the optimization problem using the Lattice Boltzmann

Method (LBM) as discretization technique coupled to a Level Set Method (LSM) for material boundary representation in the domain.

The FVM is based on discretizing macroscopic continuum equations while the LBM deals with microscopic models and mesoscopic kinetic equations where the displacement and collision of particles are solved via the Boltzmann equation [44][62]. In addition to this, both approaches use gradient-based local optimization algorithms complemented by the continuous adjoint method for sensitivity analysis. Both the optimization approaches try to maximize the same thermal objective function, however Dugast et al. [44] refers it as the heat exchange efficiency characterized by the amount of heat evacuated from the fluid. On the other hand, in the he present study it referred as the thermal power recovered by the fluid. Essentially, both the objective function are the same as they aim to maximize the term $T(\mathbf{u} \cdot \mathbf{n})$ at the outlet boundary Γ_{out}.

The 2D design domain and the boundary conditions of the optimization problem by [44] are shown in Fig. 21. The gray and white zones near the boundary are fixed solid and fluid parts, respectively. The rest of the geometry is very similar to the original problem description of the fluid channel with an inlet and an outlet as shown in Fig. 1. The length of the heated segment at the bottom wall (0.04 m) is longer that the top wall (0.02 m) in order to introduce an asymmetric effect.

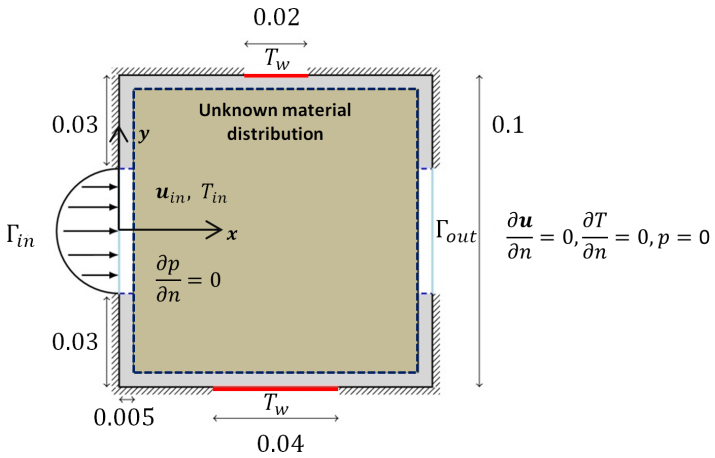

Figure 21: Initial configuration of the optimization problem (adapted from Dugast et al.[44]): All dimensions are in m.

The physical and numerical parameters for the above optimization problem based on the works by Dugast et al. [44] are as the following:

- fluid material: water (constant physical properties at $T = 45°$)
- solid material: constant thermal properties of water
- spatial discretization of the domain: 100×100 elements
- maximum allowed porosity: $\phi_{max} = 0.5$

– Reynolds number at inlet: $Re = 25$

– inlet fluid temperature: $20°C$

– heated segment temperature at top and bottom walls: $100°C$.

– initialization: full fluid

In order to ensure consistency and better compare the performance of the optimal fluid channel designs, the two optimal structures obtained from the present OpenFOAM TO numerical platform and from that by Dugast et al. [44], respectively for the same optimization problem are extracted and then simulated in STAR-CCM+®commercial CFD software package using identical grid settings and numerical schemes to get the objective function values. Figure 22 shows the two optimal designs and the associated velocity magnitude, temperature and pressure contours obtained from CFD simulations. Table 3 gives the objective function values and the pressure drop for two optimal designs.

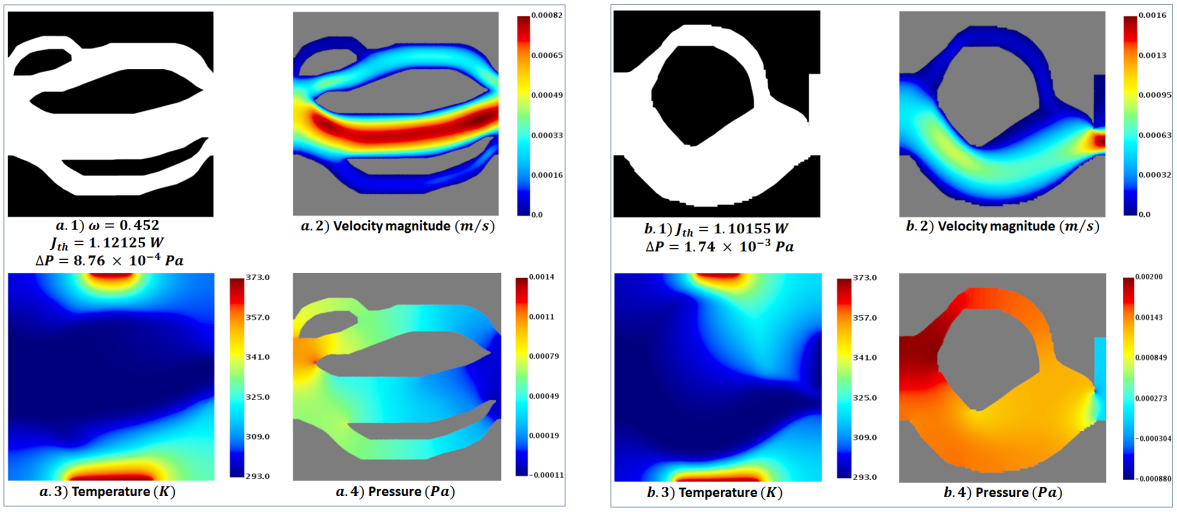

(a) Optimal design obtained in the present study.(b) Optimal design obtained by Dugast et al. [44].

Figure 22: Optimal designs obtained with : a) FVM discretization with density approach TO (present study) and b) LBM coupled to LSM for TO (Dugast et al. [44]).

Discretization method	J_{th} in (Watts)	ΔP in (Pa)
FVM (present study)	1.12125	8.76×10^{-4}
LBM (Dugast et al.)	1.10155	1.74×10^{-3}

Table 3: Objective function and pressure drop values for the optimal designs achieved from FVM and LBM dicretization methods.

Comparison the two structures, it can be observed that the objective function value (thermal power) of the optimal design obtained by the present FVM-based TO platform

is marginally higher than that obtained by Dugast et al. [44] but more importantly with around 50% less pressure drop as compared to the latter. This means that the present FVM-based TO platform coupled with the density approach produced better optimal design than that produced by [44] which is LBM-based TO platform coupled to level-sets for boundary representation. The high pressure drop values for the LBM optimal design can be attributed to the partial obstruction of the flow near the outlet (see Fig. 22b) which the LBM-based optimization approach created on purpose in order to increase the fluid velocity at the outlet which has a direct contribution in the thermal objective function. On the other hand, the bi-objective function strategy (with $\omega = 0.452$), the TO numerical platform in the present study was able to achieve similar thermal objective function values but with significantly reduced pressure drop value in the system with no obstruction at the outlet. This comparison clearly shows the advantage of using a bi-objective optimization approach particularly in topology optimization of conjugate heat transfer systems.

As for the similarities between the two designs, one can observe that both designs are asymmetric due to the asymmetric nature of the problem. Additionally, in both designs, the bulk of the fluid mass is pushed towards the bottom heated element as a direct consequence of its larger dimension compared to the top heated element. It should be noted that the thermal conductivity of the fluid and solid material are the same for this problem in Fig 21 which was taken as the thermal conductivity of water.

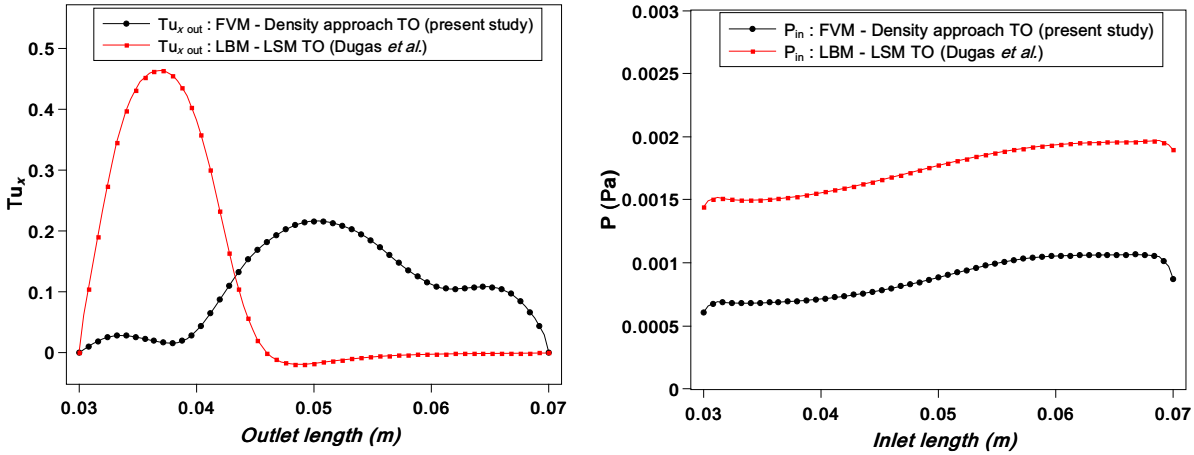

(a) Tu_x profile at outlet.

(b) Pressure profile at inlet.

Figure 23: Local analysis of the results at the domain boundary for the two designs: a) Comparison of the product Tu_x at outlet and b) Comparison of pressure profile at inlet.

Since the thermal objective function, which the optimization algorithm aims to maximize, is a product of temperature (T) and a horizontal component of velocity (u_x) at the outlet boundary, Fig. 23 represents a good methodology for deeper analysis. It illustrates the Tu_x profile at outlet and compares the pressure profile at inlet for the two obtained designs. Although there is a major increase of the product Tu_x near the bottom part at the outlet boundary for the LBM-based design, the overall average is slightly less than that of the FVM-based design due to the null fluid velocity at rest at the outlet boundary. This local analysis of results at the inlet and outlet boundaries justifies well the objective function and

pressure drop values reported in Table 3.

4. Conclusion

Topology optimization of conjugate heat transfer systems using a challenging coupled bi-objective function, for heat transfer enhancement and pressure drop reduction, has been developed and presented for laminar incompressible flows. The continuous adjoint method has been implemented for gradient computation within a density-based based approach for material distribution. The new topology optimization numerical platform is coupled to an inequality constrained optimization algorithm [56, 31] inside an open source CFD platform which uses the Finite Volume Method as the discretization technique.

The present numerical approach was then applied to an optimization problem from the literature [40] for optimizing a typical fluid channel domain with constant walls temperature different to the one imposed at the domain's inlet. The Pareto set of several optimal designs are computed, presented and analyzed.

It is found that the present developed numerical technique efficiently generates realistic topological optimal designs for conjugate heat transfer systems starting from pressure drop minimization to thermal power maximization based on the value of the weighting function. Notably, there is no fluid blockage, broken paths or other non-physical features observed in the optimal designs even at very high weighting factor of thermal objective function. Additionally, for the first time to our knowledge, an in-depth convergence study presented on the optimal structures confirmed that the developed numerical method respects well the equality (fluid continuity and momentum conservation equations) and inequality (imposed volume fraction of one material) constraints of the topology optimization problem.

A detailed analysis of the obtained optimal designs has been conducted. The friction factor has been computed as alternative performance criterion for pressure drop in the system. The obtained temperature and velocity profiles at the domain's outlet have been analyzed and justified. Moreover, an order of magnitude analysis was performed for the thermal objective function to justify its values obtained in the present study as compared to those obtained by [40].

A parametric study has been performed demonstrating the capability of the developed numerical platform in producing realistic structures (i.e., influence of the Reynolds number, spatial discretization, thermal diffusivity ratio and imposed temperature difference between the wall and the inlet).

Finally, a comparison of two different topology optimization approaches is presented for optimization of conjugate heat transfer systems. In that purpose, a recent CHT TO problem (from the literature [44]) which was solved **via a LBM-based solver coupled to level-sets** for boundary representation is solved again using the current developed TO platform but **via a FVM-based solver coupled to a density approach** for material distribution. Comparisons of results for the thermal power maximization and pressure drop reduction values of the obtained designs emphasized that the present FVM-based TO solver outperformed the LBM-based TO solver of [44] for this CHT TO problem.

Future experimental measurements, on some of the obtained optimal structures, will be conducted soon in order to quantify well the limits of validity of our topology optimization overall approach.

References

[1] W. M. Kays, A. L. London, Compact heat exchangers.

[2] M. P. Bendsøe, N. Kikuchi, Generating optimal topologies in structural design using a homogenization method, Computer methods in applied mechanics and engineering 71 (2) (1988) 197–224.

[3] T. Dbouk, A review about the engineering design of optimal heat transfer systems using topology optimization, Applied Thermal Engineering 112 (2017) 841–854.

[4] M. C. E. Manuel, P. T. Lin, Heat exchanger design with topology optimization, in: Heat Exchangers-Design, Experiment and Simulation, InTech, 2017.

[5] M. P. Bendsøe, Optimal shape design as a material distribution problem, Structural optimization 1 (4) (1989) 193–202.

[6] M. Zhou, G. Rozvany, The coc algorithm, part ii: topological, geometrical and generalized shape optimization, Computer Methods in Applied Mechanics and Engineering 89 (1-3) (1991) 309–336.

[7] H. Mlejnek, Some aspects of the genesis of structures, Structural Optimization 5 (1-2) (1992) 64–69.

[8] G. Allaire, F. Jouve, A.-M. Toader, A level-set method for shape optimization, Comptes Rendus Mathematique 334 (12) (2002) 1125–1130.

[9] M. Y. Wang, X. Wang, D. Guo, A level set method for structural topology optimization, Computer methods in applied mechanics and engineering 192 (1) (2003) 227–246.

[10] K. Yaji, T. Yamada, M. Yoshino, T. Matsumoto, K. Izui, S. Nishiwaki, Topology optimization using the lattice boltzmann method incorporating level set boundary expressions, Journal of Computational Physics 274 (2014) 158 – 181. doi:https://doi.org/10.1016/j.jcp.2014.06.004.
URL http://www.sciencedirect.com/science/article/pii/S0021999114004112

[11] J. Sokolowski, A. Zochowski, On the topological derivative in shape optimization, SIAM journal on control and optimization 37 (4) (1999) 1251–1272.

[12] B. Bourdin, A. Chambolle, Design-dependent loads in topology optimization, ESAIM: Control, Optimisation and Calculus of Variations 9 (2003) 19–48.

[13] Y. M. Xie, G. P. Steven, A simple evolutionary procedure for structural optimization, Computers & structures 49 (5) (1993) 885–896.

[14] O. Sigmund, K. Maute, Topology optimization approaches, Structural and Multidisciplinary Optimization 48 (6) (2013) 1031–1055.

[15] A. Gersborg-Hansen, M. P. Bendsøe, O. Sigmund, Topology optimization of heat conduction problems using the finite volume method, Structural and multidisciplinary optimization 31 (4) (2006) 251–259.

[16] J. Dirker, J. P. Meyer, Topology optimization for an internal heat-conduction cooling scheme in a square domain for high heat flux applications, Journal of Heat Transfer 135 (11) (2013) 111010.

[17] G. Marck, M. Nemer, J.-L. Harion, S. Russeil, D. Bougeard, Topology optimization using the simp method for multiobjective conductive problems, Numerical Heat Transfer, Part B: Fundamentals 61 (6) (2012) 439–470.

[18] F. H. Burger, J. Dirker, J. P. Meyer, Three-dimensional conductive heat transfer topology optimization in a cubic domain for the volume-to-surface problem, International Journal of Heat and Mass Transfer 67 (2013) 214–224.

[19] V. Subramaniam, T. Dbouk, J.-L. Harion, Topology optimization of conductive heat transfer devices: An experimental investigation, Applied Thermal Engineering 131 (2018) 390–411.

[20] T. Borrvall, J. Petersson, Topology optimization of fluids in stokes flow, International journal for numerical methods in fluids 41 (1) (2003) 77–107.

[21] A. Gersborg-Hansen, O. Sigmund, R. B. Haber, Topology optimization of channel flow problems, Structural and Multidisciplinary Optimization 30 (3) (2005) 181–192.

[22] L. H. Olesen, F. Okkels, H. Bruus, A high-level programming-language implementation of topology optimization applied to steady-state navier-stokes flow, arXiv preprint physics/0410086.

[23] C. Othmer, E. de Villiers, H. G. Weller, Implementation of a continuous adjoint for topology optimization of ducted flows, in: 18th AIAA Computational Fluid Dynamics Conference, June, 2007.

[24] C. Othmer, A continuous adjoint formulation for the computation of topological and surface sensitivities of ducted flows, International Journal for Numerical Methods in Fluids 58 (8) (2008) 861–877.

[25] Y. Deng, Z. Liu, P. Zhang, Y. Liu, Y. Wu, Topology optimization of unsteady incompressible navierstokes flows, Journal of Computational Physics 230 (17) (2011) 6688 – 6708. doi:https://doi.org/10.1016/j.jcp.2011.05.004.
URL http://www.sciencedirect.com/science/article/pii/S0021999111003019

[26] L. Yin, G. Ananthasuresh, A novel topology design scheme for the multi-physics problems of electro-thermally actuated compliant micromechanisms, Sensors and Actuators A: Physical 97 (2002) 599–609.

[27] T. E. Bruns, Topology optimization of convection-dominated, steady-state heat transfer problems, International Journal of Heat and Mass Transfer 50 (15-16) (2007) 2859–2873.

[28] S.-H. Ahn, S. Cho, Level set–based topological shape optimization of heat conduction problems considering design-dependent convection boundary, Numerical Heat Transfer, Part B: Fundamentals 58 (5) (2010) 304–322.

[29] A. Iga, S. Nishiwaki, K. Izui, M. Yoshimura, Topology optimization for thermal conductors considering design-dependent effects, including heat conduction and convection, International Journal of Heat and Mass Transfer 52 (11-12) (2009) 2721–2732.

[30] G. H. Yoon, Topological design of heat dissipating structure with forced convective heat transfer, Journal of Mechanical Science and Technology 24 (6) (2010) 1225–1233.

[31] K. Svanberg, The method of moving asymptotesa new method for structural optimization, International journal for numerical methods in engineering 24 (2) (1987) 359–373.

[32] E. M. Dede, Multiphysics topology optimization of heat transfer and fluid flow systems, in: proceedings of the COMSOL Users Conference, 2009.

[33] K. Lee, Topology optimization of convective cooling system designs.

[34] M. Stolpe, K. Svanberg, An alternative interpolation scheme for minimum compliance topology optimization, Structural and Multidisciplinary Optimization 22 (2) (2001) 116–124.

[35] T. Matsumori, T. Kondoh, A. Kawamoto, T. Nomura, Topology optimization for fluid–thermal interaction problems under constant input power, Structural and Multidisciplinary Optimization 47 (4) (2013) 571–581.

[36] P. E. Gill, W. Murray, M. A. Saunders, Snopt: An sqp algorithm for large-scale constrained optimization, SIAM review 47 (1) (2005) 99–131.

[37] E. Kontoleontos, E. Papoutsis-Kiachagias, A. Zymaris, D. Papadimitriou, K. Giannakoglou, Adjoint-based constrained topology optimization for viscous flows, including heat transfer, Engineering Optimization 45 (8) (2013) 941–961.

[38] J. Alexandersen, N. Aage, C. S. Andreasen, O. Sigmund, Topology optimisation for natural convection problems, International Journal for Numerical Methods in Fluids 76 (10) (2014) 699–721.

[39] A. A. Koga, E. C. C. Lopes, H. F. V. Nova, C. R. de Lima, E. C. N. Silva, Development of heat sink device by using topology optimization, International Journal of Heat and Mass Transfer 64 (2013) 759–772.

[40] G. Marck, M. Nemer, J.-L. Harion, Topology optimization of heat and mass transfer problems: laminar flow, Numerical Heat Transfer, Part B: Fundamentals 63 (6) (2013) 508–539.

[41] X. Qian, E. M. Dede, Topology optimization of a coupled thermal-fluid system under a tangential thermal gradient constraint, Structural and Multidisciplinary Optimization 54 (3) (2016) 531–551.

[42] S. Zeng, B. Kanargi, P. S. Lee, Experimental and numerical investigation of a mini channel forced air heat sink designed by topology optimization, International Journal of Heat and Mass Transfer 121 (2018) 663–679.

[43] J. H. Haertel, K. Engelbrecht, B. S. Lazarov, O. Sigmund, Topology optimization of a pseudo 3d thermofluid heat sink model, International Journal of Heat and Mass Transfer 121 (2018) 1073–1088.

[44] F. Dugast, Y. Favennec, C. Josset, Y. Fan, L. Luo, Topology optimization of thermal fluid flows with an adjoint lattice boltzmann method, Journal of Computational Physics 365 (2018) 376 – 404. doi:https://doi.org/10.1016/j.jcp.2018.03.040.
URL http://www.sciencedirect.com/science/article/pii/S0021999118302067

[45] K. Yaji, T. Yamada, M. Yoshino, T. Matsumoto, K. Izui, S. Nishiwaki, Topology optimization in thermal-fluid flow using the lattice boltzmann method, Journal of Computational Physics 307 (2016) 355 – 377. doi:https://doi.org/10.1016/j.jcp.2015.12.008.
URL http://www.sciencedirect.com/science/article/pii/S0021999115008244

[46] T. W. Athan, P. Y. Papalambros, A note on weighted criteria methods for compromise solutions in multi-objective optimization, Engineering Optimization 27 (2) (1996) 155–176.

[47] R. T. Marler, J. S. Arora, The weighted sum method for multi-objective optimization: new insights, Structural and multidisciplinary optimization 41 (6) (2010) 853–862.

[48] K. Khadra, P. Angot, S. Parneix, C. J-P, J. Numer. Methods Fluids 34 (2000) 651–684.

[49] T. DBOUK, F. PERALES, F. BABIK, R. MOZUL, A df-ibm/nscd coupling framework to simulate immersed particle interactions, Comput. Methods Appl. Mech. Engrg. 309 (2016) 610–624.

[50] M. P. Bendsoe, O. Sigmund, Topology optimization: theory, methods, and applications, Springer Science & Business Media, 2013.

[51] W. Jakob, C. Blume, Pareto optimization or cascaded weighted sum: A comparison of concepts, Algorithms 7 (1) (2014) 166–185.

[52] S. Nrgaard, O. Sigmund, B. Lazarov, Topology optimization of unsteady flow problems using the lattice boltzmann method, Journal of Computational Physics 307 (2016) 291 – 307. doi:https://doi.org/10.1016/j.jcp.2015.12.023.
URL http://www.sciencedirect.com/science/article/pii/S0021999115008426

[53] S. S. Rao, S. S. Rao, Engineering optimization: theory and practice, John Wiley & Sons, 2009.

[54] C. Hinterberger, M. Olesen, Industrial application of continuous adjoint flow solvers for the optimization of automotive exhaust systems, CFD & Optimization, Antalya, Turkey.

[55] H. K. Versteeg, W. Malalasekera, An introduction to computational fluid dynamics: the finite volume method, Pearson Education, 2007.

[56] K. Svanberg, A class of globally convergent optimization methods based on conservative convex separable approximations, SIAM J. Optim. 12 (2002) 555–573.

[57] T. Dbouk, J.-L. Harion, Performance of optimization algorithms applied to large nonlinear constrained problems, American Journal of Algorithms and Computing 2 (1) (2015) 32–56.

[58] O. Sigmund, J. Petersson, Numerical instabilities in topology optimization: a survey on procedures dealing with checkerboards, mesh-dependencies and local minima, Structural optimization 16 (1) (1998) 68–75.

[59] T. E. Bruns, D. A. Tortorelli, Topology optimization of non-linear elastic structures and compliant mechanisms, Computer Methods in Applied Mechanics and Engineering 190 (26) (2001) 3443–3459.

[60] O. Sigmund, Morphology-based black and white filters for topology optimization, Structural and Multidisciplinary Optimization 33 (4) (2007) 401–424.

[61] B. McKeon, C. Swanson, M. Zagarola, R. Donnelly, A. J. SMITS, Friction factors for smooth pipe flow, Journal of Fluid Mechanics 511 (2004) 41.

[62] S. Chen, G. D. Doolen, Lattice boltzmann method for fluid flows, Ann. Rev. of Fluid Mechanics 30 (2003) 329–364.

Chapter 5

Topology optimization applied to heat tranfer and fluid flows: Opportunities and limitations

The final chapter of this manuscript presents some of the important numerical and physical issues associated with density-based TO approach for designing optimal heat transfer and fluid flow systems, highlighting its strengths and limitations both in general and in context of the developed TO numerical tool during this thesis for its applicability in real and industrial applications. An attempt is made in this chapter to answer some of the "open" questions that currently exists in the field of TO for thermal systems. In this context, the present chapter is divided into three major sections. The first section presents a numerical verification of an optimal configuration obtained by TO. The second section demonstrates the difficulty faced by existing TO methods in literature in handling some complex boundary conditions commonly used in thermal systems. Finally, the third section presents a detailed parametric study to better understand the influence of some important numerical parameters in density-based TO with an aim to establish some guidelines for future studies in TO of heat transfer and fluid flow systems.

5.1 Numerical verification of topology optimized structure: A comparative study of Brinkman penalization approach and conventional multi-region CFD approach

It is important to examine and validate the performance of the optimal structures obtained numerically by topology optimization. For optimal designs of heat transfer and fluid flow systems, the ultimate goal should be to perform experimental validations to better investigate the performance of the topology optimized structures for real world applications. However, such experiments can sometimes be complicated and time consuming. Nonetheless, numerical verification over conventional CFD software packages may serve as a first step to qualify the performance of these optimized structures. The objective here is to estimate the accuracy of the implicit representation of solid-fluid regions via a density-based **Brinkman penalization approach** (employed in TO) by replacing it with an explicit separate modelling of solid and fluid domains using a **multi-region approach** (employed in conventional CFD) to better resolve the physics in fluid and thermal boundary layers.

In this context, the optimization problem considered in the section 3.6.5 of the article in Chapter 4 is revisited here for a comparative study of the two above mentioned numerical approaches. Figure 5.1(a) shows the 2D conjugate heat transfer TO problem under consideration. The physical and numerical parameters considered for the topology optimization problem in OpenFOAM® are as the following:

- fluid material: water (constant physical properties at $T = 45°$)
- solid material: constant thermal properties of water

– spatial discretization of the domain: 100×100 square-cell elements

– maximum allowed porosity: $\phi_{max} = 0.5$

– Reynolds number at inlet: $Re = 25$

– inlet fluid temperature: $20°C$

– heated segment temperature at top and bottom walls: $100°C$

– initialization: $\eta = 1$ (full fluid)

Fig. 5.1(b) shows the numerically obtained optimal design represented by the design variable (η) field at the end of the optimization process (where $\eta = 0$ represents the solid material and $\eta = 1$ represents the fluid material) and Fig. 5.1(c) presents the extracted CAD geometry from the design variable field for the purpose of numerical verification.

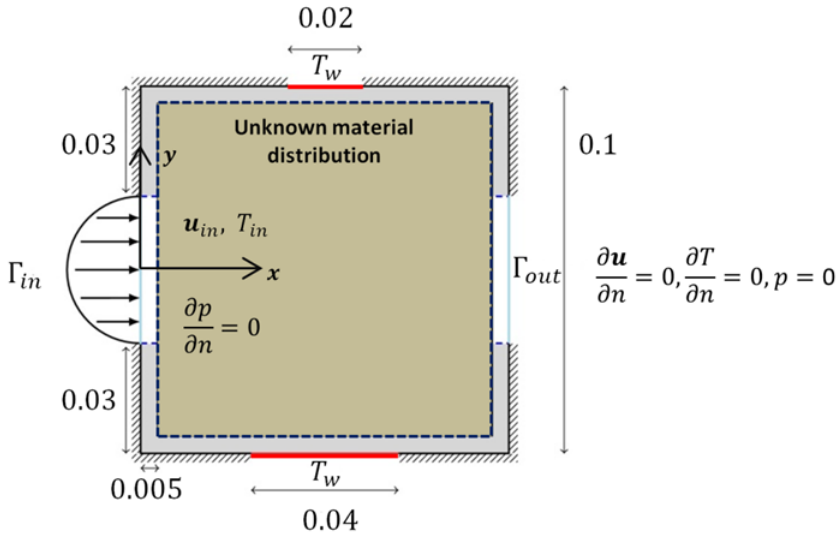

$a)$ Initial configuration and BC's for the optimization problem

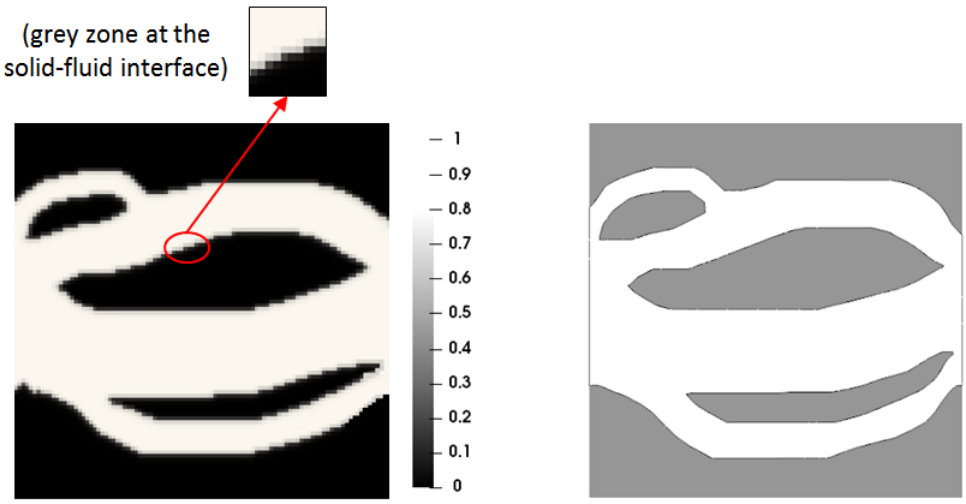

$b)$ Design variable (η) field after optimization

c) Extracted CAD geometry

Figure 5.1 – 2D CHT topology optimization problem: a) Initial configuration and boundary conditions; b) Optimal design realized in terms of design variable field (η) at the end of the optimization process where $\eta = 0$ represents the solid material and $\eta = 1$ represents the fluid material, and c) Extracted CAD geometry for numerical verification.

The extracted CAD geometry from Fig. 5.1(c) is numerically simulated in STAR-CCM+® commercial CFD software package with a multi-region approach. A conformal polyhedral mesh consisting of 42105 cells is used for the CFD simulations based on the current best practice guidelines for solving CHT problem in STAR-CCM+® [139]. Conformal meshes have faces that match exactly one-to-one at the solid-fluid interface. This ensures that heat transfer occurs smoothly across the interface. However, conformal mehses can currently be generated only by using the polyhedral mesher in STAR-CCM+® [139]. All other physical parameters and boundary conditions for the numerical simulations are kept exactly identical to the ones used for the OpenFOAM® TO problem.

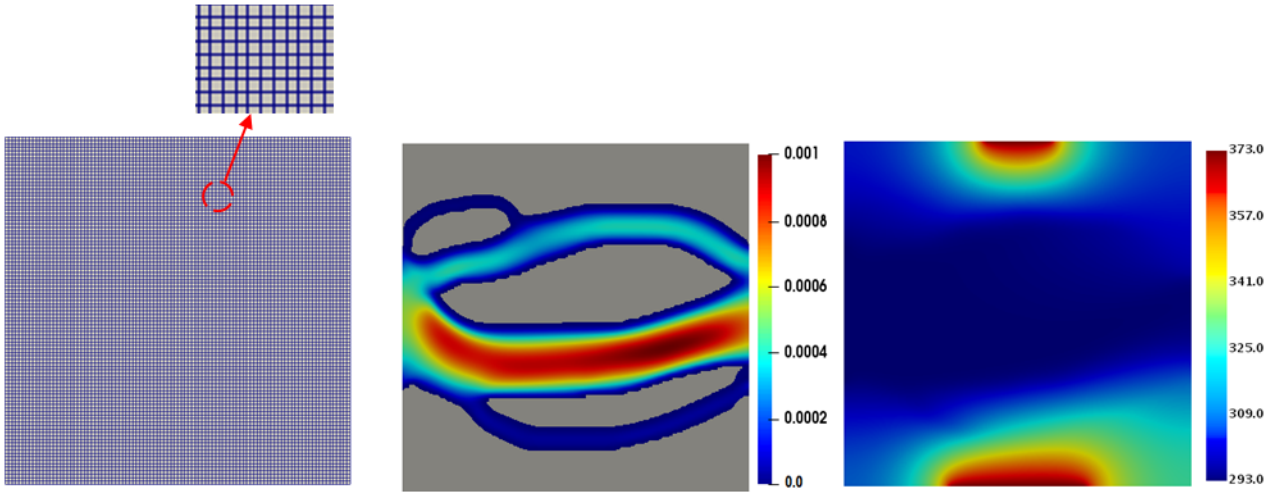

$a.1)$ Non-conformal Cartesian mesh | $a.2)$ Velocity magnitude (m/s) | $a.3)$ Temperature (K)

a) Solution using Brinkman penalization approach (used in TO in OpenFOAM solver)

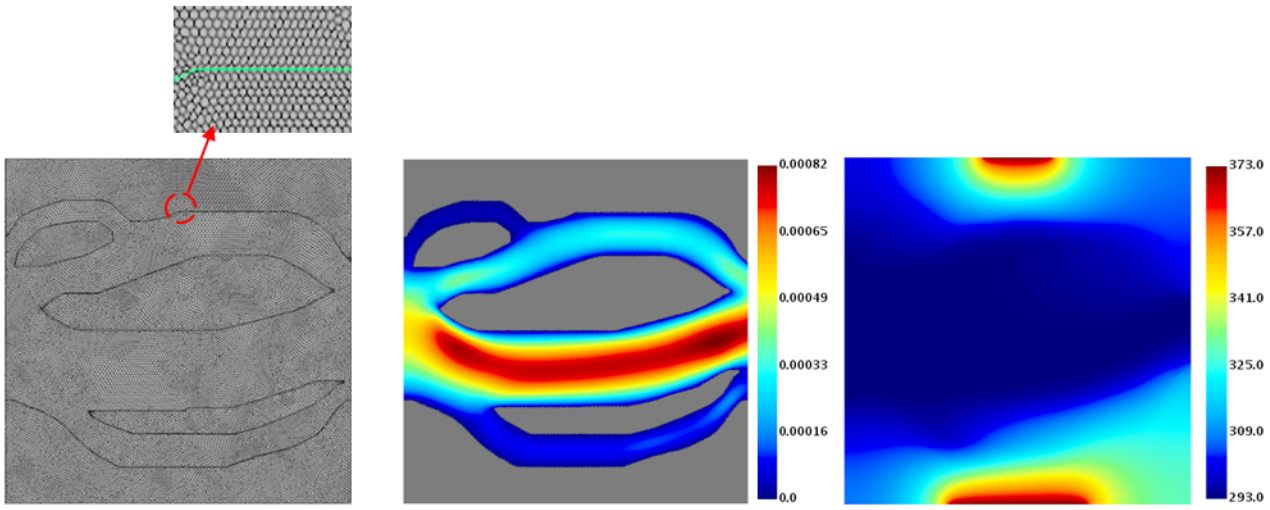

$b.1)$ Conformal polyhedral body-fitted mesh | $b.2)$ Velocity magnitude (m/s) | $b.3)$ Temperature (K)

b) Solution using multi-region approach (used in conventional CFD (STAR-CCM+®) solver)

Figure 5.2 – Numerical verification of 2D topology optimized configuration: a) **OpenFOAM® TO results**: Implicit solid-fluid representation in the iteartive Brinkman penalization approach used in TO, and b) **STAR-CCM+® CFD results**: Explicit solid-fluid representation used in conventional multi-region CFD approach.

Fig. 5.2(a) and (b) shows the mesh used for computation, contours of velocity magnitude and temperature fields in the domain obtained by iterative Brinkman penalization approach (used in TO) and multi-region approach (used in conventional CFD), respectively. Additionally, Table 5.1 gives the thermal objective function and pressure drop values as computed by the two numerical approaches.

The two results are in fair agreement with each other. It can be seen that slightly higher velocity magnitude values are obtained in the system when applying a Brinkman penalization approach. As a consequence, around $12\ \%$ higher pressure drop is reported in the system for TO results as compared to the CFD results. Moreover, the density-based Brinkman penalization TO approach predicts around $10\ \%$ less recoverable thermal power at the outlet as compared to the multi-region CFD approach.

Numerical approach	J_{th} in (Watts)	ΔP in (Pa)
Brinkman penalization (TO)	0.99895	9.83×10^{-4}
Multi-region (CFD)	1.12125	8.76×10^{-4}

Table 5.1 – Objective function and pressure drop values for the optimal designs reported by Brinkman penalization approach (used in TO) and multi-region approach (used in CFD).

As already described in Chapter 4, the thermal objective function (which is to be maximized during optimization) is a product of temperature (T) and the component of velocity (u_x) in the flow direction at the outlet boundary. Fig. 5.3(a) compares the (Tu_x) profiles obtained by the two different numerical approaches. Additionally, Fig. 5.3(b) compares their respective pressure profiles at inlet boundary. A slightly lower Tu_x values at outlet and higher pressure values at inlet obtained by the Brinkman penalization TO approach justifies the lower thermal recoverable power and higher pressure drop values reported by TO in Table 5.1.

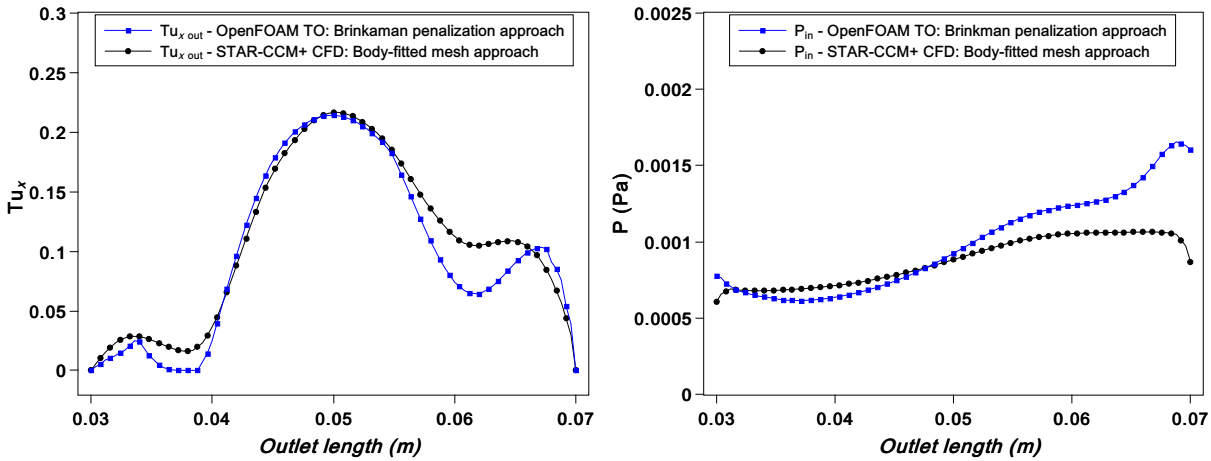

(a) Tu_x profile at outlet.

(b) Pressure profile at inlet.

Figure 5.3 – Local analysis of the results at the domain boundary for the two numerical approaches: a) Comparison of the product Tu_x at outlet and b) Comparison of pressure profile at inlet.

To understand the differences in the two results it is important to have a deeper understanding of the two approaches.

Brinkman penalization approach: Brinkman penalization approach is a particular type of immersed boundary (IB) method introduced to simulate fluid flows around stationary or moving solid obstacles of complex geometry on fixed non-conformal Cartesian grid. Here, the solid obstacles are modeled as porous media. The presence of a solid obstacle in the computational domain is modeled by adding a penalty term, depending on a *penalization* parameter, in the incompressible Navier-Stokes equations. The governing N-S equations for fluid region and penalized N-S equations for porous media are solved, simultaneously. As a result, it is not required to explicitly specify the solid-fluid interface conditions as they are automatically solved from the governing equations [140].

The governing equations for the CHT TO problem as described in section 2 of Chapter 4 are as follows:

$$\nabla \cdot \boldsymbol{u} = 0 \tag{5.1a}$$

$$(\boldsymbol{u} \cdot \nabla)\boldsymbol{u} = -\nabla p + \nabla \cdot (\nu \nabla \boldsymbol{u}) - \alpha(\eta)\boldsymbol{u} \tag{5.1b}$$

$$(\boldsymbol{u} \cdot \nabla)T = \nabla \cdot (D(\eta)\nabla T) \tag{5.1c}$$

As already described in Chapter 4, in the above equations, α, the inverse permeability is the *penalization* parameter appearing in the Brinkman penalization source term (αu) in Eqn. 5.1b which is used to force a zero velocity inside the stationary solid material regions when this *penalization* parameter, α, tends to a very large value ($\alpha >> 1$) which makes the local velocity zero. Hence, in fluid regions, the Brinkman penalization term αu approaches zero to recover the classical N-S equations in Eqn. 5.1b. Therefore, the Brinkman penalization approach can be seen as using a fictitious porous material as a tool to continuously interpolate between fluid and solid regions during the optimization process. This interpolation between fluid and solid regions is accomplished by using the following RAMP-type interpolation functions:

$$\alpha(\eta) = \alpha_s + (\alpha_f - \alpha_s)\eta\frac{1+k}{\eta+k} \tag{5.2a}$$

$$D(\eta) = D_s + (D_f - D_s)\eta\frac{1+k}{\eta+k} \tag{5.2b}$$

As for the thermal field modelling, as a result of the penalization technique and the above interpolation function, Eqn. 5.1c takes the following form in the fluid and solid regions, respectively:

$$\text{In fluid regions}: \quad (\boldsymbol{u} \cdot \nabla)T = \nabla \cdot (D_f \nabla T) \tag{5.3}$$

$$\text{In solid regions}: \quad 0 = \nabla \cdot (D_s \nabla T) \tag{5.4}$$

It is important to note that in Brinkman penalization approach, it is not required to explicitly specify the solid-fluid interface boundary conditions as they are automatically solved from the governing equations taking the appropriate values of inverse permeability $\alpha(\eta)$ and thermal diffusivity $D(\eta)$ from the RAMP-type interpolation functions in Eqn. 5.2 depending upon whether it is a solid cell $(\eta = 0)$ or a fluid cell $(\eta = 1)$.

Multi-region CFD approach: The most common approach in CFD simulations involving complex geometries is to use a multi-region approach which utilizes a body-fitted mesh [141, 142], wherein the grid is generated in a way to conform to complex boundaries. As a result, this approach makes it comparatively easy to specify solid-fluid interface boundary conditions and to attain high accuracy by putting fine mesh for boundary layers, where high resolutions are required, especially for high Reynolds number flows. For conjugate heat transfer problems, the real time coupling of fluid and solid regions by means of energy conservation is the central component of CHT methodology. The goal is to ensure energy conservation across the fluid-solid interface. Though simple in concept, it can sometimes be complex to implement it in a CFD code in a stable and efficient manner.

Most commercial CFD software packages use the so-called *coupled method* strategy [143] for solving CHT problems. This approach simulates the flow and thermal fields separately in the solid and the fluid regions followed by some specific coupling techniques [143–146] implemented at the interface. With the use of these coupling techniques, the temperature distribution and heat flux are expected to be continuous at the solid-fluid interface. For most commercial CFD codes, this method focuses on specification of the single boundary temperature at the interface, shared by the neighbouring cells on the opposite sides of the boundary as shown in Fig. 5.4. During each iteration, the boundary temperature is adjusted so that the calculated heat flux on the fluid side exactly matches the heat flux on the solid side. This interface boundary temperature based method provides stable and satisfactorily accurate estimation of the temperature field at the solid-fluid interface [147].

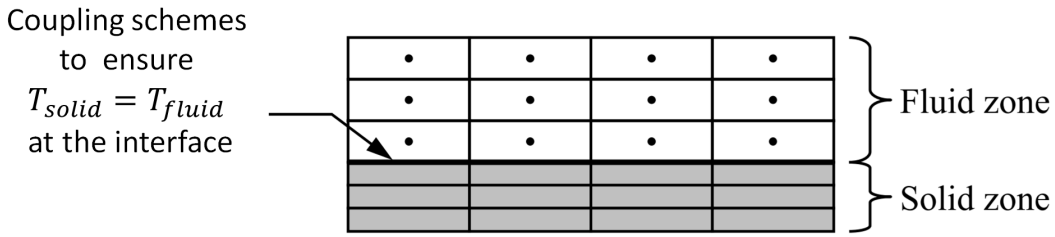

Figure 5.4 – CHT methodology used in conventional multi-region CFD approach.

After summarizing the two modeling approaches for solving CHT problems, the differences in the two results can be primarily attributed to the following three factors:

- *Grey zone at the solid-fluid interface:* The implicit solid-fluid representation based on the design variable field (η) obtained via the Brinkman penalization approach suffers from some grey zone at the interface as shown in Fig. 5.1(b). This phenomenon is inherent to density-based TO approach. These grey cells tend to introduce an undesirable third material having intermediate physical properties at the solid-fluid interface. On the contrary, the multi-region approach used in CFD has clearly predefined boundaries with no such unknown material at the solid-fluid interface.

- *Treatment of pressure field in the solid regions:* On closer observation of the momentum equation Eqn. 5.1b considered in the TO formulation, it can be seen that the Brinkman approach penalizes only the velocities in the domain but does not explicitly control the pressure [148]. This is because the Brinkman penalization approach and other similar immersed boundary methods treat solid obstacles as porous media [101]. As a result, this approach allows a continuous pressure distribution in the solid regions as well. This is the key difference from the multi-region CFD approach where no pressure values are computed in the solid regions. This justifies the higher pressure drop values reported by the TO numerical model in Table 5.1 and the difference in the inlet pressure profile in Fig. 5.1b. The same fact is also acknowledged by other studies in literature which performed similar numerical verification of the topology optimized configurations [11, 123].

- *Difference in methodology used to solve the governing equations:* The Brinkman penalization approach does not require an explicit specification of solid-fluid interface condition for solving the CHT problem and the interface is implicitly controlled by the RAMP-type interpolation technique. On the other hand, when solving CHT problem using the multi-region CFD approach, special attention is required to ensure energy conservation at solid-fluid interface by introducing some specific coupling schemes for this purpose. Moreover, the multi-region CFD approach captures the boundary layer phenomena that occurs in thermal and momentum boundary layer with much higher accuracy resulting in a much accurate representation of the sharp temperature and velocity changes occurring at such small length scales .

As a conclusion, the above comparison clearly suggests the urgent need for innovative and computationally less-expensive mesh-adaptive techniques to be implemented for resolving boundary layer phenomena occurring at much smaller length scales, in addition to better regularization techniques to obtain perfectly clear black and white (0/1) solution without any grey cells at the interface for TO of CHT systems. Apart from this, the above comparison also demonstrates that experimental validations are absolutely necessary to better quantify and qualify the performance of numerically obtained optimal configurations by TO.

5.2 Surface heat flux boundary condition for the "Volume-to-Point" heat conduction TO problem

When a heat flux boundary condition is imposed at the wall surface that borders a solid region, conventional Finite Volume based CFD software solves the following equation to compute the wall surface temperature T_w:

$$q = \frac{K_s}{\Delta n}(T_w - T_s) \tag{5.5}$$

which in turn gives:

$$T_w = \frac{q\Delta n}{K_s} + T_s \tag{5.6}$$

where

- q = imposed heat flux in $[Wm^{-2}]$,
- T_w = wall surface temperature in $[K]$ (to be computed),
- T_s = neigbouring solid cell temperature in $[K]$ (specified through solution initialization),
- Δn = distance between the wall surface and the neighbouring solid cell, and
- K_s = thermal conductivity of the solid in the neigbouring cell in $[Wm^{-1}K^{-1}]$.

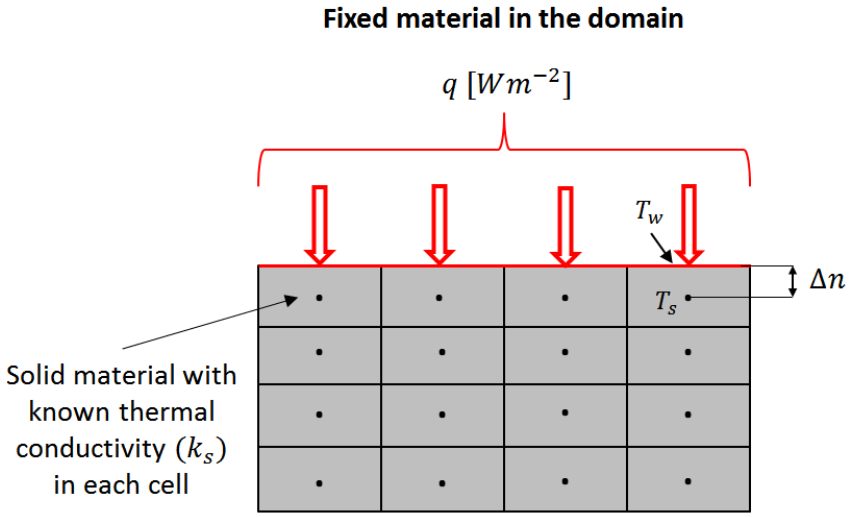

Figure 5.5 – Implementation of surface heat flux boundary condition in conventional CFD codes.

It is clearly evident from Eqn. 5.6 that to compute the heat transfer from wall surface to the interior domain, an exact knowledge of thermal conductivity of the neighbouring solid cell (K_s) is required. In conventional CFD simulations, the above computation is fairly straightforward as the location of solid material in each cell of the computational domain is predefined and fixed through out the computational process. Consequently, the value of thermal conductivity of the neighbouring solid cell throughout the computational domain is known (and fixed) a priori as represented in Fig. 5.5. On the contrary, in a TO numerical solver, the correct estimation of thermal conductivity of the neighbouring solid cell (K_s) is rather very complex. In conventional topology optimization methods, it is not easy to clearly define boundary locations in the middle of the process, since they are blurry and constantly changing. As a result, the thermal conductivity of the neighbouring cell is continuously changing at the surface during the entire optimization process as a virtue of SIMP or

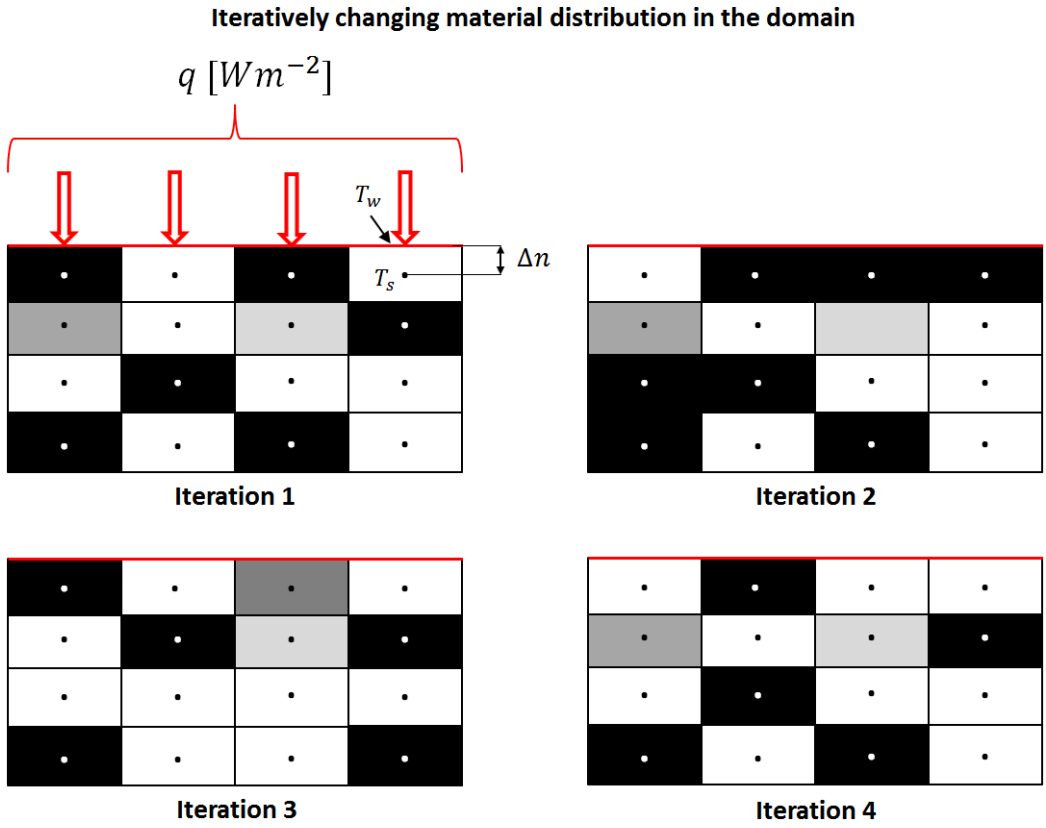

Figure 5.6 – Schematic representation of difficulty in implementation of surface heat flux boundary condition in TO.

RAMP-type material interpolation schemes used in TO (see Fig. 5.6). Additionally, Fig. 5.7, shows the actual design changes occurring in the domain during the topology optimization process.

For this particular reason, in classical volume-to-point heat conduction TO problem, almost all of the studies in literature used an internal volumetric heat source $[Wm^{-3}]$ in the low conductivity material and no instance was found which tackled a surface heat source as the boundary condition [45]. The imposed surface heat flux boundary condition for heat conduction systems is one of the most common BC that can be found in real world applications. According to the author, the inability of existing TO methods in literature to handle the surface heat flux boundary condition can be seen as a major limitation for the use TO in optimizing heat conduction systems where such boundary conditions are important. In the future, it will be important to characterize properly a surface heat flux BC $[Wm^{-2}]$ taking into account the effective thermal conductivity in the neighbouring solid cell in TO formulation where the structure is continuously changing in the domain with iterations until convergence.

A simple yet efficient solution to tackle this problem can be to fix a thin layer ($\approx$ 1 cell thickness) of either of the two material at the boundary. In this way, the fixed solid part, with the known thermal conductivity, do not participate in the optimization process and facilitates the correct imposition of surface heat flux BC $[Wm^{-2}]$ at the boundary. As an example, Fig. 5.8 shows a schematic representation where a thin layer of material 1 (with thermal conductivity K_1) is fixed at the boundary during the complete optimization process.

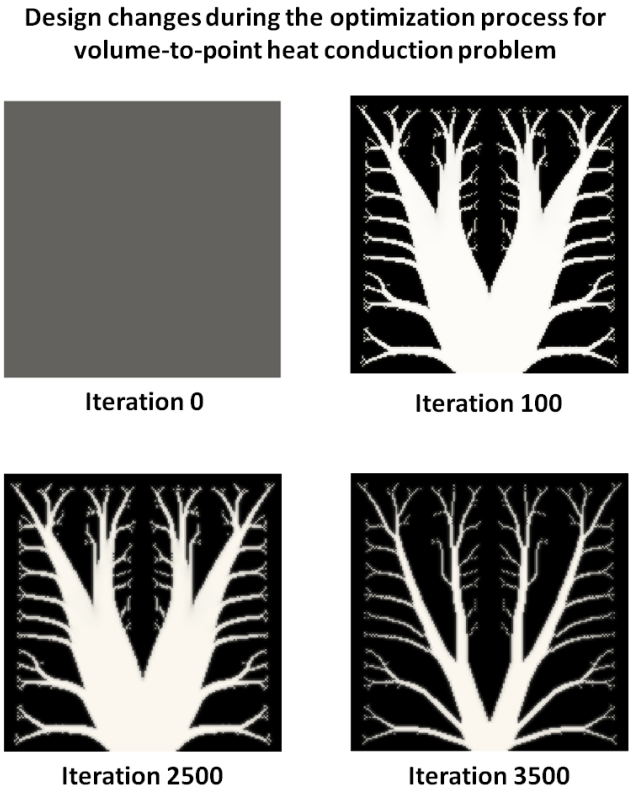

Figure 5.7 – Iteratively changing material distribution in the domain during the optimization process for a volume-to-point heat conduction TO problem.

5.3 Influence of numerical parameters on topology optimized configurations

This section investigates the influence of some important numerical parameters associated with density-based TO approach on the final optimal topology of CHT systems. The objective here is to develop a deeper understanding of the behaviour of these parameters and in the process, establish some guidelines for future studies in optimization of thermal systems using density-based TO approach by minimizing the number of tuning parameters. For the sake of simplicity and better analysis, the results in this section are presented for six different values of ω (ω = 0, 0.5, 0.7, 0.94, 0.97 and 0.99).

5.3.1 Spatial discretization

As the first parameter, the influence of spatial discretization of the computational domain on the topology optimized designs is analysed. The original CHT TO problem described in section (2) of Chapter 4 is solved on five different meshes (consisting of 3600, 6400, 10000, 14400 and 19600 square-cell designs elements, respectively) and the two objective function values are monitored on the converged solution. The corresponding optimal designs and the associated objective function values (J_f and J_{th}) for the six different values of ω in an ascending order are shown in Figure 5.9. For each value of ω, the design with the best (lowest) fluid objective function values is highlighted with a blue box and the one with best (highest) thermal objective function value is highlighted with red box. Additionally, Fig. 5.10 plots the variation of the fluid objective function (J_f) and the thermal objective function (J_{th}) with increasing mesh size.

As a first observation, it can can be seen that the final optimal designs share similar design forms, however, with better and clearer description of fluid channel boundaries with increasing mesh size. Similar observation was also made by Dugast *et al.* [131] for an unconstrained CHT TO problem handled using a level-set approach. Moreover, the two plots in Fig. 5.10 depicts the general trend of

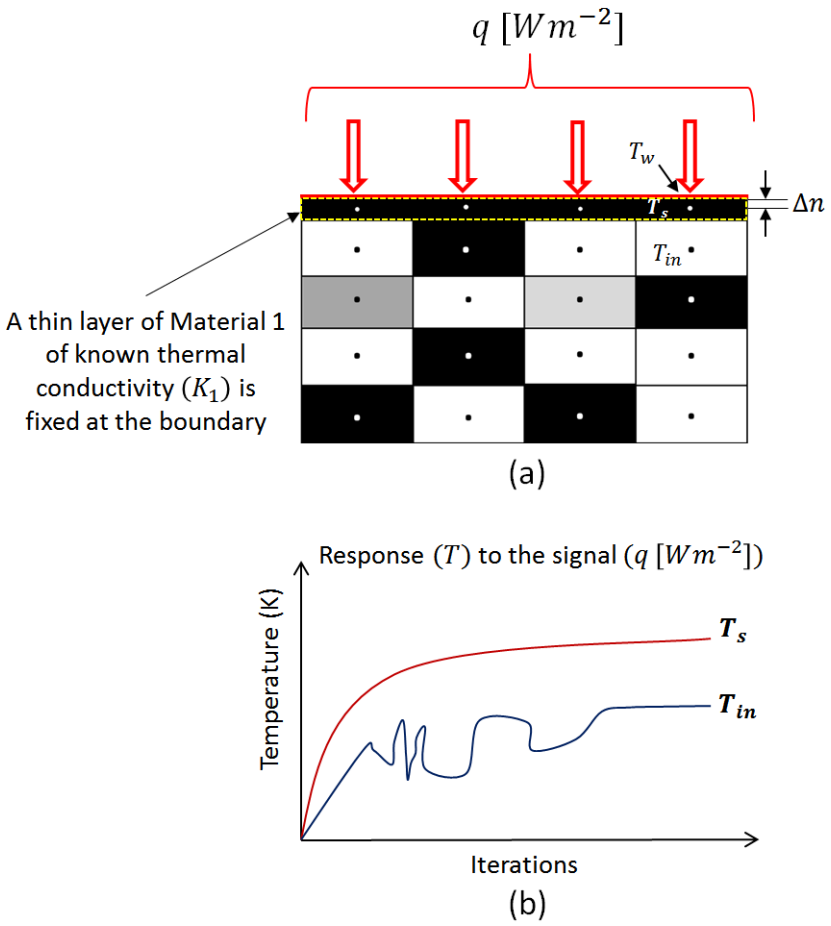

Figure 5.8 – Schematic representation of implementation of surface heat flux boundary condition in TO: a) A thin layer of material with known thermal conductivity is fixed at the boundary, and b) Temperature response to the signal ($[Wm^{-2}]$) at the boundary and interior cell, respectively, as the solution approaches convergence.

obtaining better objective function values with higher mesh size. On further observation, it can be seen that very close objective function values are obtained with the last two meshes which use 14400 and 19600 design elements, respectively with the only exception of the design obtained at $\omega = 0.99$ where the thermal objective functions is still considerably highest at 19600 mesh size as compared to the other designs. Hence, it can be said that mesh independent designs for the current problem can be obtained by using a mesh resolution of around 19600 cells. Though, at extremely high values of ω ($\omega > 0.97$), there is still a possibility of achieving higher thermal objective function values on further refining the mesh because, at these value of ω, the TO algorithm aims to further refine the fluid micro-structures located between the two major fluid branches in order to extract the maximum possible heat from the system and the optimization problem is least concerned about the pressure drop minimization in the domain. It is important to note that the smallest length scale achieved by the TO algorithm is restricted by the minimum cell size in the computational domain.

Generally, density-based TO approach is believed to suffer from mesh-dependence problem i.e., the problem of not obtaining qualitatively the same solution for different spatial discretization also reffered as obtaining *non-unique solutions* or several optima. This problem is acknowledged by several authors who dealt with heat conduction or structural TO problems [5, 35]. However, the results in Fig. 5.9 clearly show that the current TO model does not suffer from mesh-dependency numerical instability when using a Cartesian grid with orthogonal square elements.

Effect of mesh-cell type: In order to examine the effect of mesh type, the same CHT TO problem is solved on a non-uniform unstructured mesh consisting of approximately 10000 triangular elements

ω	3600 Cells	6400 Cells	10000 Cells	14400 Cells	19600 Cells
0				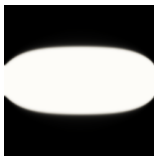	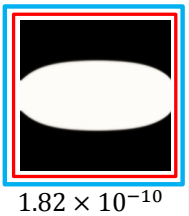
$J_f(W)$	1.94×10^{-10}	1.9×10^{-10}	1.87×10^{-10}	1.86×10^{-10}	1.82×10^{-10}
$J_{th}(W)$	0.25	0.28	0.3	0.3	0.31
0.5					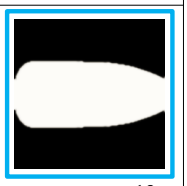
J_f	5.21×10^{-10}	2.345×10^{-10}	2.66×10^{-10}	2.34×10^{-10}	2.20×10^{-10}
J_{th}	0.52	0.59	0.61	0.63	0.62
0.7					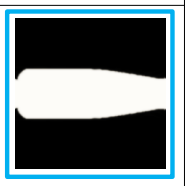
J_f	1.17×10^{-9}	6.77×10^{-10}	5.42×10^{-10}	4.13×10^{-10}	4.07×10^{-10}
J_{th}	0.54	0.61	0.64	0.66	0.65
0.94	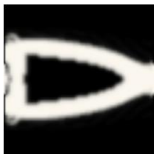		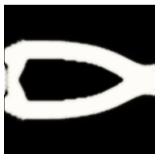		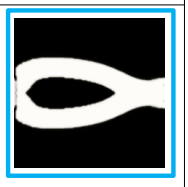
J_f	1.20×10^{-8}	1.04×10^{-8}	9.15×10^{-9}	7.81×10^{-9}	6.76×10^{-9}
J_{th}	0.73	0.85	0.86	0.90	0.87
0.97	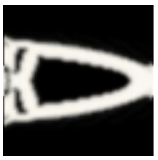	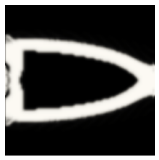	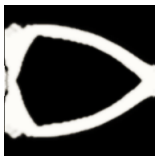	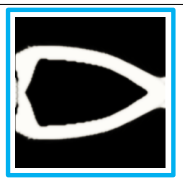	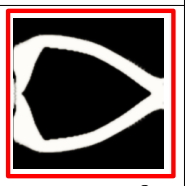
J_f	2.33×10^{-8}	2.17×10^{-8}	1.9×10^{-8}	1.35×10^{-8}	1.38×10^{-8}
J_{th}	0.77	0.87	1.13	1.05	1.17
0.99		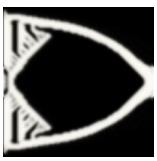		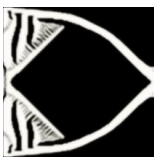	
J_f	5.13×10^{-8}	6.65×10^{-8}	4.96×10^{-8}	6.32×10^{-8}	6.57×10^{-8}
J_{th}	0.83	1.21	1.23	1.7	1.82

Figure 5.9 – Optimal designs obtained with five different mesh sizes (consisting of 3600, 6400, 10000, 14400 and 19600 designs elements, respectively): Starting from fluid objective J_f minimization ($\omega = 0$) to thermal objective J_{th} maximization ($\omega = 0.99$).

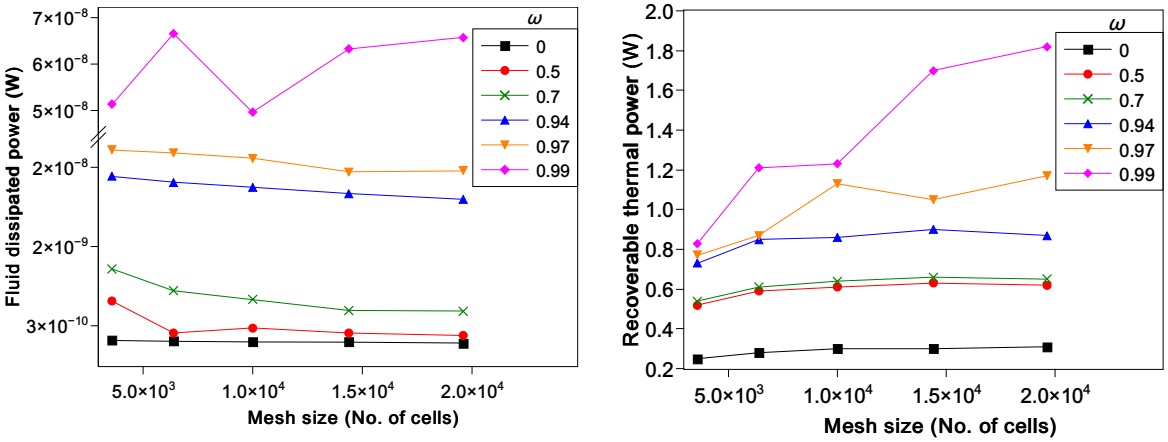

(a) Fluid dissipated power.

(b) Recoverable thermal power.

Figure 5.10 – Variation of objective function values with increasing mesh size.

and results obtained are compared to the orthogonal square mesh counterpart consisting of same number of cells. Fig. 5.11 shows the optimal designs and corresponding objective function values for the two mesh types. For most cases the orthogonal square mesh reports a noticeably better final optimal design in terms of objective function values. At $\omega = 0$, the unstructured triangular mesh gives the optimal design with a marginally (not significant) better fluid objective function value. At $\omega = 0.99$, the optimal design obtained by the triangular mesh predicts a significantly high thermal objective function value and high fluid objective function value. The reason for the latter may be that at extremely high values of ω, a triangular mesh element type unstructured arrangement may provides more degree of freedom to the optimization algorithm to form designs for heat flux orientation that are more difficult to reach using a structured orthogonal mesh arrangement. Mathematically, it represents the existence of *non-uniqueness* of solution described previously. From the above illustration, it can be concluded that the problem of existence of *non-uniqueness* of solution with the current TO model, which uses the method of moving asymptotes algorithm (MMA), is linked to the type of mesh-cell and not to the size of the mesh.

5.3.2 Design field initialization

Next, the influence of design variable field (η) initialization on the final optimal designs is investigated. A uniform initialization of the η field is used starting with a full solid initialization ($\eta = 0$), slowly increasing the fluid percentage in each cell (η= 0.25 , 0.5 , 0.75), leading to a full fluid initialization (η =1). Fig. 5.12 shows the converged optimal designs and the corresponding objective function values for the five different uniform initial design field in the ascending order of ω values. In addition to this, Fig. 5.13 shows the variation of the fluid objective function (J_f) and the thermal objective function (J_{th}) with changing initialization conditions.

It can be observed that the present TO numerical model, based on gradient-based MMA algorithm, is highly sensitive to initialization conditions. As an example, for $\omega = 0$ (when the only objective is pressure drop minimization), $\eta_{initial} = 0$ and $\eta_{initial} = 0.25$, produce totally different optimal design as compared to other values of $\eta_{initial}$, resulting in very high value of fluid objective function. On closer observation, from Fig. 5.13a, it can be seen that a full solid initialization ($\eta_{initial}$ = 0) always results in worst fluid objective function (J_f) values for all values of ω and best thermal objective function (J_{th}) for most values of ω (with the exception of $\omega = 0.94$ and $\omega = 0.97$, where it reports second best and third best values of J_{th}, respectively). On the contrary, best fluid objective function values are achieved with a design field initialization of $\eta_{initial} \geq 0.5$ (i.e., higher fluid percentage in each cell). In a sense, a full solid initialization seems to favour the thermal objective function may be due to the higher thermal conductivity of solid material. Another important observation worth mentioning that the higher the percentage of solid material in each cell in the initial design field the longer the computational time required to reach convergence. As an example,

ω	Orthogonal square	Non-ortho triangular
0		
$J_f(\mathbf{W})$	1.87×10^{-10}	1.84×10^{-10}
$J_{th}(W)$	0.3	0.29
0.5		
J_f	2.66×10^{-10}	3.85×10^{-10}
J_{th}	0.61	0.585
0.7		
J_f	5.42×10^{-10}	1.48×10^{-9}
J_{th}	0.64	0.596
0.94	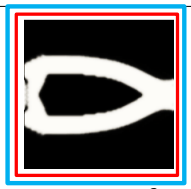	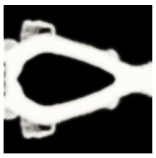
J_f	9.15×10^{-9}	1.1×10^{-8}
J_{th}	0.86	0.82
0.97	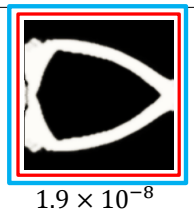	
J_f	1.9×10^{-8}	1.97×10^{-8}
J_{th}	1.13	0.87
0.99	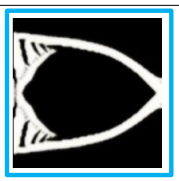	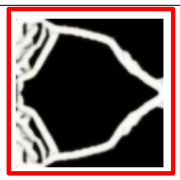
J_f	4.96×10^{-8}	9.47×10^{-8}
J_{th}	1.23	1.7

Figure 5.11 – Optimal designs obtained with uniform orthogonal square mesh elements and non-uniform triangular mesh elements keeping the number of design elements same: Starting from fluid objective J_f minimization ($\omega = 0$) to thermal objective J_{th} maximization ($\omega = 0.99$).

η_{ini} / ω	0	0.25	0.5	0.75	1
0					
$J_f(W)$	3.67×10^{-10}	3.28×10^{-10}	1.89×10^{-10}	1.89×10^{-10}	1.87×10^{-10}
$J_{th}(W)$	0.57	0.52	0.3	0.3	0.3
0.5					
J_f	4.95×10^{-10}	4.74×10^{-10}	2.61×10^{-10}	2.75×10^{-10}	2.66×10^{-10}
J_{th}	0.632	0.62	0.543	0.54	0.61
0.7					
J_f	1.12×10^{-9}	9.40×10^{-10}	5.31×10^{-10}	5.52×10^{-10}	5.42×10^{-10}
J_{th}	0.65	0.646	0.56	0.64	0.64
0.94		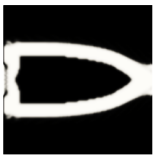		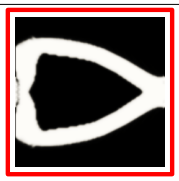	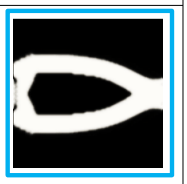
J_f	1.86×10^{-8}	1.55×10^{-8}	9.24×10^{-9}	1.04×10^{-8}	9.15×10^{-9}
J_{th}	0.90	0.88	0.86	0.94	0.86
0.97				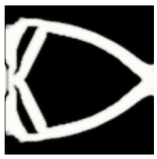	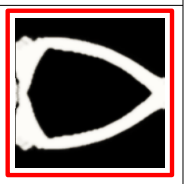
J_f	2.96×10^{-8}	2.85×10^{-8}	1.75×10^{-8}	2.05×10^{-8}	1.9×10^{-8}
J_{th}	0.96	0.94	0.93	1.03	1.13
0.99	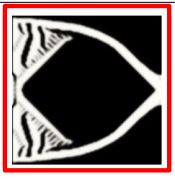				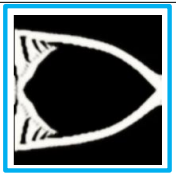
J_f	6.14×10^{-8}	9.45×10^{-8}	5.58×10^{-8}	5.79×10^{-8}	4.96×10^{-8}
J_{th}	1.38	1.28	1.04	1.12	1.23

Figure 5.12 – Optimal designs obtained with five different values of uniform design variable (η) field initialization (η = 0, 0.25, 0.5, 0.75 and 1, respectively): Starting from fluid objective J_f minimization ($\omega = 0$) to thermal objective J_{th} maximization ($\omega = 0.99$).

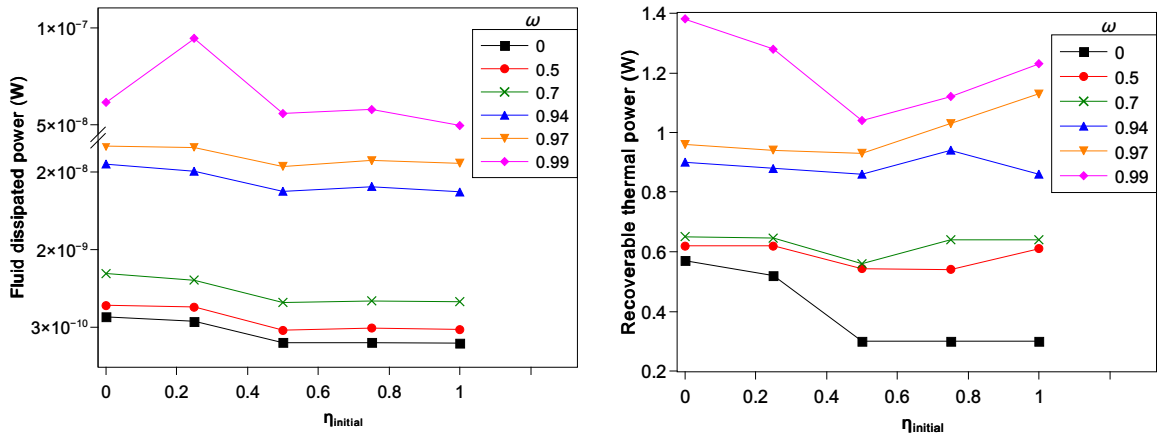

(a) Fluid dissipated power

(b) Recoverable thermal power

Figure 5.13 – Variation of objective function values with different uniform design variable field initialization values.

Table 5.2 shows the number of iterations required to reach convergence for the optimal designs with $\omega = 0.99$. On the basis of the optimal designs obtained in Fig. 5.12, objective function values in Fig. 5.13 and number of iterations required before convergence in Table 5.2, it can be concluded that a full fluid initialization ($\eta_{initial} = 1$) seems to provide the best balance of all the factors and is the best uniform initial guess that can be made for the present CHT TO problem.

Another issues that clearly emerges from this investigation is the numerical issue of obtaining multiple local optima (minima or maxima) when using a local optimization technique involving the gradient based MMA algorithm. Local optima refer to the numerical problem of obtaining different local optimal solutions to the same discretized problem when choosing different algorithmic parameters [35]. For example, on closer observation of optimal designs for ω =0.97 and ω =0.99 in Fig. 5.12, totally different final optimal structures are obtained with $\eta_{initial} = 0.5$ and $\eta_{initial} = 1.0$. For non-convex optimization problems, gradient-based algorithms in general, tends to converge to a nearby stationary point which may or may not be the global solution. This investigation highlights the need to pay more attention while choosing the MMA optimization algorithm settings in solving future topology optimization problems. This choice might affect the non-uniqueness of a solution for optimization problems where several local minima/maxima may exist.

$\eta_{initial}$	0 (Full solid)	0.25	0.5	0.75	1 (Full fluid)
Optimization iterations	16118	15213	6275	5130	4210

Table 5.2 – No. of iterations required to reach convergence for the optimal design with $\omega = 0.99$.

Non-uniform design field initialization: Recently, some authors in literature have started recommending the use of a non-uniform design field initialization when using a gradient-based local optimization algorithm like MMA for heat transfer and fluid flows [8, 129]. Hence, to investigate the influence of a non-uniform design variable field initialization, the final optimal designs obtained by using a full fluid initialization ($\eta_{initial} = 0$) from Fig. 5.12 is used as an initial guess for the same CHT TO problem. This is referred as a multi-stage optimization process where the final design obtained from one stage is used as a design field initialization for the next stage [129]. Figure. 5.14 compares the results obtained by a non-uniform initialization of the design field to the full fluid uniform initialization ($\eta_{initial} = 0$). As as first observation, it can be seen that a non-uniform initialization does not change the overall design but improves the existing designs in terms of objective function values for most of the cases. For extremely high value of ω ($\omega \geq 0.97$), a multi-stage optimization process refines the final structure by removing the smallest fluid branches (which may be undesirable

η_{ini} / ω	Uniform (Full fluid)	Non-uniform
0		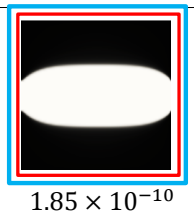
$J_f(\mathbf{W})$	1.87×10^{-10}	1.85×10^{-10}
$J_{th}(W)$	0.3	0.3
0.5		
J_f	2.66×10^{-10}	2.65×10^{-10}
J_{th}	0.61	0.615
0.7		
J_f	5.42×10^{-10}	5.27×10^{-10}
J_{th}	0.64	0.646
0.94	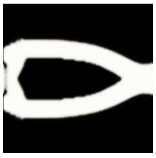	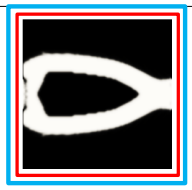
J_f	9.15×10^{-9}	9.05×10^{-9}
J_{th}	0.86	0.88
0.97	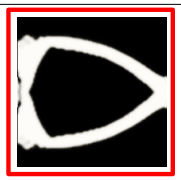	
J_f	1.9×10^{-8}	1.84×10^{-8}
J_{th}	1.13	1.09
0.99		
J_f	4.96×10^{-8}	5.32×10^{-8}
J_{th}	1.23	1.21

Figure 5.14 – Optimal designs obtained with uniform (full fluid) and non-uniform design variable (η) field initialization: Starting from fluid objective J_f minimization ($\omega = 0$) to thermal objective J_{th} maximization ($\omega = 0.99$).

for some conventional fabrication methods like water-jet and laser-jet cutting techniques) without compromising much on the thermal and fluid objective function values. Similar behavior was also reported by Zeng *et al.* [129] who used a multi-stage optimization process for a single-objective CHT TO problem. As a conclusion, whenever possible a multi-stage optimization process should be implemented for a better description of the final optimized structures.

5.3.3 Density filter radius

It is very common for density-based TO approach to exhibit numerical issues like checkerboard solutions, if no regularization technique is used. Hence, a density filtering techniques (as described in Appendix D) can be applied in order to avoid such numerical difficulties. As mentioned earlier, in density filtering technique, the design variable (η) value in each cell is redefined as weighted average of η values in a mesh-independent neighbourhood of that cell, before calling the FVM solver, and afterwards the sensitivities are modified in a consistent way [149]. Hence the final optimal design is represented by the filtered design variable values ($\widetilde{\eta}$) rather than the original design variable values (η) as shown in Eqn. D.1. Thus, it becomes important to investigate the influence of size of the mesh-independent neighbourhood used to represent the final optimal designs. This mesh-independent neighbourhood is controlled by the size of a density filter radius (r_{min}). By using this density filter technique in the present TO numerical model, a new length scale r_{min} is introduced, below which structural variation is not permitted during the optimization process.

In addition to this, the ideal density filter radius is expected to meet most (if not all) of the three below mentioned requirements:

1 Mesh-independent and checkerboard-free designs.

2 Minimized grey zone at the interface: Clear black and white (0/1) solutions.

3 Suitability to the available fabrication technique.

Sigmund [70] recommends that *"r_{min} should always be chosen greater than or equal to 1.1 times the smallest element's size to prevent formation of checkerboards"*. Accordingly, four different filter radius were investigated for $\frac{r_{min}}{a} = 1.1$, 1.5, 2 and 2.5, where a is the base cell size in the domain, in addition to a case, where no filtering technique is used. Fig. 5.15 shows the converged optimal designs and the corresponding objective function values for the five above mentioned cases in the ascending order of ω values. Additionaly, Fig. 5.1 shows the variation of the fluid objective function (J_f) and the thermal objective function (J_{th}) with changing density filter radius.

As a first clear observation, checkerboard solutions are obtained when no filtering is used at $\omega = 0.97$ and $\omega = 0.99$. This clearly demonstrates that regularization techniques are indispensable for obtaining good optimal design for CHT problems. The checkerboards are reduced (but not totally removed) when using a density filter with the smallest radius ($\frac{r_{min}}{a} = 1.1$). Staring from $\frac{r_{min}}{a} \geq 1.5$, the density filter is able to completely eliminate the checkerboards from the final optimized designs.

Secondly, from Fig. 5.16, two observations can be made: i) when fluid objective function is more prioritized ($\omega \in [0 - 0.7]$), design with no filter produces best fluid objective function (J_f) values (with the exception of $\omega = 0$, where the values are extremely close for all the designs) and increasing the filter radius has a negative impact on the fluid objective function values and, ii) similarly, when thermal objective function is more prioritized ($\omega > 0.7$), the design produced with no filter has the best thermal objective function (J_{th}) values, and increasing the filter radius has a negative impact on the thermal objective function values as well.

There are two reasons for the above observation:

– The minimum length scale that can be achieved in the final optimal designs is now controlled by the size of the filter radius (see Table 5.3). Consequently, when there is no restriction at all (i.e., no filter), the optimization algorithm is able to produce smaller fluid branches to maximize the heat transfer in the domain and produces mathematically, the best design in

ω	No Filter	$\frac{r_{min}}{a} = 1.1$	$\frac{r_{min}}{a} = 1.5$	$\frac{r_{min}}{a} = 2$	$\frac{r_{min}}{a} = 2.5$
0					
$J_f(W)$	1.89×10^{-10}	1.87×10^{-10}	1.87×10^{-10}	1.88×10^{-10}	1.88×10^{-10}
$J_{th}(W)$	0.29	0.3	0.3	0.3	0.3
0.5	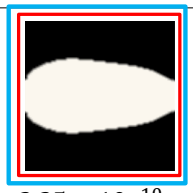				
J_f	2.25×10^{-10}	2.45×10^{-10}	2.66×10^{-10}	3.73×10^{-10}	4.52×10^{-10}
J_{th}	0.62	0.6	0.61	0.6	0.57
0.7					
J_f	2.5×10^{-10}	3.78×10^{-10}	5.42×10^{-10}	7.15×10^{-10}	8.21×10^{-10}
J_{th}	0.68	0.65	0.64	0.62	0.59
0.94					
J_f	9.52×10^{-9}	1.20×10^{-8}	9.15×10^{-9}	1.12×10^{-8}	7.94×10^{-9}
J_{th}	1.06	0.87	0.86	0.85	0.76
0.97			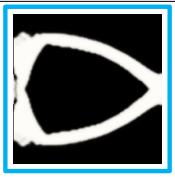	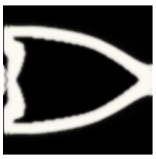	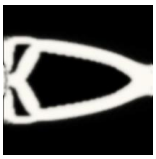
J_f	2.41×10^{-8}	2.28×10^{-8}	1.9×10^{-8}	1.98×10^{-8}	1.92×10^{-8}
J_{th}	1.56	1.42	1.13	0.92	0.84
0.99			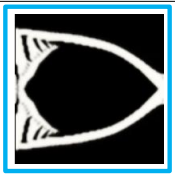	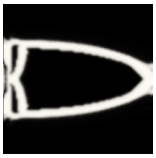	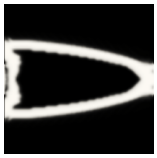
J_f	1.09×10^{-7}	7.69×10^{-8}	4.96×10^{-8}	5.94×10^{-8}	5.40×10^{-8}
J_{th}	2.32	2.12	1.23	1.05	0.87

Figure 5.15 – Optimal designs obtained without filtering and with density filter of four different filter radius size ($\frac{r_{min}}{a}$ = 1.1, 1.5, 2 and 2.5, respectively): Starting from fluid objective J_f minimization ($\omega = 0$) to thermal objective J_{th} maximization ($\omega = 0.99$).

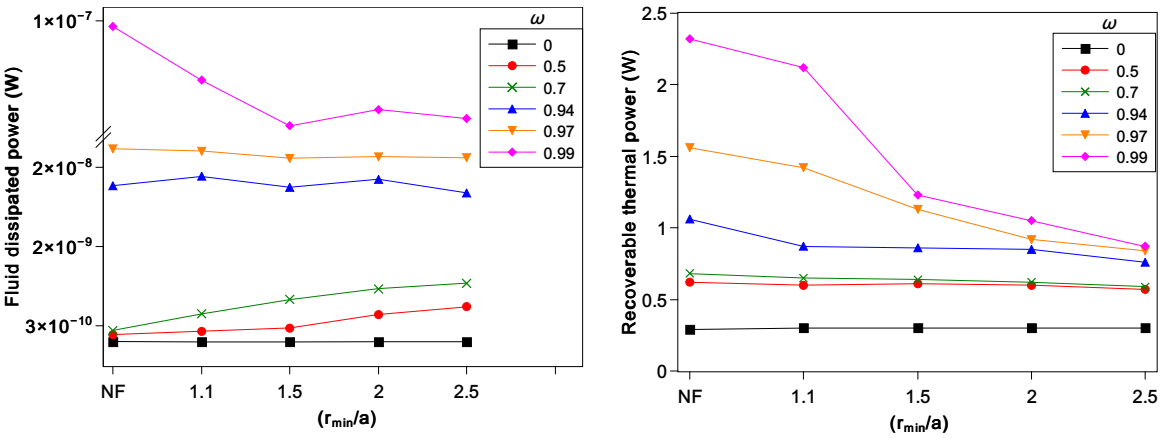

(a) Fluid dissipated power

(b) Recoverable thermal power

Figure 5.16 – Variation of objective function values with increasing filter radius size.

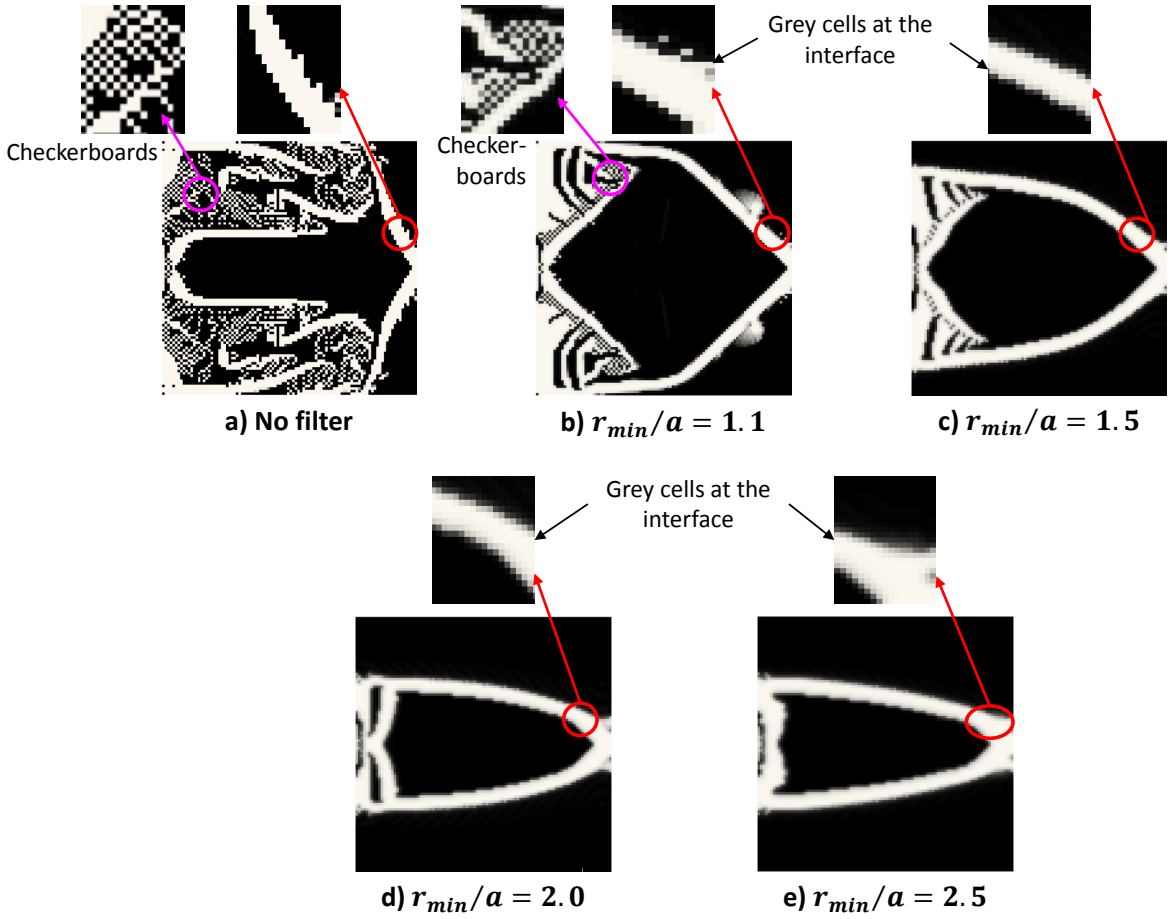

Figure 5.17 – Influence of density filter radius size on the optimal design with $\omega = 0.99$: Conflicting behaviour of reduction in occurrence of checkerboard solution and increment of grey zone at the fluid-solid interface with increasing filter radius size.

terms of thermal objective function values. While introducing the filter, the minimum size of the smallest fluid branch is now limited to the new introduced length scale r_{min}. As a result, for the same reason, an increasing filter radius has a negative impact on the thermal objective function values.

– The present density filter technique efficiently counters the checkerboard problem in the domain, however, in the process introduces grey zones at the fluid-solid interface. As an example,

Figure. 5.17 shows the final optimal designs for $\omega = 0.99$ for the five cases. It can be seen that the density filter technique is effective in removing the checkerboards in the domain. On the other hand, when the filter is introduced, the grey zone starts to appear at the fluid-solid interface and the number of grey cells at the interface continuously increases with increasing size of filter radius. When no filter is used, a crisp interface and a perfect black and white (0/1) solution is obtained. This further justifies the reason for obtaining better fluid and thermal objective function values when no filter is used.

$\frac{r_{min}}{a}$	No filter	1.1	1.5	2.0	2.5
Minimum length scale	$1\ mm$	$1.1\ mm$	$1.5\ mm$	$2\ mm$	$2.5\ mm$

Table 5.3 – Minimum length scale permitted in the final optimized design for each filter radius for a 100×100 spatial discretization and base cell size of $a = 1\ mm$.

Thus, selection of an appropriate size of filter radius (r_{min}) depends on number of factors where, density filters are capable of efficiently handling the checkerboard numerical problem. On the other hand, a high r_{min} value results in significant undesirable grey cells at the interface. Moreover, one should also keep in mind the minimum length scale that can be fabricated with the available fabrication technique before selecting the correct value of r_{min}. For the current problem, $r_{min} = 1.5 \times a$ seems to provide an appropriate compromise of the above mentioned factors. As a conclusion, it is highly important to pay attention when selecting the appropriate filtering technique for CHT TO problems.

5.3.4 FVM interpolation schemes

All the results presented in Chapter 4 were obtained using a first-order accurate Upwind-difference interpolation schemes for calculation of convection terms in both primal and adjoint system of equations. This is because of extremely high numerical instabilities encountered in terms of convergence when solving the CHT TO problem for very high values of ω ($\omega > 0.9$) with a second-order accurate Central-difference scheme. The description of the first-order and second-order FVM schemes can be found in Appendix B. As the flow under consideration is laminar and also aligned with the orthogonal square mesh, a first-order upwind discretization may produce acceptable results [150]. However, it is very important to reconsider the same problem using higher order schemes and to identify the underlying cause of extremely high numerical difficulties at higher values of ω. In this context, the primal and adjoint system of equations described in detail in Chapter 4 are represented here. Consequently, a term by term anlaysis is carried out thanks to the flexible OpenFOAM® architecture that facilitates individual specification of FV interpolation schemes for each term separately in each equation.

Primal flow eqautions:

$$\nabla \cdot \boldsymbol{u} = 0 \tag{5.7a}$$

$$\underbrace{(\boldsymbol{u} \cdot \nabla)\boldsymbol{u}}_{\text{Velocity convection}} = -\nabla p + \nabla \cdot (\nu \nabla \boldsymbol{u}) - \alpha(\eta)\boldsymbol{u} \tag{5.7b}$$

$$\underbrace{(\boldsymbol{u} \cdot \nabla)T}_{\text{Temperature convection}} = \nabla \cdot (D(\eta)\nabla T) \tag{5.7c}$$

ω	I Order	P: II Order A: I Order	P: II Order A: pr. II Order	I Order → II Order	II Order
0			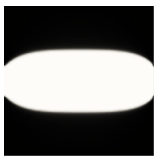		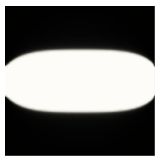
$J_f(W)$	1.87×10^{-10}	1.86×10^{-10}	1.87×10^{-10}	1.87×10^{-10}	1.865×10^{-10}
$J_{th}(W)$	0.3	0.29	0.3	0.3	0.3
0.5					
J_f	2.66×10^{-10}	2.63×10^{-10}	2.62×10^{-10}	2.66×10^{-10}	5.02×10^{-10}
J_{th}	0.61	0.59	0.6	0.6	0.58
0.7					
J_f	5.42×10^{-10}	5.34×10^{-10}	5.30×10^{-10}	5.44×10^{-10}	9.72×10^{-10}
J_{th}	0.64	0.63	0.63	0.631	0.596
0.94	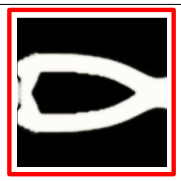	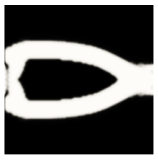		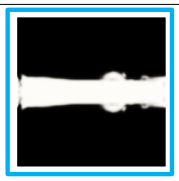	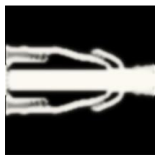
J_f	9.15×10^{-9}	9.22×10^{-9}	8.89×10^{-9}	5.42×10^{-9}	6.25×10^{-9}
J_{th}	0.86	0.82	0.81	0.67	0.64
0.97	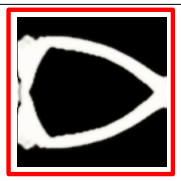	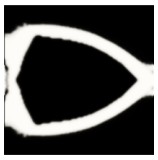	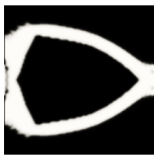	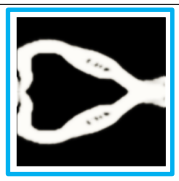	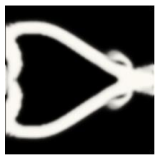
J_f	1.9×10^{-8}	1.89×10^{-8}	1.78×10^{-8}	1.45×10^{-8}	2.03×10^{-8}
J_{th}	1.13	1.0	1.03	0.99	0.84
0.99	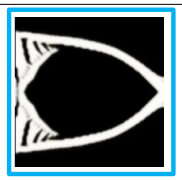			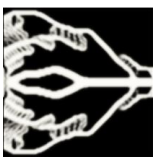	
J_f	4.96×10^{-8}	7.77×10^{-8}	7.94×10^{-8}	6.56×10^{-8}	5.8×10^{-8}
J_{th}	1.23	1.58	1.62	1.61	0.91

Figure 5.18 – Optimal designs obtained by using five different FVM interpolation schemes (**[I]**, **[P: II, A: I] [P: II, A: pr. II]**, **[P: II, A: I]** and **[I], respectively**): Starting from fluid objective J_f minimization ($\omega = 0$) to thermal objective J_{th} maximization ($\omega = 0.99$).

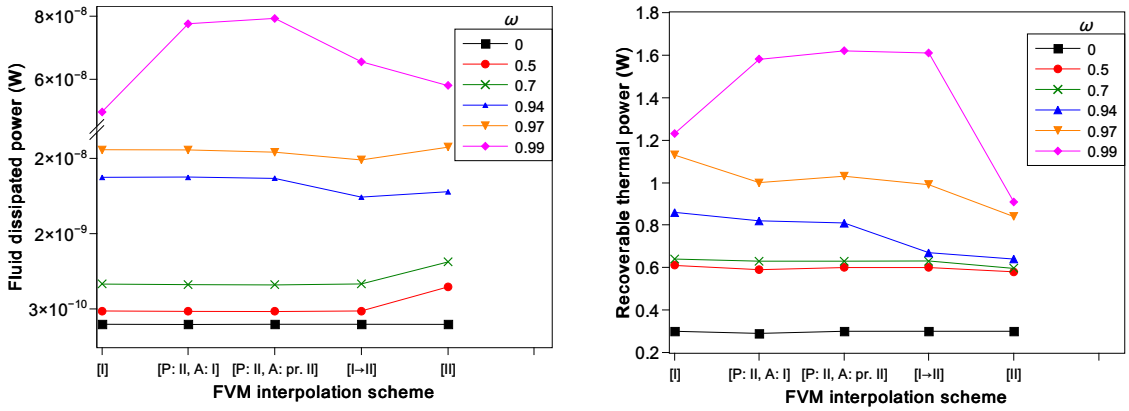

(a) Fluid dissipated power

(b) Recoverable thermal power

Figure 5.19 – Variation of objective function values with changing FVM interpolation schemes.

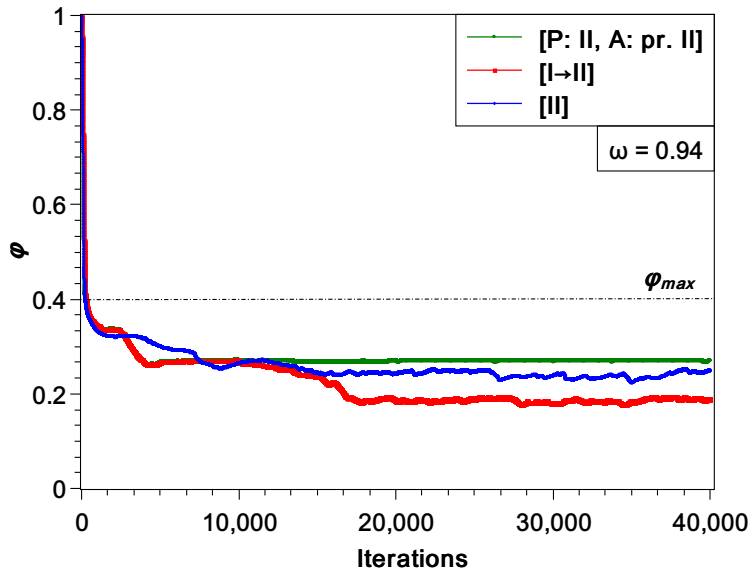

Figure 5.20 – Convergence history of the TO problem for the optimal design obtained by $\omega = 0.94$: Evolution of the volume fraction of the fluid material (ϕ) with iteration.

Continuous adjoint equations:

$$\nabla \cdot \boldsymbol{u} = \frac{\partial F_\Omega}{\partial p} \tag{5.8a}$$

$$\underbrace{-2\mathbf{E}(\boldsymbol{u}_a) \cdot \boldsymbol{u}}_{\text{Adj. velocity convection}} = -\nabla p_a + \nabla \cdot (2\nu \mathbf{E}(\boldsymbol{u}_a)) - \alpha(\eta)\boldsymbol{u}_a + T\nabla T_a - \frac{\partial F_\Omega}{\partial \boldsymbol{u}} \tag{5.8b}$$

$$\underbrace{-\boldsymbol{u} \cdot \nabla T_a}_{\text{Adj. temperature convection}} = \nabla \cdot (D(\eta)\nabla T_a) - \frac{\partial F_\Omega}{\partial T} \tag{5.8c}$$

There are two convection terms each in primal and adjoint systems of equations as shown in equations 5.7 and 5.8. Accordingly, the following five cases are investigated:

1. **I order (denoted by [I]):** All the four convection terms in primal and adjoint equations are evaluated using the first-order accurate Upwind-difference scheme.

2. **Primal equations by II order; Adjoint equations by I order (denoted by [P: II, A: I]):** The velocity convection and temperature convection terms in primal flow equations are solved

using the second-order accurate Central-difference scheme. On the other hand, the adjoint velocity convection term and the adjoint temperature convection term are evaluated using the first-order accurate Upwind-difference scheme.

3. **Primal equations by II order; Adjoint equations partially by II order (denoted by [P: II, A: pr. II]:** The velocity convection and temperature convection terms in primal flow equations are solved using the second-order accurate Central-difference scheme. On the other hand, the adjoint velocity convection term is also solved using the second-order accurate scheme but the adjoint temperature convection term is evaluated using the first-order accurate scheme.

4. **Start with I order; switch to II order (denoted by [I→II]):** In order to provide a better initial guess for second-order calculations, all the fours terms are solved with a first-order Upwind-difference scheme and then all the four terms are switched to second-order Central-difference scheme after reaching convergence with the first order scheme.

5. **II order (denoted by [II]):** All the four terms are solved using the second-order Central-difference scheme from the start of the calculation using a full fluid uniform initialization of the design domain.

Fig. 5.18 shows the converged optimal designs and the corresponding objective function values for the five above mentioned FVM schemes in the ascending order of ω values. Additionaly, Fig. 5.19 shows the variation of the fluid objective function (J_f) and the thermal objective function (J_{th}) with the different FVM schemes implemented here.

The first major observation is that using a 2^{nd} order scheme from the beginning (scheme **[II]**) with a full-fluid initialization is highly unstable and witness numerical difficulties towars convergence. Even after convergence, there is significant instability and the final structure design is oscillating at each iteration for all values of ω (except at $\omega = 0$). Hence, this scheme should be avoided. This scenario is numerically quite analogous to a high-Mach number flow calculation in aerodynamics, where the initial solution is much different than the expected final solution, and hence, it is advised to begin with a 1^{st} order scheme and switch to 2^{nd} order after few iterations [150].

Next, when using the **[I→II]** scheme, numerical difficulties are minimized and stable optimal designs are obtained atleast when fluid objective function is prioritized (i.e, $\omega \leq 0.7$). However, at higher values of ω (i.e., $\omega \geq 0.9$) there are still oscillations after convergence, however, significantly less than that observed with the **[II]** scheme. As an example, to better demonstrate the stability of FVM schemes, the volume fraction of the fluid material is plotted in figure 5.20 to show the convergence of the numerical TO problem for three different FVM schemes (**[II]**, **[I→II]** and **[P: II, A: I]**) for the optimal design with $\omega = 0.94$.

Apart from the above two cases, very stable and fairly easy to converge optimal design were obtained at all values of ω when using the remaining three schemes: **[P: II, A: pr. II]**, **[P: II, A: I]** and **[I]**. This investigation clearly shows that all the numerical instabilities in the present CHT TO problem is caused by the upstream convection of adjoint temperature term ($-\boldsymbol{u} \cdot \nabla T_a$), specifically when thermal objective function is more prioritized. The numerical behaviour of this particular term is still unclear and further in depth analysis is required in future to establish ways to correct this instability.

Nonetheless, it is important to note that the adjoint variables ($\boldsymbol{u}_a,\ p_a,\ T_a$) do not have any physical meaning to them unlike their primal counterparts ($\boldsymbol{u},\ p,\ T$). Hence, the term $-\boldsymbol{u} \cdot \nabla T_a$, i.e., the transport of adjoint temperature T_a into the control volume due to convection, actually does not have any physical meaning to it. Furthermore, on closer observation of Fig. 5.19, it can be seen that very similar objective function values are obtained by using **[I→II]** and **[P: II, A: pr. II]** for almost all the cases. Hence momentarily, it seems fairly accurate to use **[P: II, A: pr. II]** for future TO CHT problems.

Apart from this, it can be observed that, a purely first-order scheme (scheme **[I]**) tends to over estimate the values of thermal and fluid objective function for most of the cases whenever the final structure is exactly identical as compared to higher order schemes, only except at $\omega = 0.99$, where

the final structure is structurally completely different than what is obtained by other higher order schemes.

5.4 Conclusions

Based on the work realized in this chapter, examining different numerical and physical aspects of the density-based TO approach, following are the important conclusions in the form of recommendations for future studies in topology optimization of heat transfer and fluid flow systems:

- Numerical verification over a conventional CFD software package performed using a multi-region approach could serve as the first step towards validation of optimal configurations obtained by topology optimization of CHT systems. However, the ultimate goal should always be to conduct experimental measurements to better analyze the overall thermal performance of the topology optimized configurations.
- Implementation of the surface heat flux BC $[Wm^{-2}]$ in finite volume based TO solvers is rather complicated due to continuously changing material distribution on the domain surface with iterations until convergence. The ideal solution to this problem would be to search for an appropriate method to characterize the effective thermal conductivity (K_{eff}) at the surface. Nonetheless, a simple yet effective solution as proposed in this chapter could be to fix a thin layer of approximately one cell thickness of either of the two material at the boundary which does not participate in the optimization process. In doing so, the fixed solid part, with known thermal conductivity (K_s), allows accurate implementation of surface heat flux BC at the boundary.
- It is important to check for mesh-dependency issues for the results produces by the developed TO solver. In this way, one can ensure that only mesh-independent solutions are used for future experimental investigations.
- Whenever a gradient-based local optimization algorithm is used (like the method of moving asymptotes algorithm used in the present thesis), it is highly important to quantify the influence of design variable field initialization so that the best initialization conditions can be used to generate optimal solutions. Moreover, if time and resources permit, a multi-stage optimization approach using a non-uniform design field initialization can be used for a better description of the final optimized structures.
- Regularization techniques, like the density filtering technique used in this study, are absolutely necessary to generate checkerboards-free physically logical optimal designs. However, the filter radius (which decides the choice of the neighborhood over which the filtering is realized, see appendix D for more details) should be carefully selected in order to minimize undesirable grey zone at the solid-fluid interface in density-based topology optimization.

Conclusions and Perspectives

Concluding remarks

The present doctoral thesis was dedicated to application of topology optimization to explore innovative unconventional optimal designs for thermal systems. A density based TO approach from literature [18] was used for this purpose. The thesis is composed of two major parts: The first part deals with experimental investigation of the thermal performance of tree-like conductive structures obtained numerically by topology optimization formulated as a bi-material volume-to-point (VP) heat conduction problem. The second part of the thesis is devoted to numerical developments, simulations and investigations on TO of conjugate heat transfer systems inder a laminar flow regime. The key question is: Do the topology optimization numerical methods in literature have the ability to really place material points in certain zones of the flow for enhancing global heat transfer without causing flow-blockages when designing optimal thermal systems ? If yes, to what extent ? If no, then what kind of objective functions or numerical techniques may be introduced numerically to do the job better ? In this context, following are the main conclusions derived from the research conducted during this doctoral thesis:

Experimental investigation of topology optimized configuration

This work is a first approach dedicated to thermal measurements in conductive heat transfer tree-like structures obtained by topology optimization applied to VP heat conduction problem with an objective to analyze experimentally the thermal behaviour of the optimized structure under some specific thermal loads and boundary conditions. The bi-material optimal configuration obtained numerically from TO was fabricated in Aluminum-polymer combination and infrared thermography was used to measure the steady state temperature distribution on the optimal tree structure. Two different types of optimal structures were fabricated using water-jet cutting for two values of the amount of high diffusivity material in the structure, $17.92\ \%$ Al and $28.6\ \%$ Al, respectively. CFD simulations were performed on the optimized structure to mimic exactly the same initial and boundary conditions that prevailed during the experiments whose results are then eventually compared to the experimental measurements.

As a first conclusion, the optimal configurations obtained by TO were experimentally found to be effective in reducing the overall average temperature in the domain. Secondly, the values of objective function measured by IR thermography and those obtained by CFD simulations were found to be very close for the two optimal structures under observation with $\phi_{max} = 28.6\%$ and $\phi_{max} = 17.92\%$, respectively. However, for the maximum temperature in the domain (hot spot), there was a significant difference observed between the CFD and experimental results for the tree structure with $\phi_{max} = 17.92\%$ which is due to the proximity of the location of hot spot to the boundary edges and as a result the maximum temperature in the system is significantly affected by the conditions prevailing at the boundary. Further thermal measurements were performed on the existing optimal structures performed by modifying the heat sink boundary condition. The thermal behavior of the optimal structures remained consistent on modified boundary conditions as well. Finally, results of IR measurement reproduced on additional fabricated sample for the given optimal structure was found to be in line with the original IR thermal measurement thus ensuring reproducibility of experimental results. Apart from this, there are some important considerations when performing such experimental examinations for topology optimized configurations:

– It is important to ensure that a mesh-independent solution obtained from TO is used for fabricating the optimal configurations to be experimentally investigated, however, the minimum mesh size to be used in indirectly dependent on the minimum length scale that can be conveniently fabricated with the available fabrication technique. For example, the water-jet fabrication technique used in this study was capable of fabricating a minimum feature length of $0.1\ mm$. Hence, the minimum mesh size to be used in TO had to be greater than $0.1\ mm$. Fortunately, in the present study, mesh-independent solution obtained from TO had resulted in a minimum feature curve length of $0.4\ mm$ in the tree structure which was well above the minimum required criteria for fabrication. Otherwise, a higher precision fabrication technique would have been required to fabricate the optimal tree-structure.

– When extracting the CAD geometry from the final topology optimized structure represented by the contours of design variable field values, either manually or by using an automated image processing script, there will always be some minor difference in the final percentage of the two materials in the total domain volume. This may be due to the uncertainty associated with inclusion or non-inclusion of the intermediate densities (grey cells) at the interface of two materials in the final CAD geometry to be exported. For example, the original percentage of 20% and 30% of Aluminum in the total domain volume for the two tree structure were reduced to 17.92% and 28.6%, respectively, due to the post-processing of the results obtained from the TO solver. However, while doing so, it is very important to ensure that the stipulated design constraint of the original optimization problem is still respected and optimality of the solution is not affected. In other words, the final structures should not altered in a way that the extracted CAD geometry is significantly different form the numerically obtained optimal solution.

Topology optimization of conjugate heat transfer systems

Topology optimization of conjugate heat transfer systems using an innovative coupled bi-objective function, for heat transfer enhancement and pressure drop reduction, has been developed and presented for laminar incompressible flows using the Finite Volume based OpenFOAM® CFD package. The density-based TO numerical platform used an inequality constrained gradient-based optimization algorithm in conjugation with the continuous adjoint method for gradient computation.

The developed numerical tool was first applied to optimize a fluid channel with constant wall temperature numerical example from literature [15] to generate Pareto optimal solutions characteristic to multi-objective optimization problems. As a first conclusion, physically realistic optimal designs were obtained which form a Pareto frontier starting from pressure drop minimization leading to thermal power maximization based on the value of the scalar-valued weighting function. But more importantly, in contrast to the previous studies in literature [13, 15, 128], no fluid blockage, broken paths or other non-physical artifacts were observed especially when the thermal objective function was more prioritized.

In addition to this, an in-depth convergence study performed on the final topology optimized structure confirmed that the developed numerical method respects well the equality and inequality constraints associated with the topology optimization problem. Apart from this, various global and local numerical analysis methods like the evaluation of friction factor as a measure of pressure drop in the systems, examination of fluid velocity and temperature profiles at domain outlet and an order of magnitude analysis for the objective function values provides further deep insights into the obtained topology optimized designs. Furthermore, the developed numerical platform was capable to generate realistic optimal structures on varying the important physical parameters associated with the optimization problem like the Reynolds number, boundary conditions, thermal diffusivity ratio and the maximum temperature gradient in the system.

Next, in order to analyse the influence of the discretization technique and in an attempt to establish some benchmark-like cases for topology optimization of conjugate heat transfer systems, a recent numerical example solved using the Lattice Boltzmann method based topology optimization solver from literature [131] was solved again using the present Finite Volmue based OpenFOAM solver.

Comparison of the two results based on their respective objective function values demonstrate that the present FVM-based TO solver outperformed the existing LBM-based TO solver. To be specific, marginally higher thermal power is obtained but with 50% less pressure drop in the system. This further advocates the need for using a bi-objective function strategy for optimizing conjugate heat transfer systems.

As a first step towards validation of topology optimized conjugate heat transfer configuration, numerical verification over a conventional CFD software package (STAR-CCM+®) is performed to qualify the performance of the optimal CHT structures obtained by topology optimization. The goal was to evaluate the accuracy of the implicit representation of solid-fluid regions via a density-based Brinkman penalization approach (used in TO) by replacing it with an explicit separate modelling of solid and fluid domains using a multi-region approach (used in conventional CFD). The two results were in fair agreement with each other with around 12% higher pressure drop and 10% lower recoverable thermal power reported by the density-based Brinkman penalization TO approach as compared to the multi-region CFD approach. On further analysis, the difference in the two results were mainly due to three important factors. Firstly, due to the undesirable grey zones at the solid-fluid interface in desnity-based TO which introduced an unkown third material in the system, secondly, due to erroneous treatment of pressure-field in the solid regions in desnity-based TO and finally, due to the difference in methodology used to solve the governing equations in the two approaches. Nonetheless, the comparison clearly revealed that experimental validations are indispensable to better evaluate the performance of topology optimized CHT configurations.

Finally, a detailed parametric study was performed to better understand the influence of some critical numerical parameters on the present density-based topology optimization numerical platform. The mesh-sensitivity study performed for five different spatial discretization of the computational domain (based on mesh size) showed that the present TO numerical platform does not suffer from mesh-dependency problem when using a Cartesian grid with orthogonal square elements and a higher mesh resolution resulted in a better description of existing boundaries. However, when the computational domain was discretized with a non-uniform unstructured mesh consisting of triangular elements, qualitatively different configurations were obtained specially when the thermal objective function was more prioritized. Physically, this outcome can be attributed to the the nature of triangular type mesh elements which seems to provide more degree of freedom to the optimization algorithm to form designs for heat flux orientation that is more difficult to reach using a structured orthogonal mesh arrangement. Mathematically, this highlights the problem of existence of *non-uniqueness* of solution associated with the gradient-based local optimization algorithms like the one used in the present TO platform.

Furthermore, it was found that the final topologies obtained by the present TO numerical model, based on gradient-based MMA algorithm are highly sensitive to design variable field initialization. This highlights the problem of obtaining several local optimal inherent to such local optimization techniques. Additionally, a non-uniform design field initialization based on a better initial guess improved the existing solution with better description of fluid-solid interface without compromising much on the final objective function values. This outcome is in agreement with other studies in literature that used a non-uniform initialization for topology optimization of heat transfer and fluid flow systems [8, 129].

Apart form this, the influence of the size of density filter radius on the final topologies was investigated. It was clearly shown that, checkerboard solutions are produced when no filtering is used especially at very high weighting factor of thermal objective function. These checkerboard solutions were totally eradicated when using a density filter with an appropriate size of filter radius. Hence, filtering techniques are absolutely necessary for TO of CHT systems in order to generate checkerboard free solutions. On the other hand, when the filter is introduced, the grey zone starts to appear at the fluid-solid interface which keeps on growing with increasing filter radius size. Thus, it is very important to pay attention when selecting the appropriate filtering technique for TO of CHT systems.

Finally, when using a higher order FVM interpolation scheme from the start of the calculation, it was observed that the present TO numerical platform is highly unstable and encounters numerical

difficulties towards convergence specifically when the thermal objective function is more prioritized. This is because, for the current TO numerical platform, use of a higher order FVM scheme demands a better initial guess to obtain stable solutions due to the complexity induced in the system as a result of the conflicting nature of the two participating objective functions. Two solutions were proposed to encounter this issue. First, to begin with a less accurate but more stable 1^{st} order scheme and then switch to the more accurate 2^{nd} order scheme after reaching convergence with the former. Secondly, to use a 2^{nd} order scheme for all the convection terms except for the convective transport for adjoint temperature which is interpolated using a 1^{st} order scheme to obtain stable topology optimized solutions for the conjugate heat transfer problem.

As a final conclusion, it can be said that optimization of conjugate heat transfer system falls under the scope of bi-objective optimization problems due to simultaneous consideration of both the heat transfer enhancement and pressure drop reduction in the systems. However, TO of CHT systems using a bi-objective function strategy proved to be numerically a very challenging task and all the involved numerical parameters need to carefully monitored and adjusted accordingly in order to obtain physically realistic solutions in this field of optimization.

Perspectives

The research performed during this doctoral thesis gives rise to several perspective for future studies for topology optimization of conjugate heat transfer systems. Some of the most crucial and high priority requirements for the developed topology optimization numerical platform in this study can be listed as following:

- The present MMA algorithm based TO solver is computationally very expensive when handling large scale 3D problems. For example, an asymmetric computational model consisting of a quarter of the domain of the typical fluid channel with constant wall temperature numerical example discretized with 250000 cells takes approximately six to eight weeks to complete one simulation on a single Intel® Core™ i3 processor clocked at 3.70 GHz. Hence, in order to handle large scale 3D problems, the developed OpenFOAM® TO solver needs to be parallelized to make use of multiple CPU and GPU cores simultaneously, in order to minimize the overall computational time.

- Th numerical verification of topology optimized configuration pointed out some difference in the objective function values reported by the conventional CFD code as compared to the current Brinkamn penalization based TO numerical platform. This comparison clearly highlights the need to implement innovative and computationally inexpensive mesh-adaption techniques for accurately resolving boundary layer phenomena occurring at much smaller length scales. This requirement will be even more important for high Reynolds number flows where there will be sharp changes happening in the thermal and momentum boundary layers. However, implementation of appropriate mesh-adaption technique in topology optimization can be numerically very challenging as the number of design variables in the domain will be changed after each iteration due to the real time mesh-adaption happening on the boundaries and this information will have to be communicated back-and-forth to the coupled MMA optimizer after every iteration.

- It will be very interesting to see the performance of the currently used Method of Moving Asymptotes algorithm (MMA) as compared to the Optimality Criteria Method (OCM) algorithm from literature [18] in terms of overall computational time and objective function values. For example, during some preliminary testing, an another in-house developed OCM based TO solver was observed to be significantly less computationally expensive as compared to its MMA counterpart. However, the OCM based TO solver is still in its early stages and needs to be validated by solving some benchmark cases for TO of fluid flow systems before using it for solving TO of CHT systems.

– Further experimental measurements, on some of the obtained optimal structures for conjugate heat transfer problems in this study, needs to be conducted in order to better quantify and qualify the limits of the developed topology optimization numerical approach.

– The topology optimization research community is continuously developing new methods and splitting in different directions. According to the authors, it is highly important to improve existing methods in literature instead of developing alternative strategies which may or may not be better than the already existing ones. Therefore, it is important for the topology optimization community to get together and set up some benchmark cases for TO of heat transfer and fluid flow systems in order to find the best optimization approach and further improve upon it in order to handle wide variety of complex industrial optimization problems.

Bibliography

[1] Yue-Tzu Yang and Huan-Sen Peng. Numerical study of pin-fin heat sink with un-uniform fin height design. *International Journal of Heat and Mass Transfer*, 51(19-20):4788–4796, 2008.

[2] Yue-Tzu Yang and Huan-Sen Peng. Numerical study of the heat sink with un-uniform fin width designs. *International Journal of Heat and Mass Transfer*, 52(15-16):3473–3480, 2009.

[3] Haipeng Jia, HG Beom, Yuxin Wang, Song Lin, and Bo Liu. Evolutionary level set method for structural topology optimization. *Computers & Structures*, 89(5):445–454, 2011.

[4] Yongcun Zhang and Shutian Liu. Design of conducting paths based on topology optimization. *Heat and Mass Transfer*, 44(10):1217–1227, 2008.

[5] Gilles Marck, Maroun Nemer, Jean-Luc Harion, Serge Russeil, and Daniel Bougeard. Topology optimization using the simp method for multiobjective conductive problems. *Numerical Heat Transfer, Part B: Fundamentals*, 61(6):439–470, 2012.

[6] Jaco Dirker and Josua P Meyer. Topology optimization for an internal heat-conduction cooling scheme in a square domain for high heat flux applications. *Journal of Heat Transfer*, 135(11):111010, 2013.

[7] Francois H Burger, Jaco Dirker, and Josua P Meyer. Three-dimensional conductive heat transfer topology optimisation in a cubic domain for the volume-to-surface problem. *International Journal of Heat and Mass Transfer*, 67:214–224, 2013.

[8] Suna Yan, Fengwen Wang, and Ole Sigmund. On the non-optimality of tree structures for heat conduction. *International Journal of Heat and Mass Transfer*, 122:660 – 680, 2018.

[9] Thomas Borrvall and Joakim Petersson. Topology optimization of fluids in stokes flow. *International journal for numerical methods in fluids*, 41(1):77–107, 2003.

[10] Georg Pingen and Kurt Maute. Optimal design for non-newtonian flows using a topology optimization approach. *Computers & Mathematics with Applications*, 59(7):2340–2350, 2010.

[11] Sebastian Kreissl, Georg Pingen, and Kurt Maute. Topology optimization for unsteady flow. *International Journal for Numerical Methods in Engineering*, 2011.

[12] Carsten Othmer, Eugene de Villiers, and Henry G Weller. Implementation of a continuous adjoint for topology optimization of ducted flows. In *18th AIAA Computational Fluid Dynamics Conference, June*, 2007.

[13] Ercan M Dede. Multiphysics topology optimization of heat transfer and fluid flow systems. In *proceedings of the COMSOL Users Conference*, 2009.

[14] Joe Alexandersen, Niels Aage, Casper Schousboe Andreasen, and Ole Sigmund. Topology optimisation for natural convection problems. *International Journal for Numerical Methods in Fluids*, 76(10):699–721, 2014.

[15] Gilles Marck, Maroun Nemer, and Jean-Luc Harion. Topology optimization of heat and mass transfer problems: laminar flow. *Numerical Heat Transfer, Part B: Fundamentals*, 63(6):508–539, 2013.

[16] FLIR Systems, Inc., 9 Townsend West Nashua, NH 03063 USA. *The Ultimate Infrared Handbook for R&D Professionals*, 2012.

[17] Oleg Evsutin, Alexander Shelupanov, Roman Meshcheryakov, Dmitry Bondarenko, and Angelika Rashchupkina. The algorithm of continuous optimization based on the modified cellular automaton. *Symmetry*, 8(9):84, 2016.

[18] Martin Philip Bendsoe and Ole Sigmund. *Topology optimization: theory, methods, and applications*. Springer Science & Business Media, 2013.

[19] Yogesh Jaluria. *Design and optimization of thermal systems*. CRC press, 2007.

[20] Kyoungwoo Park, Dong-Hoon Choi, and Kwan-Soo Lee. Numerical shape optimization for high performance of a heat sink with pin-fins. *Numerical Heat Transfer, Part A: Applications*, 46(9):909–927, 2004.

[21] Abdus Samad, Ki-Don Lee, and Kwang-Yong Kim. Multi-objective optimization of a dimpled channel for heat transfer augmentation. *Heat and Mass Transfer*, 45(2):207, 2008.

[22] Carlos Silva, Doseo Park, et al. Optimization of fin performance in a laminar channel flow through dimpled surfaces. *Journal of Heat Transfer*, 131(2):021702, 2009.

[23] Noel Leon, Jose Cueva, Cesar Villarreal, Sergio Hutron, and German Campero. Automatic shape variations for optimization and innovation. In *Trends in Computer Aided Innovation*, pages 179–188. Springer, 2007.

[24] Yan Zhang, Ying Gao, Da Wei Qu, and Chang Qing Song. Optimization design for water jacket of 4g24 gasoline engine. In *Power and Energy Engineering Conference (APPEEC), 2011 Asia-Pacific*, pages 1–4. IEEE, 2011.

[25] Martin Philip Bendsøe and Noboru Kikuchi. Generating optimal topologies in structural design using a homogenization method. *Computer methods in applied mechanics and engineering*, 71(2):197–224, 1988.

[26] Maria B Dühring, Jakob S Jensen, and Ole Sigmund. Acoustic design by topology optimization. *Journal of sound and vibration*, 317(3-5):557–575, 2008.

[27] Erin Kuci, François Henrotte, Pierre Duysinx, Patrick Dular, and Christophe Geuzaine. Design sensitivity analysis for shape optimization of nonlinear magnetostatic systems. *IEEE Transactions on Magnetics*, 52(3):1–4, 2016.

[28] Yoshifumi Okamoto, Masaya Ohtake, and Norio Takahashi. Magnetic shield design of perpendicular magnetic recording head by using topology optimization technique. *IEEE transactions on magnetics*, 41(5):1788–1791, 2005.

[29] Anton Evgrafov, Georg Pingen, and Kurt Maute. Topology optimization of fluid domains: kinetic theory approach. *ZAMM-Journal of Applied Mathematics and Mechanics/Zeitschrift für Angewandte Mathematik und Mechanik: Applied Mathematics and Mechanics*, 88(2):129–141, 2008.

[30] Laurits H Olesen, Fridolin Okkels, and Henrik Bruus. A high-level programming-language implementation of topology optimization applied to steady-state navier-stokes flow. *arXiv preprint physics/0410086*, 2004.

[31] ChunGang Zhuang, ZhenHua Xiong, and Han Ding. A level set method for topology optimization of heat conduction problem under multiple load cases. *Computer methods in applied mechanics and engineering*, 196(4):1074–1084, 2007.

[32] Gil Ho Yoon. Topological design of heat dissipating structure with forced convective heat transfer. *Journal of Mechanical Science and Technology*, 24(6):1225–1233, 2010.

[33] Krister Svanberg. The method of moving asymptotes—a new method for structural optimization. *International journal for numerical methods in engineering*, 24(2):359–373, 1987.

[34] Ole Sigmund and Kurt Maute. Topology optimization approaches. *Structural and Multidisciplinary Optimization*, 48(6):1031–1055, 2013.

[35] Ole Sigmund and Joakim Petersson. Numerical instabilities in topology optimization: a survey on procedures dealing with checkerboards, mesh-dependencies and local minima. *Structural optimization*, 16(1):68–75, 1998.

[36] Martin P Bendsøe. Optimal shape design as a material distribution problem. *Structural optimization*, 1(4):193–202, 1989.

[37] M Zhou and GIN Rozvany. The coc algorithm, part ii: topological, geometrical and generalized shape optimization. *Computer Methods in Applied Mechanics and Engineering*, 89(1-3):309–336, 1991.

[38] HP Mlejnek. Some aspects of the genesis of structures. *Structural Optimization*, 5(1-2):64–69, 1992.

[39] Grégoire Allaire, François Jouve, and Anca-Maria Toader. A level-set method for shape optimization. *Comptes Rendus Mathematique*, 334(12):1125–1130, 2002.

[40] Michael Yu Wang, Xiaoming Wang, and Dongming Guo. A level set method for structural topology optimization. *Computer methods in applied mechanics and engineering*, 192(1):227–246, 2003.

[41] Jan Sokolowski and Antoni Zochowski. On the topological derivative in shape optimization. *SIAM journal on control and optimization*, 37(4):1251–1272, 1999.

[42] Blaise Bourdin and Antonin Chambolle. Design-dependent loads in topology optimization. *ESAIM: Control, Optimisation and Calculus of Variations*, 9:19–48, 2003.

[43] Yi M Xie and Grant P Steven. A simple evolutionary procedure for structural optimization. *Computers & structures*, 49(5):885–896, 1993.

[44] Martin P Bendsøe and Ole Sigmund. Material interpolation schemes in topology optimization. *Archive of applied mechanics*, 69(9-10):635–654, 1999.

[45] T Dbouk. A review about the engineering design of optimal heat transfer systems using topology optimization. *Applied Thermal Engineering*, 112:841–854, 2017.

[46] Nico P van Dijk, K Maute, M Langelaar, and F Van Keulen. Level-set methods for structural topology optimization: a review. *Structural and Multidisciplinary Optimization*, 48(3):437–472, 2013.

[47] Mark Christian E Manuel and Po Ting Lin. Heat exchanger design with topology optimization. In *Heat Exchangers-Design, Experiment and Simulation*. InTech, 2017.

[48] Peter D Dunning and H Alicia Kim. A new hole insertion method for level set based structural topology optimization. *International Journal for Numerical Methods in Engineering*, 93(1):118–134, 2013.

[49] Hans A Eschenauer, Vladimir V Kobelev, and Axel Schumacher. Bubble method for topology and shape optimization of structures. *Structural optimization*, 8(1):42–51, 1994.

[50] Julian A Norato, Martin P Bendsøe, Robert B Haber, and Daniel A Tortorelli. A topological derivative method for topology optimization. *Structural and Multidisciplinary Optimization*, 33(4-5):375–386, 2007.

[51] Mathias Stolpe and Martin P Bendsøe. Global optima for the zhou–rozvany problem. *Structural and Multidisciplinary Optimization*, 43(2):151–164, 2011.

[52] Virginia Young, Osvaldo M Querin, GP Steven, and YM Xie. 3d and multiple load case bi-directional evolutionary structural optimization (beso). *Structural optimization*, 18(2-3):183–192, 1999.

[53] Raphaël Boichot, Lingai Luo, and Yilin Fan. Tree-network structure generation for heat conduction by cellular automaton. *Energy Conversion and Management*, 50(2):376–386, 2009.

[54] X Huang and YM Xie. Evolutionary topology optimization of geometrically and materially nonlinear structures under prescribed design load. *Structural engineering & mechanics*, 34(5):581, 2010.

[55] M Zhou and GIN Rozvany. On the validity of eso type methods in topology optimization. *Structural and Multidisciplinary Optimization*, 21(1):80–83, 2001.

[56] Stephen Wright and Jorge Nocedal. Numerical optimization. *Springer Science*, 35(67-68):7, 1999.

[57] Gerhard Venter. Review of optimization techniques. *Encyclopedia of aerospace engineering*, 2010.

[58] Singiresu S Rao and SS Rao. *Engineering optimization: theory and practice*. John Wiley & Sons, 2009.

[59] Garret N Vanderplaats. *Multidiscipline design optimization*. Vanderplaats Research & Development, Incorporated, 2007.

[60] Jasbir S Arora. Introduction to optimum design, 1989. *McGraw-Mill Book Company*, 1967.

[61] Kyungjun Lee. Topology optimization of convective cooling system designs. 2012.

[62] John Holland. Adaptation in natural and artificial systems: an introductory analysis with application to biology. *Control and artificial intelligence*, 1975.

[63] Scott Kirkpatrick, C Daniel Gelatt, and Mario P Vecchi. Optimization by simulated annealing. *science*, 220(4598):671–680, 1983.

[64] Russell Eberhart and James Kennedy. A new optimizer using particle swarm theory. In *Micro Machine and Human Science, 1995. MHS'95., Proceedings of the Sixth International Symposium on*, pages 39–43. IEEE, 1995.

[65] Lawrence J Fogel, Alvin J Owens, and Michael J Walsh. Artificial intelligence through simulated evolution. 1966.

[66] Xianghua Xu, Xingang Liang, and Jianxun Ren. Optimization of heat conduction using combinatorial optimization algorithms. *International journal of heat and mass transfer*, 50(9-10):1675–1682, 2007.

[67] M Yoshimura, K Shimoyama, T Misaka, and S Obayashi. Topology optimization of fluid problems using genetic algorithm assisted by the kriging model. *International Journal for Numerical Methods in Engineering*, 109(4):514–532, 2017.

[68] Alejandro Diaz and Ole Sigmund. Checkerboard patterns in layout optimization. *Structural optimization*, 10(1):40–45, 1995.

[69] Martin Philip Bendsøe, Alejandro Díaz, and Noboru Kikuchi. Topology and generalized layout optimization of elastic structures. In *Topology design of structures*, pages 159–205. Springer, 1993.

[70] Ole Sigmund. *Design of Materials Structures Using Topology Optimization*. Department of Solid Mechanics, Technical University of Denmark, 1994.

[71] Hans A Eschenauer and Niels Olhoff. Topology optimization of continuum structures: a review. *Applied Mechanics Reviews*, 54(4):331–390, 2001.

[72] G Allaire and GA Francfort. A numerical algorithm for topology and shape optimization. In *Topology design of structures*, pages 239–248. Springer, 1993.

[73] JM Guedes and JE Taylor. On the prediction of material properties and topology for optimal continuum structures. *Structural optimization*, 14(2-3):193–199, 1997.

[74] Theodore L Bergman, Frank P Incropera, David P DeWitt, and Adrienne S Lavine. *Fundamentals of heat and mass transfer*. John Wiley & Sons, 2011.

[75] YA Cengel. *Introduction to thermodynamics and heat transfer+ EES software*. New York: McGraw Hill Higher Education Press, 2007.

[76] Abram S Dorfman. *Conjugate problems in convective heat transfer*. CRC Press, 2009.

[77] Abram Dorfman and Zachary Renner. Conjugate problems in convective heat transfer: Review. *Mathematical Problems in Engineering*, 2009, 2009.

[78] James D Heidmann, Alain J Kassab, Eduardo A Divo, Franklin Rodriguez, and Erlendur Steinthorsson. Conjugate heat transfer effects on a realistic film-cooled turbine vane. In *ASME Turbo Expo 2003, collocated with the 2003 International Joint Power Generation Conference*, pages 361–371. American Society of Mechanical Engineers, 2003.

[79] David L Rigby and Jan Lepicovsky. Conjugate heat transfer analysis of internally cooled configurations. In *ASME Turbo Expo 2001: Power for Land, Sea, and Air*, pages V003T01A084–V003T01A084. American Society of Mechanical Engineers, 2001.

[80] Seongwon Kang. *An improved immersed boundary method for computation of turbulent flows with heat transfer*. PhD thesis, Stanford University, 2008.

[81] Gianluca Iaccarino and Stéphane Moreau. Natural and forced conjugate heat transfer in complex geometries on cartesian adapted grids. *Journal of fluids engineering*, 128(4):838–846, 2006.

[82] C Othmer. A continuous adjoint formulation for the computation of topological and surface sensitivities of ducted flows. *International Journal for Numerical Methods in Fluids*, 58(8):861–877, 2008.

[83] Christof Hinterberger and Mark Olesen. Automatic geometry optimization of exhaust systems based on sensitivities computed by a continuous adjoint cfd method in openfoam. Technical report, SAE Technical Paper, 2010.

[84] Ch Hinterberger and M Olesen. Industrial application of continuous adjoint flow solvers for the optimization of automotive exhaust systems. *CFD & Optimization, Antalya, Turkey*, 2011.

[85] Daria Jakubek and Claus Wagner. Shape optimization of train head cars using adjoint-based computational fluid dynamics, 2012.

[86] A Lincke and T Rung. Adjoint-based sensitivity analysis for buoyancy-driven incompressible navier-stokes equations with heat transfer. In *Proceedings of the Eighth Internat. Conf. on Engineering Computational Technology, Dubrovnik, Croatia*, 2012.

[87] Eugene de Villiers and Carsten Othmer. Multi-objective adjoint optimization of intake port geometry. Technical report, SAE Technical Paper, 2012.

[88] C Othmer, EM Papoutsis-Kiachagias, and K Haliskos. Cfd optimization via sensitivity-based shape morphing. In *Proceedings of the 4th ANSA & μETA Internat. Conf., Thessaloniki, Greece, BETA CAE Systems SA*, 2011.

[89] Adrian Bejan. Constructal-theory network of conducting paths for cooling a heat generating volume. *International Journal of Heat and Mass Transfer*, 40(4):799–816, 1997.

[90] Alberto Donoso. Numerical simulations in 3d heat conduction: minimizing the quadratic mean temperature gradient by an optimality criteria method. *SIAM Journal on Scientific Computing*, 28(3):929–941, 2006.

[91] Ercan M Dede, Shailesh N Joshi, and Feng Zhou. Topology optimization, additive layer manufacturing, and experimental testing of an air-cooled heat sink. *Journal of Mechanical Design*, 137(11):111403, 2015.

[92] Qing Li, Grant P Steven, Osvaldo M Querin, and YM Xie. Shape and topology design for heat conduction by evolutionary structural optimization. *International Journal of Heat and Mass Transfer*, 42(17):3361–3371, 1999.

[93] Yongcun Zhang and Shutian Liu. The optimization model of the heat conduction structure. *Progress in Natural Science*, 18(6):665–670, 2008.

[94] Allan Gersborg-Hansen, Martin P Bendsøe, and Ole Sigmund. Topology optimization of heat conduction problems using the finite volume method. *Structural and multidisciplinary optimization*, 31(4):251–259, 2006.

[95] T Gao, WH Zhang, JH Zhu, YJ Xu, and DH Bassir. Topology optimization of heat conduction problem involving design-dependent heat load effect. *Finite Elements in Analysis and Design*, 44(14):805–813, 2008.

[96] Alberto Pizzolato, Ashesh Sharma, Kurt Maute, Adriano Sciacovelli, and Vittorio Verda. Topology optimization for heat transfer enhancement in latent heat thermal energy storage. *International Journal of Heat and Mass Transfer*, 113:875 – 888, 2017.

[97] A.V. Cherkaev. Relaxation of problems of optimal structural design. *International Journal of Solids and Structures*, 31(16):2251 – 2280, 1994.

[98] Mathias Stolpe and Krister Svanberg. An alternative interpolation scheme for minimum compliance topology optimization. *Structural and Multidisciplinary Optimization*, 22(2):116–124, 2001.

[99] MP Rossow and JE Taylor. A finite element method for the optimal design of variable thickness sheets. *Aiaa Journal*, 11(11):1566–1569, 1973.

[100] Khodor Khadra, Philippe Angot, Sacha Parneix, and Jean-Paul Caltagirone. Fictitious domain approach for numerical modelling of navier–stokes equations. *International journal for numerical methods in fluids*, 34(8):651–684, 2000.

[101] T DBOUK, F PERALES, F BABIK, and R MOZUL. A df-ibm/nscd coupling framework to simulate immersed particle interactions. *Comput. Methods Appl. Mech. Engrg.*, 309:610–624, 2016.

[102] Niclas Wiker, Anders Klarbring, and Thomas Borrvall. The darcy-stokes topology optimization problem. In *IUTAM Symposium on Topological Design Optimization of Structures, Machines and Materials*, pages 551–558. Springer, 2006.

[103] Allan Gersborg-Hansen, Ole Sigmund, and Robert B Haber. Topology optimization of channel flow problems. *Structural and Multidisciplinary Optimization*, 30(3):181–192, 2005.

[104] Niels Aage, Thomas H Poulsen, Allan Gersborg-Hansen, and Ole Sigmund. Topology optimization of large scale stokes flow problems. *Structural and Multidisciplinary Optimization*, 35(2):175–180, 2008.

[105] Casper Schousboe Andreasen, Allan Roulund Gersborg, and Ole Sigmund. Topology optimization of microfluidic mixers. *International Journal for Numerical Methods in Fluids*, 61(5):498–513, 2009.

[106] Fridolin Okkels and Henrik Bruus. Scaling behavior of optimally structured catalytic microfluidic reactors. *Physical Review E*, 75(1):016301, 2007.

[107] Gil Ho Yoon. Topology optimization for stationary fluid–structure interaction problems using a new monolithic formulation. *International journal for numerical methods in engineering*, 82(5):591–616, 2010.

[108] Xueye Chen. Topology optimization of microfluidics — a review. *Microchemical Journal*, 127:52 – 61, 2016.

[109] Xianbao Duan, Yichen Ma, and Rui Zhang. Optimal shape control of fluid flow using variational level set method. *Physics letters A*, 372(9):1374–1379, 2008.

[110] Georg Pingen, Anton Evgrafov, and Kurt Maute. Topology optimization of flow domains using the lattice boltzmann method. *Structural and Multidisciplinary Optimization*, 34(6):507–524, 2007.

[111] Georg Pingen, Anton Evgrafov, and Kurt Maute. 3d topology optimization of fluids by the lattice boltzmann method. In *Proceedings of the 11th AIAA/ISSMO multidisciplinary analysis and optimization conference, Portsmouth*, 2006.

[112] Yongbo Deng, Zhenyu Liu, Ping Zhang, Yongshun Liu, and Yihui Wu. Topology optimization of unsteady incompressible navier–stokes flows. *Journal of Computational Physics*, 230(17):6688 – 6708, 2011.

[113] Sebastian Nørgaard, Ole Sigmund, and Boyan Lazarov. Topology optimization of unsteady flow problems using the lattice boltzmann method. *Journal of Computational Physics*, 307:291 – 307, 2016.

[114] Xian-Bao Duan, Fei-Fei Li, and Xin-Qiang Qin. Adaptive mesh method for topology optimization of fluid flow. *Applied Mathematics Letters*, 44:40 – 44, 2015.

[115] Kristian Ejlebjerg Jensen. Topology optimization of stokes flow on dynamic meshes using simple optimizers. *Computers & Fluids*, 2018.

[116] J.R.L. Koch, E.M. Papoutsis-Kiachagias, and K.C. Giannakoglou. Transition from adjoint level set topology to shape optimization for 2d fluid mechanics. *Computers & Fluids*, 150:123 – 138, 2017.

[117] Gil Ho Yoon. Topology optimization for turbulent flow with spalart–allmaras model. *Computer Methods in Applied Mechanics and Engineering*, 303:288 – 311, 2016.

[118] Cetin B. Dilgen, Sumer B. Dilgen, David R. Fuhrman, Ole Sigmund, and Boyan S. Lazarov. Topology optimization of turbulent flows. *Computer Methods in Applied Mechanics and Engineering*, 331:363 – 393, 2018.

[119] Luzhong Yin and GK Ananthasuresh. A novel topology design scheme for the multi-physics problems of electro-thermally actuated compliant micromechanisms. *Sensors and Actuators A: Physical*, 97:599–609, 2002.

[120] Tyler E Bruns. Topology optimization of convection-dominated, steady-state heat transfer problems. *International Journal of Heat and Mass Transfer*, 50(15):2859–2873, 2007.

[121] Seung-Ho Ahn and Seonho Cho. Level set–based topological shape optimization of heat conduction problems considering design-dependent convection boundary. *Numerical Heat Transfer, Part B: Fundamentals*, 58(5):304–322, 2010.

[122] A Iga, S Nishiwaki, K Izui, and M Yoshimura. Topology optimization for thermal conductors considering design-dependent effects, including heat conduction and convection. *International Journal of Heat and Mass Transfer*, 52(11):2721–2732, 2009.

[123] Tadayoshi Matsumori, Tsuguo Kondoh, Atsushi Kawamoto, and Tsuyoshi Nomura. Topology optimization for fluid–thermal interaction problems under constant input power. *Structural and Multidisciplinary Optimization*, 47(4):571–581, 2013.

[124] Philip E Gill, Walter Murray, and Michael A Saunders. Snopt: An sqp algorithm for large-scale constrained optimization. *SIAM review*, 47(1):99–131, 2005.

[125] EA Kontoleontos, EM Papoutsis-Kiachagias, AS Zymaris, DI Papadimitriou, and KC Giannakoglou. Adjoint-based constrained topology optimization for viscous flows, including heat transfer. *Engineering Optimization*, 45(8):941–961, 2013.

[126] Adriano A Koga, Edson Comini C Lopes, Helcio F Villa Nova, Cicero R de Lima, and Emílio Carlos Nelli Silva. Development of heat sink device by using topology optimization. *International Journal of Heat and Mass Transfer*, 64:759–772, 2013.

[127] Jan H.K. Haertel and Gregory F. Nellis. A fully developed flow thermofluid model for topology optimization of 3d-printed air-cooled heat exchangers. *Applied Thermal Engineering*, 119:10 – 24, 2017.

[128] Xiaoping Qian and Ercan M Dede. Topology optimization of a coupled thermal-fluid system under a tangential thermal gradient constraint. *Structural and Multidisciplinary Optimization*, 54(3):531–551, 2016.

[129] Shi Zeng, Bugra Kanargi, and Poh Seng Lee. Experimental and numerical investigation of a mini channel forced air heat sink designed by topology optimization. *International Journal of Heat and Mass Transfer*, 121:663–679, 2018.

[130] Jan HK Haertel, Kurt Engelbrecht, Boyan S Lazarov, and Ole Sigmund. Topology optimization of a pseudo 3d thermofluid heat sink model. *International Journal of Heat and Mass Transfer*, 121:1073–1088, 2018.

[131] Florian Dugast, Yann Favennec, Christophe Josset, Yilin Fan, and Lingai Luo. Topology optimization of thermal fluid flows with an adjoint lattice boltzmann method. *Journal of Computational Physics*, 365:376 – 404, 2018.

[132] Pascal Häußler, Ioannis Nitsopoulos, Jürgen Sauter, and Markus Stephan. Topology and shape optimization methods for cfd problems. In *24th CADFEM Users' Meeting*, page 140, 2006.

[133] Carsten Othmer, Thomas Kaminski, and Ralf Giering. Computation of topological sensitivities in fluid dynamics: cost function versatility. In *ECCOMAS CFD 2006: Proceedings of the European Conference on Computational Fluid Dynamics, Egmond aan Zee, The Netherlands, September 5-8, 2006*. Delft University of Technology; European Community on Computational Methods in Applied Sciences (ECCOMAS), 2006.

[134] Gil Ho Yoon and Yoon Young Kim. The element connectivity parameterization formulation for the topology design optimization of multiphysics systems. *International Journal for Numerical Methods in Engineering*, 64(12):1649–1677, 2005.

[135] Bing-Chung Chen and Noboru Kikuchi. Topology optimization with design-dependent loads. *Finite Elements in Analysis and Design*, 37(1):57–70, 2001.

[136] Talib Dbouk and Jean-Luc Harion. Performance of optimization algorithms applied to large nonlinear constrained problems. *American Journal of Algorithms and Computing*, 2(1):32–56, 2015.

[137] Timothy Ward Athan and Panos Y Papalambros. A note on weighted criteria methods for compromise solutions in multi-objective optimization. *Engineering Optimization*, 27(2):155–176, 1996.

[138] Kentaro Yaji, Takayuki Yamada, Masato Yoshino, Toshiro Matsumoto, Kazuhiro Izui, and Shinji Nishiwaki. Topology optimization in thermal-fluid flow using the lattice boltzmann method. *Journal of Computational Physics*, 307:355 – 377, 2016.

[139] PLM Siemens. Star-ccm+ user's manual version 13.02, 2018.

[140] Qianlong Liu and Oleg V. Vasilyev. A brinkman penalization method for compressible flows in complex geometries. *Journal of Computational Physics*, 227(2):946 – 966, 2007.

[141] Joe F Thompson, Zahir UA Warsi, and C Wayne Mastin. Boundary-fitted coordinate systems for numerical solution of partial differential equations—a review. *Journal of computational Physics*, 47(1):1–108, 1982.

[142] Dimitri J Mavriplis. Accurate multigrid solution of the euler equations on unstructured and adaptive meshes. *AIAA journal*, 28(2):213–221, 1990.

[143] Tom Verstraete and Rene Van den Braembussche. A novel method for the computation of conjugate heat transfer with coupled solvers. In *ICHMT DIGITAL LIBRARY ONLINE*. Begel House Inc., 2009.

[144] MB Giles. Stability analysis of numerical interface conditions in fluid–structure thermal analysis. *International Journal for Numerical Methods in Fluids*, 25(4):421–436, 1997.

[145] Sébastien Chemin. *Etude des interactions thermiques fluide-structure par un couplage de codes de calcul*. PhD thesis, Reims, 2006.

[146] Emmanuel Radenac, JÈrÈmie Gressier, and Pierre Millan. Methodology of numerical coupling for transient conjugate heat transfer. *Computers & Fluids*, 100:95–107, 2014.

[147] William York. A robust conjugate heat transfer methodology with novel turbulence modeling applied to internally-cooled gas turbine airfoils. 2006.

[148] Philippe Angot, Charles-Henri Bruneau, and Pierre Fabrie. A penalization method to take into account obstacles in incompressible viscous flows. *Numerische Mathematik*, 81(4):497–520, 1999.

[149] Ole Sigmund. Morphology-based black and white filters for topology optimization. *Structural and Multidisciplinary Optimization*, 33(4-5):401–424, 2007.

[150] ANSYS Fluent. 15.0 user's manual, ansys documentation n fluent n user's guide & theory guide—release 15.0. *ANSYS Inc., ANSYS Inc.*

[151] Optris infrared thermometers, Ferdinand-Buisson-Str. 14 ▪ 13127 Berlin ▪ Germany. *Basic principles of non-contact temperature measurement*, 2006.

[152] Joel H Ferziger and Milovan Peric. *Computational methods for fluid dynamics*. Springer Science & Business Media, 2012.

[153] Henk Kaarle Versteeg and Weeratunge Malalasekera. *An introduction to computational fluid dynamics: the finite volume method*. Pearson Education, 2007.

[154] Christopher J Greenshields. Openfoam user guide. *OpenFOAM Foundation Ltd, version*, 3(1), 2015.

[155] Suhas Patankar. *Numerical heat transfer and fluid flow*. CRC press, 1980.

[156] Magnus Rudolph Hestenes and Eduard Stiefel. *Methods of conjugate gradients for solving linear systems*, volume 49. NBS Washington, DC, 1952.

[157] Henk A Van der Vorst. Bi-cgstab: A fast and smoothly converging variant of bi-cg for the solution of nonsymmetric linear systems. *SIAM Journal on scientific and Statistical Computing*, 13(2):631–644, 1992.

[158] DAH Jacobs. Preconditioned conjugate gradient methods for solving systems of algebraic equations: Central electricity research laboratories report. Technical report, RD/L, 1980.

[159] Tim Behrens. Openfoam's basic solvers for linear systems of equations. *Chalmers, Department of Applied Mechanics*, 18(02), 2009.

[160] Erik Andreassen, Anders Clausen, Mattias Schevenels, Boyan S Lazarov, and Ole Sigmund. Efficient topology optimization in matlab using 88 lines of code. *Structural and Multidisciplinary Optimization*, 43(1):1–16, 2011.

[161] Tyler E Bruns and Daniel A Tortorelli. Topology optimization of non-linear elastic structures and compliant mechanisms. *Computer methods in applied mechanics and engineering*, 190(26-27):3443–3459, 2001.

Appendix A

Infrared camera setup

Infrared (IR) radiation is a type of electromagnetic radiation which falls in between the visible light and the microwaves on the electromagnetic spectrum. It covers a part of the spectrum from approximately around $0.78\ \mu m$ to $1\ mm$. All bodies with temperature above the absolute zero (-273.15° C = 0 Kelvin) emits an electromagnetic radiation from its surface, which is proportional to its intrinsic temperature. A part of this so-called intrinsic radiation is infrared radiation, which can be used to measure a body's temperature. This radiation penetrates the atmosphere. While IR radiation can not be detected by the human eye, an infrared camera has the ability to transform it into a visual image that can represent the temperature variation across a body. Infrared thermography is a type of non-contact thermal measurement technique where imaging is performed through an infrared camera calibrated to show the thermal variation across a body.

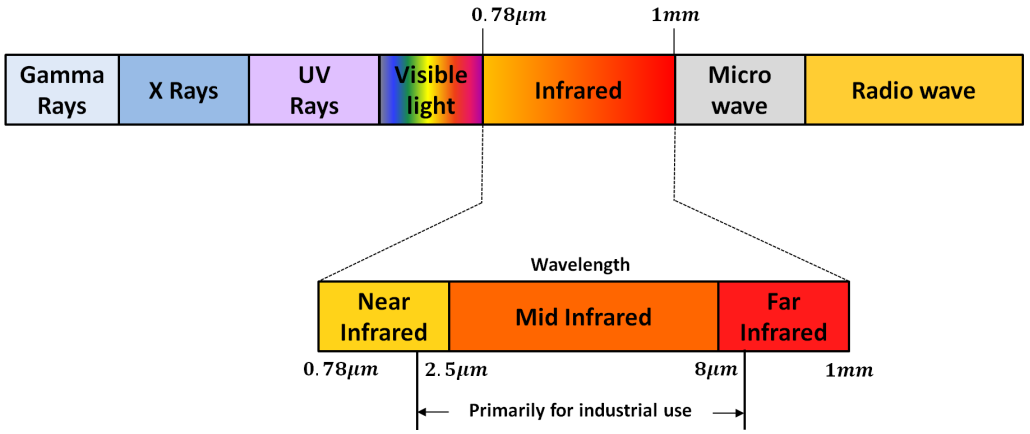

Figure A.1 – Spectrum of electromagnetic radiation.

The main components of an IR camera consists of an optical lens that focuses infrared radiation onto a detector and some specific electronics for processing the signals and related software for displaying the images (see Fig. A.2). With the help of a lens (input optics) the beams are focused on a detector element, which generates an electrical signal proportional to the radiation. The signal is amplified and, using successive digital signal processing, is transformed into an output signal proportional to the object temperature. The measuring value may be shown on a screen or released as analog output signal, which supports an easy connection to control systems of the process management [151].

The infrared camera detector is a focal plane array (FPA) of micrometer sized pixels made up of various materials sensitive to IR wavelengths. FPA resolution can range from about 160×120 pixels up to 1024×1024 pixels. An IR detector can be broadly classified into two main types: thermal detectors and quantum detectors. The operation of a quantum detector is based on the change of state of electrons in a crystal structure reacting to incident photons. These detectors are generally faster and more sensitive than thermal detectors. However, they require cooling, sometimes down

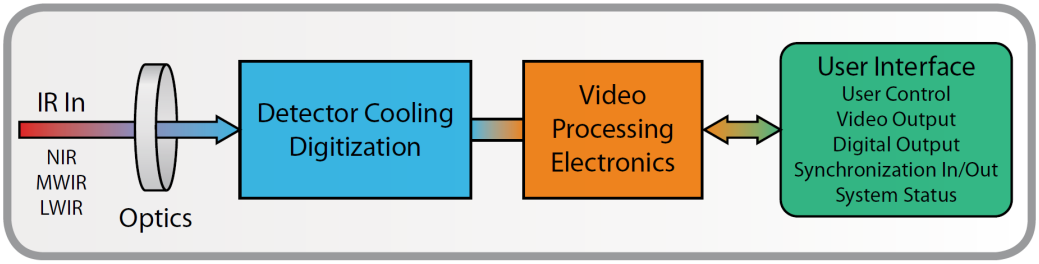

Figure A.2 – A simplified block diagram of an IR camera [16].

to cryogenic temperatures using liquid nitrogen or a small Stirling cycle refrigerator unit [16]. The Cedip Titanium 550M IR camera with a Indium antimonide (InSb) quantum detector is used in this experiment. It has a FPA resolution of 320×256 pixels. The key technical specifications of this IR camera is listed below in table A.1.

Focal length	Field of view ($\theta_H \times \theta_V$)	Aperture	Pixels (resolution)	Pixel size (pitch)	Spectral band
50 mm	$11° \times 8.8°$	$f/2.0$	320×256	30 μm	3.6 -5.1 μm

Table A.1 – Infrared camera specifications.

A.1 Field of view of the IR camera

Based on the above camera specifications, the best focal distance between the IR camera and the test section under consideration is to be calculated in order to perform accurate IR measurements. The angle of view or field of view (FOV, denoted as θ) is the amount of given scene shown on the detector/sensor. As the detector is usually rectangular, it is expressed in terms of horizontal and vertical filed of view (θ_H and θ_V). The Cedip Titanium 550M IR camera has a horizontal and a vertical field of view of 11 ° and 8.8 °, respectively. The Cedip user manual provides the following two relation to estimate the object distance accurately:

$$d_{horizontal} = \frac{(w_{obj}/2)}{tan(\frac{\theta_H}{2})} \tag{A.1a}$$

$$d_{vertical} = \frac{(l_{obj}/2)}{tan(\frac{\theta_V}{2})} \tag{A.1b}$$

Where, $d_{horizontal}$ is the minimum distance required to capture the complete width of the object, $d_{vertical}$ is the minimum distance required to capture the complete length of the object, w_{obj} and l_{obj} are the width and length of the object, respectively. Fig. A.3 shows the vertical field of view for a camera lens.

For $100\ mm \times 100\ mm$ test section (i.e., for $l_{obj} = 100\ mm$ and $w_{obj} = 100\ mm$), based on the above relations, $d_{Horizontal}$ is calculated to be $519.2\ mm$ and $d_{Vertical}$ is calculated to be $649.80\ mm$. Therefore, the square test section has to be kept at a distance of around $650\ mm$ $(0.65\ m)$ in order to accurately capture the complete thermal scene.

A.2 Calibration of the IR Camera

An infrared camera is a "photon counting device". Depending on the amount of photons received, it returns an electrical voltage (in volts) expressed as a digital level (DL). A non-linear transfer

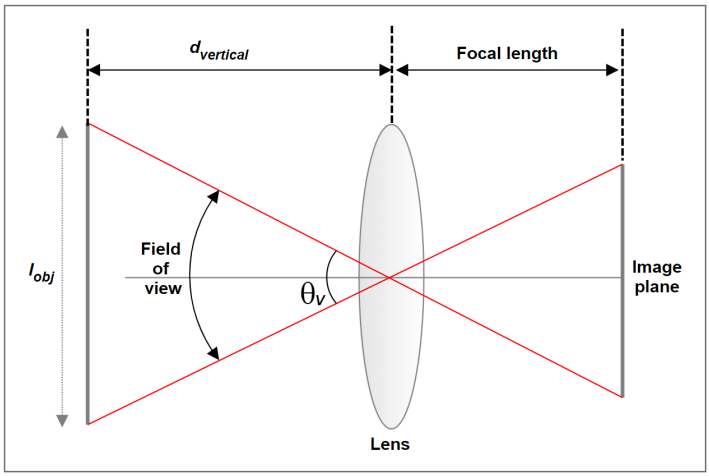

Figure A.3 – Vertical field of view over a lens.

function can convert the digital levels returned by the camera into temperatures. The purpose of calibration is to define this experimental transfer function.

Prerequisites: There are certain equipment and parameters which are necessary requirements for performing calibration of the IR camera:

- *Black body:* IR camera calibration process being a metrology operation can only be realized using some specific temperature measurement standard that gives a validated reference. For IR applications, this measurement standard is a black body. The concept of black body is very crucial in the field of IR imaging. A perfect black body absorbs all incoming radiations and radiates the maximum possible energy at each wavelength. It does not reflect or transmit the incoming radiations. A temperature regulated copper plate is used as a black body whose surface is coated with a specific black paint coating to maximize the emissivity in order to avoid undesirable reflections. For this purpose, the copper plate is uniformly coated with a high emissivity black paint $(\epsilon = 0.974)$.
- *Dynamic range:* A dynamic range must be defined for which the camera is to be calibrated. Generally, it is the operating temperature range in which the IR camera is to be used during the experiments. As an example, the thermal measurements for the topology optimized structure with 28.6% Al are performed in the operating temperature range of $0° - 70°$ C.
- *Integration time:* It refers to the amount of time an IR camera takes to acquire a single thermal image. It is analogous to the shutter speed of a traditional visible light camera. This parameter is especially very critical if the target object is in motion or if the thermal acquisitions are made under transient conditions (i.e., the target temperature is constantly fluctuating). However, in the present study all thermal measurements are made at steady state on a stationary test section. Nevertheless, for the present study the integration time is set to 1.35 milliseconds following the manufacturer recommendation such that the optimal position of the digital level count of the maximum dynamic temperature range should be around 75 % of the saturation point.
- *Thermocouple:* A k-type thermocouple is used to measure accurately the reference temperature of the black body based on which the infrared camera is be calibrated.

Standard calibration procedure:

The camera calibration is performed using the Altair software application from Cedip Infrared Systems provided along with the IR camera. To draw the calibration curve, several points at regular

intervals must be identified along this curve. Each point is described by a pair of values (block body temperature as measured by the thermocouple and the digital level (DL) value returned by the IR camera). To reduce the influence of the camera's internal temperature, it is recommended to work with a temperature-stable camera (after warming up for atleast two hours).

1. For the first measurement point, set the black body to the low end of the dynamic range ($0°C$ in this example).
2. Determine some points at regular intervals over the dynamic range (For example $0°C$, $10°C$, $20°C$, $30°C$, $40°C$, $50°C$, $60°C$ and $70°C$).
3. Place the camera at a distance of $1038\ mm$ from the black body. This distance is evaluated from FOV calculations for the black body dimensions of $200\ mm \times 150\ mm$ used in this process.
4. Focus the camera on the black body reference area and aim the camera to place the black body image in the middle of the field.
5. Successively, and for each measurement point, produce a thermal acquisition from an average of atleast hundred images. This operation eliminates virtually all the time noise.
6. In the Altair software, create a new calibration file and for every measure measurement, successively enter: i) The black body temperature as measured by the thermocouple and, ii) The digital level returned by the camera.
7. The curve is built as the data is entered. It is always increasing. Any "break" in the curve indicates a data entry error.
8. Once all the points have been entered, record the calibration file. The file's storage location (path) must correctly defined in Altair so that it can be taken into account for future measurements.

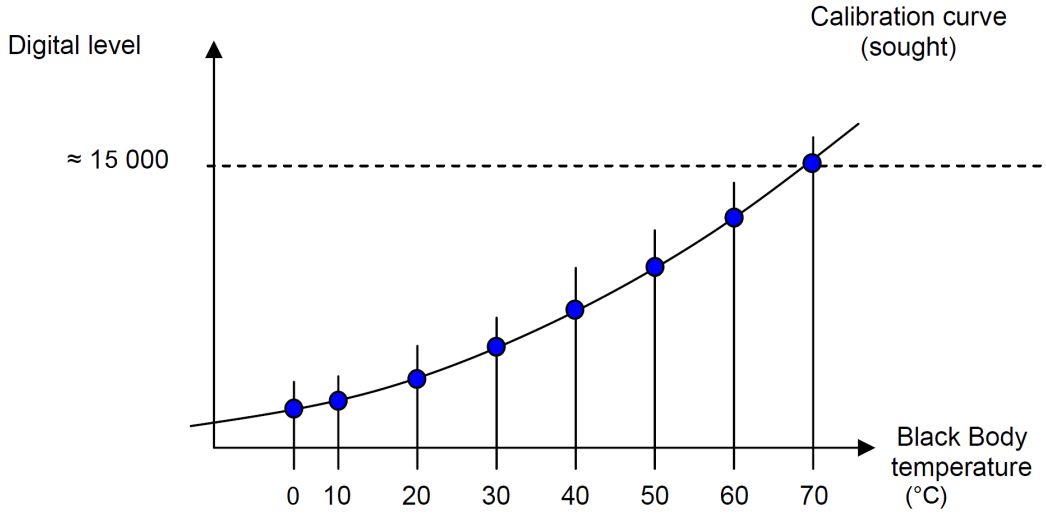

Figure A.4 – Example of calibration process for a $0°C$ - $70°C$ dynamic range.

A.3 Non Uniformity Correction

The first infrared cameras that appeared on the market were fitted with a single detector. A scanner, a mirror equipped mechanism, was used to scan the surface to be measured. The entire image provided by this single detector was implicitly coherent.

The present IR camera (Cedip Titanium 550M), on the contrary, is equipped with a matrix made up of a multitude of detectors and not fitted with a scanner. The present camera has 320×256 (76,800 pixel) matrix of detectors (see Fig. A.5). This technology makes possible extremely high image capture rates and ensures higher reliability (with no mechanical elements in motion and detectors that are independent of each other). This does however come at the cost of disparate detector characteristics, something that affects the image quality. Non Uniformity Correction (NUC) is provided to compensate for these disparities. NUC is therefore essential to provide a coherent image.

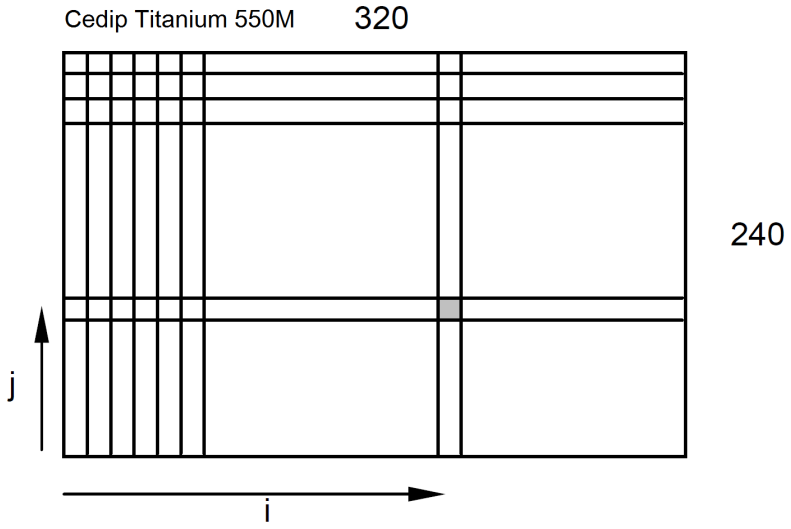

Figure A.5 – Cedip Titanium 550M IR camera: 320×256 (76,800 pixel) matrix of detectors.

Every detector (with coordinates ij) of the IR camera has its own gain (α_{ij}) and offset (β_{ij}) parameters. Correction comprises bringing the curve for each detector into line with the average curve for the entire matrix. Hence, it becomes important to obtain the following:

$$\overline{X} = Y_{ij} = \alpha_{ij} X_{ij} + \beta_{ij} \tag{A.2}$$

where $\overline{X}$ is the average of detector responses and X_{ij} corresponds to raw pixels. The response from each detector after correction equals the average of all of the detector responses. It is important to note that NUC corrects image resolution, it does not affect thermal measurements. NUC is influenced by the integration time and the optical path formed by the lens and any other component like a window, a filter, etc. Thus , the NUC will introduce, for each detector, α and β coefficients to produce a coherent image, taking the influences into account.

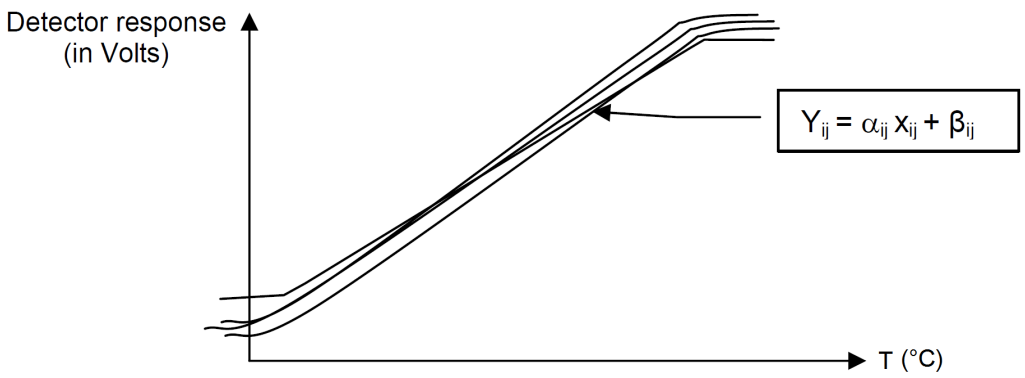

Figure A.6 – Non Uniformity Correction: Curve superposition to obtain average of detector response.

NUC procedure: A standard "two point" correction based on the black body method [16] is performed. To create NUC, two reference points are needed. These references are taken at around $30\ \%$ and $70\ \%$ of the dynamic range. The reference used is ideally a black body with extensive surface area. The latter will be placed a few centimeters from the lens (in an unfocused area). The specific temperature value of each reference point is not of major importance as long as the lower temperature value reference point is more than the lowest temperature of interest, and that the higher temperature value reference point is far from saturation. This operating mode uses the CIRRUS software package supplied with the IR camera. In the present case, for the lower temperature reference point the black body (painted copper plate) was kept at around $20°$C and for the higher temperature reference point it was kept at around $50°$C and the IR image is captured. Using the digital level (DL) values corresponding to these two reference points, the CIRRUS software automatically determines the NUC correction (gain (α_{ij}) and offset (β_{ij})) for each detector based on a proprietary CEDIP algorithm. It is important to note that a new NUC is required every time when the integration time or the optical path is changed.

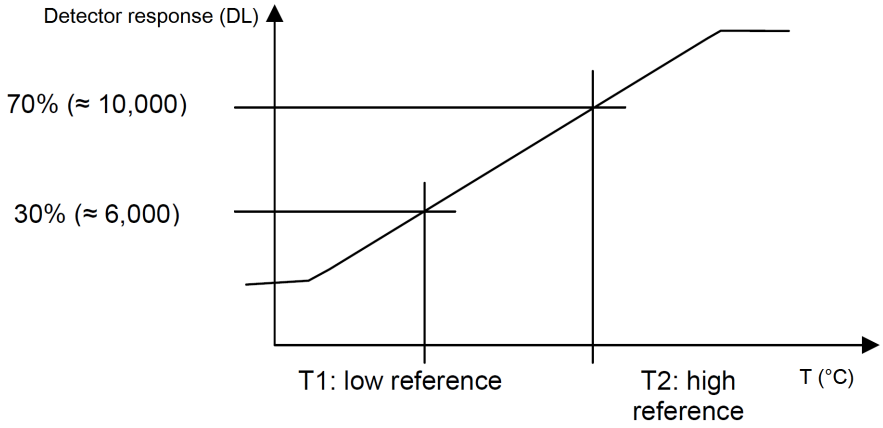

Figure A.7 – "Two point" NUC procedure.

Appendix B

The Finite Volume Method

The finite volume method is a technique for representing and evaluating partial differential equations in the form of algebraic equations [152]. The Finite Volume Method (FVM) deals with the integral form of conservation equations. The computational domain is divided into a finite number of control volumes (CVs) each having a centroid represented by the calculation node **P**. The computational domain has boundaries and each CV in the domain is surrounded by its neighbouring CVs through surfaces. Specific interpolation schemes are required to represent flow variable values at the surface **f** in terms of nodal values. The main advantage of the FVM over other discretization techniques is that this method is conservative in nature as the surface integrals values are the same for the control volumes sharing the same face.

B.1 Discretization of the computational domain

The conservative form of equations in the FVM are solved over a solution domain in space and time which itself is divided into a finite number of control volumes or cells (see Fig. B.1). Each control volume has a central computational node **P** and it is surrounded by neigbouring volume having central node **N**. Every control volume is also surrounded by different faces each defined by its surface vector S_f normal to the face **f** ($\mathrm{S}_f = \boldsymbol{n}\mathrm{S}_f$; $\mathrm{S}_f = Area\ magnitude$; **n** $= unit\ normal\ vector$), points outwards from the control volume, and has the magnitude of its surface area.

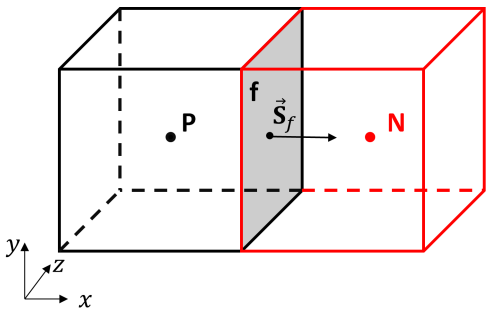

Figure B.1 – Control volume "P".

The computational node **P** is situated at the centroid of the CV such that:

$$\int_{V_p} (\boldsymbol{X} - \boldsymbol{X_P}) dV = 0 \tag{B.1}$$

where $\boldsymbol{X}(x, y, z)$ is the position vector in 3D cartesian coordinate system. The control volume faces in the mesh are also divided into two sets, boundary faces and internal faces.

B.2 Discretization of the transport equation

The general convection-diffusion transport equation for any fluid property (Ψ) is given as follows:

$$\underbrace{\frac{\partial \rho \Psi}{\partial t}}_{\text{Temporal term}} + \underbrace{\boldsymbol{\nabla} \cdot (\rho \mathbf{U} \Psi)}_{\text{Convection term}} = \underbrace{\boldsymbol{\nabla} \cdot (\rho \Gamma \boldsymbol{\nabla} \Psi)}_{\text{Diffusion term}} + \underbrace{S\Psi}_{\text{Source term}} \tag{B.2}$$

Where $\mathbf{U}(u, v, w)$ is the velocity vector, Γ is the diffusion coefficient, ρ is the density, S represents a general source term. The FVM requires that Eqn. B.2 to be satisfied over the control volume V_P around the node **P** in the integral form in both space and time such that

$$\int_t^{t+\Delta T} \left[\int_{V_P} \frac{\partial \rho \Psi}{\partial t} dV + \int_{V_P} \boldsymbol{\nabla} \cdot (\rho \mathbf{U} \Psi) dV \right] dt = \int_t^{t+\Delta T} \left[\int_{V_P} \boldsymbol{\nabla} \cdot (\rho \Gamma \boldsymbol{\nabla} \Psi) dV + \int_{V_P} S\Psi dV \right] dt \tag{B.3}$$

Physically, the first term on the left $\int_t^{t+\Delta T} \left(\int_{V_P} \frac{\partial \rho \Psi}{\partial t} dV \right) dt$ denotes the rate of change of the fluid property Ψ inside the CV, the second term from the left $\int_t^{t+\Delta T} \left(\int_{V_P} \boldsymbol{\nabla} \cdot (\rho \mathbf{U} \Psi) dV \right) dt$ denotes the net transport rate of the property Ψ into the CV due to convection, the term $\int_t^{t+\Delta T} \left(\int_{V_P} \boldsymbol{\nabla} \cdot (\rho \Gamma \boldsymbol{\nabla} \Psi) dV \right) dt$ denotes the net transport rate of the property Ψ out of the CV due to diffusion and the last term $\int_t^{t+\Delta T} \left(\int_{V_P} S\Psi dV \right) dt$ is the net rate of increase of Ψ due to sources inside the control volume.

The discretization of Eqn. B.3 is analysed in the subsequent sections with special attention on the specific schemes used for the spatial terms. However, the discretization process of the temporal terms is not discussed as it falls outside the scope of the steady state topology optimization numerical solver developed for solving optimization problems in Chapter 4.

B.2.1 Storage and arrangement of flow quantities

One important consideration when discretizing the governing equations is to the appropriate locations in the domain at which the values of flow quantities will be stored. There are two possibilities for this. First possibility is to use a "collocated grid" arrangement where in all the fluid dynamic quantities are stored at cell centers. Second possibility is to use a "staggered grid" arrangement, where in the volume based quantities like pressure, density and temperature are stored at cell centers and flux based quantities like velocity is stored on the cell faces [153].

OpenFOAM®'s FVM uses a "collocated grid" arrangement where the flow quantities are centered on the cell centroids. Collocated grids require more interpolation than staggered grid, as quantities at the control volume faces must first be interpolated before integration can be performed. A variety of available interpolation, discretization, and matrix solution schemes can be selected at runtime. These are specified in the *fvSchemes* and *fvSolutions* files inside the OpenFOAM® library. OpenFOAM® loads these schemes through its *runTimeSelection* mechanism which is flexible enough to allow different schemes to apply for each individual term in the state equation [154].

B.2.2 Discretization of spatial terms

1. **The diffusion term:** The term $\boldsymbol{\nabla} \cdot (\rho \Gamma \boldsymbol{\nabla} \Psi)$ of Eqn. B.2, after using the Gauss divergence theorem, can be discretized over node **P** of the central control volume as follows:

$$\int_{V_P} \boldsymbol{\nabla} \cdot (\rho \Gamma \boldsymbol{\nabla} \Psi) dV = \int_S d\mathbf{S}_f \cdot (\rho \Gamma \boldsymbol{\nabla} \Psi) = \sum_f \mathbf{S}_f \cdot (\rho \Gamma \boldsymbol{\nabla} \Psi)_f = \sum_f (\rho \Gamma)_f \mathbf{n} S_f \cdot (\nabla \Psi)_f \tag{B.4}$$

The term $(\nabla \Psi)_f$ can be evaluated in several different ways depending upon the type of interpolation scheme being used. The following scheme is used for the calculation of this term at

the surface **f**

$$\mathbf{n}S_f \cdot (\nabla\Psi)_f = S_f \frac{\Psi_N - \Psi_P}{|\mathbf{d}|} \tag{B.5}$$

where the vector **d** between the node **P** and the neighbouring node **N** is perpendicular to the face plane as sown below in Fig. B.2.

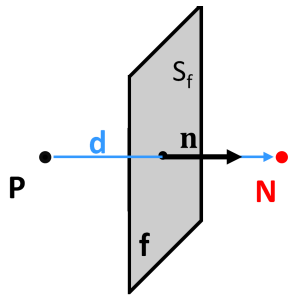

Figure B.2 – Orthogonal mesh interface **f**.

2. **The convection term:** The convection term $\boldsymbol{\nabla} \cdot (\rho \mathbf{U}\Psi)$ of Eqn. B.2, after using the Gauss divergence theorem, can be discretized over node **P** of the central control volume as follows:

$$\int_{V_P} \boldsymbol{\nabla}\cdot(\rho\mathbf{U}\Psi)dV = \int_S d\mathbf{S}_f\cdot(\rho\mathbf{U}\Psi) = \sum_f \mathbf{S}_f\cdot(\rho\mathbf{U}\Psi)_f = \sum_f \mathbf{n}S_f\cdot(\rho\mathbf{U})_f\Psi_f = \sum_f J_f\Psi_f \tag{B.6}$$

where $J_f = \mathbf{n}S_f \cdot (\rho\mathbf{U})_f$ denotes the mass flux through face **f**. Additionally, the kinematic flux Φ_f through the face **f**, for incompressible flows can be defined as follows

$$\Phi_f = \frac{J_f}{\rho} \tag{B.7}$$

The FVM often require interpolation of the variable values at cell-centers to face-center. Several interpolation schemes exists in literature to interpolate the variable values at interface **f** [152, 153, 155]. The two of the commonly used interpolation schemes in fluid flow problems are listed below.

- *The Upwind-difference scheme:* This interpolation scheme is only a first-order accurate, but it ensures boundedness of the solution. The convection term is calculated here according to the direction of the flow. The value Ψ_f at the CV interface **f** is taken as the value of Ψ that exists on the node on the *upwind* of the face such that:

$$\Psi_f = \begin{cases} \Psi_P, & \text{for } \Phi_f \geq 0 \\ \Psi_N, & \text{for } \Phi_f < 0 \end{cases} \tag{B.8}$$

  and it means

$$J_f\Psi_f = \rho[\Psi_P \cdot max(\Phi_f, 0) - \Psi_N \cdot max(-\Phi_f, 0)] \tag{B.9}$$

- *The Central-difference scheme:* This interpolation scheme is second-order accurate, however, the solution can be unbounded. Here, The value Ψ_f at the CV interface **f** is evaluated as follows:

$$\Psi_f = f_x\Psi_P + (1 - f_x) \cdot \Psi_N \tag{B.10}$$

  where

$$f_x = \frac{|\mathbf{X}_f - \mathbf{X}_N|}{|\mathbf{X}_f - \mathbf{X}_N| + |\mathbf{X}_f - \mathbf{X}_P|} \tag{B.11}$$

3. **The source term:** The source term S_Ψ of Eqn. B.2 can be a constant or a function of the fluid property Ψ. However, it must be linearised before discretization as described by Patankar [155] in a way that:

$$S_\Psi = Su + Sp\Psi \tag{B.12}$$

where Su and Sp can also be the function of the fluid property Ψ with the additional condition $(Sp < 0)$ for calculation stability. Therefore, after linearization, the dicretization of the source term over the CV is as follow:

$$\int_{V_P} S\Psi dV = \int_{V_P} (Su + Sp\Psi)dV = SuV_P + SpV_P\Psi_P \tag{B.13}$$

B.2.3 Solution methods for system of linear algebraic equation

The transport equation in its final discretized form is obtained by assembling together the individual spatially discretized terms in Eqn. B.4, B.6 and B.13. This gives an algebraic equation for each control volume of the following form:

$$a_P\Psi_P + \sum a_N\Psi_N = \boldsymbol{\Upsilon_P} \tag{B.14}$$

The value of Ψ_P depends on the values in the neighbouring control volumes, therefore creating a matrix system of algebraic equation as follow:

$$\mathbf{A\Psi} = \boldsymbol{\Upsilon} \tag{B.15}$$

with $\mathbf{A}$ being a sparse matrix of coefficients a_P on the diagonal and coefficients a_N out of the diagonal, $\boldsymbol{\Psi}$ is the vector of all Ψ's for all control volumes and $\boldsymbol{\Upsilon}$ is the source term vector. It is to be noted that $\mathbf{A}$ and $\boldsymbol{\Upsilon}$ contains the combined terms of Eqn. B.14 from both the current and the previous steps.

Several iterative methods exists in literature for solving the systems of equations of the form B.15. Some of the iterative methods are Jacobi method, Gauss Siedel method, the Tri-Diagonal Matrix Algorithm (TDMA) [153], the Conjugate Gradient (CG) method [156], the Bi-CGSTAB method [157] and the Incomplete Cholesky preconditioned Conjugate Gradient (ICCG) method [158]. In the present study, *smoothSolver* OpenFOAM® iterative method is used which uses smoother for symmetric and asymmetric matrices during run-time. *GaussSiedel* smoother is used for this purpose. The method is an improved version of the Jacobi method. It is defined on matrices with non-zero diagonals, but convergence is only guaranteed if the matrix is either diagonally dominant, or symmetric and positive definite [159].

B.2.4 Boundary conditions

The control volumes of the mesh in Fig. B.1 may have one or more faces that coincide with the boundary faces of the computational grid. These faces (denoted as *patches* in OpenFOAM®) may have imposed numerical boundary conditions, hence distinguishing them from the other internal faces of the control volumes. These *patches* are numerically treated differently in OpenFOAM®'s FVM architecture in the sense that the value of the fluid property Ψ is evaluated in a different manner for these boundary faces. Generally, the numerical boundary conditions (BC's) are of two types:

- *Dirichlet boundary condition:* These BC impose directly the value of the variable itself on the boundary. In OpenFOAM® such BC's are prescribed using the *fixed value* type of BC on the patch. It forces the value of Ψ at the boundary patch $\mathbf{b}$ to be equal to $\Psi_\mathbf{b}$.
- *Neumann boundary condition:* These BC impose the gradient of the variable on the boundary. In OpenFOAM® these are referred as the *fixed gradient* type of BC. Here, the dot product of the outward pointing unit normal vector and the gradient is prescribed on the boundary as following:

$$(\mathbf{n} \cdot \boldsymbol{\nabla}\Psi)_\mathbf{b} = g_\mathbf{b} \tag{B.16}$$

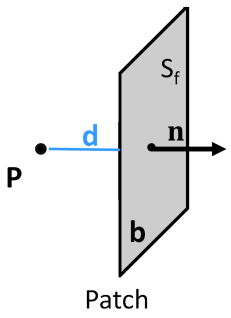

Figure B.3 – Boundary face **b** (patch).

It should be noted that the BC's for any problem are built in the algebraic system of equations B.14 before solving it. However, while performing the discretization of terms that include the sum over faces, $\sum_f$, it is important to handle appropriately the faces which coincide with the boundary.

Note:

The fluid under consideration in Chapter 4 is assumed to be incompressible, Newtonian and under steady-state laminar flow regime with a kinematic viscosity of $6.6 \times 10^{-6}\ m^2 s^{-1}$.

Appendix C

The Method of Moving Asymptotes optimization algorithm (MMA)

The method of moving asymptotes by Svanberg [33] is based on first-order Taylor series expansion of the objective and constraint functions. This method introduces an explicit convex subproblem to approximate the implicit nonlinear problem. The generation of subproblem is controlled by the "moving asmptotes". The method, by moving the asymptotes, stabilises and speeds up the convergence rate of the optimization problem. This algorithm has proved to be well suited for various structural and multi-disciplinary optimization problems, especially where reciprocal and reciprocal-like approximations are used and therefore MMA has gained remarkable interest from the optimization community [45].

A general description of this method bases on the works of Svanberg [33] is as follows:
The objective is to minimize a function, f_0:

Minimize:

$$f_0(\boldsymbol{x}) \qquad (\boldsymbol{x} \in R^n) \tag{C.1}$$

subjected to constraints:

$$f_i(\boldsymbol{x}) \leq \hat{f}_i, \qquad for\ i = 1, .., l \tag{C.2}$$

and the design variable for each cell is restricted to:

$$\underline{x}_j \leq x_j \leq \overline{x}_j, \qquad for\ j = 1, .., nCells \tag{C.3}$$

where $\underline{x}_j$ and $\overline{x}_j$ are the lower and upper bounds on the design variable. The following approach is used to generate and solve a sequence of explicit subproblems:

- *Step 0:* Choose a starting point $\boldsymbol{x}^{(0)}$, and let the iteration index be m =0.
- *Step I:* Given an iteration point $\boldsymbol{x}^{(m)}$, calculate $f_i(\boldsymbol{x}^{(m)})$ and the gradients $\nabla f_i(\boldsymbol{x}^{(m)})$ for $i = 1, .., l$.
- *Step II:* Generate a subproblem $P^{(m)}$ by replacing, in P, the (usually implicit) functions f_i by approximating the explicit function f_i^m, based on the calculations from step *I*.
- *Step III:* Solve $P^{(m)}$ and let the optimal solution of the subproblem be the next iteration point $\boldsymbol{x}^{(m+1)}$. Let $m = m + 1$ and go to step *I*.

The above process is terminated when some sort of convergence criteria is met, or simply when a satisfactory solution $\boldsymbol{x}^{(m)}$ is reached.

Reformulating the above problem (Eqn. C.1- C.3), the following form of the optimization problem holds:

Minimize: $f_0(\boldsymbol{x})$

subject to:

$$f_i(\boldsymbol{x}) \leq 0, \quad i = 1, 2, ..., m \tag{C.4}$$
$$\boldsymbol{x} \in \mathbf{X},$$

where $\boldsymbol{x} = (x_1, ...x_n)^T \in R^n$ are the so called design variables with $\mathbf{X} = \{\boldsymbol{x} \in R^n \mid x_j^{min} \leq x_j \leq {x_j}^{max}, j = 1, ..., n\}$ and $f_0, f_1, f_2, .., f_m$ are provided continuously differentiable (at least twice) real valued function on $\mathbf{X}$. x_j^{min} and x_j^{max} belongs to R such that $x_j^{min} \leq x_j^{max}\ \forall j$. The design variable $\boldsymbol{x}$ is bounded numerically such that its final value represents only one value i.e., either x_j^{min} or x_j^{max}. This represents the interpolation of two materials in the design domain which is obtained by a penalization technique. It should be noted that for the current problem, $n = nCells$ (number of square elements used to discretize uniformly the design domain), $x_j^{min} = 0$ and $x_j^{max} = 1$.

Following Svanberg's approach, by introducing artificial variables, problem C.4 can be written as the following general form:

Minimize: $f_0(\boldsymbol{x}) + a_0 z + \sum_{i=1}^{m} \left(c_i y_i + \frac{1}{2} d_i {y_i}^2\right)$

subject to:

$$f_i(\boldsymbol{x}) - a_i z - y_i \leq 0, \quad i = 1, 2, ..., m \tag{C.5}$$
$$\boldsymbol{x} \in \mathbf{X}, \boldsymbol{y} \geq \boldsymbol{0}, z \geq 0.$$

$\boldsymbol{y} = (y_1, .., y_m)^T \in R^m$ and $z \in R$ are the introduced artificial variables. $a_0,\ a_i,\ c_i$ and d_i are given real numbers such that $a_0 > 0,\ a_i \geq 0,\ c_i \geq 0,\ d_i \geq 0$ and $c_i + d_i > 0\ \forall i$. Moreover, $a_i c_i > a_0$ for all i with $a_i > 0$.

Now, if one sets $a_0 = 1;\ a_i = 0;\ d_i = 1;\ c_i >> 1\ \forall i$ then respectively, z is equal to 0 and $\boldsymbol{y}$ is equal to $\boldsymbol{0}$, in any optimal solution of problem C.5, and their corresponding $\boldsymbol{x}$ is an optimal solution of problem C.4. In that sense, both problems are equivalent. The main benefit of this reformulation is that problem C.5 has always feasible solution i.e., atleast one optimal solution.

Below here is a description of MMA to solve optimization of the form C.5: Given a point $(x^{(k)}, y^{(k)}, z^{(k)})$ as a start at an iteration k, the MMA algorithm generates the following subproblem:

Minimize: $\xi_0^{(k)}(\boldsymbol{x}) + a_0 z + \sum_{i=1}^{m} \left(c_i y_i + \frac{1}{2} d_i {y_i}^2\right)$

subject to:

$$\xi_0^{(k)}(\boldsymbol{x}) - a_i z - y_i \leq 0, \quad i = 1, 2, ..., m \tag{C.6}$$
$$\boldsymbol{x} \in X^{(k)}, \boldsymbol{y} \geq \boldsymbol{0}, z \geq 0.$$

$X^{(k)} = \{\boldsymbol{x} \in R^n \mid 0.9 l_j^{(k)} + 0.1 x_j^{(k)} \leq x_j \leq 0.9 u_j^{(k)} + 0.1 x_j^{(k)}, j = 1, ..., n\}$. The above subproblem C.6 is obtained by replacing the functions $f_0(\boldsymbol{x})$ and $f_i(\boldsymbol{x})$ of C.5 by some chosen convex functions $\xi_0^{(k)}(\boldsymbol{x})$ and $\xi_0^{(k)}(\boldsymbol{x})$, respectively. These convex functions, are then updated iteratively, based on the gradient information at the current iteration point $(x^{(k)}, y^{(k)}, z^{(k)})$ and also on the lower and upper moving asymptotes $(l_j^{(k)} \text{and} u_j^{(k)})$ that are updated based on information from the two previous iterations $(x^{(k-1)}, y^{(k-1)}, z^{(k-1)})$ and $(x^{(k-2)}, y^{(k-2)}, z^{(k-2)})$.

The subproblem C.6 can be solved then at the iteration k, and the optimal solution is updated becoming the next iteration point$(x^{(k+1)}, y^{(k+1)}, z^{(k+1)})$. Then, a new subproblem is regenerated from this last point, and the iterative loop continues by regenerating subproblems until a certain convergence criterion is satisfied (when the squared-norm of the Karush-Kuhn-Tucker (KKT) conditions becomes less than a positive real number ε such that $\varepsilon << 1$).

In the literature, there are many numerical techniques for solving the subproblem C.6, such as the "primal-dual" (PD) interior point technique and the dual approach (DA) [58]. The first approach is based on a sequence of relaxed KKT conditions that are solved by Newton's method (approach used in the present manuscript). The second approach used by Svanberg [33] is based on solving the dual problem corresponding to the subproblem C.6 (thus maximization) by a modified Newton method (Fletcher-Reeves method) that consider well the non-negativity constraints on the dual variables. Figure C.1 gives a process flow of the MMA algorithm.

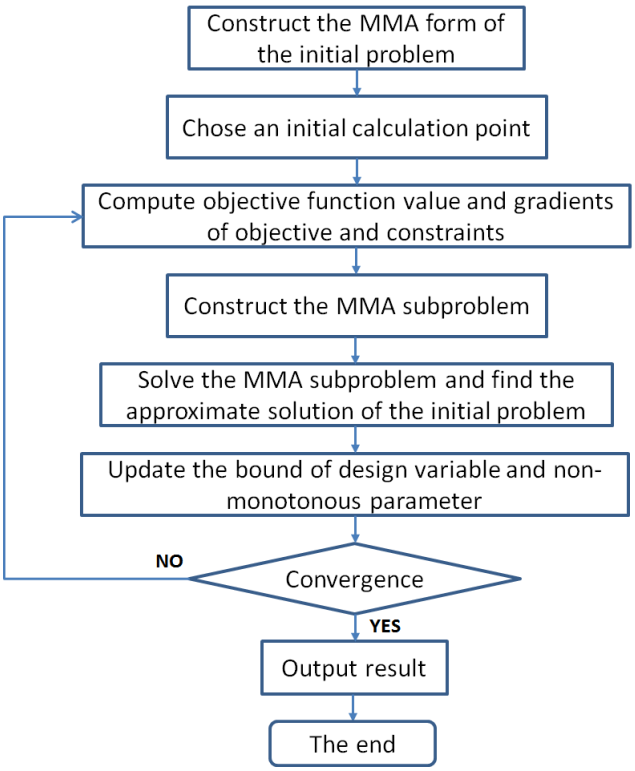

Figure C.1 – Flowchart of the MMA approach.

Appendix D

Density filtering technique

In order to ensure existence of solutions to the TO problem and and to avoid numerical instabilities like the occurrence of checkerboards in the final optimized structure, some restrictions on the design variable must be imposed [160]. A common approach in literature is to use either sensitivity filtering or density filtering, which filters either the derivative of the objective function or the design variable. The developed TO numerical method presented in Chapter 4 uses a mesh-independent density filtering technique proposed by Bruns and Tortorelli [161].

In conventional density based topology optimization, a value of density design variable η_i ranging from $\eta = 0$ (for material 1) to $\eta = 1$ (for material 2), is assigned to each cell i by the optimization algorithm in order to satisfy the desired objective. Density filters work by modifying the value of the design variable of a particular cell based on the design variable values in a specified neighbourhood of that cell. As a result, the final design of a optimization solution and its computational cost is influence by the choice of the neighbourhood. To define a neighbourhood of a cell, one can use the methodology that corresponds to a disk of radius r and take into account all elements inside that disk as shown in Fig. D.1.

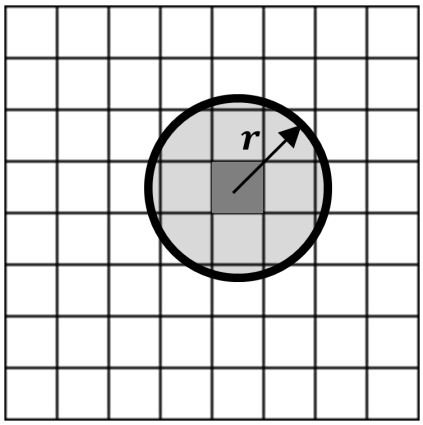

Figure D.1 – A spatial filter of a disk of radius r.

Although overall computational time can be very high for the above mentioned methodology. Another technique called *Neighbourhoods* and *Levels* can be used to define the specified neighbourhood of a cell as depicted in Fig. D.2. For a uniform structured orthogonal mesh, a level-1 von Neumann neighbourhood is formed by 5 cells: the central cell and its four adjacent cells wheres a level-1 Moore neighbourhood is formed by 9 cells. Likewise for level-2, a von Neumann neighbourhood is formed by 13 cells, whereas a Moore neighbourhood is formed by 25 cells. The computational time is generally higher with the Moore's neighbourhood. Moreover, the CPU time increases significantly with an increase in the neighbourhood level.

According to Bruns and Tortorelli [161], the design variable value for the cell i is defined by a weighted distribution of the design variable values in cells over the specified surrounding neighbour-

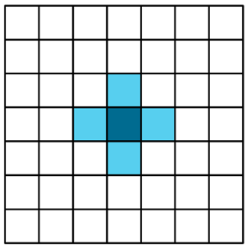

a.1) von Neumann level-1

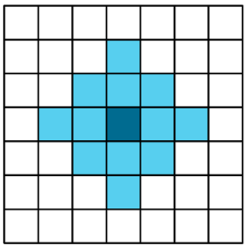

a.2) von Neumann level-2

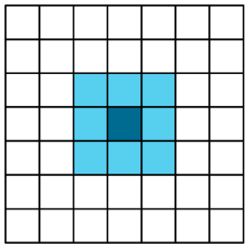

b.1) Moore level-1

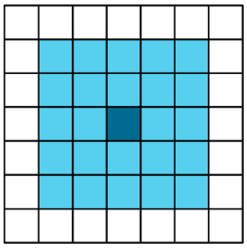

b.2) Moore level-2

Figure D.2 – Neighbourhoods and Levels: a) von Neumann neighbourhood and b) Moore neighbourhood (adapted from [17]).

hood. The density filter the transforms the original design variable value η_i as follows:

$$\widetilde{\eta_i} = \frac{1}{\sum_{N_i} H_{ie}} \sum_{N_i} H_{ie}\eta_e \tag{D.1}$$

where N_i is the set of cells e in the specified neighbourhood for which the center to center distance $\Delta(i,e)$ to cell i is smaller than the filter radius r_{min} and H_{ie} is the weight-factor described as follows:

$$H_{ie} = max(0, r_{min} - \Delta(i,e)) \tag{D.2}$$

A filter radius of $r_{min} = 1.51$ mm is used for the optimal design presented in this chapter.

Topology Optimization of Conjugated Heat Transfer Devices
- Experimental and Numerical Investigations -

Résumé : Concevoir des dispositifs thermiques plus compacts, nécessitant moins de masse de matière, produisant moins de pertes de charge et présentant un rendement thermique accru représente un enjeux clé pour des performances améliorées à un coût moindre. La présente thèse étudie le potentiel et la validité de l'optimisation topologique en tant qu'outil CFD viable permettant de générer des designs thermiques optimaux par rapport aux approches conventionnelles telles que l'optimisation de forme et paramétrique. La première partie de la thèse présente une étude expérimentale de structures bi matériaux arborescentes optimales obtenues par optimisation topologique. Le problème mathématique d'optimisation topologique est formulé et implémenté dans OpenFOAM®. Il est appliqué au problème d'optimisation de la conduction thermique dans une configuration de type volume-vers-point. Des mesures thermiques expérimentales sont effectuées sur les structures optimisées, en utilisant la thermographie infrarouge afin de quantifier leurs performances de transfert de chaleur et ainsi validé les performances des structures optimales déterminées par le code d'optimisation topologique développé. La deuxième partie de la thèse présente une technique bi-objectif innovante d'optimisation topologique des systèmes de transferts de chaleur conjugués (CHT, Conjugate Heat Transfer) en régimes d'écoulement laminaires. Pour cela, le problème est développé mathématiquement et implémenté dans le solveur OpenFOAM® basé sur une méthode directe par volumes finis. La fonction objectif est formulée par la pondération linéaire de deux fonctions objectifs, l'une pour la réduction de la perte de charge et l'autre pour l'augmentation du transfert de chaleur. Ceci représente une cible très difficile du point de vue numérique en raison de la concurrence entre les deux objectifs (minimisation de la perte de charge et maximisation de la puissance thermique récupérable). Des designs non intuitifs, mais optimaux au sens de Pareto, ont été obtenus, analysés, discu-tés et justifiés à l'aide de diverses méthodes d'analyses numériques globale et locale. De plus, une configuration identique à une optimisation par une méthode Lattice Boltzmann issue de la bibliographie a été optimisée en utilisant le solveur OpenFOAM® développé. L'objectif, en complément de la comparaison des solutions optimales, est également d'initier un cas de référence pour de futures études dans ce domaine de recherche et d'innovation de façon à pouvoir pleinement comparer les solutions optimales obtenues par différentes méthodes et différents solvers. Enfin, les différents points expérimentaux et numériques mis en lumière et illustrés dans cette thèse démontrent l'importance de la méthodologie et potentiel très important de l'optimisation topologique pour la conception de systèmes thermiques industriels plus performants.
Mots clés : Optimisation topologique, échangeurs de chaleur, Conduction, Convection, Transferts thermiques conjugués, CFD

Abstract : Designing thermal devices that are more compact with less mass, less frictional losses and increased thermal efficiency is a key requirement for enhanced performances at a lower cost. The present PhD thesis investigates the potential and validity of topology optimization numerical method as a viable CFD tool to generate optimal thermal designs as compared to conventional approaches like shape and parametric optimization. The first part of the thesis presents an experimental investigation of topology optimized tree-like structures made of two materials. The topology optimization mathematical problem is formulated and implemented in OpenFOAM®. It is applied to the topology optimization problem of volume-to-point heat removal. Experimental thermal measurements are carried out, on the optimal structures, using infrared thermography in order to quantify their heat transfer performances and thus validate the performances of the optimal structures determined by the developed topology optimization code. The second part of the thesis presents an innovative bi-objective optimization technique for topology optimization of conjugate heat transfer (CHT) systems under laminar flow regimes. For that purpose, an inequality constrained bi-objective topology optimization problem is developed mathematically and implemented inside the Finite Volume based OpenFOAM® solver. The objective function is formulated by linear combination of two objective functions for pressure drop reduction and heat transfer enhancement which is numerically a very challenging task due to a competition between the two objectives (minimization of pressure drop and maximization of recoverable thermal power). Non-intuitive Pareto-optimal designs were obtained, analyzed, discussed and justified with the help of various global and local numerical analysis methods. Additionally, a recent Lattice Boltzmann topology optimization problem form the literature was solved using the developed OpenFOAM® solver. The objective, in addition to the comparison of the optimal solutions, is also to initiate a case of reference for future studies in this field of research and innovation so as to be able to fully compare the optimal solutions obtained by different methods and different solvers. Finally, the various experimental and numerical findings highlighted and illustrated in this PhD thesis, demonstrate the importance of the methodology and immense potential behind topology optimization method for designing efficient industrial thermal systems.
Keywords : Topology optimization, Heat exchangers, Conduction, Convection, Conjugate heat transfer, CFD